



Investigating sodium-hydrogen exchanger 1 (NHE1) inhibition as a potential therapy for Duchenne muscular dystrophy

PERSEFONI IOANNOU

A thesis submitted for the degree of Doctor of Philosophy

Newcastle University

Faculty of Medical Sciences

Institute of Genetic Medicine

March 2018



**Investigating sodium-hydrogen exchanger 1 (NHE1) inhibition as a
potential therapy for Duchenne muscular dystrophy**

PERSEFONI IOANNOU

Declaration

This thesis is submitted for the degree of Doctor of Philosophy at Newcastle University. I, Persefoni Ioannou, declare that the presented work in this thesis is a result of my own original research. I confirm that the work done by others is clearly acknowledged and any published work is clearly attributed, and the source is always given. I certify that this thesis contains no material that has been submitted for any other academic degree and has not been published previously before submission.

Abstract

The absence of dystrophin in Duchenne muscular dystrophy (DMD) muscle cells results in increased membrane permeability and subsequent intracellular calcium (Ca^{2+}) overload. We postulated that the dysregulation of Ca^{2+} homeostasis is exacerbated by the increased activity of the sodium-hydrogen exchanger 1 (NHE1). NHE1 over-activity leads to an increased influx of sodium (Na^+), which in turn switches the sodium-calcium exchanger (NCX) into reverse mode, resulting in an increased Ca^{2+} influx. Selective NHE1 inhibitors can be used to reduce the Na^+ influx and thereby revert the NCX to normal mode with a subsequent decrease in the cellular Ca^{2+} load. This observation has led to the hypothesis that the use of specific NHE1 inhibitors could improve the Ca^{2+} homeostasis and alleviate pathology in DMD muscle.

The current study investigated the efficacy of a specific NHE1 inhibitor, KR-33028, that has a good safety and potency profile in several pre-clinical studies. In order for the efficacy of the drug to be determined, dystrophin-deficient *mdx* mice were treated chronically via drug in chow. The Ca^{2+} dynamics in both skeletal and cardiac muscles were studied using manganese-enhanced magnetic resonance imaging (MEMRI). Additionally, cine cardiac MRI was carried out to assess the development and progression of cardiomyopathy. Interestingly, four-limb functional grip strength tests that were carried out throughout the treatment demonstrated a significant increase of the grip strength of the drug-treated mice, in comparison to the vehicle-treated ones; and histological analysis demonstrated a significant decrease of fibrosis in the diaphragm of treated mice. Additionally, proteomic analysis showed that chronic treatment with KR-33028 resulted in a significant change of abundance of key skeletal muscle proteins and impacted on the Ca^{2+} machinery, further providing evidence to support our theory.

The proposed studies with a first prototype NHE1 inhibitor are an important step towards potential clinical trials for dystrophinopathies with this class of compounds.

“Remember to look up at the stars and not down at your feet. Try to make sense of what you see and wonder about what makes the universe exist. Be curious. And however difficult life may seem, there is always something you can do and succeed at. It matters that you don't just give up.”

Stephen Hawking (1942–2018)

Dedicated to Duchenne muscular dystrophy patients and their families.

Acknowledgements

The past three years have been a period of intense learning for me both in the scientific arena and on a personal level. I would like to reflect on the people who supported me during this period.

I would like to express my deepest appreciation to my supervisors Prof Volker Straub, Dr Umar Burki, and Dr Steven Laval for giving me the opportunity to undertake this project, but also for their expert guidance, supervision, and support. I also owe many thanks to my PhD progress assessors, Dr Guy MacGowan, and Prof Deborah Henderson, for their invaluable help. Additionally, I would like to express my gratitude to Peacock Pharma (Goch, Germany), especially Stefan Schäfer, for providing the compound tested during this project.

I am very grateful to my colleagues at the John Walton Muscular Dystrophy Research Centre and the Newcastle University, past and present, for their contributions. Special thanks to Emily O'Connor, Dr Emine Bagdatlioglu, Dr Yasmin Issop, and Dr Sally Spendiff, for your help with laboratory work and for being so supportive. Many thanks to Dr Andreas Roos for your contribution to the proteomic work incorporated in this project, and Lisa Hodgson for your help with microscopy. Dr Keith Healy, Dr Alistair Henderson and Prof Bernard Golding, NewChem Technologies (Newcastle University), many thanks for your help with HPLC and stability testing. Thanks to Elizabeth Greally, Kathleen Allinson, Dr Hadeel Alrohaif and Dr Anne Oyewole for your support and for always reminding me that the storm will pass; I will miss our lunch breaks.

I would also like to thank the teaching staff of the Biomedical Sciences School, especially Dr Michèle Sweeney, for giving me the opportunity to acquire teaching and demonstration skills during the course of my PhD.

Nduka Okwose, thank you for your immeasurable support. Your words of encouragement and comfort gave me confidence and optimism and kept me going at my lowest of times.

Finally, I want to thank my family, especially my brother Philippos. Thank you for always being there to support me no matter how far away we are from each other. Mum and dad, without your sacrifices, love and care I would not have been able to complete this thesis.

This work was funded by Barbour Foundation and Medical Research Council (MRC) UK.

Table of Contents

Declaration	i
Abstract	ii
Acknowledgements	iv
List of Tables	x
List of Figures	xi
List of Abbreviations	xiv
Chapter 1 Introduction	1
1.1 Duchenne muscular dystrophy (DMD).....	1
1.2 DMD – Phenotype and diagnosis.....	2
1.2.1 DMD clinical manifestations	2
1.2.2 Diagnostics	3
1.3 DMD – Genetics and dystrophin protein	4
1.3.1 <i>DMD</i> Gene	4
1.3.2 Dystrophin protein structure and function	5
1.3.3 Mutations in the <i>DMD</i> gene and DMD.....	7
1.4 Animal models of DMD.....	7
1.4.1 Dystrophin-deficient mice.....	8
1.4.2 Dystrophin-deficient dogs.....	9
1.4.3 Other animal DMD models.....	10
1.5 DMD – Mechanisms of muscle damage	10

1.5.1 Mechanical damage of the sarcolemma	11
1.5.2 Impaired calcium (Ca ²⁺) handling in DMD	11
1.5.3 Inflammation	15
1.5.4 Fibrosis	15
1.5.5 Oxidative Stress	16
1.6 Therapeutic approaches in DMD	17
1.6.1 Current pharmacological management	17
1.6.2 Therapeutic approaches targeting primary pathology in DMD	18
1.6.2.1 Viral gene therapy	18
1.6.2.2 Exon-skipping agents	19
1.6.2.3 Read-through agents	20
1.6.2.4 Utrophin upregulation	20
1.6.2.5 Cell therapy	21
1.6.3 Therapeutic approaches targeting secondary pathology in DMD	22
1.6.3.1 Therapeutic strategies targeting Ca ²⁺ dysregulation	22
1.7 Sodium-hydrogen exchanger (NHE) and DMD	24
1.7.1 NHE1 inhibition as a potential therapy in DMD	26
1.7.1.1 KR-33028, a small-molecule NHE1 inhibitor	27
1.8 Statement of aims	30

Chapter 2. Materials and methods31

2.1 List of reagents	31
2.2 List of solutions	32
2.3 List of antibodies	33
2.4 Chow formulation with KR-33028	34
2.5 <i>In vivo</i> experimental procedures	34
2.5.1 Animal care and husbandry	34
2.5.2 Magnetic resonance imaging (MRI)	34
2.5.2.1 Mouse preparation for MRI	34
2.5.2.2 Cine cardiac MRI	35
2.5.2.3 Manganese-enhanced MRI (MEMRI)	35

2.5.3 Four-limb hanging test	36
2.5.4 Whole blood collection	36
2.6 Histological analysis	37
2.6.1 Muscle collection and storage	37
2.6.2 Cryosectioning of muscle tissue	37
2.6.3 Masson's trichrome staining	37
2.6.4 Haematoxylin and eosin (H&E) staining	38
2.6.5 Imaging of slides and image analysis	38
2.7 Creatine kinase (CK) assay	39
2.8 Protein isolation, detection and quantification	40
2.8.1 Protein extraction	40
2.8.2 Protein quantification using BCA	40
2.8.3 SDS polyacrylamide gel electrophoresis (PAGE)	40
2.8.4 Western blotting	41
2.8.5 Coomassie brilliant blue staining	41
2.8.6 Quantification of protein expression	42
2.9 Proteomic analysis of tibialis anterior (TA) muscles	42
2.9.1 Tissue lysis and sample preparation	42
2.9.2 Protein extraction and digestion	43
2.9.3 Liquid chromatography tandem-mass spectrometry (LC-MS/MS)	43
2.9.4 Data processing	44
2.9.5 Gene ontology and protein-protein interaction analysis	45
2.10 Pharmacokinetic (PK) study	45
2.11 High-performance liquid-chromatography (HPLC) for stability testing of KR-33028-formulated chow	46
2.12 Cell culture	47
2.12.1 Standard cell culture conditions for human myoblasts	47

2.12.2 Single muscle fibre isolation and culture	47
2.13 Statistical analysis	48
Chapter 3. Pharmacokinetic (PK) study of KR-33028 and stability testing.....	49
3.1 Introduction and aims.....	49
3.2 Stability of KR-33028 in mouse chow.....	53
3.3 Pharmacokinetic (PK) study of KR-33028	54
3.4 Discussion and conclusions.....	56
Chapter 4. Investigating the effects of KR-33028 on muscle histology, serum creatine kinase activity and functional strength	58
4.1 Introduction and aims.....	58
4.2 Treatment of <i>mdx</i> mice with KR-33028 NHE1 inhibitor.....	63
4.3 Histological assessment of muscle pathology in KR-33028- and vehicle-treated <i>mdx</i> mice	64
4.3.1 Quantitative analysis of fibrosis.....	64
4.3.2 Evaluation of muscle fibre size variation.....	69
4.3.3 Quantitation of centrally nucleated muscle fibres.....	72
4.4 Assessment of CK levels in KR-33028- and vehicle-treated <i>mdx</i> mice	73
4.5 Assessment of functional grip strength in KR-33028- and vehicle-treated <i>mdx</i> mice	74
4.6 Discussion and conclusions.....	76
Chapter 5. Applying magnetic resonance imaging (MRI) to investigate the effects of KR-33028	78
5.1 Manganese-enhanced magnetic resonance imaging (MEMRI)	78
5.1.1 Introduction and aims.....	78
5.1.2 Effects of long-term treatment with KR-33028 on Ca ²⁺ influx in skeletal and heart muscles of <i>mdx</i> mice.	80
5.2 Cine cardiac magnetic resonance imaging	85
5.2.1 Introduction and Aims	85
5.2.2 Effects of chronic treatment with KR-33028 on the development and progression of cardiomyopathy in <i>mdx</i> mice	87

5.3 Discussion and conclusions.....	90
Chapter 6. Investigating the effects of KR-33028 treatment on the proteome of dystrophic skeletal muscle.....	92
6.1 Introduction and aims.....	92
6.2 Proteome profiling of TA muscles collected from KR-33028-treated and vehicle-treated <i>mdx</i> mice	96
6.3 Pathway and protein-protein interaction (PPI) analysis of proteins down- and up-regulated in KR-33028-treated TA samples	99
6.4 Verification of proteomics data.....	103
6.5 Discussion and conclusions.....	105
Chapter 7. General discussion and future directions	109
7.1 Investigating the effects of KR-33028 <i>in vivo</i>	110
7.1.1 Efficacy of KR-33028 in improving DMD pathology of <i>mdx</i> skeletal muscles	112
7.1.2 Efficacy of KR-33028 in improving DMD pathology of <i>mdx</i> cardiac muscles	114
7.2 Future directions.....	116
7.3 Conclusion.....	122
Appendix A.	123
References	125

List of Tables

Table 2.1. List of reagents used in this project.	32
Table 2.2. List of buffers and solutions used in this project.	33
Table 2.3. List of primary and secondary antibodies used in this project.....	33
Table 2.4. Blood sampling times for mice treated with KR-33028-formulated chow....	45
Table 4.1. Suitability of different mouse muscles for morphological, biochemical, and functional pre-clinical studies..	60
Table 5.1. Cardiac function of drug-treated and vehicle-treated <i>mdx</i> mice before and at the end of the treatment.....	89
Table 6.1. Proteins found to be significantly different between the KR-33028- and vehicle-treated samples.	98
Appendix A. Table 1. List of solutions used for fluorescent pH assay.....	123

List of Figures

Figure 1.1. <i>DMD</i> gene structure and location on the X chromosome.....	4
Figure 1.2. Structure of the full-length dystrophin protein and its isoforms.....	5
Figure 1.3. Dystrophin-glycoprotein complex (DGC).....	6
Figure 1.4. Representation of calcium (Ca ²⁺) signalling and dynamics in muscle fibres.	12
Figure 1.5. Schematic representation of the calcium (Ca ²⁺)-handling proteins and downstream Ca ²⁺ -regulated effectors that are involved in Ca ²⁺ dysregulation in muscular dystrophy.....	14
Figure 1.6. Schematic representation of pharmacologic agents that have been or could be used to improve calcium (Ca ²⁺) homeostasis in DMD.	23
Figure 1.7. NHE1 over-activity results in indirect increase of calcium (Ca ²⁺) influx in dystrophic muscle.....	25
Figure 1.8. Chemical structure of KR-33028 (N-4-cyano (benzo[b]thiophene-2-carbonyl) guanidine, C ₁₁ H ₈ N ₄ OS), a recently developed NHE1 inhibitor.....	27
Figure 1.9. Effects of oral administration of KR-33028 to <i>mdx</i> mice for 6 weeks.	29
Figure 3.1. Basic principles of Pharmacokinetics (PK).	50
Figure 3.3. A typical plasma concentration-time curve obtained after oral administration of a single dose of a drug showing descriptive pharmacokinetic (PK) parameters.	51
Figure 3.4. KR-33028 Standard curve developed using high performance liquid chromatography (HPLC).....	53
Figure 3.5. Mean plasma concentration-time profiles of KR-33028 in mice after intravenous (IV) injection, oral administration and drug-formulated chow.	55
Figure 4.1. Skeletal muscle tissue regeneration process in healthy vs dystrophic muscle tissues.	59
Figure 4.2. Average body weight of drug-treated and vehicle-treated <i>mdx</i> mice measured during the 28-week treatment.....	63
Figure 4.3. Quantitative analysis of fibrosis in diaphragm, heart, and quadriceps muscles harvested from KR-33028-treated and vehicle-treated <i>mdx</i> mice and C57BL/10 mice.	64
Figure 4.4. Masson's trichrome staining of diaphragm harvested from A. control (C57BL/10) mice, B. vehicle-treated <i>mdx</i> mice and C. KR-33028-treated <i>mdx</i> mice....	66
Figure 4.5. Masson's trichrome staining of cardiac muscle tissues harvested from A. control (C57BL/10) mice, B. vehicle-treated <i>mdx</i> mice and C. KR-33028-treated <i>mdx</i> mice.	67
Figure 4.6. Masson's trichrome staining of quadriceps muscle tissues harvested from A. control (C57BL/10) mice, B. vehicle-treated <i>mdx</i> mice and C. KR-33028-treated <i>mdx</i> mice.	68

Figure 4.7. Minimal Feret's diameter of diaphragm muscle fibres in control (C57BL/10), and KR-33028-treated and vehicle-treated <i>mdx</i> mice.....	69
Figure 4.8. Variance coefficient of minimal Feret's diameter of diaphragm muscle fibres in control (C57BL/10), KR-33028-treated and vehicle-treated <i>mdx</i> mice.....	70
Figure 4.9. Haematoxylin and eosin (H&E) staining of diaphragm muscle tissues harvested from A. control (C57BL/10) mice, B. vehicle-treated <i>mdx</i> mice and C. KR-33028-treated <i>mdx</i> mice.	71
Figure 4.10. Average percentage of centrally nucleated muscle fibres in diaphragm samples of control (C57BL/10), and KR-33028-treated and vehicle-treated <i>mdx</i> mice.	72
Figure 4.11. Serum creatine kinase (CK) in control (C57BL/10), KR-33028-treated and vehicle-treated <i>mdx</i> mice.....	73
Figure 4.12. Assessing functional four limb grip strength of KR-33028- and vehicle-treated <i>mdx</i> mice.	75
Figure 5.1. Representative Mn ²⁺ -enhanced MRI (MEMRI) scan.....	79
Figure 5.2. Mean manganese (Mn ²⁺) uptake in myocardium, forelimb and chest-wall muscle of drug-treated <i>mdx</i> mice before and after treatment with KR-33028.....	82
Figure 5.3. Mean manganese (Mn ²⁺) uptake in myocardium, forelimb and chest-wall muscle of vehicle-treated <i>mdx</i> mice before and after treatment with KR-33028.	83
Figure 5.4. Mean manganese (Mn ²⁺) uptake in myocardium, forelimb and chest-wall muscle of drug- and vehicle-treated <i>mdx</i> at the end of treatment with KR-33028.	84
Figure 5.5. Basic principles of cine cardiac magnetic resonance imaging (MRI) acquisition.	86
Figure 5.6. Segmentation of a typical cine scan of a mouse heart.	88
Figure 6.1. Types of proteomics and their applications to biology.....	92
Figure 6.2. Main components of a mass spectrometer.....	93
Figure 6.3. Anatomical position of the tibialis anterior (TA) and extensor digitorum longus (EDL) muscles in mouse hindlimb. A.....	94
Figure 6.4. Subcellular localization of proteins found to be regulated in TA samples collected from KR-33028-treated <i>mdx</i> mice.	99
Figure 6.5. Molecular function enrichments in the network of proteins found to be significantly different between KR-33028-treated and vehicle-treated <i>mdx</i> mice.....	100
Figure 6.6. Protein-protein interaction (PPI) network of proteins found to be regulated in KR-33028-treated skeletal muscle samples.	101
Figure 6.7. Protein-protein interaction (PPI) network of proteins found to be significantly altered in abundance in TA samples harvested from KR-33028-treated <i>mdx</i> mice.....	102
Figure 6.8. Western blot (WB) investigation of CAB39 levels in KR-33028- and vehicle-treated TA samples.....	104

Figure 7.1. Study plan for the investigation of KR-33028 efficacy in the <i>mdx</i> mouse model.	111
Figure 7.2. Monitoring NHE1 activity using an artificial acid-load procedure.....	117
Figure 7.3. Calcium (Ca ²⁺) uptake in DMD and control human myotubes.	118
Appendix A. Figure 1. Preliminary results of fluorescent pH assay carried out in control human myotubes using the BCECF-AM pH fluorescent indicator.....	124

List of Abbreviations

AAV	Adeno-associated virus
AON	Antisense oligonucleotide
AR	Autosomal recessive
BMD	Becker muscular dystrophy
bp	Base pairs
BSA	Bovine serum albumin
C57BL/10	control mouse model
Ca ²⁺	Calcium ions
CI	Cardiac input
CK	Creatine kinase
cM	Centimorgan
CO	Cardiac output
CO ₂	Carbon dioxide
DAPC	Dystrophin-associated protein complex
DCM	Dilated cardiomyopathy
DGC	Dystrophin glycoprotein complex
dH ₂ O	Distilled water
DMD	Duchenne muscular dystrophy
DMEM	Dulbecco's modified Eagle's medium
DNA	Deoxyribonucleic acid
EC	Excitation-contraction coupling
ECG	Electrocardiogram

ECM Extracellular matrix

ED End diastole

EDL Extensor digitorum longus muscle

EDVI End diastolic volume index

EF Ejection fraction

ES End systole

ESVI End systolic volume index

FDB Flexor digitorum brevis muscle

GI Gastrointestinal

H&E Haematoxylin and eosin staining

H⁺ Hydrogen ions (protons)

HPLC High-performance liquid-chromatography

HS Horse serum

IP3Rs Inositol 1,4,5-trisphosphate receptors

kb Kilo bases

kDa Kilo Daltons

LC-MS/MS Liquid chromatography tandem-mass spectrometry

LETM1 Leucine zipper EF-hand containing transmembrane protein 1

LGMD Limb-girdle muscular dystrophy

LV Left ventricle

LVMi Left ventricular mass index

Mbp Mega base pairs

MCU Mitochondrial calcium uniporter

mdx C57BL/10ScSn-Dmd^{*mdx*} mouse model

Mdx Murine dystrophy X-linked, dystrophic animal model

MEMRI Manganese-enhanced Magnetic Resonance Imaging

mm Millimetres

Mn²⁺ Manganese ions

MPTP Mitochondrial permeability transition pore

MRI Magnetic resonance imaging

mRNA Messenger RNA

ms Milliseconds

Na⁺ Sodium ions

NCBI National Centre for Biotechnology Information

NCLX Mitochondrial sodium-calcium exchanger

NCX Sodium-calcium exchanger

NHE Sodium-hydrogen exchanger

ORAI1 Calcium release-activated calcium modulator 1

PAGE Polyacrylamide gel electrophoresis

Pen/strep Penicillin/streptomycin

PK Pharmacokinetic

PMCA Plasmalemmal calcium-ATPase

PTP Permeability transition pore

RIPA Radio-immunoprecipitation assay buffer

RMW Respiratory muscle weakness

RNA Ribonucleic acid

ROS Reactive oxygen species

RT Room temperature

RV Right Ventricle

RVEDVI Right ventricular end diastolic volume index

RVEF Right ventricular ejection fraction

RVESVI Right ventricular end systolic volume index

RyRs Ryanodine receptors

SD Standard deviation

SDS-PAGE Sodium dodecyl sulphate polyacrylamide gel electrophoresis

SEM Standard error of the mean

SERCA Sarco/endoplasmic reticulum luminal calcium-ATPase

SOCE Store-operated calcium entry

SR Sarcoplasmic reticulum

STIM1 Stromal interaction molecule 1

SVI Stroke volume index

TA Tibialis anterior

TRPC Transient receptor potential cation channel

Chapter 1 Introduction

1.1 Duchenne muscular dystrophy (DMD)

The term “muscular dystrophies” refers to a group of genetic muscle diseases that are characterized by progressive muscle wasting and weakness (Emery, 2002; Wicklund, 2013). Based on their historic discovery and the predominant sites of muscle weakness, the muscular dystrophies can be subdivided into seven major forms: Duchenne (DMD), Becker (BMD), Emery-Dreifuss (EDMD), congenital (CMD), facioscapulohumeral (FSHMD), oculopharyngeal (OPMD), and limb-girdle muscular dystrophy (LGMD) (Emery, 2002). The different forms of muscular dystrophies differ by the degree of severity, age of onset, the muscle groups that are primarily affected and the mode of inheritance (Dalkilic and Kunkel, 2003).

DMD is the most common and best characterised form of muscular dystrophy – affecting 1 in 3500 to 5000 live male births (Emery, 1991; Drousiotou *et al.*, 1998; Parsons *et al.*, 2003). It is an X-linked recessive disease that is characterised by progressive muscle weakness and wasting and which, almost exclusively, affects males (Wicklund, 2013). DMD was named after Guillaume Benjamin Amand Duchenne who in his seminal publications of 1861 and 1868 described the clinical features of the disease and the muscle histology in detail (Duchenne, 1861; Duchenne, 1868). Duchenne named the disease as “paralysie musculaire pseudohypertrophique” (pseudohypertrophic muscle paralysis); the term “muscular dystrophy” was not introduced until 1884 by the German neurologist Dr W.H. Erb (Erb, 1884).

Isolated cases of DMD were initially described in the 19th century papers of Gaetano Conte, Charles Bell, Richard Partridge, and Edward Meryon (Tyler, 2003; Pearce, 2005). Edward Meryon, an English physician, was the first to provide a systematic genetic, clinical and pathological study of DMD. He described eight affected boys in three families. His work was presented to a meeting of the Royal Medico-Chirurgical Society in 1851 and was published in “The Transactions of the Society” the following year (Meryon, 1852). Meryon demonstrated that DMD is a familial muscle disease characterised by muscle wasting and weakness and which affects only males. Additionally, autopsy and histological examinations revealed that the spinal cord and the nervous system were normal but sarcolemma in the muscle tissue was broken down and destroyed (Emery, 1993; Pearce, 2005).

1.2 DMD – Phenotype and diagnosis

1.2.1 DMD clinical manifestations

The first clinical features of DMD appear around the age of 3 to 5 years. Weakness in DMD is progressive and starts with proximal lower limb and truncal weakness followed by weakness of upper limb and distal muscles (Yiu and Kornberg, 2015). Presenting symptoms of DMD include delayed motor milestones, speech delay, frequent falls, a waddling gait, difficulty running and jumping, and a mildly lordotic posture (Nigro and Piluso, 2015; Yiu and Kornberg, 2015; Van Ruiten *et al.*, 2016). Additionally, due to weakness of the knee and hip extensors, children suffering from DMD use their hands and arms “climbing up” themselves in order to rise from the ground (Gower’s manoeuvre) (Emery, 2002). Calf hypertrophy with fatty replacement of the gastrocnemius and soleus muscles is also a typical sign of DMD (Nigro and Piluso, 2015). Notably, strength and motor skills in DMD boys are developed to a lesser extent than in their peers and increase only up to 6–7 years of age when strength first plateaus and then deteriorates. Ultimately, in most cases, a wheelchair is required by the age of 12 years old (Emery, 2002; Yiu and Kornberg, 2015).

As the disease progresses, DMD patients develop cardiac complications, including dilated cardiomyopathy (DCM), heart failure and arrhythmias (Judge *et al.*, 2011). The incidence of cardiac complications increases with age and pre-clinical cardiac involvement is evident by the age of 6 years in ~25% of the patients and between the ages of 6 and 10 in ~59% of patients. After the age of 18 all DMD patients develop cardiac involvement (Nigro *et al.*, 1990). Cardiomyopathy is one of the leading causes of death in DMD (Judge *et al.*, 2011).

Progressive respiratory muscle weakness (RMW) is also a major characteristic of DMD. RMW is defined as the inability of the respiratory muscles, i.e. the diaphragm, external intercostal and accessory muscles, to produce normal levels of flow and pressure during inspiration and expiration. RMW results in alterations of ventilatory mechanics, and subsequent restriction of chest movements, carbon dioxide (CO₂) retention and respiratory failure (Perrin *et al.*, 2004). Respiratory failure is directly or indirectly responsible for ~90% of the DMD deaths (Mosqueira *et al.*, 2013). A number of studies have demonstrated that the average life expectancy without ventilatory support is around 20 years. Death is usually caused by retained secretions, atelectasis (lung collapse), pneumonia, or respiratory muscle fatigue and failure (Perrin *et al.*, 2004).

In addition to muscle impairments, approximately a third of the DMD boys exhibit distinct cognitive profiles and neurobehavioral comorbidities which are thought to be non-progressive (Blake and Kroger, 2000; Muntoni *et al.*, 2003; Wicklund, 2013). Furthermore, attention-deficit/hyperactivity disorder (ADHD), autism spectrum disorders, and obsessive-compulsive disorder (OCD) are prevalent in DMD patients (Wicklund, 2013). DMD patients may also exhibit a high risk for development of anxiety and depression (Banihani *et al.*, 2015).

Females heterozygous for a *DMD* allele are usually asymptomatic carriers of the disease. However, a small subset of female carriers (manifesting carriers; MCs), develop a spectrum of DMD symptoms ranging from a very mild late-onset presentation to a severe DMD-like phenotype (Soltanzadeh *et al.*, 2010). DMD phenotypes in MCs are in the majority of cases attributed to skewed X chromosome inactivation (Giliberto *et al.*, 2014). Approximately 10–20% of female carriers present symptoms, including cognitive impairment, cardiac complications, and muscle weakness (Emery, 2002; Yiu and Kornberg, 2015). Furthermore, serum creatine kinase (CK) levels may be mildly elevated in 30 to 60% of carriers, whether symptomatic or asymptomatic (Wicklund, 2013).

1.2.2 Diagnostics

A physician should suspect DMD when a 3–5 years old boy presents with toe walking, partial Gower's manoeuvre, neck weakness, large calves and highly elevated CK levels (up to 200 fold) (Wicklund, 2013). CK levels in DMD patients are high from birth. Therefore, newborn screening 24–48 hours after birth has been considered in order to reduce the diagnostic delay and enable earlier treatments (Ellis *et al.*, 2013). The concentrations of aspartate aminotransferase (AST) (Ervasti, 2007) and alanine aminotransferase (ALT) might be elevated as well (Wicklund, 2013).

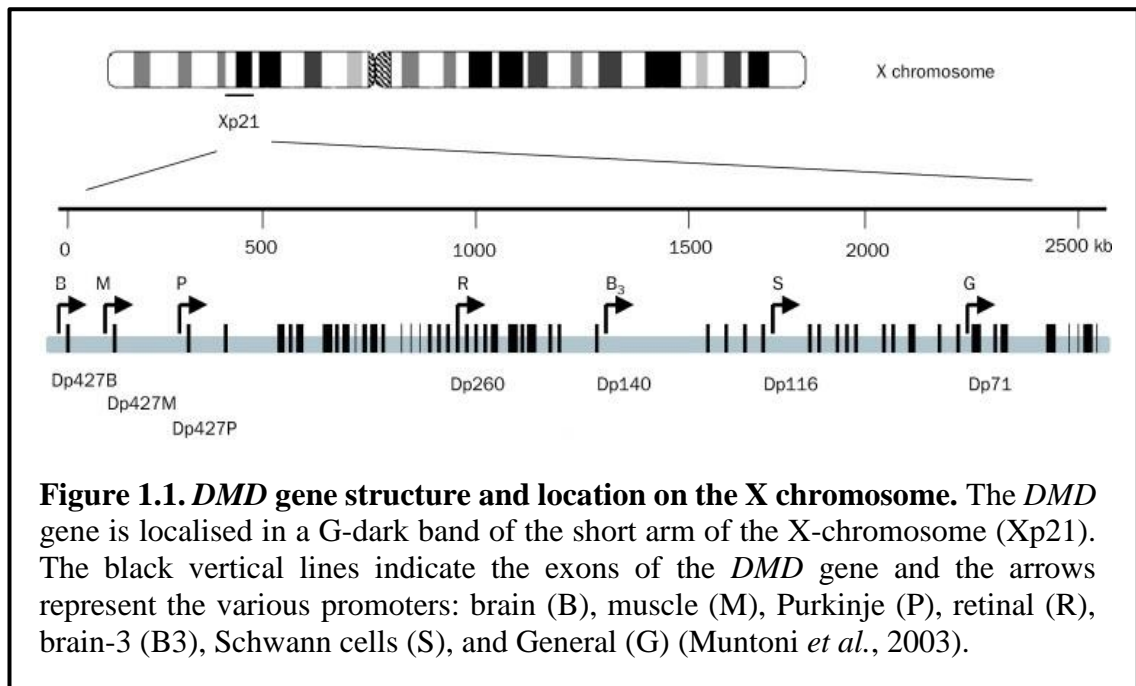
The first diagnostic procedure in DMD is the mutation analysis of the *DMD* gene (Wicklund, 2013). Deletions and duplications are detected by multiplex ligation-dependent probe amplification (MLPA) or oligonucleotide-based array comparative genomic hybridisation (array-CGH). In the case of negative results in MLPA and array-CGH tests, a full sequence analysis is undertaken in order to detect possible point mutations (Laing *et al.*, 2011).

A muscle biopsy is not required to establish the diagnosis in DMD patients unless the genetic testing is negative and the clinical phenotype suggestive of DMD. Muscle

histology investigates fibre size variation, fibre necrosis, invasion of macrophages and significant replacement of muscle by fat and connective tissue (Emery, 2002; Yiu and Kornberg, 2015). Furthermore, immunohistochemistry and western blot analysis allow for quantification of the amount of dystrophin protein expressed and assessment of its size. In DMD, dystrophin expression in skeletal muscle is absent or significantly reduced (Yiu and Kornberg, 2015).

1.3 DMD – Genetics and dystrophin protein

1.3.1 DMD Gene

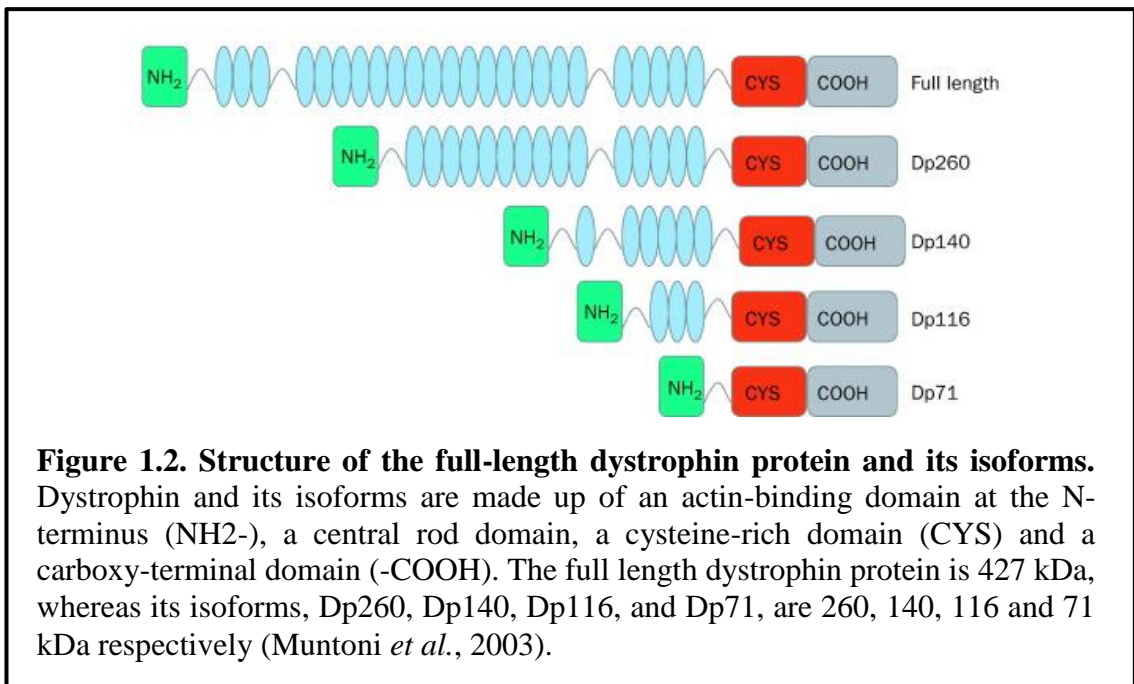


DMD is the result of mutations that disrupt the reading frame of the *DMD* gene leading to residual or no production of functional dystrophin protein. The *DMD* gene was the first human gene to be cloned by positional cloning (Koenig *et al.*, 1987) and is to date the largest gene in the human genome. It spans ~2.5 Mbp in a G-dark band of the short arm of the X-chromosome (Xp21) (Figure 1.1) (Nigro and Piluso, 2015). This corresponds to ~0–1% of the entire human genome and ~1–5% of the entire X chromosome (Kunkel *et al.*, 1989; Mandel, 1989; Manole, 1995). As shown in Figure 1.1, the *DMD* gene possesses 84 average-size exons that are separated by large introns. Notably, ~99% of the *DMD* sequence corresponds to introns (Muntoni *et al.*, 2003).

The *DMD* gene encodes for the dystrophin protein and its isoforms. The gene has a total of 7 promoters which are linked to unique first exons and are activated in a tissue-specific way (Figure 1.1). The full-length dystrophin isoform is produced by the activation of the

brain (B), muscle (M) and Purkinje (P) promoters. The name of the promoters refers to the major sites of expression of the protein. The B promoter produces a protein that is localised in the cortical neurons and the hippocampus of the brain, the M promoter drives the expression of dystrophin in skeletal muscle and cardiomyocytes, but also in some glial cells of the brain at lower concentrations, and the P promoter regulates the expression of dystrophin in skeletal muscle, at lower concentrations (Nudel *et al.*, 1989; Bies *et al.*, 1992a; Bies *et al.*, 1992b; Torelli *et al.*, 1999; Muntoni *et al.*, 2003; Doorenweerd *et al.*, 2017). In addition to the full length isoform; four truncated isoforms of dystrophin are produced by the four internal promoters: retinal (R), brain-3 (B3), Schwann cell (S), and general (G) (Blake *et al.*, 2002). Those transcripts result from different promoters – each isoform can also have alternative splicing. The R promoter is active in the retina, the B3 in the brain, kidney and retina, the S in the peripheral nervous system, and the G in most non-muscle tissues, including lung, kidney, liver, brain, and cardiac muscle (Blake *et al.*, 2002; Muntoni *et al.*, 2003).

1.3.2 Dystrophin protein structure and function



The full-length dystrophin protein is 427 kDa, whereas the isoforms produced by the retinal (R), brain-3 (B3), Schwann cell (S) and general (G) promoters are 260, 140, 116 and 71 kDa, respectively. Dystrophin is a cytoskeletal protein and is a member of the β -spectrin/ α -actinin protein family. As shown in Figure 1.2, dystrophin has four major domains: a) an actin-binding domain at the NH₂-terminus, b) a central rod domain, c) a

cysteine-rich domain and d) a carboxy-terminal domain (Blake *et al.*, 2002; Nigro and Piluso, 2015).

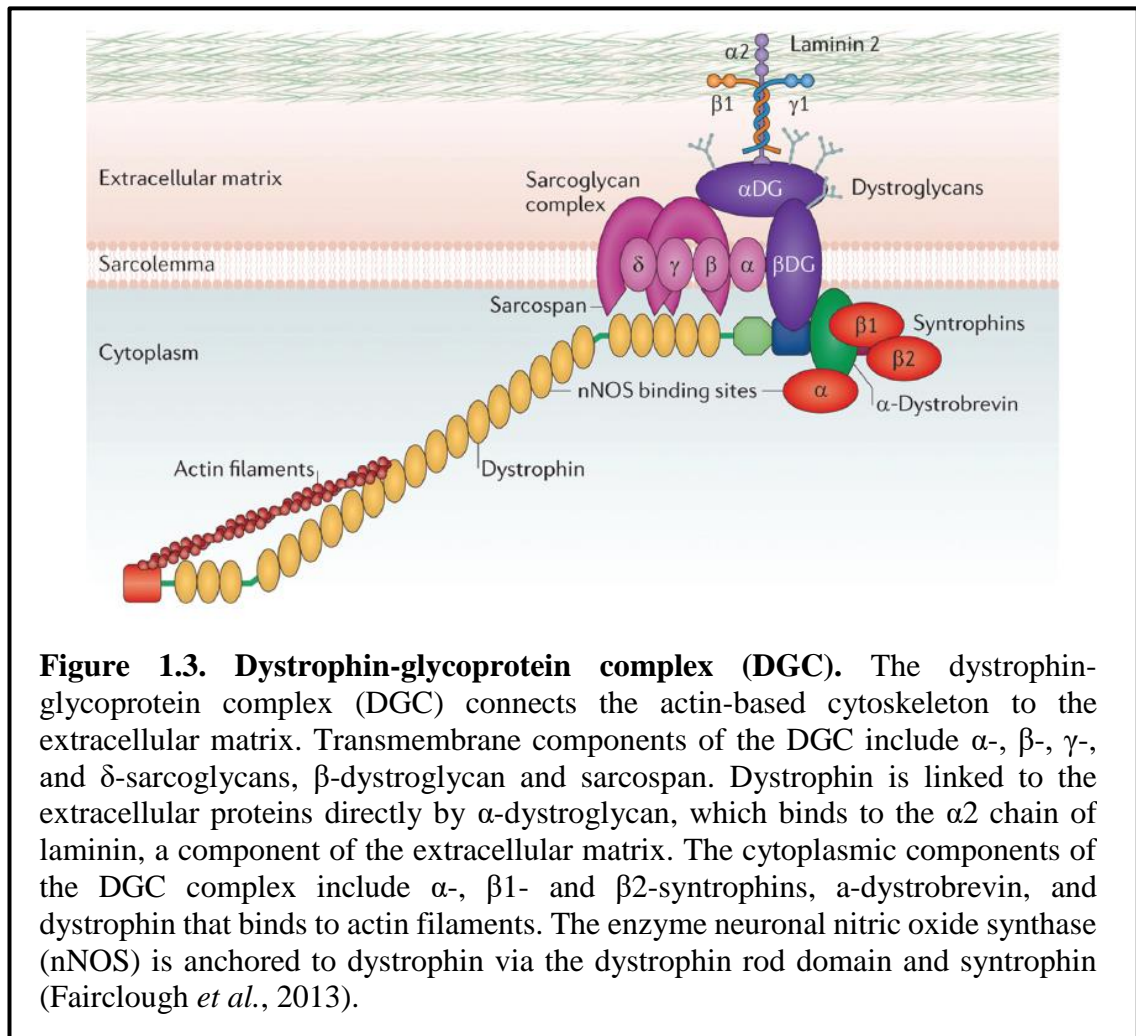


Figure 1.3. Dystrophin-glycoprotein complex (DGC). The dystrophin-glycoprotein complex (DGC) connects the actin-based cytoskeleton to the extracellular matrix. Transmembrane components of the DGC include α -, β -, γ -, and δ -sarcoglycans, β -dystroglycan and sarcospan. Dystrophin is linked to the extracellular proteins directly by α -dystroglycan, which binds to the $\alpha 2$ chain of laminin, a component of the extracellular matrix. The cytoplasmic components of the DGC complex include α -, $\beta 1$ - and $\beta 2$ -syntrophins, α -dystrobrevin, and dystrophin that binds to actin filaments. The enzyme neuronal nitric oxide synthase (nNOS) is anchored to dystrophin via the dystrophin rod domain and syntrophin (Fairclough *et al.*, 2013).

Dystrophin is located on the cytoplasmic side of the plasma membrane of cardiac and skeletal muscles (Muntoni *et al.*, 2003). It associates with several proteins, including the α -, β -, γ - and δ -sarcoglycans, β -dystroglycan, sarcospan, the syntrophins, dystrobrevin, and nitric oxide synthase (NOS), in order to form a large protein complex known as the dystrophin-glycoprotein complex (DGC) (Figure 1.3) (Ervasti *et al.*, 1990; Ervasti and Campbell, 1991; Straub and Campbell, 1997; Wicklund, 2013). The DGC spans the sarcolemma and forms a molecular bridge between the extracellular matrix (ECM) and the muscle cytoskeleton by linking actin filaments through the transmembrane protein complex to laminin in the ECM (Nigro and Piluso, 2015). The assembly of the DGC is dependent on the presence of dystrophin and therefore, in dystrophin-deficient muscle the DGC is destabilized (Blake and Kroger, 2000).

In addition to its structural function, dystrophin is involved in cellular signalling cascades by interacting with neuronal NOS (nNOS), transient receptor potential channels 1 and 4 (TRPC1 and TRPC4 respectively), and other transmembrane proteins, such as the acetylcholine receptor (AChR), the voltage-gated sodium channel (Nav) and aquaporin (AQP). It is involved in vital cellular processes, such as excitation-contraction (EC) coupling, calcium (Ca²⁺) homeostasis, gene expression, mitochondrial function, and motor protein interaction (Mosqueira *et al.*, 2013).

1.3.3 Mutations in the DMD gene and DMD

The *DMD* gene has a high mutation rate due to its large size and the high intragenic recombination rate (over 12 cM) (Wicklund, 2013; Nigro and Piluso, 2015). Large intragenic deletions account for 43–67% of the DMD cases, small mutations for 16–26%, duplications for 9–11%, and splice site mutations for 5–6% of the cases (Flanigan *et al.*, 2009; Tuffery-Giraud *et al.*, 2009; Takeshima *et al.*, 2010; Mah *et al.*, 2011). Two deletion hotspots have been identified within the *DMD* gene, the first one being at the 3' end of the gene (exons 44–53) and the second at the 5' end (exons 3–19) (Nigro and Piluso, 2015).

The phenotype and severity of the disease do not depend on the size of the deletion but on whether the mutation disrupts the reading frame of the *DMD* gene or not. The vast majority of mutations (~90%) that cause DMD disrupt the reading frame of the *DMD* gene (out-of-frame mutations). As a result of out-of-frame mutations, the RNA transcribed from the *DMD* gene contains stop codons and is rapidly degraded. Consequently, no dystrophin protein is produced. On the other hand, in-frame mutations of the repetitive rod domain can result in the production of partly functional dystrophin protein and generally cause the allelic, but much less severe form of Becker muscular dystrophy (BMD) (Becker and Kiener, 1955; Becker, 1957). Examples of in-frame mutations that result in DMD are large deletions in the 5' end and which extend to the middle-rod domain, such as deletions of exons 3–31, 3–25, 4–18, and 4–41, and result in the removal of essential protein domains, including the cysteine-rich domain (Muntoni *et al.*, 2003).

1.4 Animal models of DMD

Investigation and understanding of several physiological and pathophysiological processes relies widely on animal models. There are a number of naturally occurring

animal models for DMD, out of which the most commonly used ones are *mdx* mice and muscular dystrophy dog (*cxmd*).

1.4.1 Dystrophin-deficient mice

The *mdx* model was first discovered by Bulfield *et al.* (1984) and is now the best characterised animal model for DMD. The *mdx* mouse carries a mutation within exon 23 of the *Dmd* gene which results in a premature stop codon and absence of dystrophin expression in muscle (Sicinski *et al.*, 1989). Despite the lack of dystrophin, compared to DMD patients, the *mdx* mouse displays a very mild clinical phenotype and its lifespan is only reduced by 25% as opposed to 75% in DMD patients. Furthermore, the limb muscles of adult *mdx* mice exhibit neither the weakness nor the progressive degeneration that characterise DMD in humans. Skeletal muscle disease in the *mdx* mice presents several distinctive phases; in the first 2 weeks, *mdx* muscle appears normal, between weeks 3 to 6, it undergoes necrosis, and, subsequently, the majority of skeletal muscle enters a relatively stable phase owing to robust regeneration. During the last phase, *mdx* limb muscles often become hypertrophic (McGreevy *et al.*, 2015). The diaphragm, however, presents a pattern of fibrosis, degeneration and severe functional deficit (Stedman *et al.*, 1991). Other pathological characteristics of *mdx* mice include elevated serum CK levels, variation of fibre size, muscle degeneration and necrosis, and centrally nucleated fibres (indicative of muscle regeneration) (Nakamura and Takeda, 2011). Additionally, the disease phenotype progressively worsens with age and severe dystrophic phenotypes, such as heart failure, scoliosis and spontaneous sarcoma, do not occur until mice are 15 months or older (Pastoret and Seville, 1995; Lynch *et al.*, 2001; Chamberlain *et al.*, 2007; Bostick *et al.*, 2009; Schmidt *et al.*, 2011; Wang *et al.*, 2014).

Since the clinical relevance of the *mdx* mouse as a model of DMD is questionable, several other mouse strains with different mutations and differential expression of dystrophin isoforms have been investigated in an attempt to mimic the human DMD phenotype (Wang *et al.*, 2009b; Rodrigues *et al.*, 2016). It has been found that inducing secondary mutations in genes with important cellular functions and modifying the genetic background may lead to more severe pathological characteristics than those observed in *mdx* (C57BL/10 genetic background) mice (Rodrigues *et al.*, 2016). For example, *mdx* mice that also carry a mutation within the *CMAH* gene (*mdx/cmah* mice; Chandrasekharan *et al.*, 2010), or a deletion in the RNA component TERC (mTR) of telomerase (*mdx/mTR* mice; Sacco *et al.*, 2010) exhibit more severe pathological

characteristics and could, therefore, constitute better DMD animal models. The double knock-out (*dko*) mouse model which lacks both dystrophin and a closely related protein, utrophin, also presents a more severe phenotype (similar to or even worse than that of DMD patients), including progressive muscle wasting, weight loss, breathing problems, joint contractures and kyphosis (Deconinck *et al.*, 1997; Grady *et al.*, 1997). However, the *dko* mice are difficult to generate and care for, and, compared with the single knockouts, often die prematurely between 4 to 20 weeks (McGreevy *et al.*, 2015). Consequently, it has recently been proposed that utrophin heterozygous *mdx* mice might represent an intermediate model between the mildly affected *mdx* mice and severely affected *dko* mice (Zhou *et al.*, 2008; Rafael-Fortney *et al.*, 2011; van Putten *et al.*, 2012). Additionally, the *mdx* mice on the DBA/2J background (DBA/2J-*mdx* model or DBA mice) which lack dystrophin as well as γ -sarcoglycan, present a more severe phenotype than *mdx* mice with C57BL/10 genetic background, including more skeletal muscle damage and inflammation, as well as an earlier onset of cardiac disease (Heydemann *et al.*, 2005; Coley *et al.*, 2016).

Despite the development of other mouse models, the *mdx* remains the most commonly used murine model for DMD. It is the mouse model that most accurately represents DMD genetically and is, therefore, essential for the preclinical development of gene therapies (Willmann *et al.*, 2009).

1.4.2 Dystrophin-deficient dogs

In contrast to the *mdx* mouse, the canine X-linked muscular dystrophy (*cxmd*) model exhibits a more severe DMD phenotype. *Cxmd* was first identified in Golden Retrievers (Cooper *et al.*, 1988; Kornegay *et al.*, 1988) and then in other breeds, including Rottweilers (Collins and Morgan, 2003) and German shorthaired pointers (Schatzberg *et al.*, 1999).

The Golden Retriever muscular dystrophy model (GRMD) has been the most extensively examined and characterized canine model amongst research institutes (Sharp *et al.*, 1992). The disease in the GRMD model results from a point mutation within the intron 6 of the *DMD* gene, which leads to skipping of exon 7, a premature stop codon and subsequent lack of dystrophin expression (Sharp *et al.*, 1992; Howell *et al.*, 1997). The pathology of GRMD dogs is characterised by progressive muscle wasting, degeneration and fibrosis,

elevated CK levels, contractures, cardiomyopathy and short life span (Valentine *et al.*, 1988; Valentine *et al.*, 1992; Howell *et al.*, 1997).

Despite the severity of the pathology that the GRMD model presents, it is less widely adopted than murine DMD models because maintenance of a dog colony is challenging and expensive (Wang *et al.*, 2009b; Kornegay, 2017), but also because the severity of the pathology in GRMD dogs is highly variable due to epigenetic effects and modifier genes (Kornegay *et al.*, 2012; Brinkmeyer-Langford and Kornegay, 2013; Yu *et al.*, 2015).

1.4.3 Other animal DMD models

In addition to the naturally occurring murine and canine models, other animal DMD models are widely used as quick and cheap alternatives even though they are more genetically divergent from humans. Those include zebrafish (Berger *et al.*, 2010; Gibbs *et al.*, 2013), *Drosophila* (Mosqueira *et al.*, 2010; Pantoja and Ruohola-Baker, 2013; Plantie *et al.*, 2015) and *Caenorhabditis elegans* (Chamberlain and Benian, 2000; Gieseler *et al.*, 2000). Moreover, a dystrophic rat model (*Dmd*^{mdx} rats) with phenotypic characteristics similar to the human DMD pathology has recently been developed and represents a promising DMD model (Larcher *et al.*, 2014; Nakamura *et al.*, 2014).

Pigs share many anatomical and physiological features with humans, including the cardiovascular system, which is of great importance in the study of dystrophinopathies. Consequently, a tremendous amount of effort has been made to genetically engineer porcine models of DMD. It has been demonstrated that, similarly to DMD patients, dystrophic pigs exhibit impaired mobility, progressive muscle weakness, and elevated serum CK levels (Klymiuk *et al.*, 2013). However, their short life span and susceptibility to sudden death due to acute stress limit their potential contribution to the field. Ongoing studies aim to further describe the pathophysiological characteristics and disease progression of different DMD pig models (Selsby *et al.*, 2015; Frohlich *et al.*, 2016; Yu *et al.*, 2016).

1.5 DMD – Mechanisms of muscle damage

Although the genetics of the disease have been well characterized, the precise mechanism that leads from the absence of dystrophin to muscle degeneration is yet to be defined in detail. The pathophysiology of DMD is complicated and involves a series of mechanisms, including the mechanical damage of the cell membrane, disruption of Ca²⁺ homeostasis, fibrosis, inflammatory responses, oxidative stress, autophagy, apoptosis, and disruption

of several signalling pathways (Deconinck and Dan, 2007; Shin *et al.*, 2013). The main mechanisms of the disease pathology are presented in more detail below.

1.5.1 Mechanical damage of the sarcolemma

The absence of dystrophin from muscle results in loss of the dystrophin-associated proteins from the membrane, destabilisation of the DGC complex and consequent disruption of the link between the cytoskeleton and the ECM. As a result, the muscle membrane becomes more fragile and susceptible to mechanical stress and damage, particularly that induced by eccentric contractions. The formation of microlesions and tears in the sarcolemma leads to increased membrane permeability. As a consequence, soluble proteins, such as CK, leak out of the cell while plasma proteins, and ions, such as Ca^{2+} , enter the cells (Deconinck and Dan, 2007; Allen and Whitehead, 2011; Yiu and Kornberg, 2015).

1.5.2 Impaired calcium (Ca^{2+}) handling in DMD

Ca^{2+} ions represent a ubiquitous second messenger molecule involved in the regulation of various metabolic and physiological processes. The temporal localization and concentration of integrated free cytosolic Ca^{2+} constitutes a specific message and therefore, Ca^{2+} signalling is highly organized in frequency, amplitude and space. A series of complex interactions between ion exchangers and pumps, voltage sensors, Ca^{2+} channels, Ca^{2+} transporters and Ca^{2+} -binding proteins mediate Ca^{2+} concentration in all eukaryotic cells (Berchtold *et al.*, 2000; Missiaen *et al.*, 2000; Berridge *et al.*, 2003).

In skeletal muscles, the levels of cytosolic Ca^{2+} dictate the overall contractile status; high Ca^{2+} levels are critical for triggering muscle contraction, while low levels are crucial for muscle relaxation (Vallejo-Illarramendi *et al.*, 2014). Skeletal muscle Ca^{2+} levels are particularly frequent and diverse; hence why Ca^{2+} cycling mechanisms and storage need to be maintained under precise spatial and temporal control. The main signalling pathways that control Ca^{2+} dynamics in muscle fibres are presented in Figure 1.4. Notably, prolonged increases in basal intracellular Ca^{2+} levels have been associated with long duration fatigue (Allen *et al.*, 2008), certain muscle diseases and ageing (Andersson *et al.*, 2011). Furthermore, abnormal expression patterns of ion-regulatory proteins have repeatedly been linked to several forms of muscular dystrophy (Gailly, 2002).

Intracellular Ca^{2+} levels in skeletal muscle are maintained at a very low concentration due to the central role that Ca^{2+} plays in EC coupling. However, in DMD muscle intracellular

Ca^{2+} levels are higher than normal (Oberc and Engel, 1977; Duncan, 1978). The elevated intracellular Ca^{2+} concentrations in DMD result in the activation of several Ca^{2+} -dependent pathways, for example mitochondrial-mediated cell death by opening the mitochondrial permeability transition pore (PTP) (Vallejo-Illarramendi *et al.*, 2014), activation of a series of muscle-dependent proteases, such as calpains, which degrade

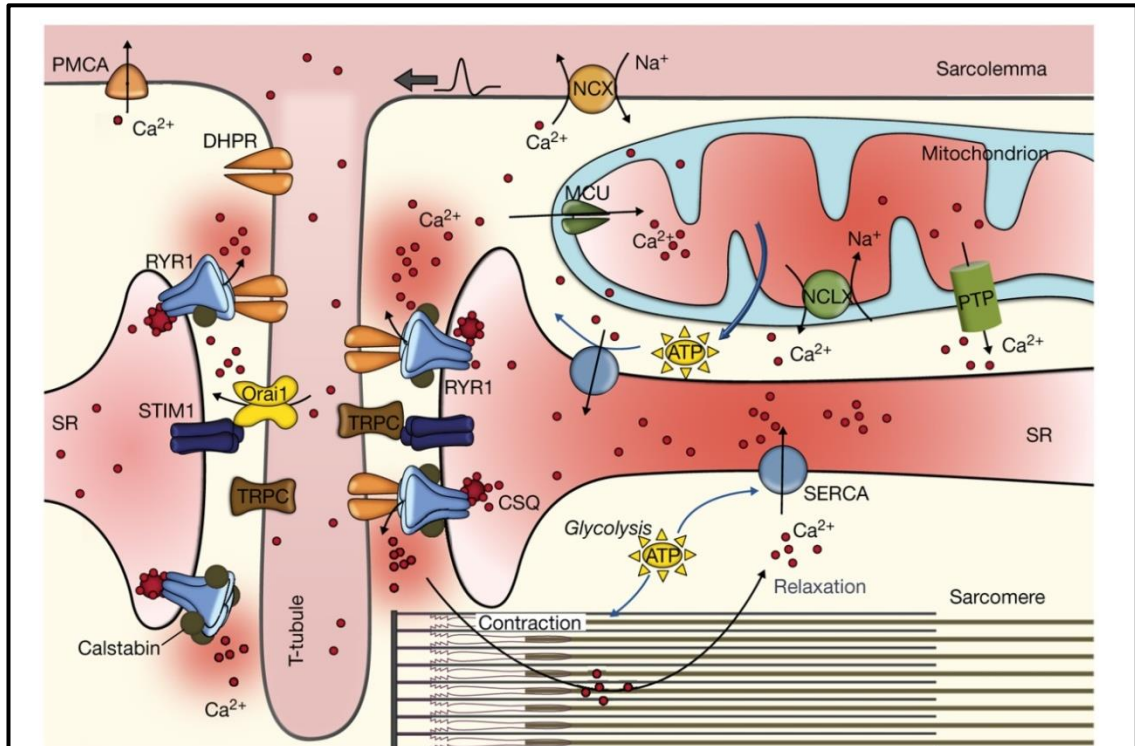


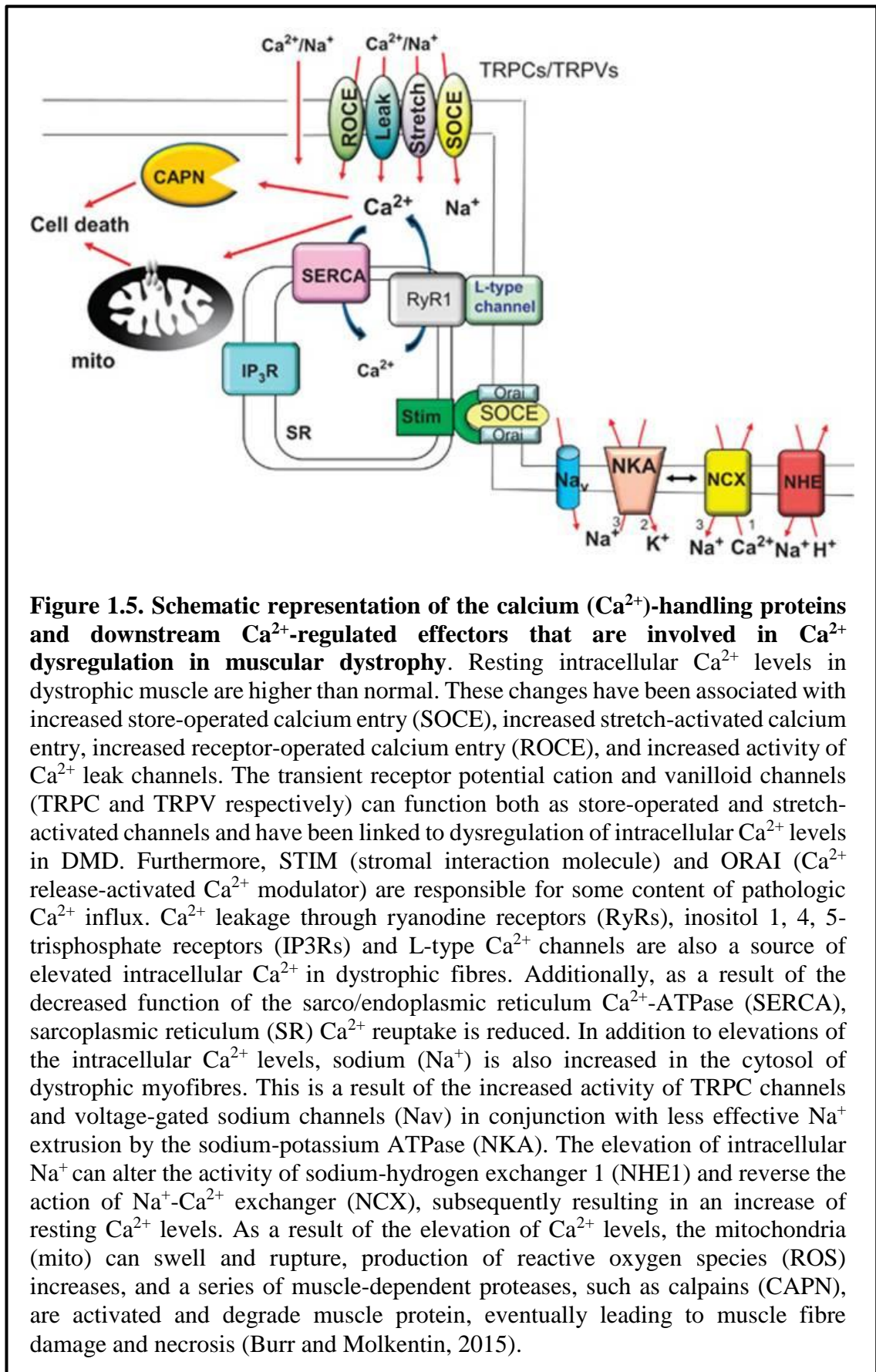
Figure 1.4. Representation of calcium (Ca^{2+}) signalling and dynamics in muscle fibres. Skeletal muscle contraction initiates when the sarcolemma is depolarised in response to release of acetylcholine from motoneurons. The sarcolemmal depolarisation travels along the T-tubules and activates the dihydropyridine receptors (DHPRs) resulting in their conformational change. Subsequently, closely apposed ryanodine receptors (RyRs; Ca^{2+} release channels localised in the sarcoplasmic reticulum (SR) membranes) are activated and release Ca^{2+} in the SR. Afterwards, Ca^{2+} diffuses throughout the sarcomere and binds to various cytosolic constituents or Ca^{2+} buffers. Binding of Ca^{2+} to troponin C triggers the contractile force of myofibrils. Relaxation is initiated as Ca^{2+} diffuses from the myofilaments to the cytosol and transferred back to the SR by the sarco/endoplasmic reticulum Ca^{2+} pump (SERCA). Furthermore, the sarcolemmal $\text{Na}^{+}/\text{Ca}^{2+}$ -exchanger (NCX) and the plasmalemmal Ca^{2+} -ATPase (PMCA) can remove cytosolic Ca^{2+} to the extracellular space. A portion of this Ca^{2+} reaches the mitochondria through the mitochondrial Ca^{2+} uniporter (MCU) and the leucine zipper and EF-hand containing transmembrane protein 1 (LTEM1), where it stimulates the production of ATP, which is required to maintain contraction. Ca^{2+} can exit the mitochondria through the mitochondrial $\text{Na}^{+}/\text{Ca}^{2+}$ -exchanger (NCLX) and the mitochondrial permeability transition pore (PTP). Low Ca^{2+} levels in the SR are detected by STIM1 (Stromal interaction molecule 1) and activate store-operated calcium entry (SOCE), an extracellular Ca^{2+} influx through the Ca^{2+} release-activated Ca^{2+} modulator 1 (ORAI1) and transient receptor potential cation channels (TRPC) to refill intracellular Ca^{2+} stores (Vallejo-Illarramendi *et al.*, 2014).

muscle protein, and increased production of reactive oxygen species (ROS) (Whitehead *et al.*, 2006). Eventually, these pathways lead to fibre damage and necrosis (Shin *et al.*, 2013).

The high influx of extracellular Ca^{2+} in dystrophic fibres has been attributed to microlesions of the damaged sarcolemma (Deconinck and Dan, 2007), Ca^{2+} leak channels (Alderton and Steinhardt, 2000), mechanosensitive Ca^{2+} channels, and store-operated Ca^{2+} entry (SOCE) channels (Mosqueira *et al.*, 2013). Figure 1.5 presents the Ca^{2+} -handling proteins and downstream Ca^{2+} -regulated effectors that are involved in Ca^{2+} dysregulation in muscular dystrophy.

TRPC channels are mechanosensitive voltage-dependent Ca^{2+} channels that are highly expressed in dystrophic fibres. TRPC channels function both as store-operated and stretch-activated channels and are therefore involved in store-operated Ca^{2+} entry (SOCE) response. SOCE is defined as an influx of intracellular Ca^{2+} in response to depletion of Ca^{2+} in the SR. A series of studies have shown that blockage of the TRPC channels in dystrophic mice reduces abnormal Ca^{2+} influx (Vallejo-Illarramendi *et al.*, 2014), whereas overexpression of TRPC3 in normal mouse skeletal muscle induces Ca^{2+} influx and the development of a phenotype that resembles dystrophin-deficient mice (Millay *et al.*, 2009). SOCE activity also disrupts Ca^{2+} homeostasis and is enhanced in dystrophic myotubes. It is induced by the action of several proteins, such as protein kinase C (PKC), phospholipase C (PLC), phospholipase A2 (iPLA2) and its derived metabolites, and by the Orai1/Stim pathway. Ca^{2+} leakage through ryanodine receptors (RyRs) and inositol 1,4,5-trisphosphate receptors (IP3Rs) is also a source of elevated intracellular Ca^{2+} in dystrophic fibres (Vallejo-Illarramendi *et al.*, 2014).

Furthermore, elevated Ca^{2+} influx in dystrophic muscle can be attributed to the sodium-calcium exchanger ($\text{Na}^+/\text{Ca}^{2+}$ exchanger, NCX) which has been found to have a reversed action in DMD myotubes (Deval *et al.*, 2002). Interestingly, recent studies have demonstrated that elevated activity of the sodium-hydrogen exchanger 1 (Na^+/H^+ exchanger 1, NHE1), an integral membrane protein that regulates Ca^{2+} levels indirectly, drives to an increase of the intracellular Na^+ concentration and a subsequent intracellular Ca^{2+} overload via reduced Ca^{2+} extrusion by the NCX (Iwata *et al.*, 2007; Koliakos *et al.*, 2008; Bkaily and Jacques, 2017). This concept is reviewed in more details in section 1.7.



1.5.3 Inflammation

A chronic inflammatory response is a major contributor to the pathology of DMD and the formation and progression of muscle lesions. Several studies have reported a high expression of proteins involved in inflammation, including cytokines (e.g. TNF- α , IL-1 β , IL-6, IL-12, IL-23), chemokines, and cell adhesion molecules (e.g. intracellular adhesion molecule-1) in dystrophin-deficient muscle (Deconinck and Dan, 2007; Shin *et al.*, 2013).

Immune cell infiltration is persistent throughout the various stages of the disease. The balance between the pro-inflammatory M1 macrophages and anti-inflammatory M2 macrophages is critical for the degeneration/ regeneration of muscle. Elevated numbers of M1 macrophages are associated with extensive tissue damage (Nigro and Piluso, 2015). Furthermore, in dystrophin-deficient muscle the resident mononuclear phagocytes cannot respond to tissue stress and thus, monocytes are recruited at the injured muscle and differentiate into mononuclear phagocytes. The newly recruited cells lyse muscle cells by producing reactive oxygen and nitrogen intermediates, including nitric oxide (NO) and superoxide, which induce aberrant inflammation and several cytokines, which activate proteolytic systems inducing muscle wasting and inhibiting muscle regeneration (Shin *et al.*, 2013; Nigro and Piluso, 2015). Additionally, neutrophils, T cells and mast cells infiltrate dystrophic muscle. CD4⁺ T cells in dystrophic muscle can produce inflammatory cytokines whereas CD8⁺ T cells can trigger muscle cell death directly. Neutrophils, however, induce muscle necrosis mainly via the production of superoxide (Shin *et al.*, 2013). It has also been reported that DMD muscle has a high concentration of mast cells. Degranulation of mast cells has been observed in the surrounding areas of damaged myofibres and it releases proteases that promote membrane lysis (Gorospe *et al.*, 1994).

1.5.4 Fibrosis

Fibrosis refers to the extensive ECM deposition and the subsequent replacement of muscle tissue with connective tissue. It is a hallmark of DMD and occurs due to chronic inflammation in dystrophin-deficient muscle. Fibrosis is progressive and deteriorates muscle force and elasticity (Nigro and Piluso, 2015).

Fibrosis is characterized by overexpression of ECM proteins, such as fibronectins, collagens, chondroitin/dermatan sulphate (e.g. biglycan and decorin), and heparan-sulphate proteoglycans (e.g. syndecan-3, perlecan, and glypican-1), by myofibroblasts (Mosqueira *et al.*, 2013). The main factors that mediate fibrotic tissue formation are: myostatin, fibrinogen, matrix metalloproteinases (MMPs), and the transforming growth

factor-beta 1 (TGF- β 1) and its interactions with the connective tissue growth factor (Zhu *et al.*, 2007; Li *et al.*, 2008; Shen *et al.*, 2008; Chen and Li, 2009; Mann *et al.*, 2011). Fibrinogen interacts with the integrin receptor Mac-1 on activated M1 macrophages and can promote inflammation. Furthermore, accumulation of fibrinogen in DMD muscle has been associated with collagen deposition but also the activation of TGF- β 1 (Vidal *et al.*, 2008). TGF- β 1 reduces the expression of matrix degradation proteases, promotes collagen synthesis, and induces growth and differentiation of fibroblasts (Ignatz and Massague, 1986; Border and Noble, 1994). Myostatin, also known as growth differentiation factor 8, is a member of the TGF- β family and it is a major regulator of muscle mass. The studies that have investigated serum myostatin concentrations in DMD patients present contradictory results (Awano *et al.*, 2008; Anaya-Segura *et al.*, 2015; Burch *et al.*, 2017). Nonetheless, the most recently published study has demonstrated that serum myostatin levels in DMD patients are lower than those found in healthy control and are dependent on disease state (Burch *et al.*, 2017). Loss of myostatin signalling results in increase of myofibre diameter and strength, and skeletal muscle mass, but also promotes progression of fibrosis by activation of fibroblasts (Bogdanovich *et al.*, 2002; Whittemore *et al.*, 2003; Malerba *et al.*, 2012; St Andre *et al.*, 2017). Moreover, myostatin activates the p38 MAPK, Smad, and AKT pathways in fibroblasts promoting ECM synthesis (Philip *et al.*, 2005; Elkina *et al.*, 2011). Additionally, MMPs play an important role in the development of fibrosis. They induce inflammation and migration of inflammatory, vascular, myogenic and fibroblastic cells to damaged tissue by degrading the ECM (Kharraz *et al.*, 2014). Furthermore, when the rate of collagen degradation by MMPs is lower than the rate of its synthesis, collagen accumulation occurs. Notably, the activity of MMPs can amplify or synergize with plasminogen activation system proteases, which activate cytokines, growth factors and angiogenic factors, and is thus crucial for ECM remodelling (Nagamine *et al.*, 2005; Chen and Li, 2009; Mann *et al.*, 2011).

1.5.5 Oxidative Stress

Oxidative stress, defined as a disturbance in the balance between the production of ROS (free radicals) and antioxidant defences (Betteridge, 2000), has been associated with muscle weakness and wasting in DMD. Several mechanisms are implicated in the excessive oxidative stress production, including infiltrating neutrophils and macrophages, mitochondria, sarcolemmal ROS-generating NAD(P)H oxidase complex (Nox2), the absence of the neuronal isoform of NOS (nNOS) and the overproduction of NO by the inducible isoform of NOS (iNOS) (Mosqueira *et al.*, 2013; Shin *et al.*, 2013).

Excessive oxidative stress results in the production of primary oxidative species, such as hydrogen peroxide (H₂O₂), superoxide anion (O₂⁻) and NO, which are then converted into secondary ROS and reactive nitrogen species (RNS). High levels of ROS and RNS can damage regulatory and structural proteins, membrane lipids and DNA (Kar and Pearson, 1979; Hauser *et al.*, 1995; Haycock *et al.*, 1996; Terrill *et al.*, 2013). Furthermore, oxidative stress is responsible for the activation of NF-κB, a transcription factor that induces muscle wasting through three major pathways: 1) augmentation of the expression of proteins implicated in the ubiquitin-proteasome system, for example the E3 ubiquitin ligase MuRF1, which promotes skeletal muscle loss, 2) increase of the expression of chemokines, cytokines, matrix-degrading proteins, and cell adhesion molecules, which stimulate inflammation, and 3) blocking of the myofibre regeneration in response to injury (Whitehead *et al.*, 2006; Shin *et al.*, 2013).

1.6 Therapeutic approaches in DMD

Muscle, the target tissue of DMD therapies, constitutes 30–40% of body mass. With over 700 muscles in the human body and DMD affecting most of them, developing an effective treatment for DMD is particularly challenging.

Treatment strategies that have been developed for DMD fall into two main categories, 1) employment of approaches for the restoration of the primary structural defect, and 2) mitigation of secondary downstream pathological mechanisms, including Ca²⁺ dysregulation, oxidative stress, inflammation, fibrosis and mitochondrial dysfunction (Guiraud and Davies, 2017). Although no effective treatment for DMD exists to date, recent advances of the management of cardiac, respiratory, psychosocial, neuromuscular, orthopaedic, nutritional, gastrointestinal, swallowing, and speech complications have improved DMD patients' quality of life and extended their life expectancy to the fourth decade (Birnkrant *et al.*, 2018a; Birnkrant *et al.*, 2018b; Birnkrant *et al.*, 2018c).

The most promising pharmacological approaches aiming to address the pathogenesis of DMD are briefly explained below.

1.6.1 Current pharmacological management

Corticosteroids, e.g. deflazacort and prednisone/prednisolone, are the current standard of care in DMD and although their exact mechanism of action is unknown, they are thought to primarily reduce inflammation. Corticosteroids have been proven to markedly improve strength and function, reduce the risk of scoliosis, delay loss of ambulation, and stabilise

pulmonary and cardiac function. Despite the benefit they confer for patients with DMD, long-term treatment with corticosteroids has serious side effects, such as impairment of glucose metabolism, excessive weight gain, behavioural changes, immunosuppression, hypertension, development of cataracts and delayed puberty. Furthermore, corticosteroids can aggravate the low bone mineral content and amplify the risk for vertebral fractures and development of osteoporosis (Bushby *et al.*, 2010; Goemans and Buyse, 2014; Reinig *et al.*, 2017).

For the treatment of cardiac manifestations, including DCM and arrhythmias, angiotensin-converting enzyme (ACE) inhibitors, β -blockers, and diuretics are administered (Goemans and Buyse, 2014; Birnkrant *et al.*, 2018a).

1.6.2 Therapeutic approaches targeting primary pathology in DMD

1.6.2.1 Viral gene therapy

Gene therapy techniques employ viral or non-viral vectors in order to transduce a functional copy of *DMD* into muscles or to repair the mutated locus. Notably, gene therapy presents some limitations, such as the large size of the *DMD* gene (Harper *et al.*, 2002), the need to restore the dystrophin in all different muscle types, the need to transduce both post-mitotic and actively dividing cells, the high risk of immunogenicity and long-term resistance (Rodino-Klapac *et al.*, 2007; Guglieri and Bushby, 2010; Fairclough *et al.*, 2013).

Different types of vectors have been constructed over the last few years in order to carry full-length dystrophin, mini-dystrophin, micro-dystrophin or full-length utrophin genes (Goyenvalle *et al.*, 2011; Leung and Wagner, 2013; Le Guiner *et al.*, 2017). Adeno-associated virus (AAV) vectors are currently the preferred viral vectors. They have small capacity (~5 kb) (Carter, 2004) and can, therefore, transfer only mini- or micro-genes (Crawford *et al.*, 2000), but present lower immunogenicity than other vectors. Local or systemic delivery of mini-dystrophin using AAVs has been successful in cardiac and skeletal muscles of DMD animal models and has been demonstrated to ameliorate muscle disease (Wang *et al.*, 2000; Harper *et al.*, 2002; Liu *et al.*, 2005; Gregorevic *et al.*, 2006; Wang *et al.*, 2009a; Hakim *et al.*, 2017).

Several clinical trials aiming to test the efficacy of gene delivery in DMD are currently ongoing. Those include: NCT03375164, which aims to test the efficacy of systemic delivery of rAAVrh74.MHCK7.micro-dystrophin to DMD patients, NCT03368742,

which aims to test the safety, efficacy and tolerability of SGT-001 micro-dystrophin gene therapy, NCT03362502, which aims to test the safety and tolerability of a single intravenous infusion of PF-06939926 mini-dystrophin in ambulatory patients, and NCT03333590, which aims to test the safety and efficacy of intravenous rAAVrh74.MCK.GALGT2 in DMD patients.

1.6.2.2 Exon-skipping agents

Exon-skipping was first proposed as a therapeutic strategy in the mid-nineties. It aims to restore the reading frame of out-of-frame *DMD* transcripts by employing RNaseH-resistant antisense oligonucleotides (AONs). AONs hybridize to complementary sequences in or close to the target exon in precursor mRNA (pre-mRNA) molecules, modulating splicing. This technique results in the expression of functional short forms of dystrophin which are assumed to be associated with a better clinical outcome than the absolute absence of dystrophin (Goyenvalle *et al.*, 2011; Fairclough *et al.*, 2013).

AONs target specific exons in an attempt to help the greatest number of patients. According to the TREAT-NMD DMD Global Database (Bladen *et al.*, 2015), ~14% of *DMD* mutations are amenable to skipping exon 51. Eteplirsen (EXONDYS 51™ Sarepta Therapeutics), a phosphorodiamidate morpholino oligomer (PMO) designed to skip *DMD* exon 51 in patients with DMD, was granted Orphan Drug Designation, Fast Track status, and Priority Review status and is the first FDA-approved medication for DMD. It is well tolerated by DMD patients and slows the progression of the disease in a dose-dependent manner (Kinali *et al.*, 2009; Cirak *et al.*, 2011; Mendell *et al.*, 2013; Mendell *et al.*, 2016). Eteplirsen is currently under evaluation by a number of ongoing trials (ClinicalTrials.gov identifiers NCT01540409, NCT02255552, NCT02286947, and NCT02420379), which will inform the FDA's decision to grant its approval. In addition to exon 51, other exon skips are possible; 8% of *DMD* mutations are amenable to skipping exon 53, 9% to skipping exon 45, 7% to exon 44, and 7% to exon 43 (Bladen *et al.*, 2015). Clinical trials with compounds that skip exons 45 and 53 are currently ongoing (ClinicalTrials.gov identifiers NCT02081625, NCT02310906, NCT02500381, NCT02530905, and NCT02740972) and it is likely that one or more may be commercially available in the coming years (Reinig *et al.*, 2017).

1.6.2.3 Read-through agents

Approximately 11% of DMD patients carry premature stop-codon mutations (Bladen *et al.*, 2015) and could therefore be treated with drugs that promote read-through of premature termination mutations, for example aminoglycoside antibiotics (e.g. gentamicin), and Translarna (formerly ataluren, PTC124/PTC Therapeutics). *In vivo* and *in vitro* studies of gentamicin and Translarna demonstrated that they can induce the production of full-length dystrophin that localizes correctly to the plasma membrane (Finkel *et al.*, 2013). In July 2014, after a Phase 2b clinical trial demonstrating improvement in the six minute walk test (6MWT) and a slower disease progression, Translarna was given orphan drug designation and conditional EMA approval (Bushby *et al.*, 2014; Ryan, 2014). Furthermore, although a Phase 3 clinical trial in 228 ambulatory DMD patients demonstrated no significant benefit in the 6MWT, the primary endpoint was met in the pre-specified subgroup. For this reason, the EMA prolonged conditional approval. (Guiraud and Davies, 2017).

1.6.2.4 Utrophin upregulation

Utrophin is an orthologue of dystrophin protein expressed abundantly during muscle development. Its expression at the sarcolemma is later replaced by dystrophin and is restricted to the neuromuscular and myotendinous junctions (Ohlendieck *et al.*, 1991; Gramolini and Jasmin, 1997). The two proteins, utrophin and dystrophin, share many of the same binding partners and as such upregulation of utrophin is considered a promising therapeutic strategy. The expression of utrophin in dystrophin-deficient muscle is upregulated, but its levels are not sufficient to compensate for the dystrophin loss and prevent the disease development (Cossu and Sampaolesi, 2007; Goyenville *et al.*, 2011).

Elevated utrophin expression can be induced by transcriptional upregulation (Tinsley *et al.*, 2011), direct delivery of the protein (Sonnemann *et al.*, 2009), or stabilization of the protein or RNA (Chakkalakal *et al.*, 2008; Moorwood *et al.*, 2013). Utrophin upregulation presents several advantages; it could be effective in all DMD patients despite their specific gene defect, and could be administered systemically because utrophin overexpression is not detrimental even in tissues other than muscle (Goyenville *et al.*, 2011).

A series of small compounds have been evaluated in pre-clinical studies for the upregulation of utrophin, including heregulin (Krag *et al.*, 2004), L-arginine (Voisin and de la Porte, 2005), nabumetone (Moorwood *et al.*, 2011), a peroxisome proliferator-

activated receptor agonist (GW501516) (Miura *et al.*, 2009), RhoA (Gauthier-Rouviere and Bonet-Kerrache, 2009), trans-activator of transcription (TAT)-utrophin (Sonnemann *et al.*, 2009) and recombinant biglycan (rhBGN) (Amenta *et al.*, 2011). It has been demonstrated that each of these compounds can improve dystrophic pathology in mice to varying degrees. Moreover, ezutromid (formally known as SMT C1100), a small molecule that acts through the promoter to induce utrophin upregulation, is a particularly promising compound. After it was shown to be well tolerated in Phase 1a and 1b clinical trials carried out by Summit Therapeutics, ezutromid has entered Phase 2 studies and has been granted Fast Track designation by the FDA (Guiraud *et al.*, 2015; Ricotti *et al.*, 2016; Johnstone *et al.*, 2017).

1.6.2.5 Cell therapy

Cell therapy is based on the idea that transplantation of muscle precursor cells with stem cell-like properties may have the ability to give rise to dystrophin-expressing myofibres in dystrophic muscle to ameliorate DMD pathology (Sienkiewicz *et al.*, 2015). Transplantation of myoblasts was tested in clinical trials in the early 1990s but demonstrated no functional benefit in the injected muscles due to poor survival of injected myoblasts, the inability of the myoblasts to migrate, but also due to an immune response against the donor myoblasts (Partridge *et al.*, 1989; Morgan *et al.*, 1990; Morgan *et al.*, 1996; Mouly *et al.*, 2005). However, the use of adult-derived stem cells, such as bone marrow-derived stem cells, muscle-derived stem cells, blood- and muscle-derived CD133⁺ cells, mesoangioblasts, side population (SP) cells, embryonic stem (ES) cells, induced pluripotent stem (iPS) cells, embryonic- and postnatal-derived fibroblasts, and Sertoli cells (Sec) opened up new possibilities for cell therapy (Cossu and Sampaolesi, 2007; Muir and Chamberlain, 2009; Sienkiewicz *et al.*, 2015; Chiappalupi *et al.*, 2017; Johnstone *et al.*, 2017).

Clinical trials using transplanted cells, e.g. autologous bone marrow mononuclear transplantation and myoblast transplantation, have yielded some promising results (Hogrel *et al.*, 2013; Sharma *et al.*, 2013; Perie *et al.*, 2014; Sharma *et al.*, 2014). Insufficient numbers and distribution of transplanted cells have, however, been a problem (Skuk *et al.*, 2007) and ongoing trials are looking to optimise transplant procedures (Cossu *et al.*, 2015; Johnstone *et al.*, 2017).

The use of allogeneic cardiosphere-derived cells (CDCs), or CAP-1002, has also been proposed as a potential therapeutic strategy for DMD. Preclinical investigations have

shown that CDCs can be effective in decreasing myocardial fibrosis, improving cardiac function, inducing cardiomyogenesis, and improving exercise capacity in DMD mouse models. Capricor is currently investigating the efficacy and tolerability of CAP-1002 in DMD patients in a Phase II clinical trial (NCT03406780).

1.6.3 Therapeutic approaches targeting secondary pathology in DMD

Development and approval of genetic approaches to treat DMD will take time and even when approved may only be suitable for a select patient population and/or able to alleviate pathology, but not relieve them completely. Consequently, therapies that either independently or in combination with other treatment strategies improve disease pathology are needed (Hollinger and Selsby, 2013). A series of pharmacological approaches that target secondary pathology downstream of dystrophin deficiency, such as Ca^{2+} dysregulation, mitochondrial dysfunction, oxidative stress, fibrosis, inflammation, muscle wasting and muscle ischaemia have been developed (Guiraud and Davies, 2017).

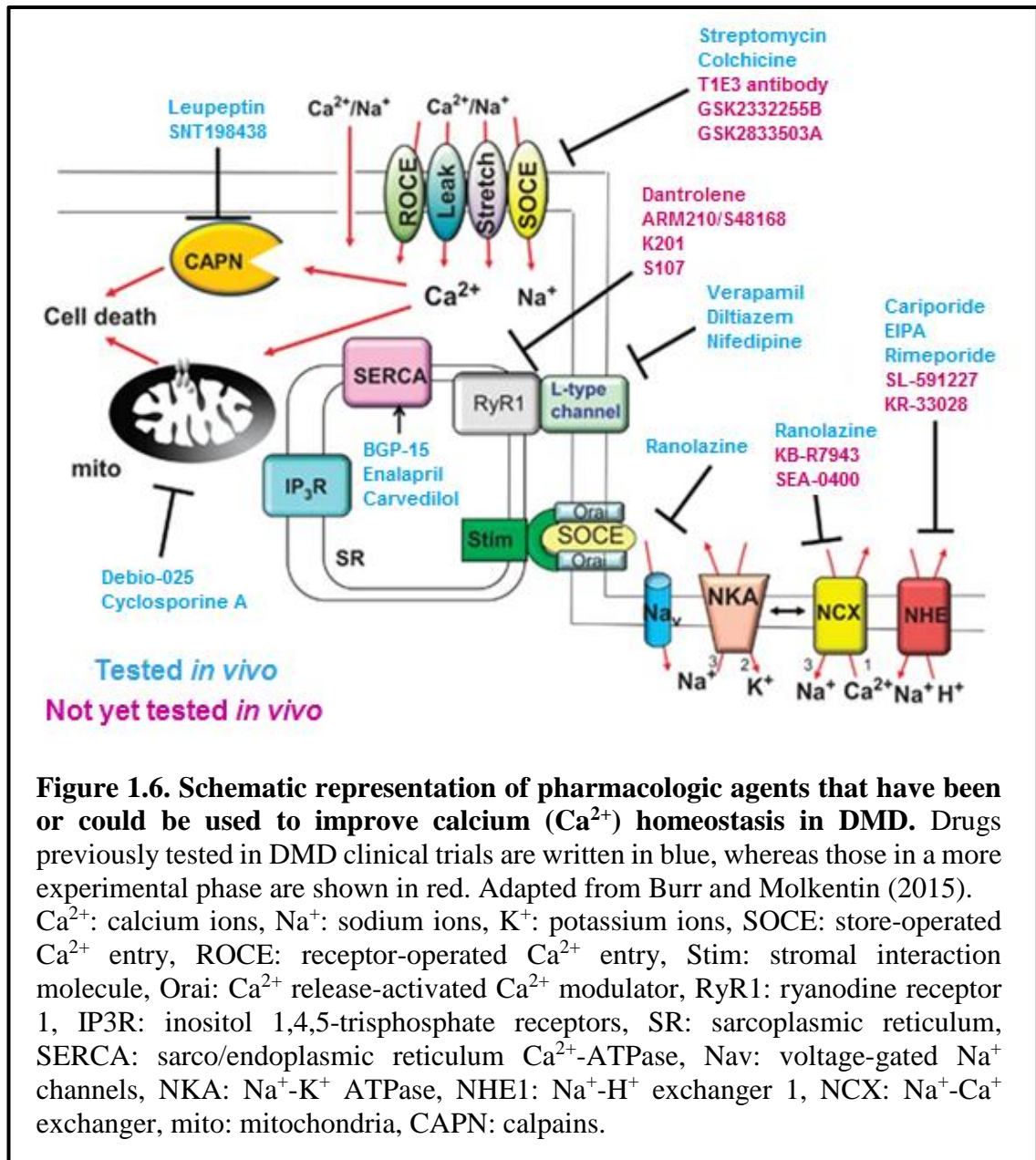
Below, therapies that target Ca^{2+} dysregulation are briefly outlined. Detailing the therapeutic strategies that target other secondary pathological characteristics is beyond the scope of this thesis; for an up-to-date detailed review of those therapies refer to: Guiraud and Davies (2017), Johnstone *et al.* (2017) and Reinig *et al.* (2017).

1.6.3.1 Therapeutic strategies targeting Ca^{2+} dysregulation

The elevation of intracellular Ca^{2+} levels observed in DMD muscle (Oberc and Engel, 1977; Duncan, 1978) can be attributed to the mechanical damage of the sarcolemma but also deficiencies in several Ca^{2+} -regulatory proteins, including Ca^{2+} leak channels, mechanosensitive Ca^{2+} channels, and store-operated Ca^{2+} entry (SOCE) channels (Vallejo-Illarramendi *et al.*, 2014; Burr and Molkentin, 2015). Therefore, Ca^{2+} homeostasis can be corrected at multiple levels including at the level of the sarcoplasmic reticulum (SR), the plasma membrane, and the mitochondria.

Over the years, several pharmacological and molecular therapies that target Ca^{2+} dysregulation have been proposed as potential treatments for DMD (Figure 1.6). A series of studies in animal models have demonstrated beneficial effects of RyR stabilisers, for example K201, S107, dantrolene and ARM210/S48168, in muscular dystrophy and heart failure (Bellinger *et al.*, 2009; Mackrill, 2010; Kendall *et al.*, 2012; Mei *et al.*, 2013; Capogrosso *et al.*, 2014). Additionally, several L-type Ca^{2+} channel inhibitors, such as verapamil, nifedipine, and diltiazem, have been shown to improve muscle structure and

function in dystrophic mice (Matsumura *et al.*, 2009; Altamirano *et al.*, 2013), but have failed to prove significant beneficial effects in DMD patients in clinical trials (Phillips and Quinlivan, 2008). Similarly, blocking the stretch-activated channels (i.e. TRPC, TRPV2) has also shown a beneficial effect in several dystrophic animal models (Yeung *et al.*, 2005; Iwata *et al.*, 2009).



The reduced SERCA activity is a contributing factor to Ca²⁺ dysregulation in DMD. Therefore, compounds that can increase the expression and/or function of SERCA2, including a number of angiotensin II-receptor blockers, β-blockers and angiotensin-converting-enzyme inhibitors, are also potential enhancers of Ca²⁺ homeostasis (Morine *et al.*, 2010; Shareef *et al.*, 2014). Notably, AAV-mediated gene therapy approaches have also been shown to have beneficial effects on several dystrophic models by increasing the

expression of SERCA1 and SERCA2 in skeletal muscle. SERCA2 viral vectors are now in phase II/III trials for human heart failure (Jaski *et al.*, 2009; Goonasekera *et al.*, 2011; Greenberg, 2015).

Furthermore, it has been demonstrated that therapeutic compounds targeting mitochondrial dysfunction can improve muscle function in different dystrophic mouse models. These include the use of cyclosporine A and cyclophilin D inhibitors (Debio 025) for impaired mitochondrial PTP opening, pargyline for excessive accumulation of ROS, overexpression of peroxisome proliferator-activated receptor γ coactivator 1-gene α (*PGC1 α*) for mitochondrial dysfunction in post-necrotic dystrophic muscles, and idebenone for improvement of mitochondrial respiratory function (Millay *et al.*, 2008; Katsetos *et al.*, 2013; Vallejo-Illarramendi *et al.*, 2014).

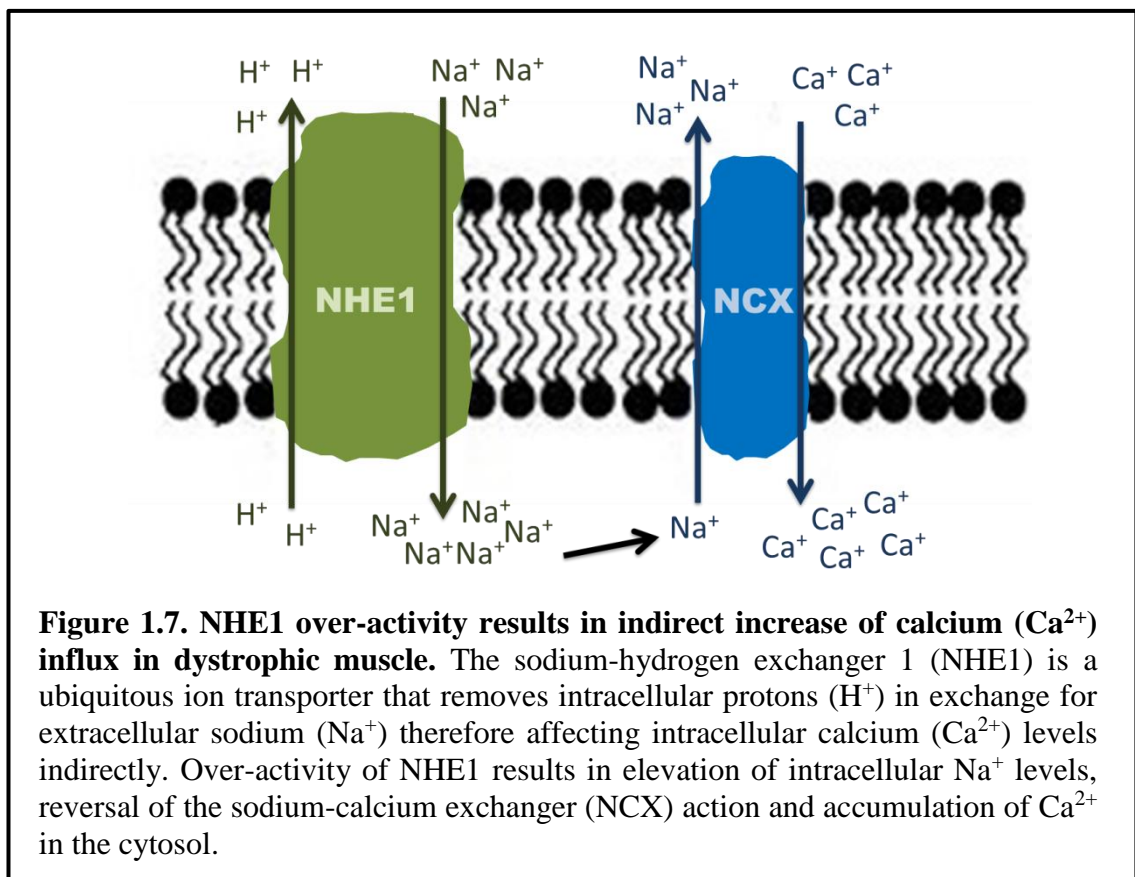
As mentioned above (section 1.5.2), the activity of NHE1 and NCX also contributes to the elevation of intracellular Ca^{2+} levels in dystrophic muscle cells (Iwata *et al.*, 2007; Burr *et al.*, 2014; Bkaily and Jacques, 2017). Inhibition of the reverse mode of NCX using compounds such as ranolazine, KB-R7943 and SEA040015 can stimulate myogenesis and reduce oxidative stress in muscle cells (Matsuda *et al.*, 2001; Egar *et al.*, 2014; Ileana *et al.*, 2016). Moreover, NHE1 has been recently proposed as a novel therapeutic target for DMD. Use of NHE1 inhibitors such as cariporide, 5-(N-ethyl-N-isopropyl)-amiloride (EIPA), and rimeporide has been shown to attenuate muscle degeneration in dystrophic mouse models (Iwata *et al.*, 2007; Bkaily and Jacques, 2017). Rimeporide prevents both inflammation and the accumulation of fibrosis in skeletal muscles, the diaphragm and heart of dystrophic mice, and is currently in Phase II/III clinical trial for DMD patients (Porte Thomé *et al.*, 2016; Gidaro *et al.*, 2017).

1.7 Sodium-hydrogen exchanger (NHE) and DMD

The NHE exchangers are ubiquitous ion transporters that remove intracellular protons (H^+) in exchange for extracellular Na^+ , therefore affecting intracellular Ca^{2+} levels indirectly. To date, thirteen NHE isoforms have been identified and have been shown to be implicated in numerous physiological processes (Fuster and Alexander, 2014).

The NHE1 was the first NHE isoform that was identified (Pouyssegur *et al.*, 1982; Sardet *et al.*, 1989). It is a major regulator of a series of physiological functions, including intracellular pH homeostasis and cell volume. It functions as a membrane anchor for the actin-based cytoskeleton and regulates a number of cell behaviours, such as adhesion,

migration, proliferation and shape determination (Putney *et al.*, 2002; Malo and Fliegel, 2006). Consequently, NHE1 is highly regulated at the transcriptional level allowing the amount of mRNA and protein that are produced to be controlled, but also at the post-transcriptional level through phosphorylation by various kinases and interactions with other cellular proteins (Slepkov *et al.*, 2007). Under normal physiological conditions, NHE1 is relatively inactive but is rapidly activated as the intracellular pH decreases (intracellular acidosis). Furthermore, NHE1 can also be activated in response to extracellular stimuli such as growth factors, hormones and mechanical stressors (Iwata *et al.*, 2007; Wakabayashi *et al.*, 2013).



Dysfunction of NHE1 has been linked to disease. The loss of NHE1 impacts on the expression and activity of other membrane transport proteins in the brain, resulting in increased neuronal excitability (Fuster and Alexander, 2014). Conversely, the elevation of the NHE1 activity is detrimental for cardiac and neural tissues during episodes of ischaemia-reperfusion. In these pathological conditions, the NHE1 over-activity causes substantial intracellular Na⁺ accumulation, which in return activates the plasmalemmal Na⁺/Ca²⁺ exchanger (NCX) inducing a deleterious increase of intracellular Ca²⁺ that triggers various pathways ultimately leading to cell death (Karmazyn, 2013; Fuster and Alexander, 2014). Additionally, NHE1 plays a pivotal role in tumorigenesis since it is

involved in cell proliferation, cell migration, invasion, metastasis, and suppression of apoptosis (Malo and Fliegel, 2006; Fuster and Alexander, 2014; Amith *et al.*, 2016).

The upregulation of NHE1 has also been implicated in muscular dystrophy. Similarly to ischaemia-reperfusion, intracellular acidosis causes NHE1 over-activity, which in turn can result in elevation of intracellular Na⁺ levels, reversal of NCX action and accumulation of Ca²⁺ (Figure 1.7) (Deval *et al.*, 2002; Iwata *et al.*, 2007; Koliakos *et al.*, 2008; Bkaily and Jacques, 2017; Gidaro *et al.*, 2017).

1.7.1 NHE1 inhibition as a potential therapy in DMD

Several NHE1 inhibitors have been developed with the aim to attenuate the harmful consequences of excessive NHE activation. NHE1 inhibitors, in their cation form, can inhibit NHE1 by binding competitively to the NHE1 extracellular Na⁺ binding site (Jin *et al.*, 2011). They can be classed into two categories based on their chemical structure: 1) the diuretic compound amiloride and its analogues, for example 5-(N, N-hexamethylene)-amiloride (HMA), 5-(N-ethyl-N-isopropyl)-amiloride (EIPA), N-methyl-isobutyl-amiloride (MIA) and pyrazinoyl guanidines, and 2) the novel benzoylguanidine derivatives including cariporide, rimeporide, zoniporide and KR-33028 (Kim *et al.*, 2007a; Mao *et al.*, 2009; Park *et al.*, 2009; Xu *et al.*, 2009; Mihaila, 2015).

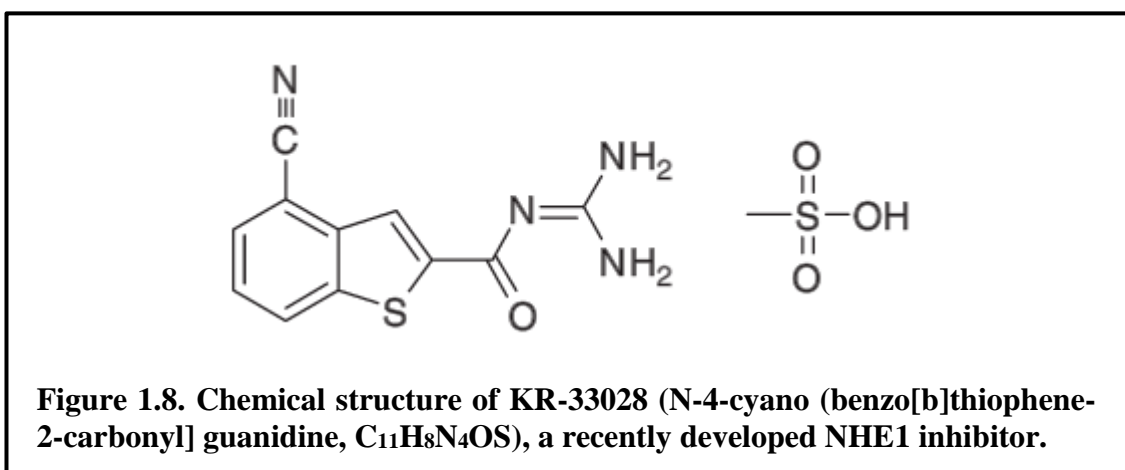
Although NHE1 inhibitors were initially developed as potential therapeutic agents for cardioprotection in ischaemic heart disease, a series of studies have now exploited the inhibition of NHE1 for the treatment of other diseases, including DMD (Masereel, 2003; Baartscheer *et al.*, 2005; Mihaila, 2015; Gidaro *et al.*, 2017). NHE1 inhibition through the use of specific NHE1 inhibitors could result in reversal of the NCX in dystrophic muscle and subsequent decrease of intracellular Ca²⁺ levels, therefore addressing the Ca²⁺ pathology issue in DMD. A recent study by Iwata *et al.* (2007) has demonstrated that NHE1 inhibitors can decrease intracellular Ca²⁺ levels in DMD animal models. Chronic administration of cariporide in both *mdx* mice and BIO-14.6 hamsters, animal models of DMD and delta sarcoglycan-deficient muscular dystrophy (LGMD2F) respectively, prevented abnormal Ca²⁺ uptake and improved several histological, biochemical and functional parameters. The two studies by Bkaily *et al.* (2015) and Bkaily and Jacques (2017) also proposed that inhibition of NHE1 may improve the cardiomyopathy present in DMD patients. Additionally, rimeporide has been shown to address skeletal muscle inflammation, fibrosis and cardiomyopathy in cardiomyopathic mice (CMH) and *mdx* mice. In 2015, rimeporide was granted a European medicines agency (EMA) orphan drug

designation (ODD) and is currently in a Phase IB clinical trial for DMD patients (Porte Thomé *et al.*, 2016; Gidaro *et al.*, 2017). These results suggest that NHE1 inhibition may have a profound impact on the disease course in a broad population of patients, regardless of their mutational status, and could be an ideal complement to treatments designed to replace or augment dystrophin.

1.7.1.1 KR-33028, a small-molecule NHE1 inhibitor

KR-33028 (N-4-cyano (benzo[b]thiophene-2-carbonyl] guanidine, C₁₁H₈N₄OS) is an NHE1 inhibitor recently developed by the Korea Research Institute of Chemical Technology (KRICT), the structure of which is shown in Figure 1.8. A series of pre-clinical studies have already demonstrated that this compound has a good safety and potency profile (Kim *et al.*, 2005; Jung *et al.*, 2006; Kim *et al.*, 2006; Kim *et al.*, 2007a; Kim *et al.*, 2007b; Kim *et al.*, 2007c; Oh *et al.*, 2007; Lee *et al.*, 2009; Amith *et al.*, 2016).

KR-33028 presents cardioprotective effects and can reduce myocardial infarction due to ischaemia-reperfusion injury in rats and dogs (Kim *et al.*, 2006; Oh *et al.*, 2007). Similarly, Lee *et al.* (2009) have demonstrated that KR-33028 is protective against cell death due to glutamate toxicity in cultured neuronal cells and can significantly reduce the size of cerebral infarcts due to ischaemic injury in rats. KR-33028 has also been evaluated for its potential chemotherapeutic effects and was shown to suppress metastatic potential of triple-negative breast cancer cells (Amith *et al.*, 2016).



No data has been published, to date, to support the efficacy of KR-33028 in treating DMD. However, a pilot study conducted prior the initiation of this project investigated the effects of oral KR-33028 treatment in *mdx* mice (Burki *et al.*, 2014). During the pilot study, a total of 6 *mdx* mice were treated with a single dose of KR-33028 for 6 weeks. A significantly reduced Ca²⁺ uptake was observed in both forelimb and chest-wall muscles,

using manganese-enhanced MRI (MEMRI) (Figure 1.9.A; B), but not in the myocardium. Additionally, the functional grip strength of the treated mice was increased but did not reach statistical significance (Figure 1.9.C). The results were nevertheless encouraging and indicate the potential of NHE1 inhibition using KR-33028 for the treatment of DMD.

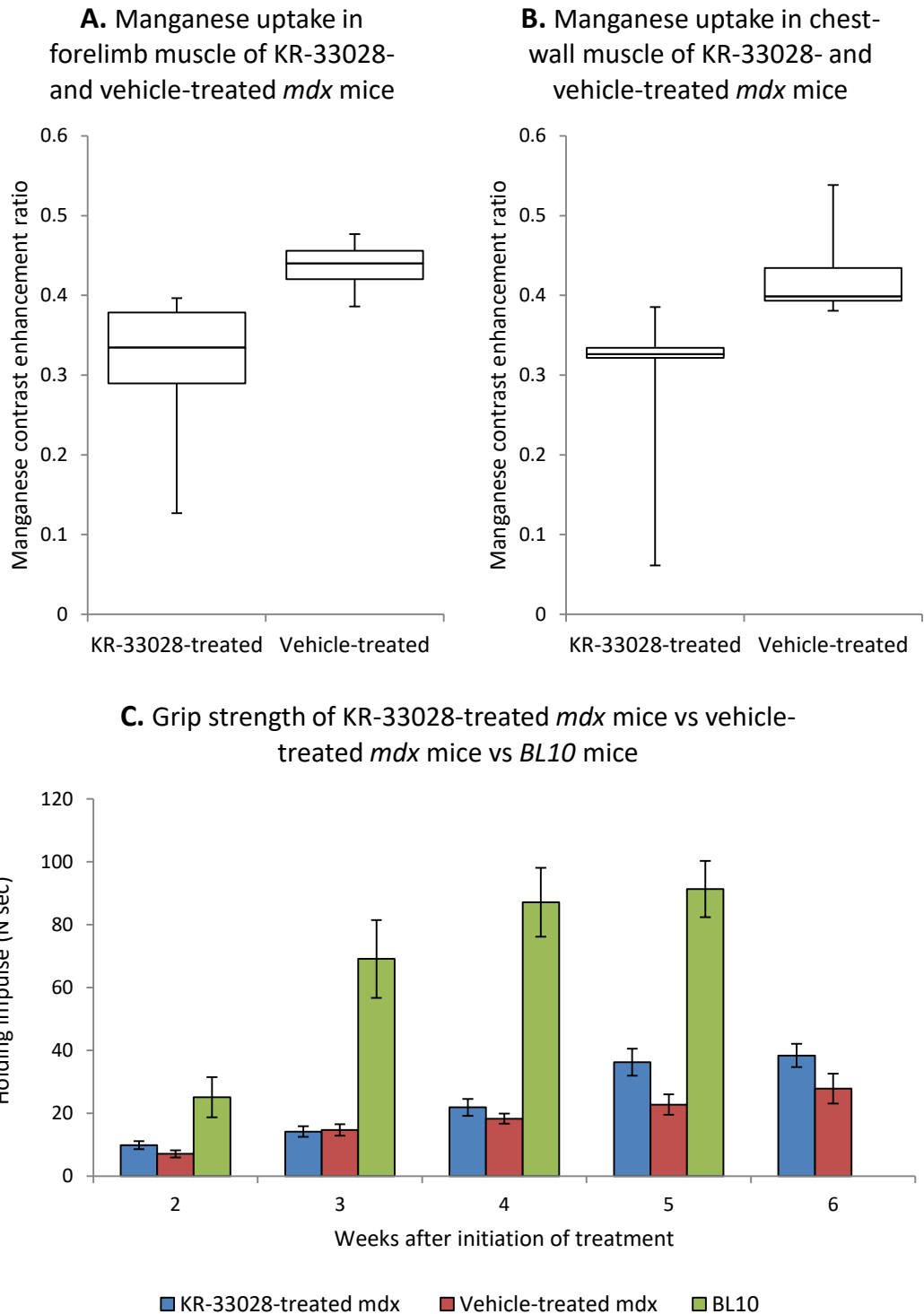


Figure 1.9. Effects of oral administration of KR-33028 to *mdx* mice for 6 weeks. A total of six 17-week-old *mdx* mice were treated with 20 mg/kg of KR-33028 for 6 weeks through oral gavage. Manganese-enhanced magnetic resonance imaging (MEMRI) demonstrated a significant decrease of calcium (Ca^{2+}) uptake in both forelimb (A.) and chest-wall (B.) muscles of KR-33028-treated mice, when compared to that of vehicle-treated *mdx* mice. Additionally, the functional grip strength of treated mice was increased, but did not reach statistical significance (C.); green bars show the grip strength of control (C57BL/10) mice, blue bars the grip strength of KR-33028-treated *mdx* mice, and red bars the grip strength of vehicle-treated *mdx* mice. Error bars show standard error of the mean (SEM).

1.8 Statement of aims

This thesis introduces the inhibition of NHE1 by using the KR-33028 compound as a way to improve DMD pathology. Several non-DMD-related pre-clinical studies have already been conducted and have demonstrated that this compound has a good safety and potency profile (Kim *et al.*, 2005; Jung *et al.*, 2006; Kim *et al.*, 2006; Kim *et al.*, 2007a; Kim *et al.*, 2007b; Kim *et al.*, 2007c; Oh *et al.*, 2007; Lee *et al.*, 2009). However, the efficacy of the compound to treat muscular dystrophy has not yet been assessed.

The aims of the results chapters were as follows:

- To collect pharmacokinetic (PK) and stability data for KR-33028.
- To determine the effects of the KR-33028 on the DMD pathology after chronic *in vivo* treatment of *mdx* mice with the compound.
- To employ the use of magnetic resonance imaging (MRI) techniques to assess the Ca²⁺ dynamics and cardiomyopathy in KR-33028-treated *mdx* mice.
- To investigate the effects of KR-33028 treatment on individual protein levels.

Chapter 2. Materials and methods

2.1 List of reagents

Product	Manufacturer	Associated assay(s)
Acetic acid, glacial	Sigma Aldrich	Masson's Trichrome
Acetone	VWR	Histology
Acrylamide/bis (30%)	Bio-Rad Laboratories	Western Blotting
Bicinchoninic Acid (BCA)	Sigma Aldrich	Protein Quantification
Bouin's solution	Sigma Aldrich	Histology
Bovine serum albumin (BSA)	Sigma Aldrich	Protein Quantification
Collagen from calf skin	Sigma Aldrich	Tissue Culture
Collagenase type II	Gibco	Single muscle fibre Isolation
cOmplete EDTA-free Protease Inhibitor Tablets	Roche Applied Science	Protein Extraction
Coomassie Brilliant Blue G250	Sigma Aldrich	Western blotting
Copper (II) sulphate	Sigma Aldrich	Protein Quantification
Creatine kinase assay kit	Abcam	Creatine kinase assay
DPX Mounting Medium	National Diagnostics	Histology
Dulbecco's modified Eagle medium (DMEM)	Gibco	Cell culture
Eosin	VWR	H&E staining
Foetal Bovine Serum (FBS)	SLI	Cell culture
Gentamicin	Life Technologies	Cell culture
GlutaMAX™ Supplement	Fisher Scientific	Cell culture
Glycine	Sigma Aldrich	Western Blotting
Haematoxylin Harris	VWR	H&E staining
Histoclear	National Diagnostics	Histology
Horse Serum (HS)	Gibco	Cell culture
Hydrochloric Acid	Thermo Scientific	pH acid
Isopropanol	VWR	Tissue harvesting

KR-33028, NHE1 inhibitor	Korea Research Institute of Chemical Technology (KRICT)	Many
Laemmli sample buffer	Bio-Rad	Western Blotting
Magnesium chloride (MgCl ₂)	Sigma Aldrich	MEMRI
Masson's Trichrome Kit	Sigma Aldrich	Masson's Trichrome
Milk, dried skimmed	TESCO/Sainsbury's/Morrisons	Western Blotting
Mounting medium with DAPI	Vectorlabs	Staining
OCT embedding matrix	Pyramid innovations	Cryosectioning
Penicillin/Streptomycin	Gibco	Cell culture
Phosphate buffered saline solution	Gibco	Cell culture
Protein ladder, PageRuler™ Plus	Thermo Scientific	Western Blotting
RIPA buffer	Thermo	Western Blotting
Skeletal Muscle Cell Growth Medium	Promocell	Cell culture
Sodium Dodecyl Sulphate (SDS)	Sigma Aldrich	Western Blotting
Sodium Hydroxide	Sigma	pH base
Supplement Mix	Promocell	Cell culture
Tris Base	Sigma Aldrich	Buffer constituent
Tris HCL	Sigma Aldrich	Buffer constituent
Trypsin EDTA (0.05%)	Gibco	Tissue culture
Tween® 20	Sigma Aldrich	Buffer constituent
Weigert's iron haematoxylin kit	Sigma Aldrich	Masson's Trichrome
Xylene	Sigma Aldrich	Histology

Table 2.1. List of reagents used in this project.

2.2 List of solutions

Buffer/Solution	Composition
10% APS	10 g ammonium persulfate (APS), 100ml dH ₂ O, stored at -20 °C
Blocking milk solution	15 g instant dried skimmed milk powder, 1.75 g NaCl, 3 ml Tris 1M pH 7.6, 300 µl Tween® 20, make up to 300 ml with dH ₂ O, stored at 4 °C

BSA-wash buffer	1.5 ml Tris 1M pH 7.6, 75 ml NaCl 2M, 2.5g Bovine serum albumin (BSA), 2ml NP-40, make up to 1L with dH ₂ O
Coomassie staining solution	1 g/L Coomassie brilliant blue G250, 400 ml ethanol, 500 ml dH ₂ O, 100 ml acetic acid
De-staining buffer 1	477.5 ml dH ₂ O, 100 ml acetic acid, 400 ml ethanol, 22.5 ml glycerin
De-staining buffer 2	827.5 ml dH ₂ O, 50 ml acetic acid, 100 ml ethanol, 22.5 ml glycerin
Human myoblast differentiation medium	490 ml Dulbecco's modified Eagle's medium (DMEM), 10 ml horse serum (HS), stored at 4 °C
Human myoblast growth medium	500 ml skeletal muscle cell growth medium, 25 ml supplement mix 50 ml foetal bovine serum (FBS), 300 µl gentamycin (50 mg/ml), 7.5 ml glutamax, stored at 4 °C
Protein lysis buffer	10 ml RIPA buffer, 1 cOmplete EDTA-free protease inhibitor tablet
SDS-PAGE gels lower buffer	181.72 g Tris base, 4 g SDS, adjust pH to 8.8, make up to 1L with dH ₂ O
SDS-PAGE gels upper buffer	30.28 g Tris base, 2 g SDS, adjust pH to 6.8, make up to 500 ml with dH ₂ O
Western blotting 10x SDS running buffer	30.3 g Tris Base, 144 g glycine, 10 g SDS, make up to 1L with dH ₂ O
Western blotting protein transfer buffer	2.4 g Tris base, 11.24 g glycine, 200 ml methanol, make up to 1L with dH ₂ O

Table 2.2. List of buffers and solutions used in this project.

2.3 List of antibodies

Primary antibodies			
Protein	Manufacturer	Host	Antigen species
CAB39	Abcam	Rabbit	Human, Mouse, Rat
Secondary antibodies			
Alexa Fluor 680 anti-rabbit	Abcam	Goat	Anti-rabbit

Table 2.3. List of primary and secondary antibodies used in this project.

2.4 Chow formulation with KR-33028

The KR-33028 compound was formulated in standard mouse chow (PicoLab® Rodent Diet 20, LabDiet 5053) using the compound to a final concentration of 750 mg per kg of chow. The drug-formulated chow was produced by TestDiet® on the 25th of February 2015 and was kept in a sealed box at room temperature (RT).

2.5 *In vivo* experimental procedures

2.5.1 *Animal care and husbandry*

Wild type *C57BL/10ScSnOlaHsd* (C57BL/10, Harlan Laboratories, Indianapolis, USA) and *C57BL/10ScSn-Dmd^{mdx}* (*mdx*, Jackson, Maine USA) mice for this study were bred by Elizabeth Greally in the Functional Genomics Unit (FGU), the animal facility at the Institute of Genetic Medicine, Newcastle University. The *mdx* colony was maintained homozygously and breeders were housed as pairs of one male and one female.

All procedures were approved by the Home Office and were carried out under Animals (Scientific Procedures) Act of 1986 under the licence number: PPL 70/8538. Numbers and age of mice used in the various experiments are detailed in the figure and table legends.

For all experiments described throughout this thesis male mice were used exclusively.

2.5.2 *Magnetic resonance imaging (MRI)*

Magnetic resonance imaging (MRI) techniques were developed in Newcastle by Dr Benjamin Davison, Elizabeth Greally, Dr Guy MacGowan, Prof Volker Straub and Prof Andrew Blamire; and were carried out with the help of Elizabeth Greally.

MRI experiments were not carried out in a blinded fashion.

2.5.2.1 *Mouse preparation for MRI*

For MRI anaesthesia was induced using 5% isoflurane and was then maintained at 1.5% oxygen with a flow rate of 0.5 L/min. The tail-vein was cannulated, and chest hair removed. The mouse was then placed on a MR-compatible sled with surface electrocardiogram (ECG) electrodes on the chest wall, cutaneous temperature probe and respiration pillow (Dazai Research Instruments, MICE, Toronto, Canada), which was in turn connected to MR-compatible monitoring equipment (SA Instruments Inc., Stony

Brook, NY 11790). The mouse on the sled was then placed on a bed holding the nose cone for anaesthesia delivery, and then all of this was slid into a 39 mm diameter quadrature birdcage volume coil (Rapid Biomedical GmbH).

Images were acquired on a 7 Tesla horizontal bore microimaging system equipped with a 12 cm microimaging gradient insert (maximum gradient: 40 gauss/cm; Varian Inc., Palo Alto, CA, USA).

2.5.2.2 Cine cardiac MRI

Following power calibration and global shimming, a series of four pilot transverse images were acquired over the heart. Single slice coronal and sagittal images were then obtained in order to view the apex and mitral valve planes. These images were used to plan for the true short axis plane.

A stack of contiguous short axis slices was acquired to cover the entire left and right ventricles of the heart using a spoiled gradient-echo cine sequence (TR= 5 ms and TE= 1.42 ms, Flip angle 15°, Field of view 30 x 30 mm, Data matrix 128 x 128, Slice thickness 1 mm). Images were ECG-triggered to the R wave with a cine delay of 15 ms and, typically, 30 phases were acquired and distributed through the cardiac cycle. Images were zero-filled to a matrix size of 256 x 256.

Scans were converted to DICOM (Digital Imaging and Communications in Medicine) files and analysed using the analysis software Segment V2.0 R4949 to measure the LV and RV functional parameters – end-systolic and end-diastolic volumes, stroke volume, ejection fraction and cardiac output.

2.5.2.3 Manganese-enhanced MRI (MEMRI)

MEMRI is an imaging technique based on the properties of manganese ions (Mn^{2+}) to act as a contrast agent in T1-weighted MRI and to mimic the entry of Ca^{2+} ions in excitable cells, such as neurons and cardiac cells (Massaad and Pautler, 2011).

Gradient echo short axis images were acquired through the heart at the level of the papillary muscles with the left upper forelimb within the field of view. This slice allowed 3 muscle groups to be analysed – myocardium, muscles of the upper forelimb and the chest wall muscles ventral to the heart.

Prior to the initiation of the Mn^{2+} infusion, four baseline images were acquired in order to average any variations due to changes in TR as a result of fluctuations in heart rate.

Intravenous infusion of 60 mM manganese chloride (MnCl₂, Sigma Aldrich) through the tail vein cannula followed at a flow-rate of 0.6 ml/h. The flow time was adjusted according to weight to give a total dose of 190 nmol per gram body weight. Seven more images were acquired; at 2.5 and 5 min, and then at 5-minute intervals for a total of 30 min following the initiation of the MnCl₂ infusion. A relative increase in T1 weighted contrast indicates increased Mn²⁺ uptake. Images acquired from each time point were opened in ImageJ (<http://rsb.info.nih.gov/ij/>) and converted to a stack using the stack builder plugin. On the first image an area of interest was drawn to fit inside the muscle/group of muscles of interest and average signal intensity was measured. Minor adjustments of this drawn region were made for subsequent images in the stack to allow for movement. The increase in contrast enhancement was expressed as a ratio of the average of the four baseline images (which showed little or no variation).

2.5.3 Four-limb hanging test

A four-limb hanging test was aimed to demonstrate neuromuscular impairment and assess the muscle strength of mice under investigation. The four-limb hang test uses a wire grid system to non-invasively measure the ability of the mice to exhibit sustained limb tension to oppose their gravitational force.

The methodology was adapted from the standard operating procedure (SOP) DMD_M.2.1.005 (George Carlson, TREAT-NMD Neuromuscular Network). During the test, the mouse was placed upside down on a wire grid with all four paws grasping the grid. The wire grid holding time was defined as the amount of time that it took for the mouse to fall from the wire grid. The hang time was measured from the time the mouse grasped the grid with all four limbs to the time that the mouse fell off the grid. The procedure was repeated four times for each mouse with a rest interval of at least 3 minutes. Additionally, due to a potential influence that body mass has on the hang time, the holding impulse was used to correlate the hang time with the body mass. The holding impulse equals the hang time multiplied by the body weight (gm sec or Newtons sec; conversion factor - 9.806×10^{-3} Newtons/gm).

These experiments were not blinded.

2.5.4 Whole blood collection

Whole blood was collected from mice under non-recovery general anaesthesia induced using 5% isoflurane and 1.5% oxygen with a flow rate of 0.5 L/min. The heart was

punctured with a 25-gauge needle and blood was collected into a syringe and then stored at 4°C for up to 30 min. Mice were humanely killed without ever regaining consciousness. Subsequently, the blood was centrifuged at 2,300 g for 10 min. The serum fraction, supernatant, was transferred to a fresh Eppendorf tube and stored at -80°C.

2.6 Histological analysis

2.6.1 Muscle collection and storage

For histology, different types of muscles, including the quadriceps, diaphragm, and heart, were used because of their well-established pathological expression profiles. The analysis of these muscle groups has been recommended in standard experimental protocols for the use of *mdx* mice in DMD pre-clinical studies (Willmann *et al.*, 2012). Other tissues that were collected include the gastrocnemius, tibialis anterior and triceps muscles.

Using a clean dissection kit, skin layers were peeled away, and skeletal muscles were excised from tendon to tendon. Following collection, muscles were flash frozen in a 1.5 mL Eppendorf tube placed in isopentane that was kept on dry ice. Tissues intended for cryosectioning, including hearts, diaphragm and quadriceps, were arranged on a cork disk in a small amount of OCT medium in a longitudinal orientation, so as to achieve transverse sections, and were flash frozen in isopentane that was kept on dry ice. All tissues were stored at -80°C.

2.6.2 Cryosectioning of muscle tissue

8 µm serial sections of frozen muscles – quadriceps, diaphragm and heart – were cut with a cryotome (Leica CM1860) along the entire muscle, separated by intervals of approximately 160 µm between the sets of serial sections. Tissue sections were mounted on Superfrost Slides (VWR).

Intervening sections were collected in Eppendorf tubes for protein extraction. Slides were wrapped in cling film and stored at -80°C.

2.6.3 Masson's trichrome staining

Masson's trichrome staining was employed to assess fibrotic and dystrophic changes in sectioned tissues. The protocol we followed was adapted from the procedure 'No. HT15' (Sigma Aldrich) that was included in the Trichrome Stain (Masson) Kit (Sigma Aldrich).

Prior to staining, slides were air dried for 60 min. Subsequently, they were treated with Bouin's solution (Sigma Aldrich) overnight at RT to intensify the final colouration. After a washing step to remove the yellow colour from the sections, Weigert's iron haematoxylin (Sigma Aldrich) was applied for 5 min to stain nuclei, followed by a 5-minute rinse under running tap water. Sections were then stained with Beibrich scarlet-acid fuchsin for 5 min followed by rinsing of the slides in dH₂O. Following this, slides were treated with phosphotungstic and phosphomolybdic acid for 5 min. Sections were then placed in aniline blue for 5 min to stain collagen. After staining, tissue sections were rinsed in 1% acetic acid (Sigma Aldrich, diluted with dH₂O), dehydrated through ascending concentrations of alcohol –70%, 90% and 100%– for 10 s each and then placed in Xylene (Fisher Scientific) twice for 5 min each. The slides were then mounted with DPX Mounting Medium (LAMB) and allowed to dry overnight.

2.6.4 Haematoxylin and eosin (H&E) staining

Haematoxylin and eosin (H&E) staining was carried out in order to assess tissue pathology. Frozen muscle sections on slides were air-dried at RT for 60 min. They were then stained with Haematoxylin Harris (VWR) for 10 min and rinsed under running tap water for 1 minute. Subsequently, they were dipped in 1% HCl (Hydrochloric Acid, Sigma Aldrich; diluted in 70% ethanol) for 5 s and rinsed in tap water for 30 s. For staining of the cytoplasm, Eosin (1% AQUEOUS, VWR) was applied for 30 s followed by rinsing under running tap water for a further 30 s. Sections were then dehydrated by dipping the slides in an ascending alcohol series of 70%, 90% and 100% for 5 s each, and placed in HistoClear (National Diagnostics) twice for 3 min each. Finally, the sections were mounted in DPX Mounting Medium (LAMB) with a glass coverslip and allowed to dry overnight.

2.6.5 Imaging of slides and image analysis

Slides of stained tissue sections were shipped to the Newcastle Biobank (Faculty of Medical Sciences, Newcastle University), where imaging was carried out. A Leica SCN400 slide scanner was used to scan and digitalise slides at a x20 magnification.

Images were processed and analysed using the image analysis software ImageJ (<http://rsb.info.nih.gov/ij/>). Disease parameters that were assessed include muscle fibre cross sectional area, Feret's diameter, number of centrally-located nuclei within muscle fibres and levels of fibrosis. Image analysis was carried out in a blinded fashion.

2.7 Creatine kinase (CK) assay

CK is an important metabolic enzyme usually restricted to the intracellular compartment. Its presence in the serum is a marker of sarcolemmal damage (Wallimann *et al.*, 2011). In order to assess the levels of CK in the serum of KR-33028- and vehicle-treated *mdx* mice, and age-matched control animals, a standard CK assay kit (Abcam) was used following the manufacturer's instructions. Briefly, 50 μ l of each sample was mixed with 50 μ l of CK enzymatic assay reagent, containing CK assay buffer, CK enzyme mix, CK developer, ATP and CK substrate, in single wells of a 96-well plate (VWR). Sample background control wells were also prepared all reagents except the CK enzyme mix. A standard series containing a set quantity of NADH serially diluted with a standard dilution buffer (0, 2, 4, 6, 8 and 10 nmol) was included in another 6 wells. Additionally, one well was reserved for a blank, and one for a positive control (provided with the kit). Output at OD 450 nm was measured on a microplate reader (Tecan Infinite® F-200) in a kinetic mode, every 2 min for a total of 40 min at 37°C protected from light.

Absorbance values were corrected by subtracting the mean absorbance value from all standard and sample readings. Using the readings for the standard series of NADH a standard curve was constructed in Microsoft Excel. In order to calculate the amount of NADH generated by CK during the reaction time (ΔT), the ΔOD was calculated based on the following equation:

$$\Delta OD_{450nm} = (A_2 - A_{2BG}) - (A_1 - A_{1BG}), \text{ where:}$$

A_1 is the sample reading at time T_1 , A_{1BG} is the background control sample at time T_1 , A_2 is the sample reading at time T_2 , and A_{2BG} is the background control sample at time T_2 .

Subsequently, CK activity (nmol/min/ml or mU/ml) in the test samples was calculated as:

$$\text{CK Activity} = (B / (\Delta T * V)) * D, \text{ where:}$$

B is the amount of NADH in sample well calculated from standard curve (nmol), ΔT is the reaction time in min, V is the original sample volume added into the reaction well (ml), and D is the sample dilution factor.

2.8 Protein isolation, detection and quantification

2.8.1 Protein extraction

Cardiac and skeletal muscles were kept on ice at all times to prevent protein degradation. Each muscle was placed in a 15 ml falcon tube and homogenised in 400 µl lysis buffer (Table 2.2) with tissue raptor. Triton X-100 was then added to a final concentration of 1% and lysates were left on ice for 30 min. Subsequently, the lysates were transferred to 1.5 ml Eppendorf tubes and were spun at 700 g for 10 min at 4°C in order to pellet debris. The supernatant was then collected and spun at 10000 g for 30 min at 4°C whereas the pellet was discarded. After spinning of the samples, the supernatant (cytosolic fraction) was collected in a new 1.5 ml Eppendorf tube and the pellet (membrane fraction) was re-suspended in 30 µl of lysis buffer. Both the cytosolic and membrane fractions were stored at -20°C.

2.8.2 Protein quantification using BCA

The bicinchoninic protein assay (BCA) is a colorimetric assay based on the conversion of Cu^{2+} to Cu^+ under alkaline conditions. The Cu^+ is then detected by reaction with BCA (Walker, 1994).

Bovine serum albumin (BSA; Sigma Aldrich) was used to prepare a linear range of protein standards between 25 and 1000 ng/µl. 10 µl of protein standard or test protein sample was added to the appropriate number of wells of a 96-well plate (VWR) in duplicate. To each standard- and sample-containing well, 200 µl of BCA working solution (1 part copper (II) sulphate solution (Sigma Aldrich), 50 parts BCA solution) was added. The plate was then left at RT for 15 min. Absorbance at 595 nm was measured using a microplate reader (Tecan Infinite® F-200). The protein concentration of the test samples was determined by using the standard curve of the absorbance versus concentration of BSA.

2.8.3 SDS polyacrylamide gel electrophoresis (PAGE)

Equal quantities of protein extracts (25 µg) were mixed 1:1 with 2x Laemmli sample buffer (Bio-Rad Laboratories) containing 5% v/v β-mercaptoethanol and heated at 100°C for 5 min. The resultant samples were then loaded to individual lanes of a two-phase polyacrylamide gel electrophoresis (PAGE) gel alongside the PageRuler™ Plus Prestained Protein Ladder (Thermo Scientific).

PAGE gels were made with a lower percentage stacking gel (4% w/v) overlaying a resolving gel (6–12% w/v). The ingredients used to make the gels are presented in more detail on Table 2.2. Stacking and resolving gel components were mixed in separate 15 ml Falcon tubes and polymerising agents: 10% APS and TEMED were added right before to pouring the gels.

Gels were assembled in a tank (Life Technologies, Novex Mini-Cell) which was filled with 1x SDS running buffer and run at 200 V for 45–60 min.

2.8.4 Western blotting

For the transfer of proteins from the gels to a PVDF membrane (GE Healthcare), gels with separated proteins were placed within a Western sandwich set up (Mini Trans-Blot Electrophoresis Transfer Cell, BioRad) containing chilled 1x transfer buffer (Table 2.2) and surrounded by ice. Transfers were run at 100 V for ~1.5 h.

Following transfer, PVDF membranes were removed and washed prior to a 1 h blocking with 5% blocking milk solution (Table 2.2). The milk solution was drained, and the membrane was placed in a plastic bag. Primary antibody diluted in BSA wash buffer (Table 2.2) was added to the membrane and incubated in the sealed bag for 2 h at RT or in the cold room overnight. The membrane was then washed in BSA wash buffer three times for 5 min. The secondary antibody incubation followed for 1 h at RT. Secondary antibodies were diluted using BSA wash buffer. The washing steps used for the primary antibody were applied and the protein bands were visualised using the Odyssey® CLx Imaging System (LI-COR Biosciences).

2.8.5 Coomassie brilliant blue staining

For the visualisation of proteins separated by SDS PAGE, Coomassie Brilliant Blue G250 (Sigma Aldrich) was used. The detection range is 0.3 to 1.0 µg per protein band (Gallagher and Chakavarti, 2008).

After electrophoresis, the gel was washed in dH₂O and was then stained with Coomassie staining solution (Table 2.2) on a shaker for 45 min or until the gel was completely blue. The Coomassie solution was then removed and de-staining buffer 1 (Table 2.2) was added for 1 h on a shaker, followed by 1 h with de-staining buffer 2 (Table 2.2) on a shaker. dH₂O was then added and the gel was left on a shaker overnight covered in tissue paper.

The protein bands were visualised using the Odyssey® CLx Imaging System (LI-COR Biosciences).

2.8.6 Quantification of protein expression

The protein expression in each sample was defined as the protein band intensity normalised against expression coefficient values which were estimated based on Coomassie brilliant blue staining. Protein band intensities were determined in ImageJ software by drawing identical rectangular regions of interest (ROIs) around protein bands of interest. The average intensity of all bands (Coomassie gel) was determined and then, individual band intensities were divided by the average value in order to determine the expression coefficient values. Subsequently, in order to get a protein expression normalised value, protein of interest band intensities (WB image) were multiplied by the corresponding coefficients. Notably, brightness and contrast of bands was only adjusted for display purposes but not before image analysis had been completed.

2.9 Proteomic analysis of tibialis anterior (TA) muscles

Tibialis anterior (TA) muscles collected from KR-33028-treated *mdx* mice (n=3) and vehicle-treated *mdx* mice (n=3) were used for comparative proteome profile analysis. The proteomic analysis was carried out by Viet Xuan Phan, Leibniz-Institute for Analytical Science (ISAS), Germany, in a blinded fashion.

2.9.1 Tissue lysis and sample preparation

Each muscle sample was grinded and lysed in 0.5 ml of 50 mM Tris-HCl buffer (pH 7.8) containing 150 mM NaCl, 1 % SDS and 1 cOmplete™ EDTA-free protease inhibitor tablet. Samples were then centrifuged at 13,500 rpm for 30 min at 4°C and tissue lysates were collected. Protein concentration of each sample was determined using the BCA assay according to the manufacturer's protocol.

Following tissue lysis, disulphide bonds in proteins were reduced using 10 mM dithiothreitol (DTT) at 56°C for 30 min. Thiol groups of cysteines were then carbamidomethylated with 30 mM iodoacetamide (IAA) for 30 min at RT in the dark. Cysteine carbamidomethylation (CAM), deliberate post-translational modification introduced to cysteine residues, is an essential step of sample preparation for mass spectrometry and allows for identification and characterisation of proteins (Wilkins *et al.*, 2008; Rombouts *et al.*, 2013).

2.9.2 Protein extraction and digestion

Filter-aided sample preparation (FASP) was performed for the extraction of proteins from the samples and proteolysis. FASP uses an ultrafiltration device with membrane pores small enough to allow contaminating detergents to pass through, while allowing proteins to be retained and concentrated in the filter unit (Coleman *et al.*, 2017). A total of 100 µg of protein was diluted 10-fold with freshly prepared 8 M urea/100 mM Tris-HCl buffer (pH 8.5) and was then filtered using a 30K Nanosep® centrifugal device with Omega Membrane at 13,800 rpm for 20 min at RT. All the following centrifugation steps were performed under the same conditions. In order to eliminate residual SDS from the samples, three washing steps were carried out with 100 µl of 8 M urea/100 mM Tris-HCl buffer (pH 8.5). Subsequently, for buffer exchange, the device was washed thrice with 100 µl of 50 mM ammonium bicarbonate (NH₅CO₃; pH 7.8). The protein samples were digested using 100 µl of proteolysis buffer, made of trypsin (1:25 w/w, protease to substrate), 0.2 M GuHCl and 2 mM CaCl₂ in 50 mM NH₅CO₃ (pH 7.8), which was added to the device and incubated at 37°C for 14 h. The generated tryptic digests were then recovered by centrifugation with 50 µl of 50 mM NH₅CO₃ and then with 50 µl of ultra-pure water. Finally, peptides were acidified by addition of 10% (v/v) trifluoroacetic acid (TFA) and digests were quality controlled in a reversed-phase high-performance liquid-chromatography (HPLC).

2.9.3 Liquid chromatography tandem-mass spectrometry (LC-MS/MS)

All samples were measured using an UltiMate™ 3000 RSLCnano System (Thermo Scientific) coupled to an Orbitrap Elite™ Mass Spectrometer (Thermo Scientific). Peptides were pre-concentrated on a C18 trapping column, 100 Å, 5 µm, 100 µm x 2 cm (Acclaim Pepmap, Thermo Scientific) using 0.1% TFA (v/v) at a flow rate of 20 µl/min followed by separation on a C18 column, 100 Å, 2 µm, 75 µm x 50 cm (Acclaim Pepmap, Thermo Scientific), with a 115 min LC gradient ranging from 3–35% of buffer containing 84% acetonitrile (ACN) and 0.1% (v/v) formic acid (FA) at a flow rate of 250 nl/min. Mass spectrometry (MS) survey scans were acquired in the Orbitrap from 300 to 1500 m/z at a resolution of 60,000 using the polysiloxane ion at 371.101236 m/z as lock mass. The fifteen most intense signals were subjected to collision-induced dissociation (CID) in the ion trap, dynamic exclusion of 30 s. CID spectra were acquired with a normalized collision energy of 42% and an activation time of 10 ms. AGC target values were set to 106 and 104 for Orbitrap MS and ion trap sequential MS (MS_n) scans respectively. Moreover, for both full MS and MS_n scans, maximum injection times were set to 100 ms.

2.9.4 Data processing

Data analysis of the acquired label-free quantitative MS data was performed using the Progenesis Qi software from Nonlinear Dynamics (Newcastle upon Tyne, UK). The MS raw data was aligned automatically by Progenesis, which selected one of the LC-MS files as reference. After peak picking, only features within m/z windows from 300-1500 m/z and retention time ranging 0–120 min, with charge states +2, +3, and +4 were considered for peptide statistics and analysis of variance (ANOVA).

MS/MS spectra were exported in a mascot generic file (mgf) format as peak lists. The mgf peak lists were searched against a list of all known mouse proteins using Mascot 2.4 (Matrix Science), X! TANDEM Vengeance (2015.12.15.2) and MS-GF+ Beta (v10282) (12/19/2014) with the help of searchGUI 3.0.0. More specifically, a concatenated target-decoy version of the mouse UniProt database (downloaded in July 2015) containing 16,716 target sequences was used for this search. Trypsin with a maximum of two missed cleavages was selected as enzyme, carbamidomethylation of cysteine was set as ‘fixed’ and oxidation of methionine was selected as ‘variable modification’. MS and MS/MS tolerances were set to 10 ppm and 0.5 Da, respectively.

In order to maximize the number of identified peptides and proteins from searchGUI and Mascot at a given quality, the PeptideShaker software 1.12.2 was used. Combined search results were filtered at a false discovery rate (FDR) of 1% on the protein level and exported using the advanced PeptideShaker features that allow direct re-import of the quality-controlled data into Progenesis Qi. To reduce unanticipated bias in quantification, peptide sequences containing oxidized methionines were excluded from further analysis. Only proteins that were quantified with unique peptides were exported. Subsequently, for each protein, the average of the normalized abundances (obtained from Progenesis Qi) from the replicate analyses was calculated to determine the ratios between the KR-33028- and vehicle-treated mice. Proteins which were a) commonly quantified in all the replicates, with b) unique peptides, c) an ANOVA p-value less than 0.05 (Progenesis Qi) and d) an average log₂ ratio of which protein that was either higher than the up-regulated cut-off or lower than the down-regulated cut-off was considered as regulated. The cut-off values were determined based on the 2x standard deviation and the normal distribution of the log₂ ratios from all identified proteins (found to be symmetric around the mean and had bell-shaped density curves). Therefore, an average log₂ ratio of a protein below -0.79 or above 0.62 (corresponding to approximately 1.5-fold regulation; log₂ ratios of 0.96) for comparative global profile were considered as regulated.

2.9.5 Gene ontology and protein-protein interaction analysis

Proteins the levels of which were found to be significantly different between the KR-33028- and vehicle-treated samples were further subjected to a gene ontology analysis. The proteins were functionally grouped into metabolic, signalling or transcriptional pathways using the STRING database (<http://string-db.org>), version 10.5 (von Mering *et al.*, 2005; Szklarczyk *et al.*, 2015). Additionally, a protein-protein interaction network depicting both physical (direct) and functional (indirect) associations between the various proteins was constructed.

2.10 Pharmacokinetic (PK) study

In order to obtain the mean plasma concentration-time profiles of the KR-33028 compound, the compound was administered to *mdx* mice by intravenous (IV) injection (n=2), oral gavage (n=3) or via drug-formulated chow (n=4). For the administration via IV and oral gavage, the compound was dissolved in 50% PEG-400 and water (v/v) and dosed at 20 mg/kg with 5 ml/kg injection volume. The drug-formulated chow was formulated using KR-33028 to a final concentration of 750 mg per kilogram of chow; and each mouse treated with drug-formulated chow ate ~4 g of chow per day which was equivalent to a daily dose of ~120 mg/kg. Drug-formulated chow was provided ad libitum.

Day Number	Time (H)	Clock
1	0	19:00
2	2	21:00
3	4	23:00
4	12	07:00
5	16	11:00
6	20	15:00
7	24	19:00

Table 2.4. Blood sampling times for mice treated with KR-33028-formulated chow.

PK profile of the KR-33028 after administration through drug-formulated chow relies on the feeding pattern of the mice, which in turn depends on the light (7am-7pm) and dark cycles (7pm-7am). In order to ensure an accurate assessment of the PK profile, bleeding time points were spread evenly over the dark and light cycles. Furthermore, bleeding of the mice can affect the feeding of the mice and in turn the PK profile. In order to minimise the effects of bleeding, each sample was taken 24 h apart.

After the drug administration, blood was sampled from the mice of each group at different time points. For the mice treated with drug-formulated chow, the dosing was dependent on their feeding pattern and therefore, the dark and light cycles (mice are nocturnal animals and are therefore more active during the dark cycle). In order to ensure an

accurate assessment of the PK profile, the bleeding time points were spread out evenly during the dark (7pm–7am) and light (7am–7pm) cycle (Table 2.4). Additionally, it was highly likely that blood sampling would affect normal feeding pattern, which in turn would affect the PK profile. In order to minimise the effects that stress due to bleeding could have on the feeding pattern, each blood sample was taken 24 h apart, allowing enough time between each bleed to recover (Table 2.4).

Following collection, each blood sample was stored at 4°C for up to 30 min. Subsequently, blood samples were centrifuged at 2,300 g for 10 min. The plasma fraction, supernatant, was transferred to a fresh Eppendorf tube and stored at -80°C. Plasma samples were sent to Cyprotex Discovery Ltd for bioanalysis.

2.11 High-performance liquid-chromatography (HPLC) for stability testing of KR-33028-formulated chow

For the purposes of this study, *mdx* mice were treated with the KR-33028 compound over the period of 6 months. The compound was formulated in standard mouse chow. Establishing the compound stability in the chow over the treatment period was essential for the determination of the drug concentration the mice were dosed with. The stability testing described below was carried out by Dr Keith Healy, Dr Alistair Henderson and Prof Bernard Golding from NewChem Technologies (Newcastle University).

An analytical method was developed for KR-33028, in which a reversed-phase HPLC system (Shimadzu LC20) employing a C18 column (250 × 4.6 mm Kinetix C18 5 µ) with elution by aqueous trifluoroacetic acid and acetonitrile was used. HPLC parameters were set as following: flow rate 1 ml/min, detection wavelength 309 nm, temperature -37°C, injection volume 5 µl and linear gradient 90% to 65% aqueous trifluoroacetic acid (0.5%) over 20 min with the balance being acetonitrile. A standard curve for KR33028 was generated for a series of known concentrations in acetonitrile and water (1:1).

A weighed quantity (between 4–6 g) of mouse chow containing KR33028 was crushed in a pestle and mortar to a fine powder. The extraction efficiency was measured by extracting the powder three times with acetonitrile/water (1:1, 50 ml) with stirring for 1 h each time and measuring the amount of KR33028 by comparing the peak area to the standard curve. It was found that the extractions removed all of the KR33028 (1st extraction: 77 %, 2nd: 19 %, 3rd: 4 %).

A total of three HPLC measurements were taken, one when the chow was first handed to NewChem technologies, one at the 3-month time point and then at the 6-month time point.

2.12 Cell culture

2.12.1 Standard cell culture conditions for human myoblasts

Human myoblasts (MRC-CNMD Biobank) were grown at 37°C and 5% CO₂, medium replaced every other day and passaged when they reached a confluency of ~70% and until appropriate yield and consistent growth was achieved. When cells attained ~70% confluency, they were split into two T-25 flasks. Cells were washed with 2 ml of sterile 1x PBS (Dulbecco's Phosphate Buffer Saline, Sigma Aldrich) and were then, incubated with 2 ml of 0.05% Trypsin-EDTA 1x (Life Technologies) for 2–3 min at 37°C. Subsequently, in order to inactivate the Trypsin-EDTA, 4 ml of growth medium was added to the cell suspension, which was then transferred into a 15 ml tube and centrifuged at 450 g for 5 min. After discarding the supernatant, the pellet was resuspended in 10 ml growth medium. 5 ml of the cell suspension along with 2 ml of growth medium was dispensed into each of the two T-25 flasks and returned to the incubator.

Myoblast differentiation into myotubes was induced by reducing the serum concentration to 2%. Once cells reached ~70% density, the medium was replaced by differentiation medium supplemented with 2% horse serum (Life Technologies). The differentiation medium was replenished every other day until cells were fused into myotubes over a period of 2–8 days.

2.12.2 Single muscle fibre isolation and culture

Extensor digitorum longus (EDL) and flexor digitorum brevis (FDB) muscles were carefully dissected from freshly killed mice, handling by tendons only, and avoiding any tension. Immediately after dissection, the muscles were placed into individual bijoux with 2 ml of DMEM solution. The muscles were then transferred in 2 ml of 0.2% collagenase solution (pre-warmed at 37°C) and incubated at 37°C and shaking with a speed of 160 rpm. EDL muscles were incubated for 90 min whereas FDB muscles for 60 min. After digestion, each muscle was transferred to an individual petri dish with PBS/10% sodium pyruvate solution. Single muscle fibres were liberated by gentle trituration with a wide-mouthed glass Pasteur pipette. After their isolation, intact fibres were transferred to a petri dish containing DMEM solution with 10% FBS and 1% PenStrep, and were kept at 37°C.

2.13 Statistical analysis

Statistical tests were performed using Microsoft Excel. For comparison of one response variable from 2 independent groups, and when sample values could be assumed, or determined, as normally distributed, a Student's t-test was chosen. Moreover, repeated ANOVA measures were used to compare the effects of two variables within dependent groups. For all analyses, an α -level of 0.05 was assumed.

Chapter 3. Pharmacokinetic (PK) study of KR-33028 and stability testing

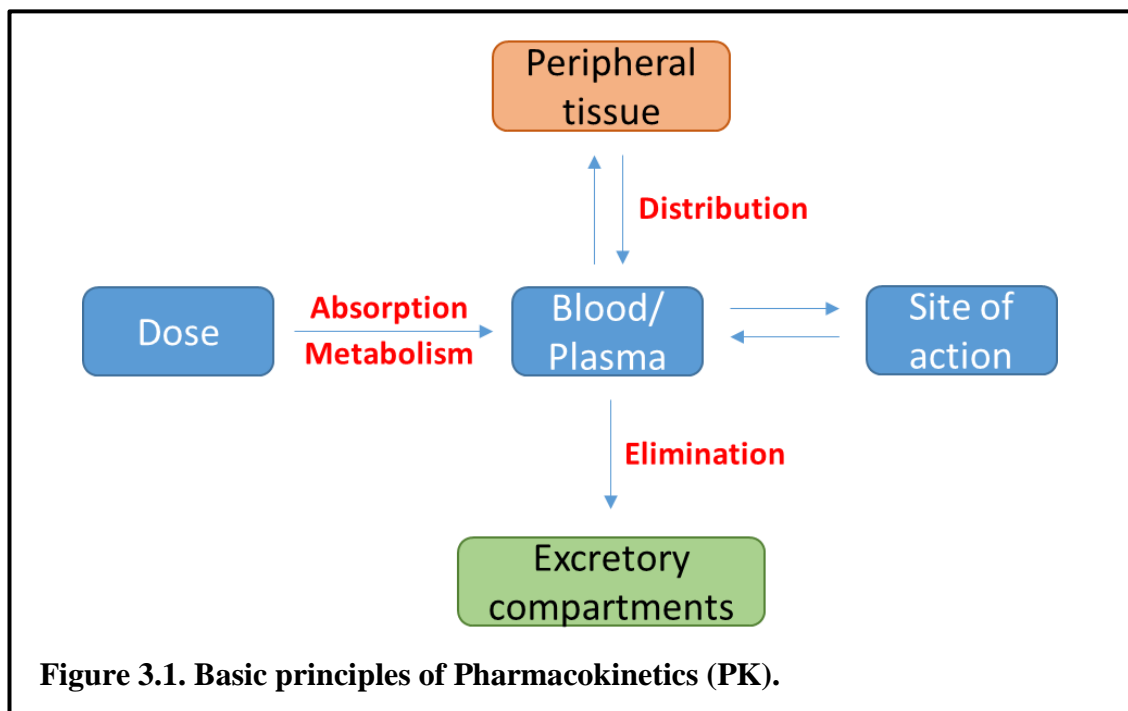
3.1 Introduction and aims

The primary purpose of this project was to investigate the effects of KR-33028 (N-4-cyano (benzo[*b*]thiophene-2-carbonyl] guanidine methanesulfonate, C₁₂H₁₂N₄O₄S₂) *in vivo* in the *mdx* mouse model for DMD. Stability studies are an essential component of pharmaceutical development, allowing evaluation of drug stability under the influence of a variety of environmental factors such as light, temperature and humidity (Bharath, 2013). Accelerated stability testing that was carried out prior to the initiation of this project demonstrated that storage of KR-33028 at 40°C, 75% relative humidity for the period of 6 months has minimal effects on the purity (0.07% decrease) and moisture (0.1% increase) of the compound and no effects on its stability. Additionally, KR-33028 dosing formulations in 0.5% hydroxypropylmellulose (HPMC), over the concentration range of 1 mg/mL to 150 mg/mL, were shown to be stable for up to 8 days when stored at ambient temperature and between 2°C to 8°C, both protected from light (unpublished data).

During this study, eleven *mdx* mice were treated with the KR-33028 NHE1 inhibitor over the period of 28 weeks. Ideally, the mice would have been treated with an intravenous (IV) injection which offers a more direct route of dosing by avoiding gastrointestinal (GI) absorption and metabolism leading to greater drug exposure (Rang *et al.*, 2015). Additionally, the study by Kim *et al.* (2007c) has demonstrated that the KR-33028 compound is readily metabolized by the liver at low doses. It was also shown that doses greater than 2 mg/ml can saturate this process thereby allowing more drug to enter the circulation. A rapid dosing, such as an IV, favours the saturation process more than slower methods such as oral dosing. However, due to the workload involved in handling all the mice, administration through an IV injection was not feasible, and therefore, the drug was formulated in standard mouse chow. Establishing the compound stability in the chow over the treatment period was essential for the determination of the drug concentration the mice were dosed with.

In addition to the stability testing, obtaining pharmacokinetic (PK) data from the compound is crucial to all drug-development studies. Pharmacokinetics is an investigation of the fate of a drug into the organism after its administration and provides

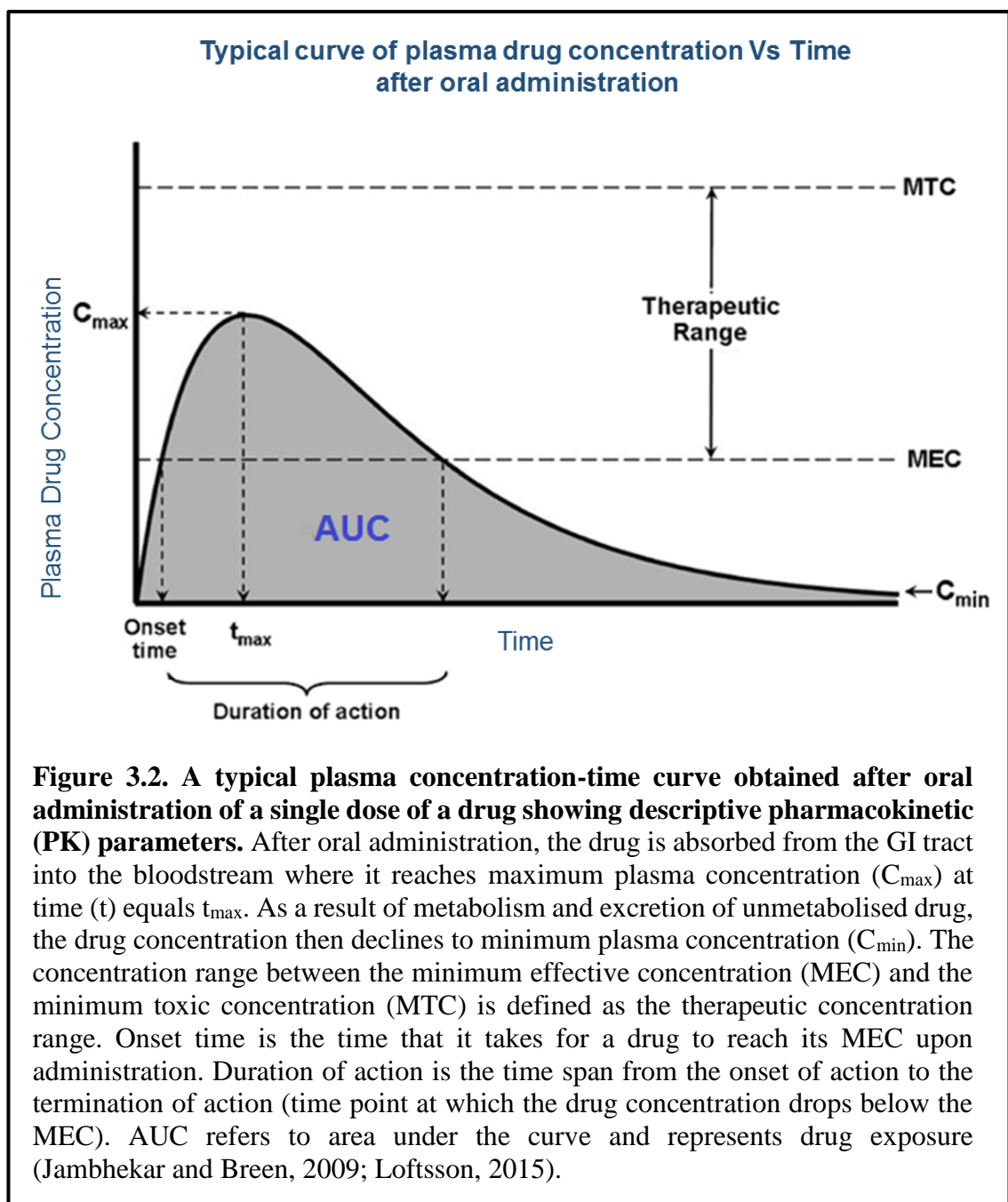
information about the drug absorption, distribution, metabolism and excretion (Figure 3.1) (Cawello and Antonucci, 1997; Benedetti *et al.*, 2009).



Absorption refers to the transfer of a drug from the site of administration into the bloodstream. It depends on the route of administration, the chemical properties and formulation of the drug, and physiological factors that can impact the site of absorption. IV administration of a compound requires no absorption, because the drug is administered directly into the bloodstream and consequently, the entire dose of the drug is available to reach the site of drug action. However, administration through other routes, for example oral gavage and drug-formulated chow, may result in less availability due to incomplete absorption. When this occurs, less of the drug is delivered by the bloodstream to the site of action. The fraction of drug that reaches the systemic blood circulation intact after administration is referred to as ‘bioavailability’. By definition, the bioavailability of a drug administered intravenously is 100% and it decreases when administered via other routes of administration (Rang *et al.*, 2015; Hilal-Dandan *et al.*, 2017).

The purpose of the second part of this chapter was to measure the plasma concentrations of KR-33028 after drug administration through IV injection, oral gavage or drug-formulated chow and calculate the bioavailability of the compound for all three different routes of administration. Furthermore, by inspecting the time course of drug concentration in plasma following dosing, some descriptive pharmacokinetic characteristics can be observed directly (Figure 3.2), including the maximum plasma

concentration (C_{max}), the time between drug administration and achieving C_{max} (t_{max}), the compound half-life ($t_{1/2}$), and area under the curve (AUC). C_{max} is dependent on the dose administered. Together with C_{min} , the minimum concentration a drug achieves after dosing, C_{max} can determine whether a dose is within the therapeutic concentration range and therefore whether it is sub-therapeutic, therapeutic or toxic (Rosenbaum, 2011). The therapeutic concentration range (also referred to as therapeutic window) of a drug is the concentration range from the minimum effective concentration (MEC) to the minimum toxic concentration (MTC) (Loftsson, 2015). T_{max} can control the onset of action of the drug (Rosenbaum, 2011), the time it takes for the drug to reach its MEC (Jambhekar and Breen, 2009). AUC refers to the overall amount of drug in the bloodstream after a dose



and represents drug exposure to the tissues and organs. Furthermore, $t_{1/2}$ is the rate of decrease of the drug concentration in the plasma and refers to the time it takes for the drug concentration to fall by one half (Kolthammer and Korjonen-Close, 2007).

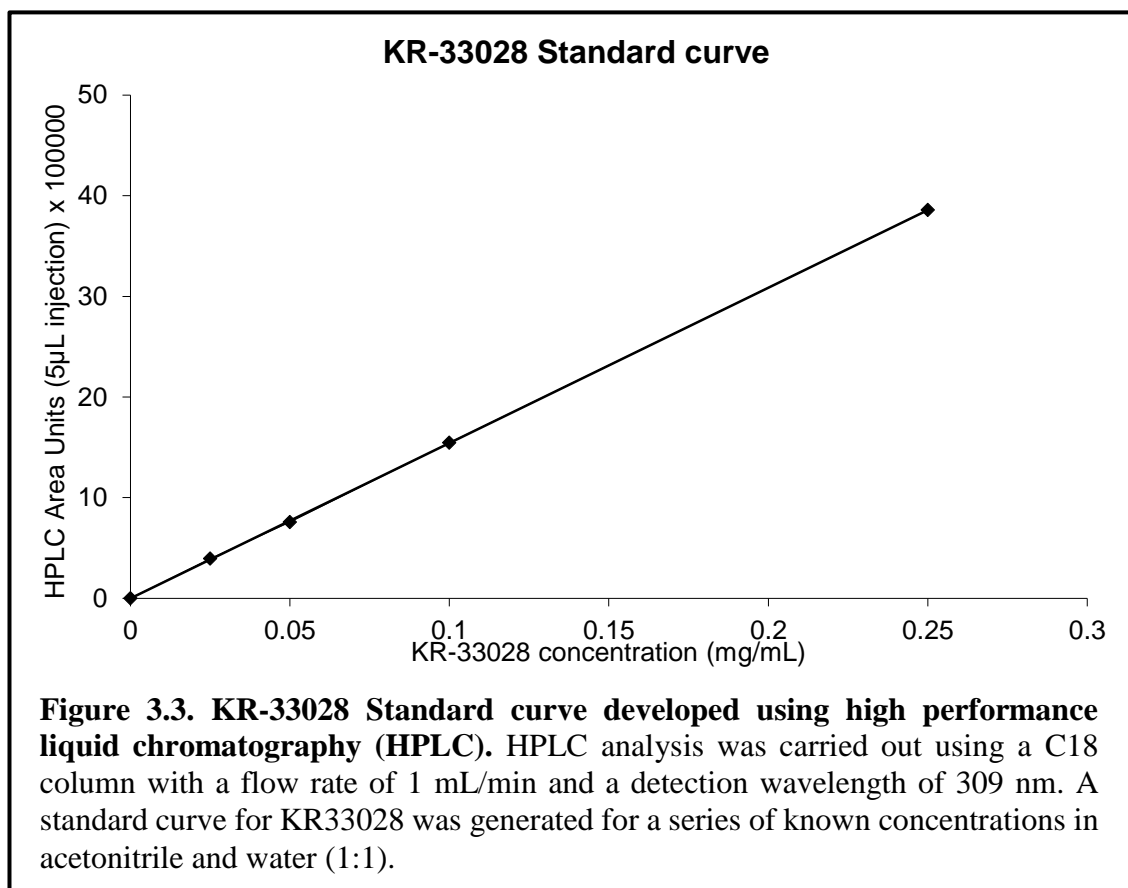
Aims of the experiments described in this chapter:

- Investigate the stability of KR-33028 in the formulation of standard mouse chow.
- Establish the PK profile of KR-33028 after administration to *mdx* mice via IV injection, oral gavage or drug-formulated chow.

3.2 Stability of KR-33028 in mouse chow

Based on the availability of the compound for this study (~10g), the number of mice that were treated (11), the length of period for which the study took place (6 months), and previous reports of efficiency and toxicity of the compound (Jung *et al.*, 2006; Kim *et al.*, 2007a; Kim *et al.*, 2007c; Oh *et al.*, 2007; Lee *et al.*, 2009), it was decided to use 750 mg of compound per kilogram of chow. The drug was formulated into the standard mouse chow by Test Diet® Europe.

The stability testing of the compound was carried out by NewChem Technologies (Newcastle University) ~1 year after the end of the treatment of the mice with the KR-33028-formulated chow. During this period, the chow was stored at -80°C.



In order to measure the concentration of the KR-33028 compound in the drug-formulated chow, high performance liquid chromatography (HPLC) analysis was carried out and a calibration curve was obtained using a series of known KR-33028 concentrations (Figure 3.3). It was observed that the mouse chow had a concentration of 590 mg of KR-33028 per kilogram of chow when it was first supplied to NewChem Technologies, compared to the expected concentration of 750 mg/kg after formulation of the drug in standard

mouse chow. The relative concentration of KR-33028 in chow was found to be 580 mg/kg after 6 months of storage at ambient temperature demonstrating minimal degradation of the KR-33028 in the chow formulation.

It was postulated that the difference between the expected and the actual concentration of the KR-33028 compound in the chow (~21.3% less) could be attributed either to inefficient formulation of the drug into the standard mouse chow or degradation of the compound due to freeze/thaw effects. In order to investigate this further, an additional measurement of the drug concentration was taken after freezing a small batch of chow and then thawing it. It was demonstrated that a cycle of freeze/thaw did not have any impact on the concentration of the KR-33028 in the drug-formulated chow, providing evidence to support the first statement; that ~21.3% of KR-33028 was lost during formulation of the chow. As a result, the mice received 590 mg of KR-33028 per kilogram of chow.

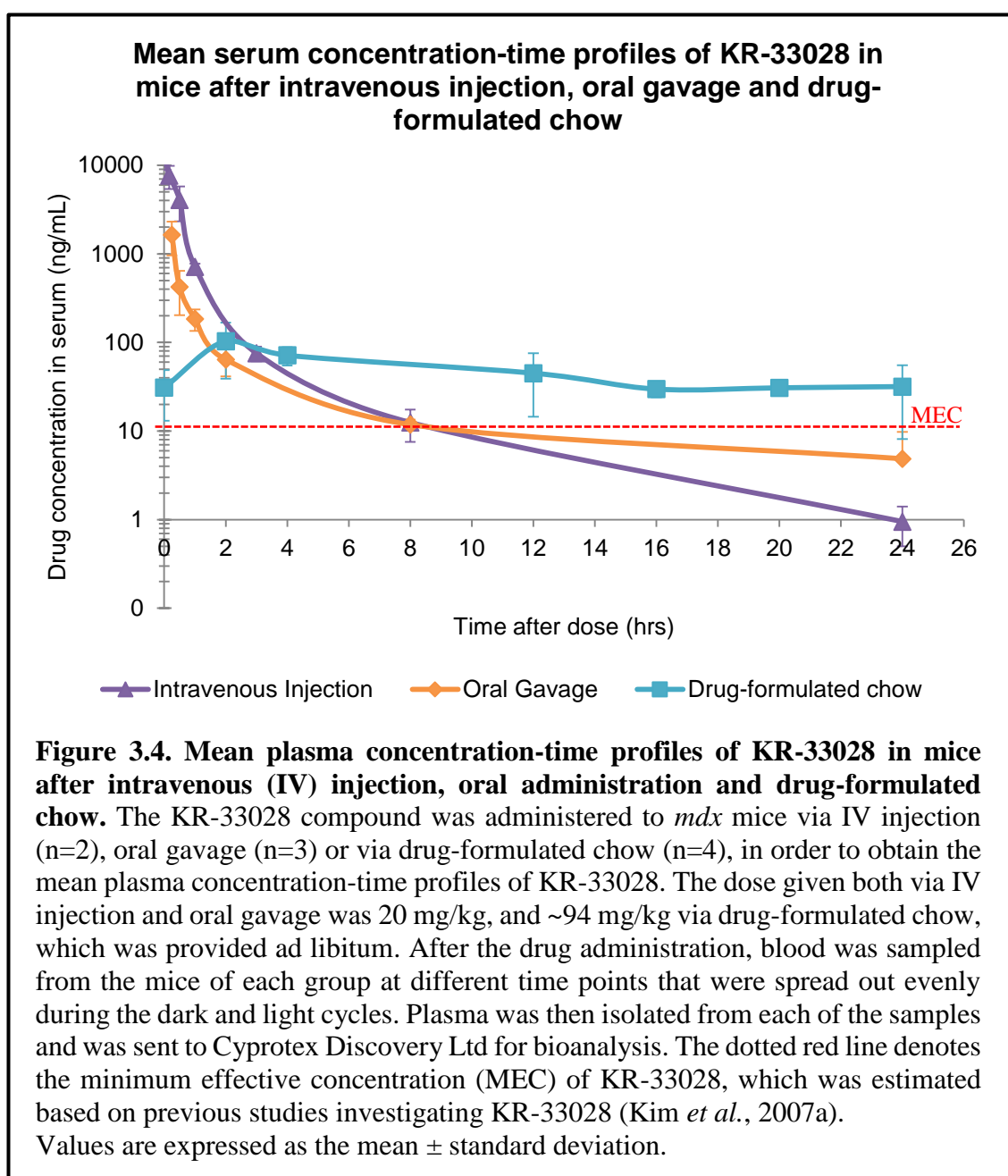
3.3 Pharmacokinetic (PK) study of KR-33028

The purpose of the PK study was to obtain the mean plasma concentration-time profiles of KR-33028 after administration to *mdx* mice via IV injection (n=2), oral gavage (n=3) and drug-formulated chow (n=4). The drug may behave differently at different doses and therefore, multiple doses at multiple routes of administration should, ideally, be investigated. However, due to limited drug availability we were only able to select a single dose. Based on the data published by Jung *et al.* (2006) and Kim *et al.* (2007c), the highest dose that could have been given safely through IV and oral gavage was 20 mg/kg. As previously mentioned, the chow was formulated by Test Diet® Europe using the KR-33028 to a final concentration of 590 mg per kg of chow; and each mouse treated with drug-formulated chow consumed ~4 g of chow per day which was equivalent to a daily dose of ~94.4 mg/kg. After the drug administration, blood was sampled from the mice of each group at different time points. For the mice treated with drug-formulated chow the bleeding time-points were spread out evenly during the dark and light cycles because the cycles affect the feeding of the mice and therefore the dosing. Plasma was then isolated from each of the samples and was sent to Cyprotex Discovery Ltd for bioanalysis.

The graph in Figure 3.4 presents the concentration of KR-33028 in the plasma at different times for all three different routes of administration. The half-life of the compound after oral gavage and IV injection was ~15–30 mins. Additionally, drug reached C_{max} within 15 mins after oral gavage dosing, suggesting remarkable GI absorption. The C_{max} of the

drug in plasma collected from mice fed with drug-formulated chow was 103.65 ng/mL and the plasma concentration did not go below 30 ng/mL at any time during the treatment.

The AUC was found to be 6.009, 1.086 and 1.160 mg.hr/L for IV injection, oral gavage and drug-formulated chow respectively. The compound bioavailability for oral gavage and chow formulation was estimated using the equation: Bioavailability (F%) = $[(AUC_{ev})/(AUC_{iv})] * 100$, where ev stands for extravascular and refers to all routes of administration other than IV injection. The KR-33028 bioavailability was found to be 18.07% and 19.30% for oral gavage and drug-formulated chow respectively.



3.4 Discussion and conclusions

In order to investigate the effects of the KR-33028 NHE1 inhibitor *in vivo*, the compound was formulated in standard mouse chow which was then fed to the mice. The drug-formulated chow was formulated using 750 mg of KR-33028 per kg of chow (expected concentration). The amount of compound that was used for the formulation of the chow was determined by the availability of the compound (~10g), the number of mice that were treated (11), the length of period for which the study took place (6 months), and previous reports of efficiency and toxicity of the compound (Jung *et al.*, 2006; Kim *et al.*, 2007a; Kim *et al.*, 2007c; Oh *et al.*, 2007; Lee *et al.*, 2009).

Prior to the initiation of the current study, stability testing of the KR-33028 compound was carried out. It was demonstrated that the compound is stable when stored in an air-tight container at ambient temperature and protected from the light. Further to those studies, it was necessary to establish whether the compound was stable in the formulation of the standard mouse chow. A sample of the drug-formulated chow was sent to NewChem Technologies ~1 year after the end of the drug-treatment study which then carried out HPLC analysis in order to determine the concentration of the KR-33028 in the chow. A total of three measurements were taken, the first one at the beginning of the study, the second one at the 3-month time point and the third one at the 6-month time point. The concentration of the compound in chow was found to be 590, 570, and 580 mg/kg for each of the time points respectively. This demonstrated that storage of the drug-formulated chow at ambient temperature over the period of 6 months had minimal effects on the degradation of the compound in the chow. It further suggests that the concentration of the compound remained stable over the 6-month treatment of the *mdx* mice. As mentioned above, the chow was formulated using 750 mg of compound per kg of chow which suggests the loss of ~21.3% of the compound during the formulation processes. Consequently, the mice were treated with a lower dose of compound (~94.4 mg/kg) than the one that was initially estimated (~120 mg/kg); the dose of compound was estimated based on the daily eating rate of the mice (~4 g of chow per day) and average mouse body weight (25 g).

After oral administration, the compound must move along the GI tract before it enters the bloodstream. It encounters a series of barriers and sites of loss which might result in poor absorption and low bioavailability (Benedetti *et al.*, 2009). PK study of three different routes of administration, IV, oral gavage and drug-formulated chow, allowed for the

investigation of the drug concentration in the plasma of *mdx* mice at different time points after administration. Drug-formulated chow presented 19.30% bioavailability, higher than the one of oral gavage (18.07%). Furthermore, the C_{max} of the drug in plasma collected from mice fed with drug-formulated chow was 103.65 ng/mL and the plasma concentration did not go below 30 ng/mL at any time during the treatment. The experiments by Lee *et al.* (2009) have demonstrated that KR-33028 is a very potent NHE1 inhibitor with an IC_{50} of 2.2 nM. It was also demonstrated that KR-33028 presents anti-apoptotic effects and can reduce intracellular Ca^{2+} levels at a concentration as low as 0.01 μ M. Furthermore, KR-33028 is four times more potent than cariporide, which can inhibit NHE1 at a mean concentration of 100 ng/ml (unpublished observations, Hoechst Marion Roussel, Frankfurt, Germany). Based on these and since the concentrations of KR-33028 did not go below 0.122 μ M at any time, it is safe to assume that the detected plasma concentrations were above the MEC of KR-33028 and within the therapeutic window of KR-33028, a range of doses that produce therapeutic response without causing any significant adverse effects and toxicity (Rang *et al.*, 2015).

In conclusion, the mice were treated with ~94.4 mg of KR-33028/kg, a dose significantly lower than the one intended at the beginning of the study. However, based on the findings of the PK study, the treatment resulted in drug plasma concentrations within the therapeutic window of KR-33028, suggesting that the dose could promote a therapeutic effect.

Chapter 4. Investigating the effects of KR-33028 on muscle histology, serum creatine kinase activity and functional strength

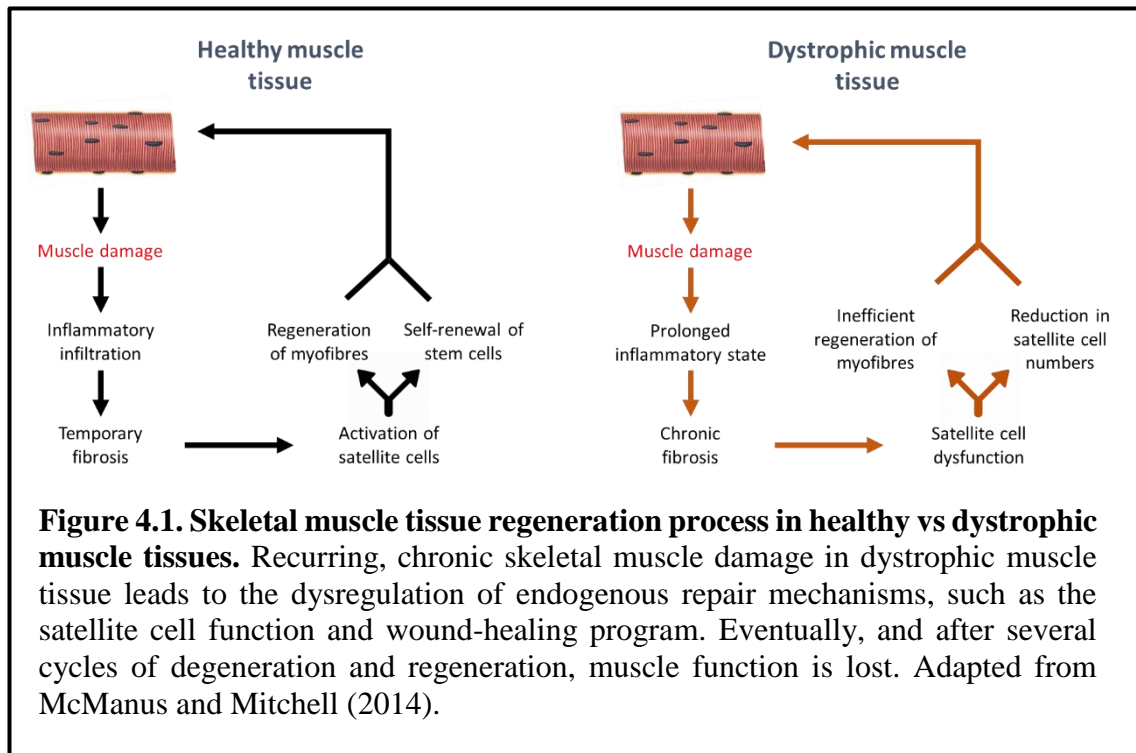
4.1 Introduction and aims

DMD is characterised by chronic muscle degeneration and tissue remodelling which result in reduced muscle force generation, dissociation of tissue ultrastructure, and the replacement of muscle with fat and connective tissue (Mann *et al.*, 2011; Klingler *et al.*, 2012). DMD skeletal muscle cells, as opposed to normal muscle cells, do not possess the capacity to fully regenerate and maintain fibre integrity in response to injury signals. Damaged skeletal muscle fibres undergo necrosis and apoptosis, which then trigger an inflammatory response and a cycle of degeneration and regeneration events (Figure 4.1) (McManus and Mitchell, 2014). Although the exact mechanism leading to sustained muscle repair is unknown, it is thought that the satellite cell pool gets depleted in response to significantly increased replication, during a process termed replicative senescence (Figure 4.1) (Schultz and Lipton, 1982; Zacharias and Anderson, 1991). This process is partly dependent on the length of telomeres, which reduces over the repeated cycles of satellite cell activation and proliferation (Decary *et al.*, 2000; Sacco *et al.*, 2010). Mice possess longer telomeres than humans and this has, therefore, been proposed as one of the reasons why *mdx* mice present a less severe phenotype than DMD patients (Sacco *et al.*, 2010).

Although the regenerative capacity of mammalian hearts is not very well understood (Kikuchi and Poss, 2012; Uygur and Lee, 2016), recent evidence proposes that similarly to the skeletal muscle, cardiac muscle of *mdx* mice might also present regenerative capacity. Richardson *et al.* (2015) propose that in the *mdx* mouse model cardiomyocyte renewal is elevated in response to chronic cardiomyocyte loss in order to maintain cardiac function. Later in life, *mdx* mice develop DCM, similar to that seen in DMD patients, with evidence of cardiomyocyte hypertrophy and cardiac fibrosis (Quinlan *et al.*, 2004; Khouzami *et al.*, 2010; Stuckey *et al.*, 2012).

Notably, the majority of muscles in the *mdx* mouse undergo continuous cycles of degeneration and regeneration instead of undergoing chronic and continuous degeneration. After an initial asymptomatic period, the *mdx* mouse undergoes pronounced muscle fibre necrosis and apoptosis at the age of ~3–6 weeks, accompanied by active

cellular infiltration and sterile inflammation mechanisms (Dangain and Vrbova, 1984; Tanabe *et al.*, 1986; Coulton *et al.*, 1988b; Roig *et al.*, 2004; Willmann *et al.*, 2012). Following the initial degeneration, *mdx* mice are able to repair and reduce muscle destruction, although, necrosis persists at low levels for the rest of their lives (Lynch *et al.*, 2001; Roig *et al.*, 2004). Histologically, the continuous cycles of muscle repair are characterised by increased numbers of centrally located myonuclei in cross-sections of muscle fibres (McManus and Mitchell, 2014).



Another histological parameter that is modified in DMD is muscle fibre size and morphology. In DMD patients after the age of ~5 years old, the number of regenerating, regenerated or split fibres rapidly increases resulting in fibres smaller and less regular in shape when compared to healthy muscle fibres (Watkins and Cullen, 1982). However, *mdx* mice present a pattern of muscle fibre size changes that differs from the one in humans (Dangain and Vrbova, 1984; Tanabe *et al.*, 1986; Coulton *et al.*, 1988b; Roig *et al.*, 2004; Willmann *et al.*, 2012). Dystrophic *mdx* muscle is characterised by a greater variability of muscle fibre sizes than control mouse muscle. During the acute phase of muscle fibre degeneration and regeneration, fibres are on average smaller. Consecutively, *mdx* muscle partially recovers, a subset of muscle fibres show hypertrophy to compensate for an inherent weakness, whereas specific muscle force remains lower (Lynch *et al.*, 2001). Finally, from ~62 weeks of age, *mdx* mouse muscles undergo a late-phase atrophy

during which muscle fibre degeneration can no-longer be compensated for by regeneration (Pastoret and Sebille, 1995).

Naturally, in the human disease smaller muscle fibres tend to be less susceptible to DMD-related damage (Karpati and Carpenter, 1986; Karpati *et al.*, 1988), potentially due to Ca²⁺ handling and cellular mechanics (Khurana *et al.*, 1995). Additionally, muscle groups of the limbs, the diaphragm, and the heart are more severely affected than others. Within affected muscle groups, fast-twitch glycolytic fibres are more susceptible to damage than slow-twitch oxidative fibres (Webster *et al.*, 1988). Similarly to humans, in the *mdx* mouse model certain muscle groups are more severely affected than others (Moens *et al.*, 1993; Ljubicic *et al.*, 2011). Additionally, over the progression of the disease, a fibre type switching from fast to slow-twitch is observed in *mdx* mice (Carnwath and Shotton, 1987; Selsby *et al.*, 2012). Consequently, different *mdx* muscles are preferred for pre-clinical testing (Willmann *et al.*, 2012) with the diaphragm and quadriceps muscles marked as ‘particularly appropriate’ for down-stream morphological and/or biochemical analyses (Table 4.1).

Muscle Name	Type	Morphology	Biochemistry	Function
Diaphragm (DIA) ^a	fast	✓ ✓	✓ ✓	✓ ✓
Extensor digitorum longus (EDL) ^b	fast	✓	✓	✓ ✓
Gastrocnemius (GC) ^c	mixed	✓ ✓	✓ ✓	✓*
Quadriceps (QD) ^d	mixed	✓ ✓	✓ ✓	X
Biceps/Triceps ^e	mixed	✓	✓	X
Tibialis anterior (TA) ^f	fast	✓ ✓**	✓	✓*
Soleus (SOL) ^g	slow	✓ ✓	✓	✓ ✓

Table 4.1. Suitability of different mouse muscles for morphological, biochemical, and functional pre-clinical studies. ✓ ✓ = particularly appropriate; ✓ = appropriate; X = not suitable. ^aSevere phenotype, should be used as much as possible; ^bSmall size: more suitable for functional assays; ^cLarge size, heterogeneous fibre type composition, affected by exercise; ^dLarge size, affected by exercise; ^eAs back-up if GC or QD not sufficient; ^fLarge size, accessible; ^gSmall size. As a purely slow muscle, Soleus is more preserved from dystrophic pathology.

*Only in in situ studies. **Less affected by standard exercise regimes that induce muscle damage and contraction-induced pathological injury; but badly affected during onset of necrosis (Willmann *et al.*, 2012).

Compromised sarcolemmal integrity in DMD leads to increased membrane permeability and the subsequent leak of soluble proteins, such as CK, out of the cell (Allen and Whitehead, 2011). Serum CK is a standard clinical diagnostic marker for DMD used to determine sarcolemmal instability and damage (Hess *et al.*, 1964). Additionally, serum

CK is a widely used marker for disease activity in dystrophic animal models including the *mdx* mouse model (Coulton *et al.*, 1988a).

The cellular and molecular dysfunctions inherent to the disease lead to a decrease in muscle force and function, primary features of DMD. Assessment of muscle strength can be used for the evaluation of disease progression and as both a measure of treatment efficacy in muscular dystrophy studies (Takeshita *et al.*, 2017). *Mdx* mice, similarly to wild-type mice, show an age-dependent increase of their grip strength between 4 and 12 weeks (Aartsma-Rus and van Putten, 2014). Subsequently, both their fore- and hindlimb grip strength decreases, when compared to wild-type animals, in an age-dependent manner (Smith *et al.*, 1995; Spurney *et al.*, 2009; Aartsma-Rus and van Putten, 2014).

The loss of dystrophin function in DMD directly compromises muscle fibre viability (Petrof *et al.*, 1993; Dudley *et al.*, 2006). Additionally, second messenger led pathways, such as apoptotic and proteolytic pathways downstream of elevated intracellular Ca^{2+} levels, are also considered integral to membrane destabilisation and contribute to elevation of oxidative stress, inflammation, and muscle fibre necrosis (Hollinger and Selsby, 2013). Consequently, targeting the elevated intracellular Ca^{2+} levels has been proposed as a way of improving DMD pathology and several pharmacological and molecular treatment approaches that target Ca^{2+} homeostasis have been developed over the years.

The elevation of intracellular Ca^{2+} levels can be attributed to the mechanical damage of the sarcolemma but also deficiencies in several Ca^{2+} -regulatory proteins (Vallejo-Illarramendi *et al.*, 2014; Burr and Molkentin, 2015). Recent data suggests that the dysregulation of calcium homeostasis is also exacerbated by the increased activity of the NHE1 exchanger (Deval *et al.*, 2002; Iwata *et al.*, 2007; Burr *et al.*, 2014; Bkaily *et al.*, 2015). NHE1 over-activity leads to an increased influx of Na^+ , which in turn switches the NCX exchanger into reverse mode, resulting in an increased Ca^{2+} influx.

This project introduces the inhibition of NHE1 by using the KR-33028 compound, a very specific and potent NHE1 inhibitor with a good safety and potency profile (Kim *et al.*, 2005; Jung *et al.*, 2006; Kim *et al.*, 2006; Kim *et al.*, 2007a; Kim *et al.*, 2007b; Kim *et al.*, 2007c; Oh *et al.*, 2007; Lee *et al.*, 2009), as a way to improve the DMD pathology. It was hypothesised that chronic treatment of *mdx* mice with the KR-33028 NHE1 inhibitor would lead to a decrease of intracellular Na^+ levels, reversal of the NCX back to normal and subsequent decrease of Ca^{2+} influx within the skeletal and cardiac muscle cells.

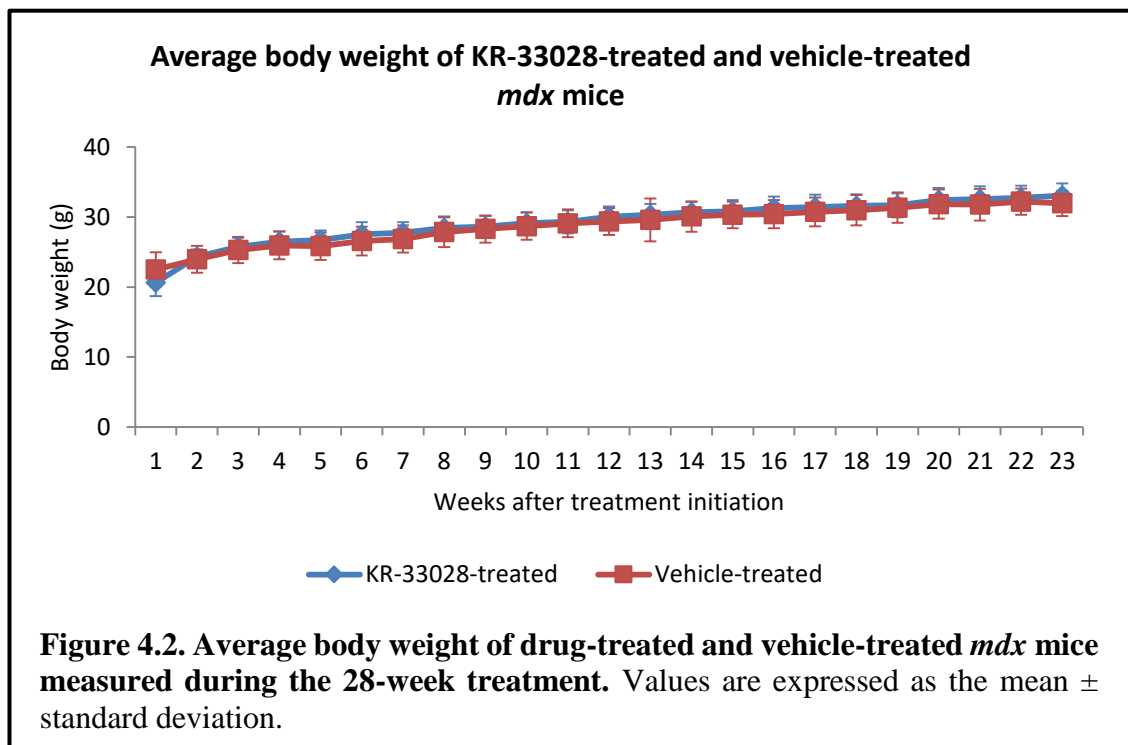
Aims of the experiments described in this chapter:

- Histological assessment of dystrophin-deficient pathology in heart, diaphragm and quadriceps muscles harvested from KR-33028-treated and vehicle-treated *mdx* mice.
- Assessment of functional four-limb grip strength of KR-33028-treated *mdx* mice in comparison to vehicle-treated *mdx* mice.
- Comparison of serum CK levels of KR-33028-treated *mdx* mice vs vehicle-treated *mdx* mice.

4.2 Treatment of *mdx* mice with KR-33028 NHE1 inhibitor

Eleven male *mdx* mice were treated chronically, for a period of 28 weeks, with the KR-33028 NHE1 inhibitor. To investigate the effects of the treatment on the development and progression of the diseases, we initiated the treatment of the mice at the youngest possible age, 6 weeks old. The drug was administered through drug-formulated chow that was formulated using the compound to a final concentration of 590 mg per kilogram of chow, and which was provided ad libitum.

The mice were monitored throughout the treatment and the chow was weighed once a week in order to estimate the eating rate of the mice. It was estimated that each mouse consumed ~4.05 g of drug-formulated chow per day, which was equivalent to a daily dose of ~94.4 mg/kg; estimated based on average mouse body weight (25 g). During the study, animals treated with KR-33028 presented no changes in behavioural response, food and water intake, or mortality. Furthermore, KR-33028-treated animals had a normal body growth and weight gain (Figure 4.2) comparable to the vehicle-treated animals during the 28 weeks of treatment. At the end of treatment, both groups of mice, drug-treated and vehicle-treated, were sacrificed and organs were harvested.

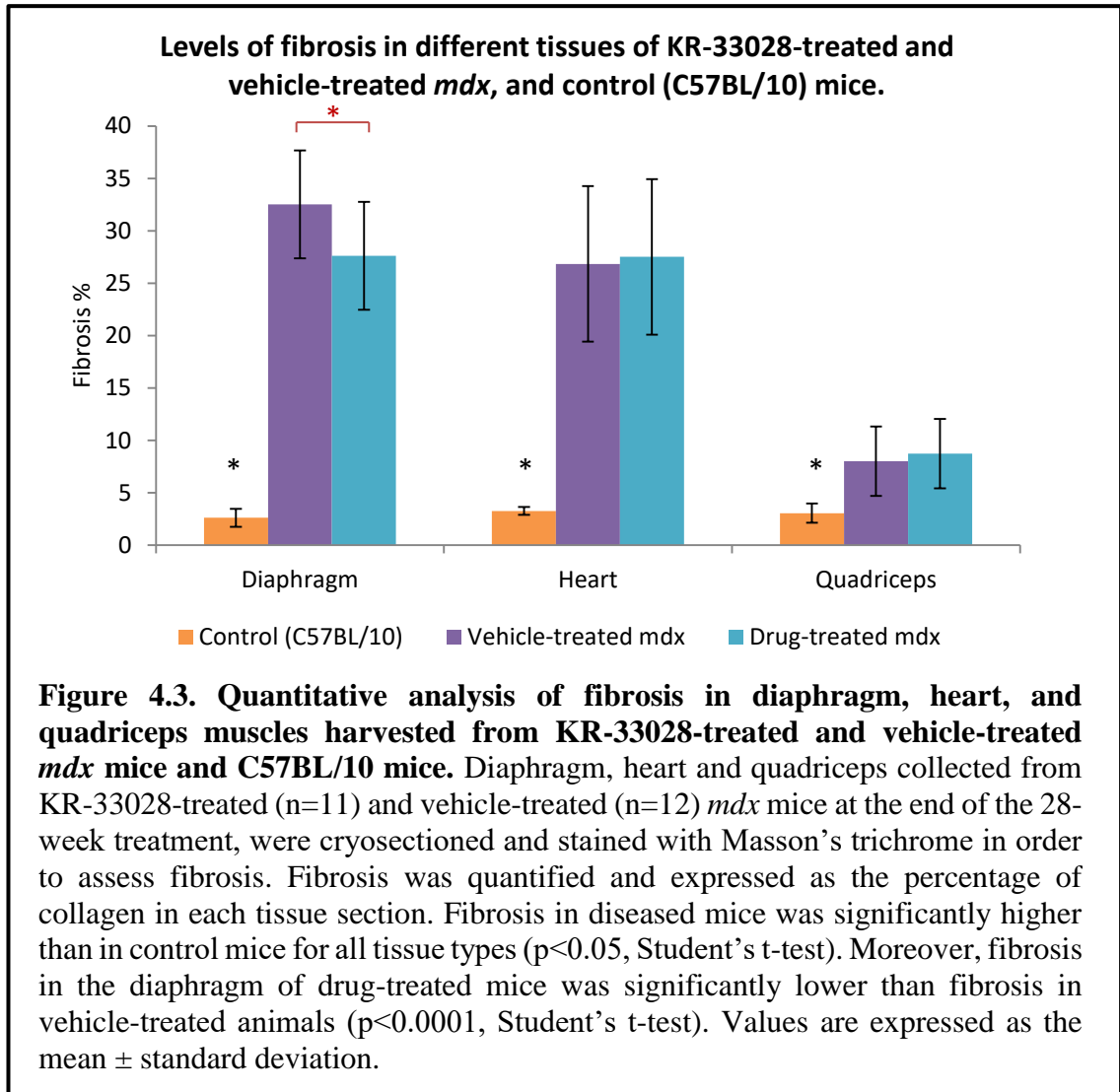


Subacute toxicity studies have previously demonstrated that high doses of KR-33028 may cause enlargement of spleen in male rats (Jung *et al.*, 2006). No evidence of drug toxicity

was observed in our study, i.e. the weight of the spleen was not significantly different between the two groups of mice, KR-33028- and vehicle-treated.

4.3 Histological assessment of muscle pathology in KR-33028- and vehicle-treated *mdx* mice

4.3.1 Quantitative analysis of fibrosis



Muscle tissues collected from KR-33028- and vehicle-treated *mdx* mice were cryosectioned and stained with Masson's trichrome (Figure 4.4; Figure 4.5; Figure 4.6), a trichrome stain intended for distinguishing connective tissue and collagen fibres from muscle fibres (Sheehan and Hrapchak, 1980). Fibrosis was expressed as the percentage of collagen tissue (blue staining) in whole tissue cross-sections. Fibrosis in vehicle-treated *mdx* mice was significantly higher than fibrosis in control tissues ($p < 0.0001$, Student's t-test). Moreover, it was demonstrated that fibrosis in the diaphragm of drug-treated mice was significantly lower than the one in the diaphragm of vehicle-treated mice. However,

fibrosis of the heart and quadriceps muscles of KR-33028-treated mice was not significantly different than the one in vehicle-treated animals (Figure 4.3).

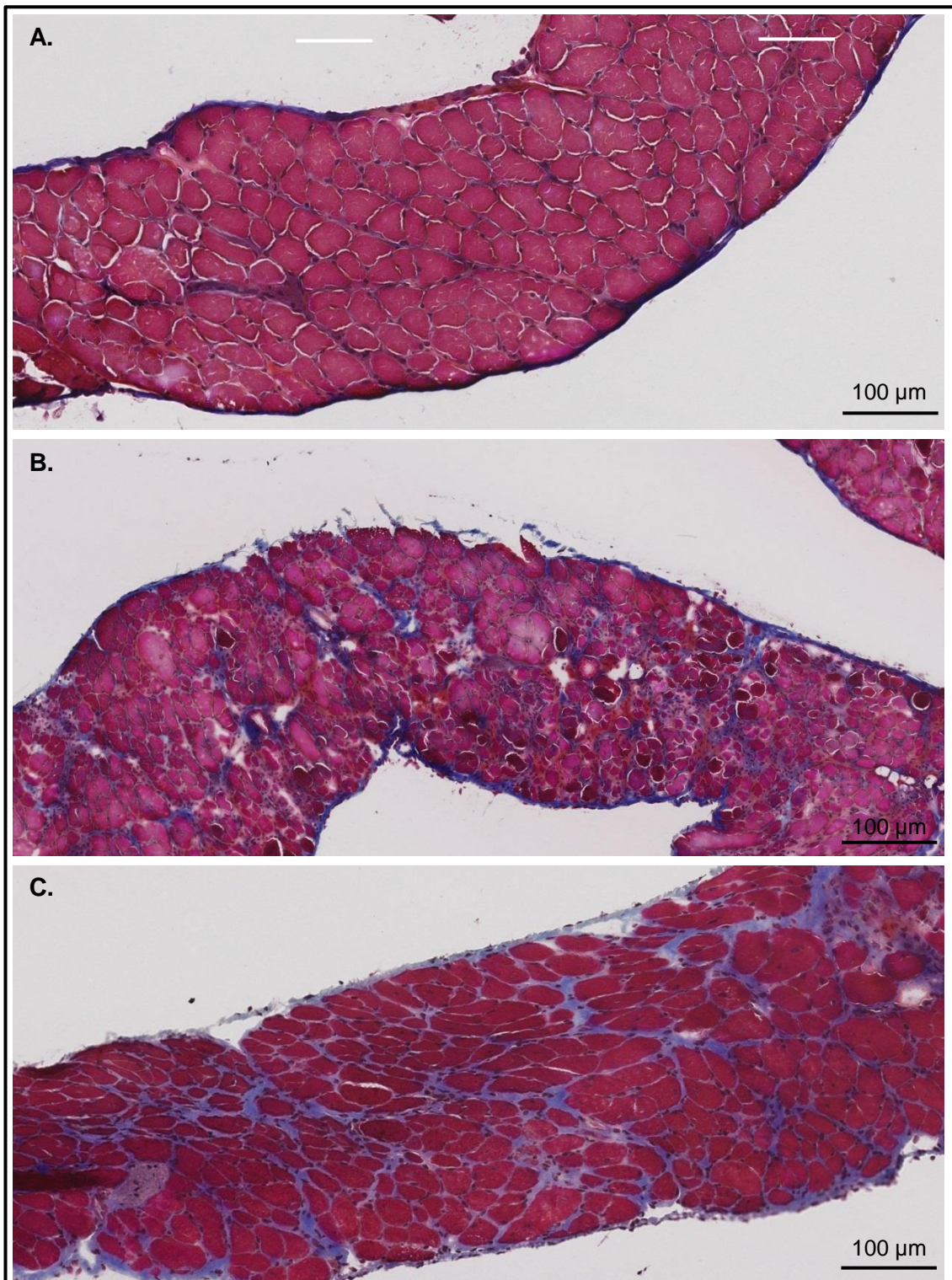


Figure 4.4. Masson's trichrome staining of diaphragm harvested from A. control (C57BL/10) mice, B. vehicle-treated *mdx* mice and C. KR-33028-treated *mdx* mice. Diaphragm tissue samples were collected from KR-33028-treated (n=11) and vehicle-treated (n=12) *mdx* mice at the end of the 28-week treatment period. Additionally, diaphragm samples from age-matched control mice (n=3) were harvested for comparative purposes. 8 µm serial sections were cut along the entire muscles, separated by intervals of about 160 µm between the sets of serial sections, and were embedded on Superfrost Slides. In order to assess fibrosis, tissue sections were stained with Masson's trichrome. As a result, cytoplasm and muscle fibres were stained red, nuclei black and collagen blue. Images were obtained using a Leica SCN400 slide scanner at a x10 magnification.

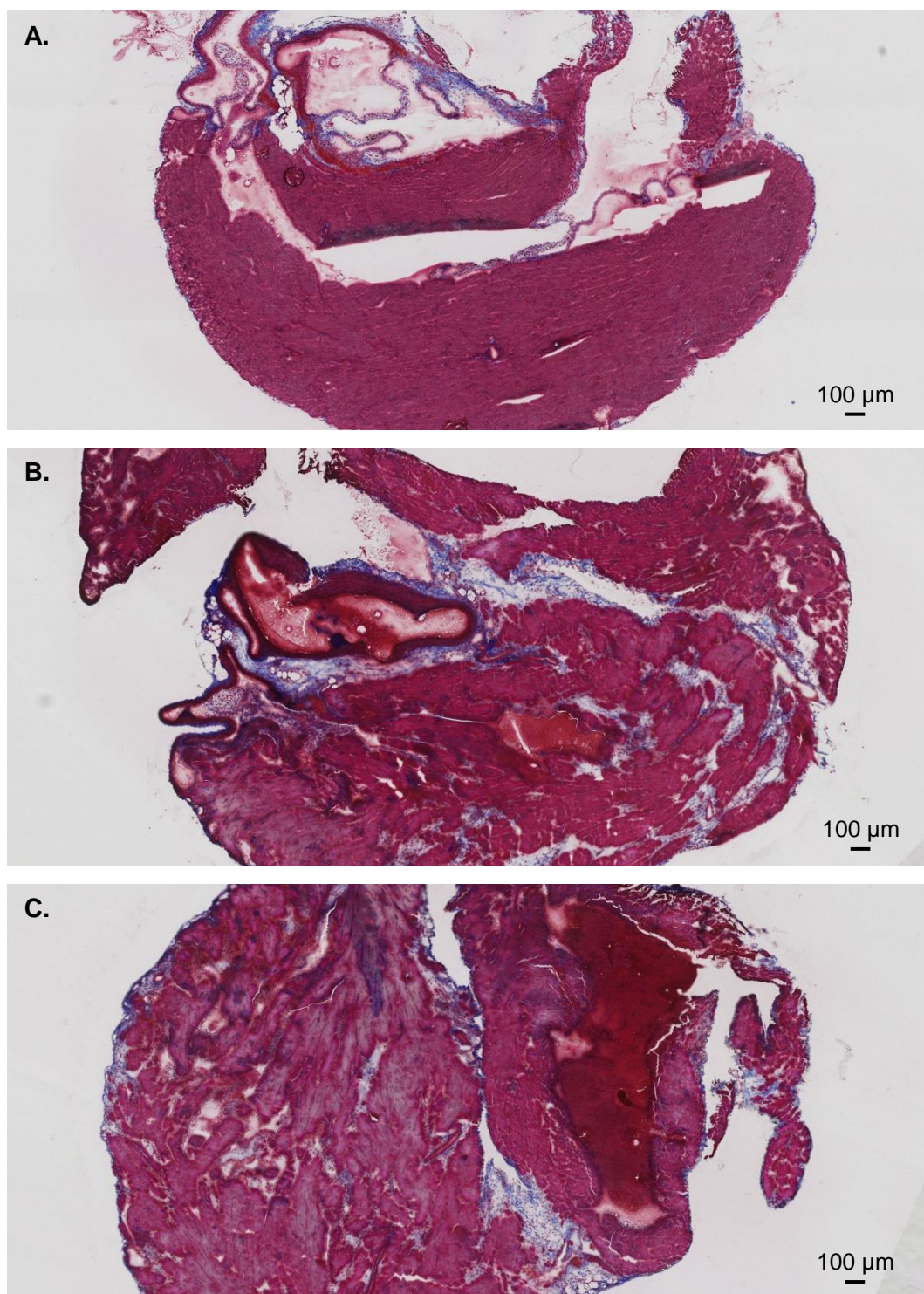


Figure 4.5. Masson's trichrome staining of cardiac muscle tissues harvested from A. control (C57BL/10) mice, B. vehicle-treated *mdx* mice and C. KR-33028-treated *mdx* mice. Hearts were collected from KR-33028-treated (n=11) and vehicle-treated (n=12) *mdx* mice at the end of the 28-week treatment period. Additionally, hearts from age-matched control mice (n=3) were harvested for comparative purposes. 8 µm serial sections were cut along the entire muscles, separated by intervals of about 160 µm between the sets of serial sections, and were embedded on Superfrost Slides. In order to assess fibrosis, tissue sections were stained with Masson's trichrome. As a result, cytoplasm and muscle fibres were stained red, nuclei black and collagen blue. Images were obtained using a Leica SCN400 slide scanner at a x4 magnification.

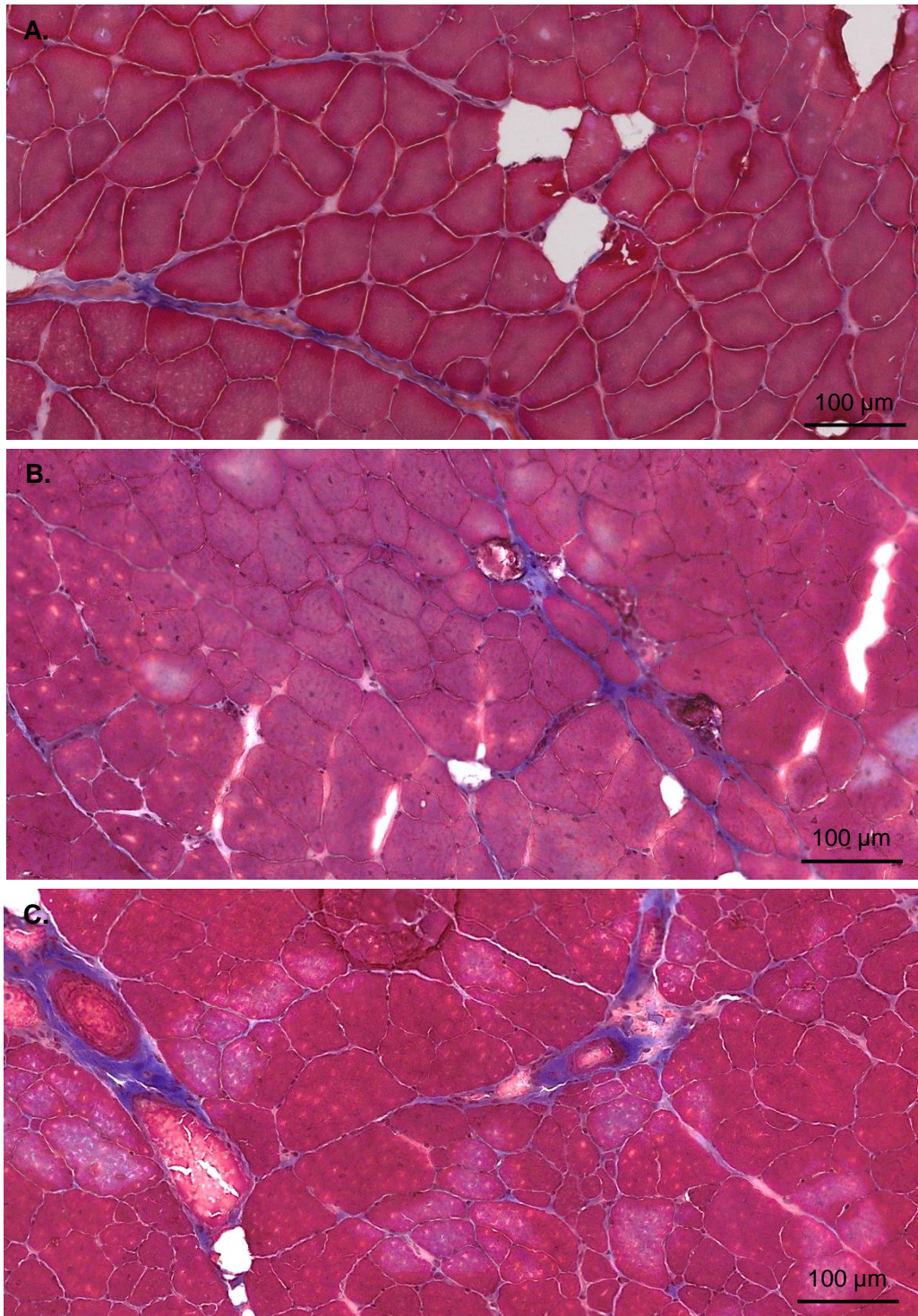
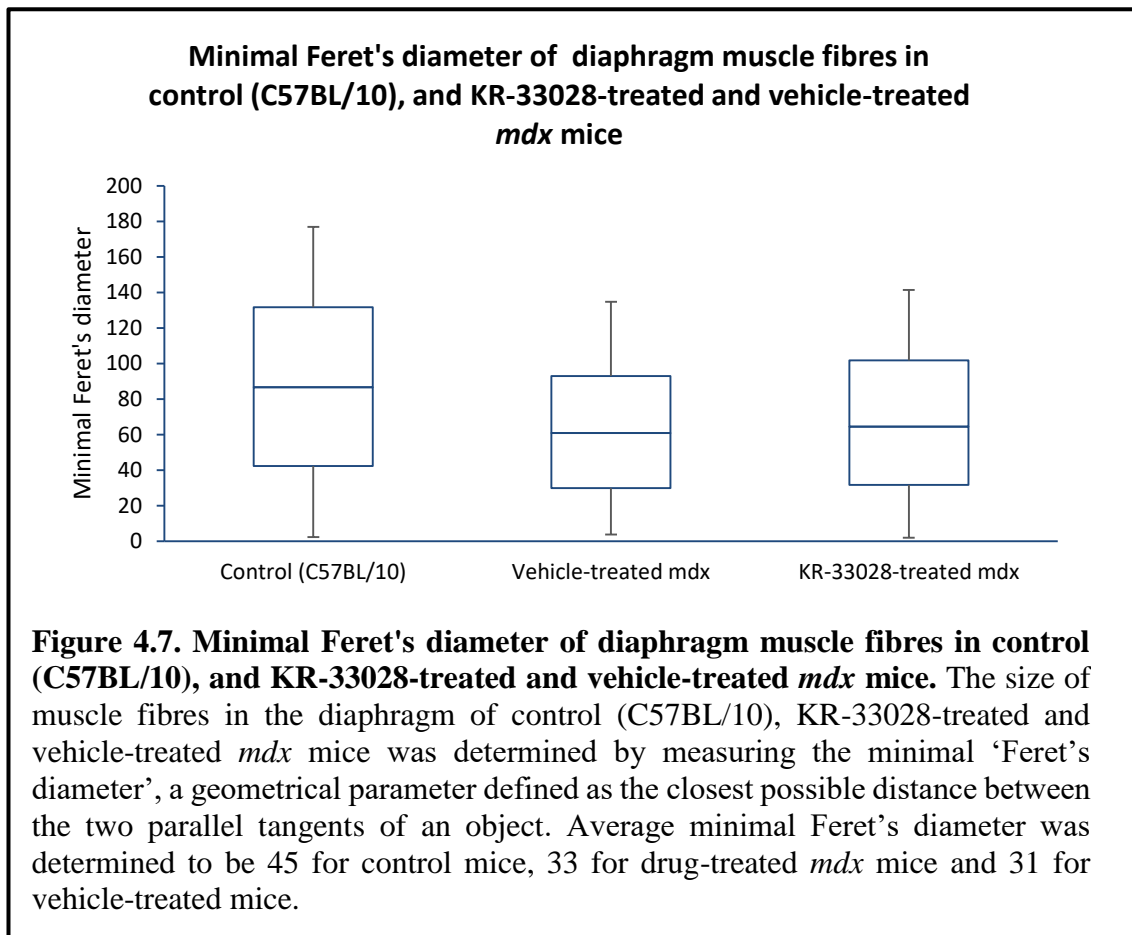


Figure 4.6. Masson's trichrome staining of quadriceps muscle tissues harvested from A. control (C57BL/10) mice, B. vehicle-treated *mdx* mice and C. KR-33028-treated *mdx* mice. Quadriceps muscles were collected from KR-33028-treated (n=11) and vehicle-treated (n=12) *mdx* mice at the end of the 28-week treatment period. Additionally, quadriceps samples from age-matched control mice (n=3) were harvested for comparative purposes. 8 µm serial sections were cut along the entire muscles, separated by intervals of about 160 µm between the sets of serial sections, and were embedded on Superfrost Slides. In order to assess fibrosis, tissue sections were stained with Masson's trichrome. As a result, cytoplasm and muscle fibres were stained red, nuclei black and collagen blue. Images were obtained using a Leica SCN400 slide scanner at a x20 magnification.

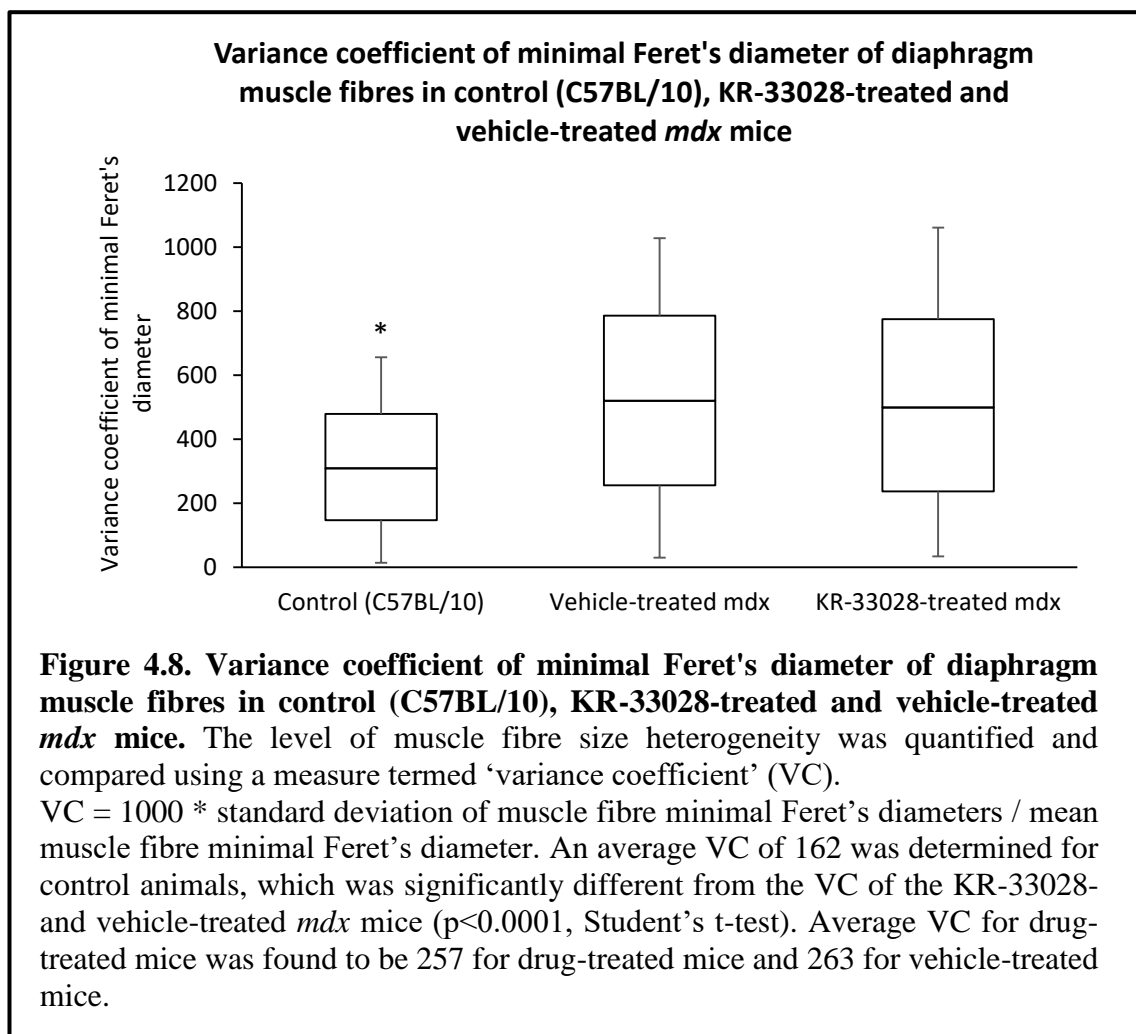
4.3.2 Evaluation of muscle fibre size variation

In order to investigate the skeletal muscle damage present in the diaphragm of vehicle-treated and KR-33028-treated *mdx* mice, nuclei and cytoplasm were delineated using standard haematoxylin and eosin (H&E) staining. For comparative purposes, diaphragm from age-matched control (C57BL/10) mice was also analysed histologically using H&E. Both groups of *mdx* mice, KR-33028- and vehicle-treated, presented clear regions of fibre size variation, mononuclear cell infiltrations, and instances of hyalinated or necrotic fibres that were absent in control tissues (Figure 4.9).



Indicative of many factors influencing muscle remodelling processes, the level of muscle fibre size heterogeneity can be quantified and compared using a measure termed 'variance coefficient' (VC). VC is defined as the standard deviation of muscle fibre minimal diameters divided by the mean muscle fibre minimal diameter, then multiplied by 1000 (Briguet *et al.*, 2004). Due to cryosectioning of tissue at variable oblique angles, fibre size inconsistencies can be introduced. To compensate for this, the size of muscle fibres was determined by measuring the minimal 'Feret's diameter' (Figure 4.7), a geometrical parameter defined as the closest possible distance between the two parallel tangents of an object (i.e. muscle fibre) (Briguet *et al.*, 2004). Using the measure of muscle fibre

variability across whole muscle cross-sections, an average VC of 257 was determined for KR-33028-treated *mdx* mice, compared to 263 for vehicle-treated *mdx* mice, and 162 for control animals (Figure 4.8).



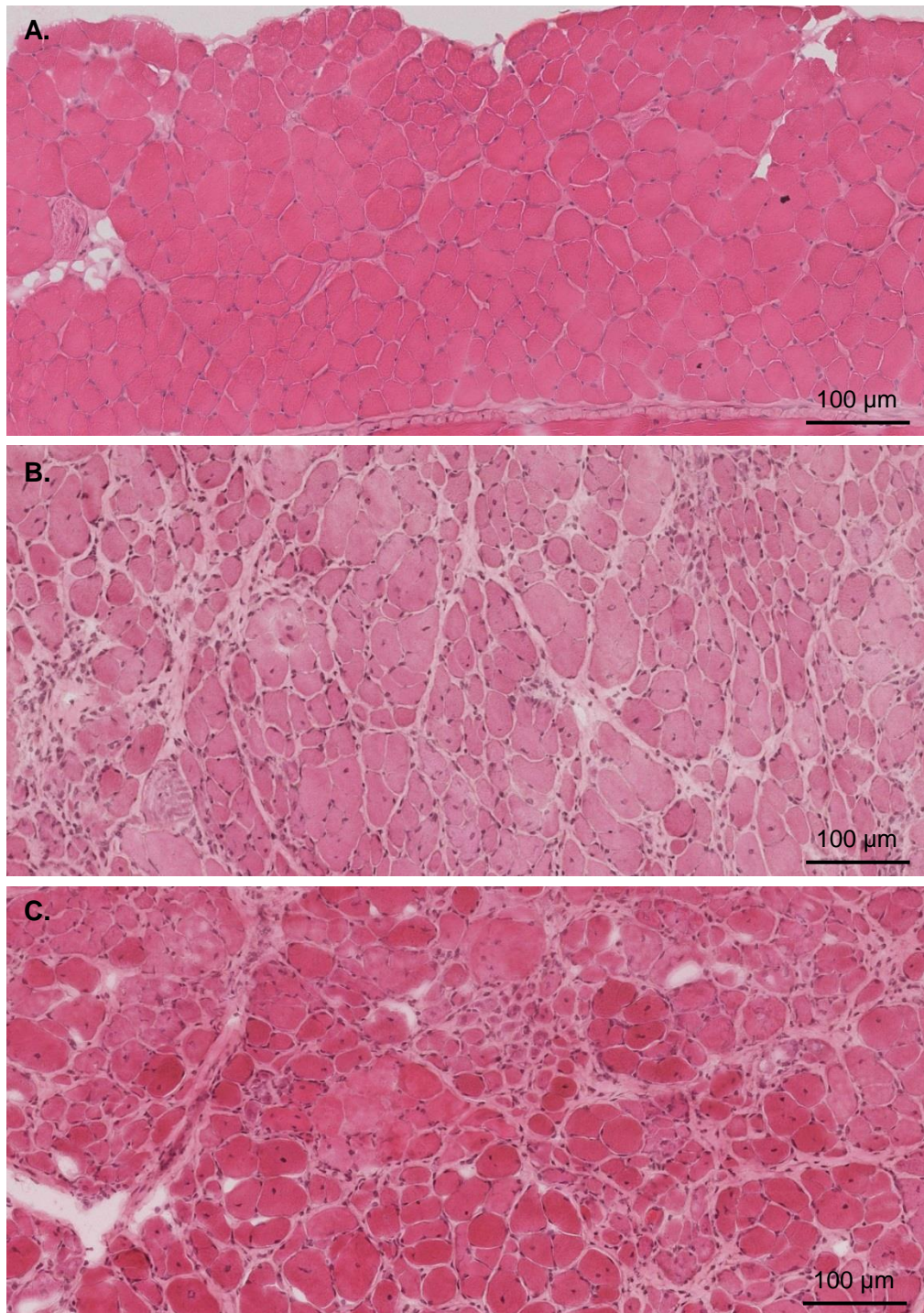
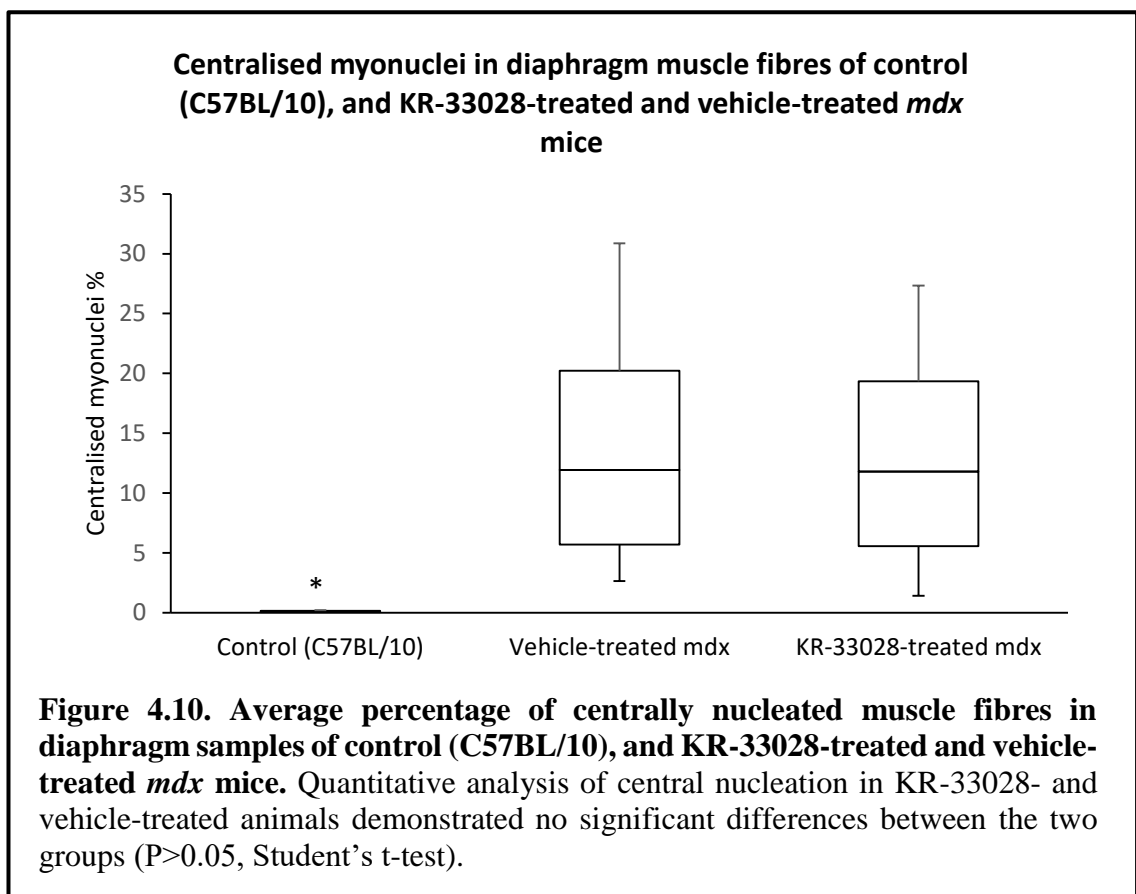


Figure 4.9. Haematoxylin and eosin (H&E) staining of diaphragm muscle tissues harvested from A. control (C57BL/10) mice, B. vehicle-treated *mdx* mice and C. KR-33028-treated *mdx* mice. Diaphragm tissue samples were collected from KR-33028-treated (n=11) and vehicle-treated (n=12) *mdx* mice at the end of the 28-week treatment period. Additionally, diaphragm samples from age-matched control mice (n=3) were harvested for comparative purposes. 8 µm serial sections were cut along the entire muscles, separated by intervals of about 160 µm between the sets of serial sections, and were embedded on Superfrost Slides. Tissue sections were stained with H&E. As a result, cytoplasm and muscle fibres were stained red, and nuclei black. Images were obtained using a Leica SCN400 slide scanner at a x10 magnification. Dystrophic *mdx* mouse tissues are characterised by increased muscle fibre size variation and central nucleation.

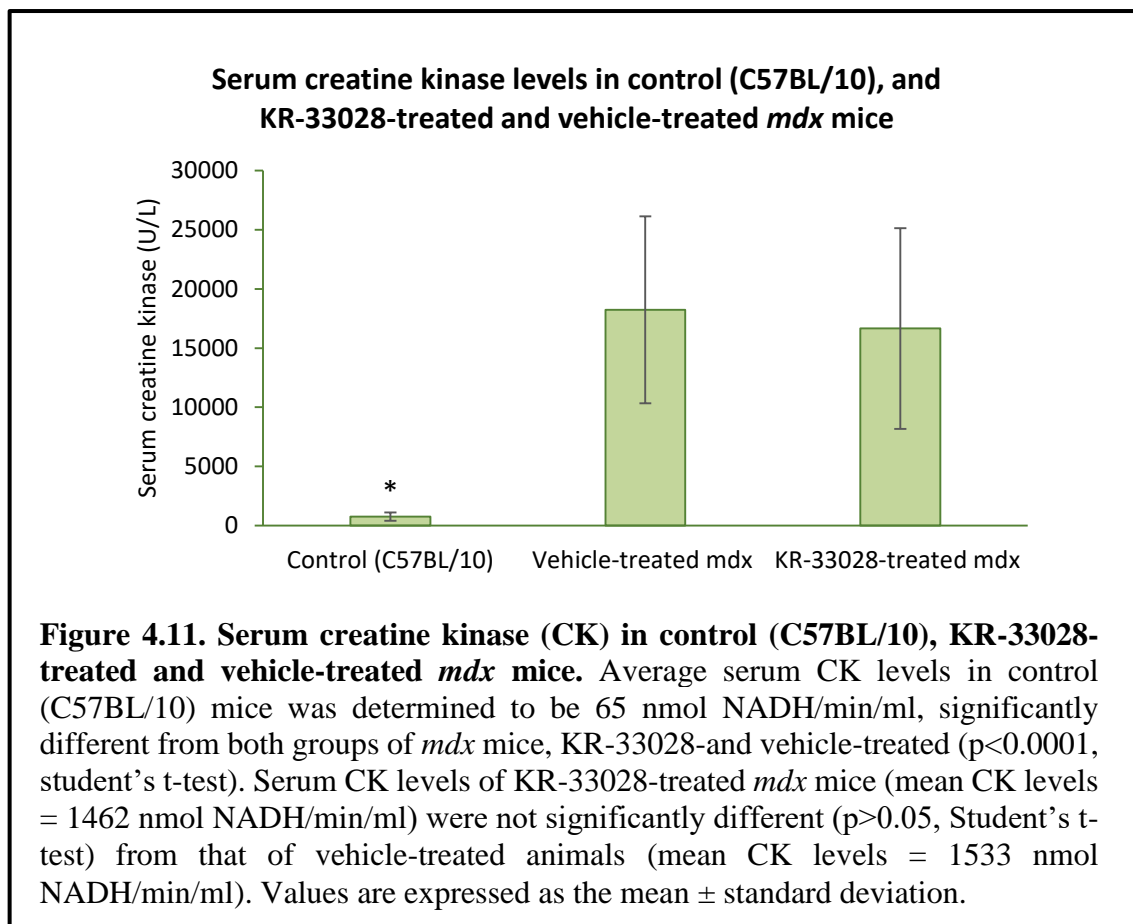
4.3.3 Quantitation of centrally nucleated muscle fibres

In addition to the muscle fibre size variation, increased numbers of centrally nucleated fibres are indicative of the degeneration-regeneration cycles dystrophic fibres undergo and are therefore used as a measure of pathological severity (Spurney *et al.*, 2009). Quantitative analysis of central nucleation in muscle fibres from diaphragm tissue samples harvested from KR-33028-treated and vehicle-treated animals, demonstrated no significant effects of KR-33028 NHE1 inhibitor on the levels of central nucleation (Figure 4.10).



4.4 Assessment of CK levels in KR-33028- and vehicle-treated *mdx* mice

Serum CK analysis provides an indication of muscle fibre damage. An enzymatic CK detection kit was used to measure the levels of CK in serum collected from KR-33028- (n=11) and vehicle-treated *mdx* (n=12) mice. Serum CK levels of KR-33028-treated *mdx* mice (mean CK levels = 1462 nmol NADH/min/ml) was not significantly different ($p>0.05$, Student's t-test) from that of vehicle-treated animals (mean CK levels = 1533 nmol NADH/min/ml) (Figure 4.11). For comparative purposes, CK was also determined in control (C57BL/10) animals (mean CK level = 65 nmol NADH/min/ml; Figure 4.11).



4.5 Assessment of functional grip strength in KR-33028- and vehicle-treated *mdx* mice

A functional four-limb hanging test was carried out throughout the treatment of the mice in order to determine the effect of KR-33028 on muscle function, most likely related to muscle strength. The four-limb hang test employed a wire grid system to non-invasively measure the ability of the mice to exhibit sustained limb tension to oppose their gravitational force (Figure 4.12.A.) (Aartsma-Rus and van Putten, 2014).

The test demonstrated a significant increase of the grip strength of the KR-33028-treated *mdx* mice in comparison to the vehicle-treated ones ($p < 0.05$, Student's t-test; Figure 4.12.B.). Towards the end of the treatment a decrease of the performance of the mice had been observed in both groups and can be attributed to altered conditions, such as lighting in the room where mice were kept, which induced external stress to the mice.

The maximum holding impulse that the group of drug-treated mice had achieved during the 28-week treatment was 74.86 N sec, in comparison to 43.61 N sec that the vehicle-treated mice achieved. Control age-matched mice (C57BL/10) achieved a maximum holding impulse of 91.3 N sec during the pilot study conducted prior the initiation of this project (unpublished data). This equates to a 65% improvement of functional grip strength as a result of the KR-33028 treatment (based on the equation: $100 \times (\text{HI}_{(\text{mdx-controls})} - \text{HI}_{(\text{mdx-test-conditions})}) / (\text{HI}_{(\text{mdx-controls})} - \text{HI}_{(\text{wild-type})})$), where: $\text{HI}_{(\text{mdx-controls})}$ is the maximum holding impulse of the vehicle-treated *mdx* mice, $\text{HI}_{(\text{mdx-test-conditions})}$ is the maximum holding impulse of the KR-33028-treated *mdx* mice, and $\text{HI}_{(\text{wild-type})}$ the maximum holding impulse of the control animals (C57BL/10)).



B. Functional grip strength of KR-33028-treated Vs vehicle-treated *mdx* mice

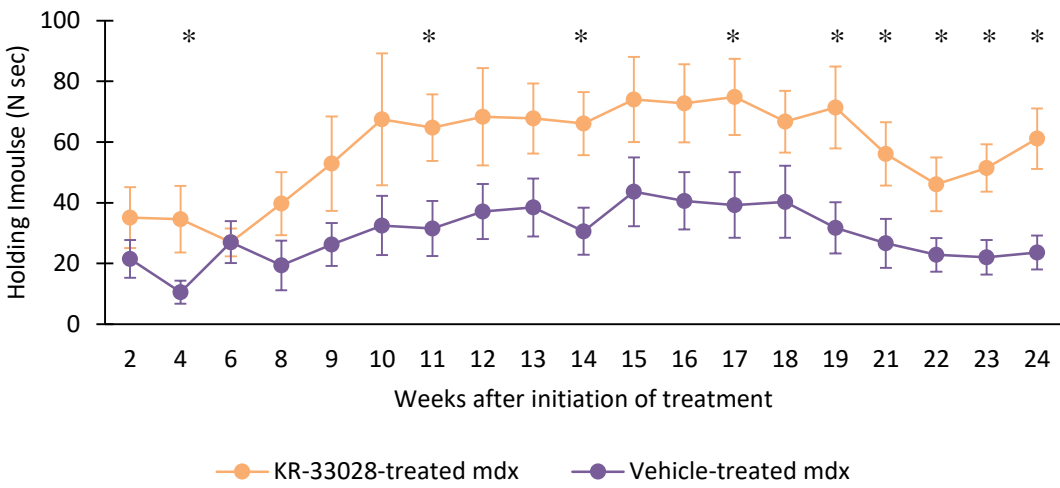


Figure 4.12. Assessing functional four limb grip strength of KR-33028- and vehicle-treated *mdx* mice. **A.** A functional four-limb grip strength test was employed to measure the grip strength of the mice throughout the treatment. Each mouse was put upside down the wire grid and the time it took for the mouse to fall off the grid was measured (hang time). The hang time was then converted into holding impulse (Holding Impulse = hang time * body weight in grams * 9.806×10^{-3} N sec). The test was repeated four times for each mouse and then the best attempt was estimated. **B.** The functional four-limb grip strength test demonstrated a significant increase of the grip strength of the drug-treated mice (n=11) as opposed to the vehicle-treated ones (n=12; $p < 0.05$, Student's t-test). Stars on the graph demonstrate significant difference between the two groups. Values are expressed as the mean \pm standard error of the mean.

4.6 Discussion and conclusions

The experiments described in the current chapter have sought to investigate the effects of the KR-33028 NHE1 inhibitor on the pathophysiology of DMD using the *mdx* mouse model of this disease. A total of 11 *mdx* mice were chronically treated (~28 weeks) with ~94.4 mg of KR-33028/kg via drug-formulated chow. Notably, KR-33028-treated animals had a normal body growth and presented no changes in their behavioural response, food and water intake, or mortality.

Following the treatment, mice were sacrificed, and selected muscle tissues were histologically stained in order to assess the impact of KR-33028 on muscle histology. It was demonstrated that the fibrosis in the diaphragm of treated animals, when compared to vehicle-treated mice, was significantly lower signifying a positive impact of the treatment on the DMD pathology of the *mdx* mice. However, fibrosis in heart and quadriceps muscles of KR-33028-treated mice did not present any significant differences from the one in vehicle-treated animals. This discordant tissue effectiveness could relate to variations in pathological severity of the analysed tissues (Moens *et al.*, 1993; Muller *et al.*, 2001; Ljubicic *et al.*, 2011). Diaphragm is the most severely affected muscle in the *mdx* mouse model with prominent dystrophic changes, which reproduce the degenerative pattern observed in DMD (Stedman *et al.*, 1991; Ragusa *et al.*, 1996; Reid and MacGowan, 1998; Jørgensen *et al.*, 2011).

Muscle fibre size variation and the number of centrally nucleated muscle fibres, both markers of ongoing muscle regeneration, in diaphragm muscle samples were not improved by the long-term treatment with KR-33028. However, as noted by Jørgensen *et al.* (2011), the presence of centrally located myonuclei only indicates that regeneration has taken place, but does not indicate the amount of times each individual muscle fibre has undergone a round of degeneration-regeneration. Consequently, it can be speculated that, if the muscles have undergone fewer degeneration-regeneration cycles, the satellite cell pool will not be exhausted enabling muscle fibre repair. This could potentially result in the observed pattern of regeneration (indicated by high muscle fibre size variation and number of centrally nucleated muscle fibres) with reduced fibrosis.

Muscle functional and strength measurements are the most clinically relevant assessments of treatment efficacy in muscular dystrophy clinical and pre-clinical studies. The most encouraging finding of this chapter was the significant increase of the functional four-limb grip strength in mice treated with KR-33028, depicting a positive effect of KR-

33028. The difference in the muscle strength between the two *mdx* mouse groups, KR-33028-treated and vehicle-treated, became apparent early on during the treatment (significance observed at 4 weeks after treatment initiation). Drug-treated *mdx* mice achieved a 65% improvement in their fore- and hindlimb grip strength as a result of the 6-month KR-33028 treatment, in comparison to the vehicle-treated *mdx* mice.

Despite the histological and functional assessments demonstrating a positive effect of KR-33028 on the *mdx* muscle damage, the serum CK levels of the drug-treated *mdx* mice did not appear significantly different from the ones in vehicle-treated animals. Notably, as highlighted by Spurney *et al.* (2009), due to the mild phenotype and the extent of regeneration observed in the *mdx* mouse model, correlation of CK levels with histological parameters and functional data is difficult. A series of studies have previously demonstrated an improvement of functional and histological parameters that was not accompanied by a decrease of the elevated CK levels (Anderson *et al.*, 1996; Granchelli *et al.*, 2000).

In conclusion, the findings of this chapter suggest that KR-33028 has the potential of improving both histological and functional aspects of DMD pathophysiology. It is also evident that using the *mdx* mouse model for pre-clinical assessment of the efficacy of treatments for DMD is not ideal due to its phenotype being milder than the one in DMD patients. Mouse models that are not characterised by continuous phases of regeneration following necrosis, and which present a more severe phenotype, would be more suitable for pre-clinical animal studies.

Chapter 5. Applying magnetic resonance imaging (MRI) to investigate the effects of KR-33028

MRI is one of the most powerful and most studied *in vivo* imaging techniques. It is of great interest in pre-clinical research, but also in clinical diagnostics, because it provides a non-invasive way to obtain high spatial resolution images of soft tissues (Silva and Bock, 2008; Malheiros *et al.*, 2015).

5.1 Manganese-enhanced magnetic resonance imaging (MEMRI)

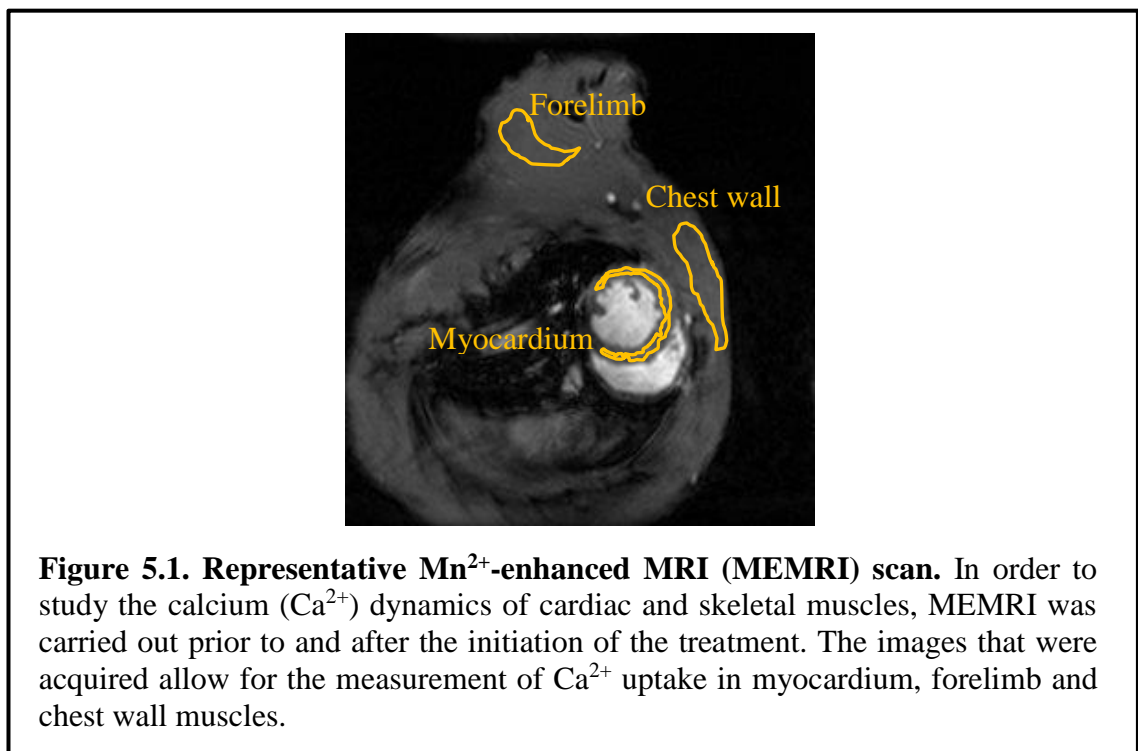
5.1.1 Introduction and aims

Great efforts have been made towards the development of contrast agents that add biochemical, molecular and physiological information to the detailed anatomical information already provided by MRI (Silva and Bock, 2008). Paramagnetic manganese ions (Mn^{2+}) are a molecular contrast agent first studied by London *et al.* (1989). They present chemical properties and ionic radius similar to that of Ca^{2+} and can enter excitable cells via several types of Ca^{2+} channels, such as voltage-gated Ca^{2+} channels and the $\text{Na}^+/\text{Ca}^{2+}$ exchanger (Murphy *et al.*, 1991; Mason *et al.*, 1993; Kerper and Hinkle, 1997; Finley, 1998). Notably, Mn^{2+} can also enter the mitochondria through the mitochondrial Ca^{2+} uniporter (Takeda, 2003). Consequently, the use of Mn^{2+} as an MRI contrast agent offers a non-invasive technique, also referred to as Mn^{2+} -enhanced MRI or MEMRI, for indirect assessment of the intracellular Ca^{2+} flux fluctuations *in vivo* (Hu *et al.*, 2001; Cacace *et al.*, 2014). MEMRI has been used to assess a series of conditions associated with Ca^{2+} ions, including neuronal tract tracing and axonal transport (Inoue *et al.*, 2011; Majid *et al.*, 2014), brain activity (Cha *et al.*, 2016; Schroeder *et al.*, 2016), cardiac function (Chen *et al.*, 2005; Andrews *et al.*, 2015), ischaemia-reperfusion (Zhao *et al.*, 2015), injury (Rodriguez *et al.*, 2016; Yang *et al.*, 2016) and muscular dystrophy (Blain *et al.*, 2013; Grealley *et al.*, 2013; Blain *et al.*, 2015; Loehr *et al.*, 2016).

One of the major pathological characteristics of dystrophic muscle is the elevation of intracellular Ca^{2+} levels. This has been attributed to the mechanical damage of the sarcolemma, but also deficiencies in several Ca^{2+} -regulatory proteins, including Ca^{2+} leak channels, mechanosensitive Ca^{2+} channels, and store-operated Ca^{2+} entry (SOCE) channels (Vallejo-Illarramendi *et al.*, 2014). Recent evidence suggests that the dysregulation of Ca^{2+} homeostasis is also exacerbated by the increased activity of the NHE1 exchanger. NHE1 over-activity leads to an increased influx of Na^+ , which in turn

switches the NCX exchanger into reverse mode, resulting in an increased Ca^{2+} influx (Deval *et al.*, 2002; Iwata *et al.*, 2007). Previous MEMRI experiments have demonstrated that *mdx* mice present elevated Mn^{2+} uptake in their myocardium, forelimb and chest-wall muscles when compared to age-matched control (C57BL/10) mice (Greally *et al.*, 2012; Greally *et al.*, 2014).

We hypothesised that the long-term treatment of *mdx* mice, a widely used DMD mouse model, with the KR-33028 NHE1 inhibitor will lead to a decrease of intracellular Na^+ levels, reversal of the NCX back to normal and subsequent decrease of the Ca^{2+} influx within the skeletal and cardiac muscle cells. In order to investigate this, MEMRI was carried out prior to and at the end of drug treatment. Gradient echo short axis images were acquired through the heart at the level of the papillary muscles. The slice was also planned to include the left upper forelimb within the field of view. This slice allowed 3 muscles/groups to be analysed – myocardium, muscles of the upper forelimb and the chest wall muscles ventral to the heart (Figure 5.1).



Experiments using MEMRI during this study aimed to:

- Compare the Ca^{2+} influx in skeletal and heart muscles of the KR-33028-treated *mdx* mice before and after the 6-month treatment.
- Compare the Ca^{2+} influx in skeletal and heart muscles of the KR-33028-treated *mdx* mice to that of vehicle-treated *mdx* mice at the end of the 6-month treatment.

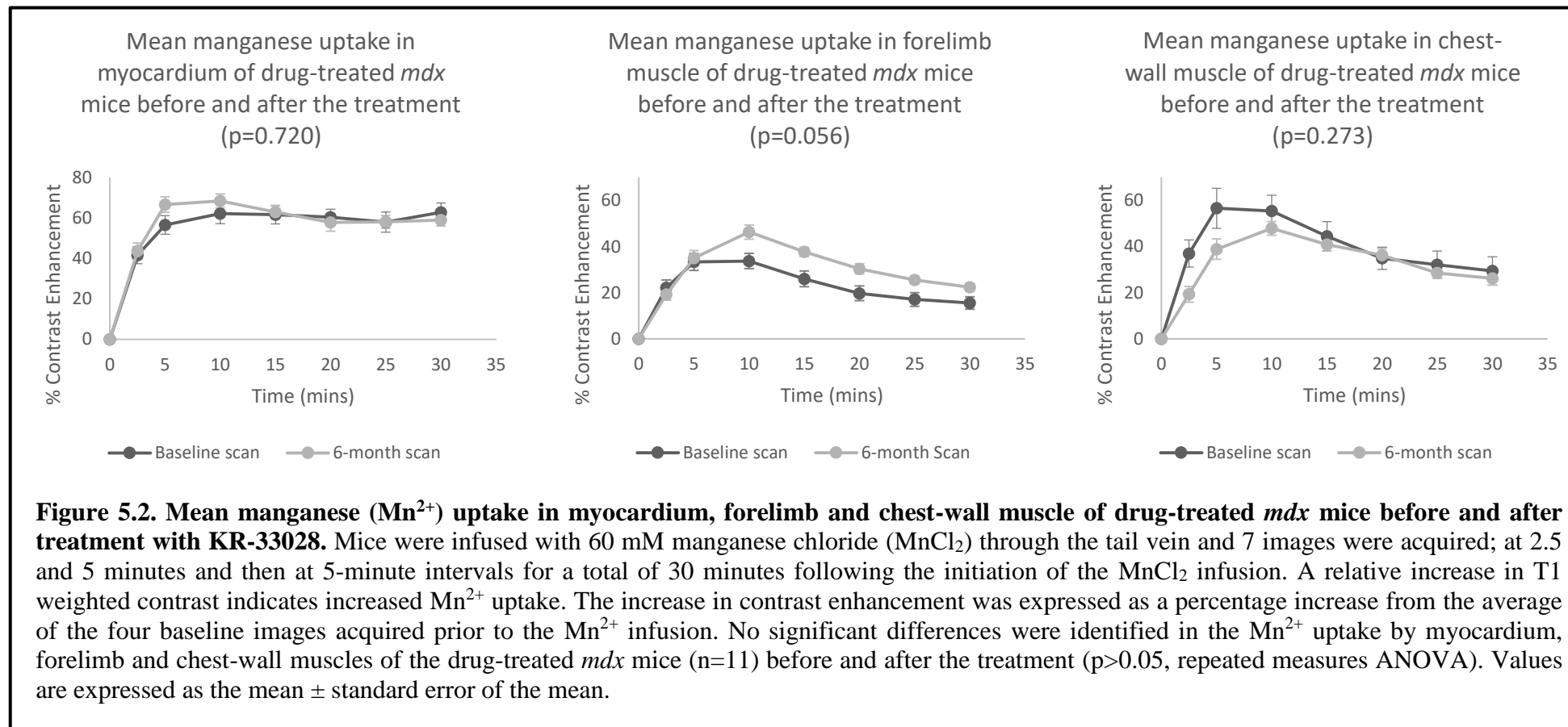
5.1.2 Effects of long-term treatment with KR-33028 on Ca²⁺ influx in skeletal and heart muscles of mdx mice.

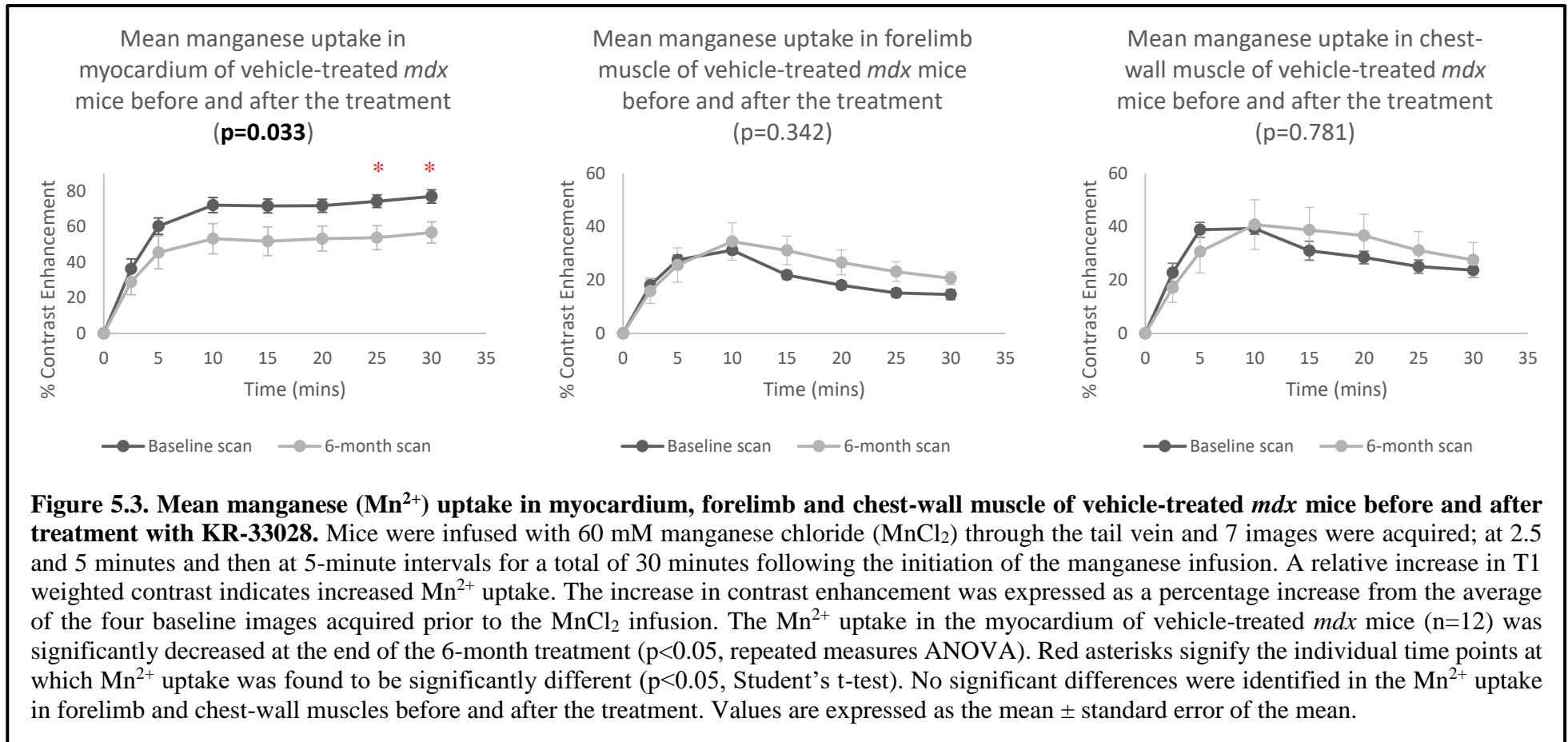
Two groups of *mdx* mice, drug-treated (n=11) and vehicle-treated (n=12), were randomly selected for this study. The mice were all scanned with MEMRI at the age of 6 weeks to establish the baseline Mn²⁺ influx prior to the initiation of drug-treatment. Mice were then treated for a 28-week period (~ 6 months) either with KR-33028-formulated chow or, for the vehicle group, regular chow which was identical to the drug-formulated chow but without the KR-33028. At the end of the 28-week treatment, mice from both groups were scanned with MEMRI.

During MEMRI, each mouse was infused with manganese chloride (MnCl₂) and a total of seven images were acquired; at 2.5 and 5 minutes, and then at 5-minute intervals for a total of 30 minutes following the initiation of the MnCl₂ infusion. A relative increase in T1 weighted contrast indicates increased Mn²⁺ uptake. Additionally, prior to the initiation of the MnCl₂ infusion, four baseline images were acquired in order to average any variations due to changes in TR (repetition time; the length of time between corresponding consecutive points on a repeating series of pulses and echoes) as a result of fluctuations in heart rate. Calculation of the contrast enhancement at each time point relative to baseline shows the Mn²⁺ uptake by muscle over a 30-minute period which in turn represents Ca²⁺ uptake.

As shown in Figure 5.2, the mean Mn²⁺ uptake in myocardium, forelimb and chest-wall muscles of drug-treated mice at the end of the treatment (6-month scan) was not significantly different from the Mn²⁺ uptake at the beginning of the study (baseline scan; Figure 5.2). The mean Mn²⁺ uptake in forelimb and chest-wall muscles of vehicle-treated mice was not significantly changed during the treatment, but the Mn²⁺ uptake in myocardium was significantly decreased (p<0.05, repeated measures ANOVA; Figure 5.3). This depicts an age-related effect on the Mn²⁺ uptake in the myocardium of *mdx* mice. This effect has been previously reported by Greally *et al.* (2013) who investigated the Mn²⁺ transients in 24- and 40-week old *mdx* mice. The age-related decrease of Mn²⁺ uptake in myocardium is only present in the vehicle-treated group of mice, suggesting that this age-related effect has been reversed by the drug-treatment. However, there was no significant difference between the vehicle-treated and drug-treated mice at 6 months (Figure 5.4).

Comparison of the Mn^{2+} uptake in forelimb and chest-wall muscles of drug-treated mice to that of vehicle-treated mice at the end of the treatment also shows no significant differences between the two groups (Figure 5.4).





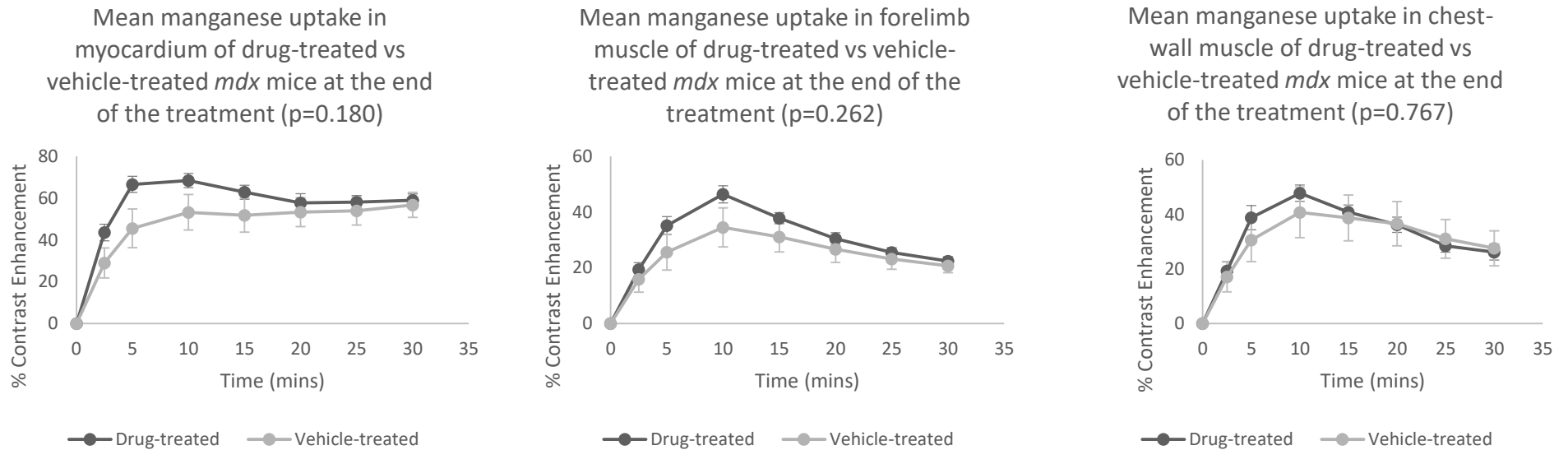


Figure 5.4. Mean manganese (Mn^{2+}) uptake in myocardium, forelimb and chest-wall muscle of drug- and vehicle-treated *mdx* at the end of treatment with KR-33028. Mice were infused with 60 mM manganese chloride ($MnCl_2$) through the tail vein and 7 images were acquired; at 2.5 and 5 minutes, and then at 5-minute intervals for a total of 30 minutes following the initiation of the Mn^{2+} infusion. A relative increase in T1 weighted contrast indicates increased Mn^{2+} uptake. The increase in contrast enhancement was expressed as a percentage increase from the average of the four baseline images acquired prior to the Mn^{2+} infusion. No significant Mn^{2+} uptake differences were identified in myocardium, forelimb and chest-wall muscles of the drug-treated *mdx* mice (n=11) vs the ones of vehicle-treated *mdx* mice (n=12) at the end of treatment (p<0.05, repeated measures ANOVA). Values are expressed as the mean \pm standard error of the mean.

5.2 Cine cardiac magnetic resonance imaging

5.2.1 Introduction and Aims

Cardiac magnetic resonance (CMR) imaging can provide non-invasive, high resolution images of both the left and right heart ventricles of small rodents and can be used to assess the heart anatomy, perfusion, viability, and function (Gilson and Kraitchman, 2007). The most commonly used technique in CMR is cine MRI; the basic principles of which are illustrated in Figure 5.5.

Progressive cardiac complications, including dilated cardiomyopathy (DCM), heart failure and arrhythmias, are one of the leading causes of death in DMD (Nigro *et al.*, 1990; Judge *et al.*, 2011). *Mdx* mice, similarly to DMD patients, experience a progressive DCM with evidence of cardiomyocyte hypertrophy and necrosis, and cardiac fibrosis (Quinlan *et al.*, 2004; Khouzami *et al.*, 2010; Stuckey *et al.*, 2012). Stuckey *et al.* (2012) have demonstrated that *mdx* mice present right ventricle (RV) dysfunction with right ventricular end systolic volume (RVESV) increased and right ventricular ejection fraction (RVEF) reduced as early as three months. Left ventricle (LV) filling and ejection rates were lower at 3 and 6 months of age, although these changes were not detected at 12 months of age suggesting that progressive remodelling and hypertrophy may compensate for dysfunction and mask the original abnormalities at later time points. In accordance, Blain *et al.* (2013) have also demonstrated that end diastolic volume index (EDVI), end systolic volume index (ESVI), stroke volume index (SVI), and cardiac output (CO) of *mdx* mice are decreased in comparison to that of wild type (C57BL/10) mice. Consequently, the *mdx* mouse model can be useful in understanding the cardiomyopathy that appears in DMD patients.

As explained above (section 5.1.1), it has been hypothesised that chronic treatment of *mdx* mice with KR-33028, an NHE1 inhibitor, will lead to a decrease of the intracellular Ca^{2+} levels within both the skeletal and cardiac muscle cells. This can in turn result in improvement of the dystrophin-deficient pathology in the heart and therefore hindering the progression of DCM.

Experiments using cine cardiac MRI aimed to:

- Investigate the effects of long-term treatment with KR-33028 on the development and progression of cardiomyopathy in *mdx* mice.

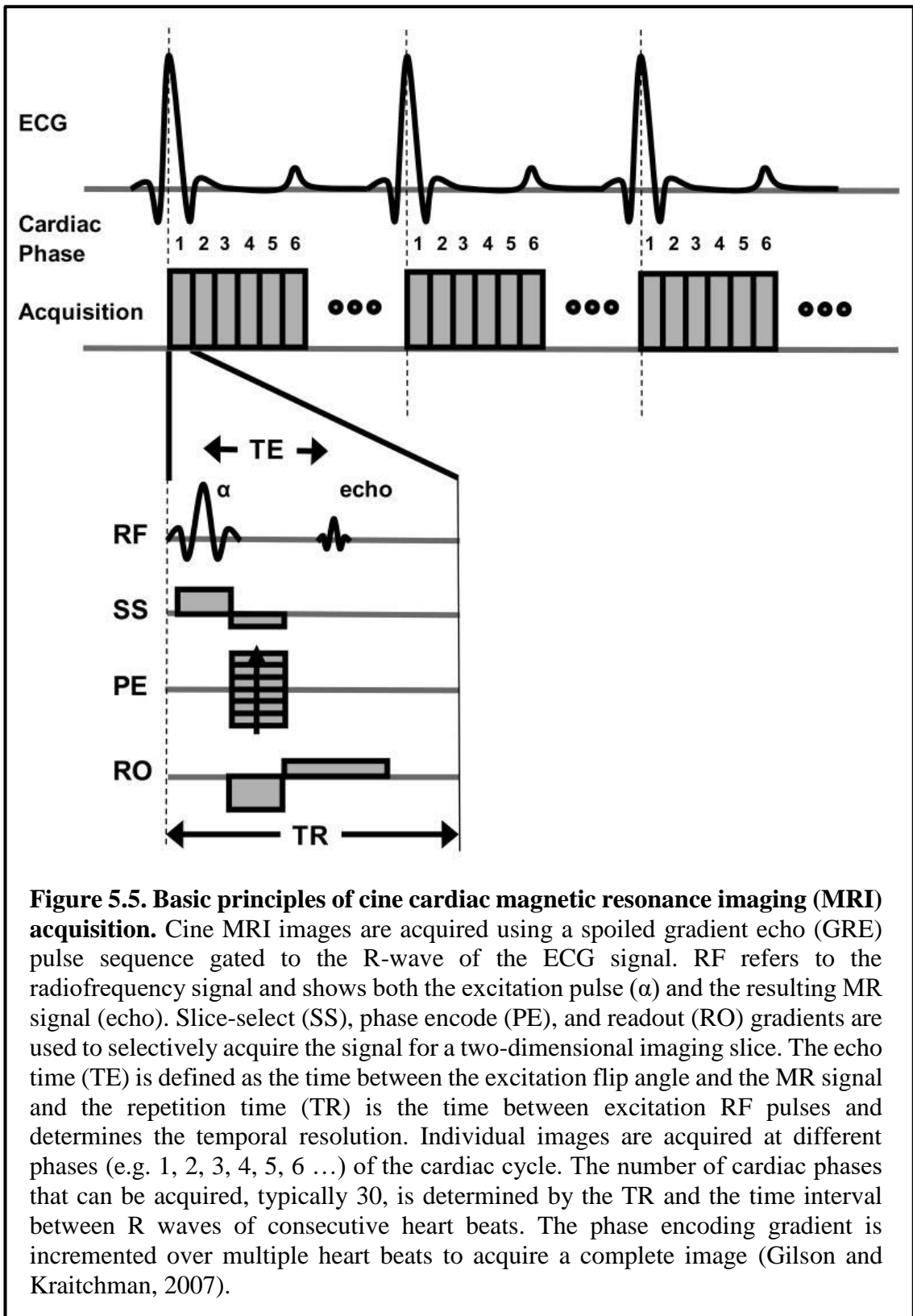


Figure 5.5. Basic principles of cine cardiac magnetic resonance imaging (MRI) acquisition. Cine MRI images are acquired using a spoiled gradient echo (GRE) pulse sequence gated to the R-wave of the ECG signal. RF refers to the radiofrequency signal and shows both the excitation pulse (α) and the resulting MR signal (echo). Slice-select (SS), phase encode (PE), and readout (RO) gradients are used to selectively acquire the signal for a two-dimensional imaging slice. The echo time (TE) is defined as the time between the excitation flip angle and the MR signal and the repetition time (TR) is the time between excitation RF pulses and determines the temporal resolution. Individual images are acquired at different phases (e.g. 1, 2, 3, 4, 5, 6 ...) of the cardiac cycle. The number of cardiac phases that can be acquired, typically 30, is determined by the TR and the time interval between R waves of consecutive heart beats. The phase encoding gradient is incremented over multiple heart beats to acquire a complete image (Gilson and Kraitchman, 2007).

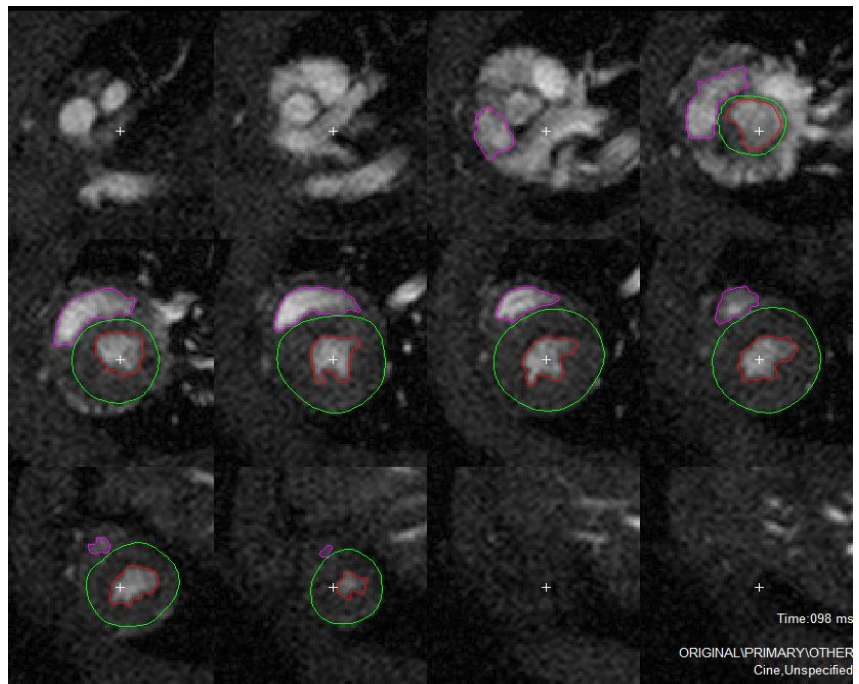
5.2.2 Effects of chronic treatment with KR-33028 on the development and progression of cardiomyopathy in *mdx* mice

Cine cardiac MRI was employed to assess the cardiac function of the drug-treated and vehicle-treated *mdx* mice. Cine MRI of the heart was performed prior to the infusion of MnCl_2 for MEMRI. A stack of contiguous short axis slices was acquired to cover the entire left and right ventricles. The acquired images were distributed throughout the cardiac cycle. Using the analysis software Segment V2.0 R4949, cine images were analysed in order to measure the left ventricle (LV) and right ventricle (RV) functional parameters. Figure 5.6 shows the segmentation of typical cine images in the RV, LV and myocardium during the end systolic (ES) and end diastolic (ED) time frames.

As seen in Table 5.1, no significant differences were identified between treated and untreated mice at the end of the treatment. However, at the end of the 6 months both groups presented a significant ($p < 0.05$, Student's t-test) decrease of end diastolic volume index (EDVI), end systolic volume index (ESVI), stroke volume index (SVI), cardiac index (CI), right ventricular end diastolic volume index (RVEDVI), right ventricular stroke volume index (RVSVI), and right ventricular ejection fraction (RVEF) when compared to the beginning of the treatment. This is a sign of development of cardiomyopathy affecting both left and right ventricular functions. Notably, the vehicle-treated mice presented a significant ($p < 0.05$, Student's t-test) decrease in their cardiac output (CO), which was not observed in the drug-treated mice. CO in drug-treated mice remained the same before and after the treatment despite a significant decrease of SVI. This could possibly be attributed to a slight increase of their heart rate (355 ± 47 bpm at baseline vs 397 ± 36 bpm at 6-months), although not significant. Furthermore, the left ventricular mass index (LVMI) in drug-treated mice was decreased at the end of the 6-month period but remained static in vehicle-treated mice.

Our findings suggest the development of diastolic dysfunction affecting both the left and right ventricles of *mdx* mice. They are consistent with the studies of Stuckey *et al.* (2012) who demonstrated that *mdx* mice present left and right ventricular dysfunction, as depicted by a decrease in EF, CO, RVEF and increase of RVESVI; and Blain *et al.* (2013) who have also demonstrated that EDVI, ESVI, SVI, and CO of *mdx* mice are decreased in comparison to that of wild type (C57BL/10) mice. It is, however, evident in our study that the 28-week long treatment with KR-33028 did not impact the development and progression of cardiomyopathy in the *mdx* mice.

End Systole



End Diastole

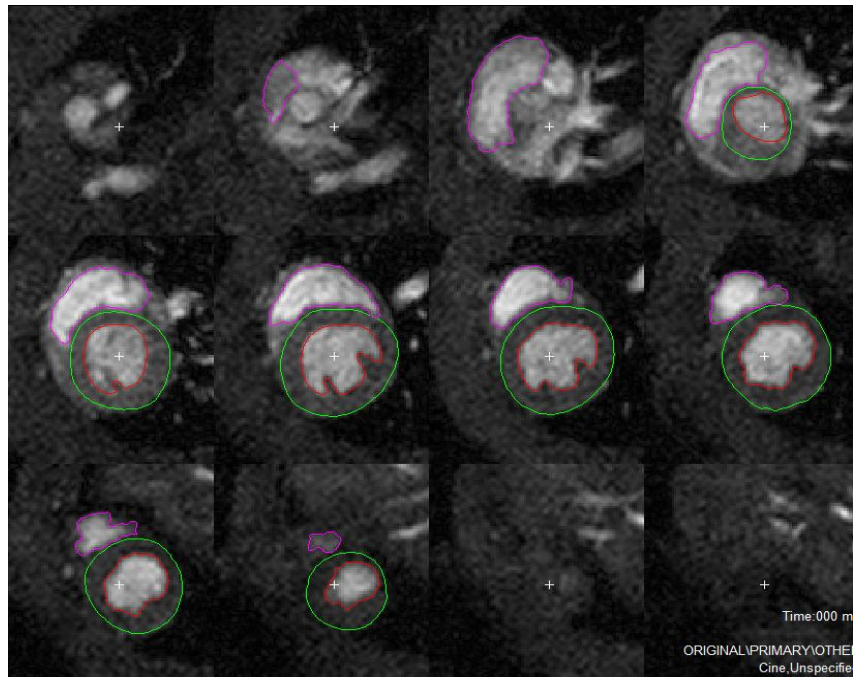


Figure 5.6. Segmentation of a typical cine scan of a mouse heart. The right and left ventricles are outlined with pink and red lines respectively. The red line delineates the endocardial border, whilst the green line marks the epicardial border. The top and bottom images depict the end systolic (ES) and end diastolic (ED) time frames respectively. The columns show contiguous slices, base to apex.

Parameters: Slice thickness 1 mm. Images were zero-filled to a matrix size of 256 x 256.

	Drug-treated <i>mdx</i> mice (n=11)		Vehicle-treated <i>mdx</i> mice (n=12)	
	Baseline Scan (6 weeks old)	6-month Scan (34 weeks old)	Baseline Scan (6 weeks old)	6-month Scan (34 weeks old)
Body Weight [g]	21.12±1.46	33.35±1.81	22.51±2.54	32.51±2.50
Heart Rate [bpm]	355±47	397±36	426±40	412±27
LVMI [$\times 10^{-3}$]	3.72±0.76	3.12±0.29*	3.47±0.32	3.38±0.37
EDVI [μ l/g]	2.69±0.9	1.43±0.21*	2.80±0.26	1.62±0.37*
ESVI [μ l/g]	1.07±0.56	0.51±0.19*	1.10±0.19	0.56±0.19*
SVI [μ l/g]	1.62±0.44	0.92±0.22*	1.70±0.20	1.06±0.24*
EF [%]	62.50±10.02	64.39±13.53	60.78±5.33	65.67±6.31
CO [ml/min]	12.07±3.50	12.11±3.12	16.16±2.19	14.18±3.50*
CI [ml/min/g]	0.57±0.17	0.36±0.09*	0.72±0.08	0.44±0.10*
RVEDVI [μ l/g]	2.82±0.48	2.04±0.36*	2.54±0.28	1.99±0.47*
RVESVI [μ l/g]	1.31±0.36	1.21±0.39	0.99±0.19	1.09±0.33
RVSVI [μ l/g]	1.51±0.30	0.83±0.27*	1.55±0.24	0.90±0.29*
RVEF [%]	54.05±7.91	41.12±13.59*	60.91±6.30	45.30±11.19*

Table 5.1. Cardiac function of drug-treated and vehicle-treated *mdx* mice before and at the end of the treatment. Asterisks denote significant differences between the baseline and 6-month scans in each group of *mdx* mice, drug- and vehicle-treated ($p < 0.05$, Student's t-test). LVMI: left ventricular mass index, EDVI: end diastolic volume index, ESVI: end systolic volume index, SVI: stroke volume index, EF: ejection fraction, CO: cardiac output, CI: cardiac index, RVEDVI: right ventricular end diastolic volume index, RVESVI: right ventricular end systolic volume index, RVSVI: right ventricular volume index, RVEF: right ventricular ejection fraction. Values are expressed as the mean \pm standard deviation.

5.3 Discussion and conclusions

The aim of this chapter was to apply MEMRI and cine cardiac MRI in order to investigate the effects of 28-week treatment with KR-33028 on the Ca^{2+} dynamics and cardiomyopathy development in *mdx* mice, respectively.

Our experiments demonstrated an age-related decrease of the Mn^{2+} uptake in the myocardium of 34-week old *mdx* mice when compared to their Mn^{2+} uptake when 6-weeks old. This effect has been previously seen and reported by Greally *et al.* (2013), who compared the Mn^{2+} transients in 24-week old *mdx* mice to those of 40-week old *mdx* mice. The mechanisms by which Mn^{2+} uptake would decrease with age are not very well understood. However, a series of studies have highlighted the fact that MEMRI measures the uptake of Mn^{2+} in viable, healthy cardiomyocytes (Waghorn *et al.*, 2009; Price *et al.*, 2010). Based on this, it is possible that the decrease of Mn^{2+} uptake could be related to an elevation of the number of damaged and necrotic cardiomyocytes in older mice. Notably, the Mn^{2+} uptake by the myocardium of drug-treated mice was not found to be significantly different at the end of the study suggesting that the chronic treatment with KR-33028 reversed the age-related effects.

In contrast to the above findings, cine cardiac MRI demonstrated that the left and right ventricular functions of the drug-treated mice were not significantly impacted by the treatment, suggesting that although chronic treatment with KR-33028 improved the Ca^{2+} levels in the hearts of dystrophin-deficient animals it did not improve the heart function. Both drug-treated and vehicle-treated *mdx* mice developed diastolic dysfunction that affected the left and right ventricular functions, including the LVMI, ESVI, SVI, CI, RVEDVI, RVSVI and RVEF, which were found to be significantly decreased in both groups of mice at the end of treatment. Our findings are consistent with the studies of Stuckey *et al.* (2012) who demonstrated that *mdx* mice present left and right ventricular dysfunction, as depicted by a decrease in EF, CO, RVEF and increase of RVESVI; and Blain *et al.* (2013) who have also demonstrated that EDVI, ESVI, SVI, and CO of *mdx* mice are decreased in comparison to that of wild type (C57BL/10) mice.

MEMRI scans were acquired through the heart at the level of the papillary muscles with the left upper forelimb within the field of view. This slice allowed for two more muscle groups, forelimb and chest-wall, to be investigated in addition to the myocardium. Interestingly, no age-effects were identified in these two muscle groups at the end of the

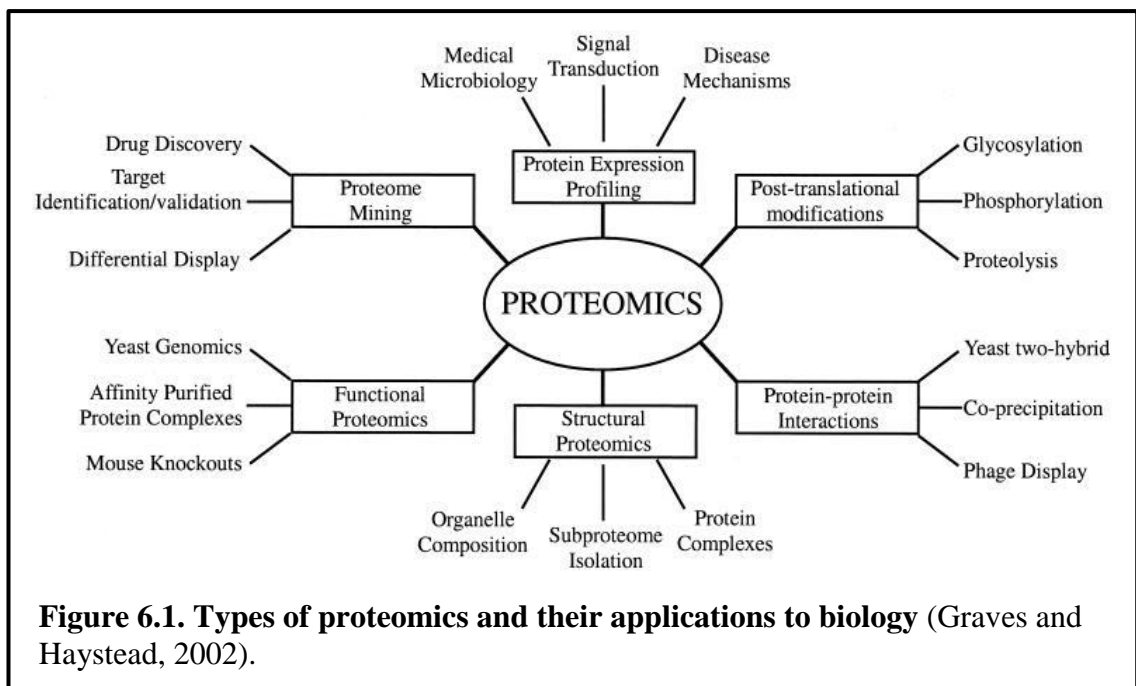
treatment. Additionally, treatment with KR-33028 did not impact the Mn^{2+} uptake in forelimb and chest-wall muscles of drug-treated mice.

MEMRI was employed for the investigation of Ca^{2+} dynamics in the cardiac and skeletal muscles of KR-33028- and vehicle-treated *mdx* mice. More specifically, the present study was intended to investigate the entry of Ca^{2+} ions through the NCX exchanger. Previous evidence suggests that Mn^{2+} can enter the cardiac and skeletal muscle cells through different Ca^{2+} transporters, including L-type Ca^{2+} channels (Blain *et al.*, 2013; Greally *et al.*, 2013), and although we have assumed that Mn^{2+} can access any route that is available to Ca^{2+} , no solid evidence exists, to our knowledge, to suggest that Mn^{2+} can also enter through the NCX exchanger. Moreover, it is possible that small transient changes were not detected by MEMRI due to the sensitivity of the technique. Consequently, the suitability of MEMRI for the assessment of the effect of KR-33028 on Ca^{2+} dynamics could not be proven in our study. In addition to technological limitations associated with the MRI techniques described in this chapter, the lack of wild type controls (C57BL/10 animals) in our experiments complicates the interpretation of the study findings.

Chapter 6. Investigating the effects of KR-33028 treatment on the proteome of dystrophic skeletal muscle

6.1 Introduction and aims

Proteomic characterisation of a biological system (e.g. cell, tissue, and organism) provides an “*en masse* interrogation of biological phenomena on the protein level” (Mallick and Kuster, 2010). Proteomic analysis offers a complementary approach to genomics technologies (Roos *et al.*, 2017). Many types of information cannot be obtained from the study of genes alone and it is impossible to study post-translational modifications, elucidate mechanisms of disease and aging, investigate environmental effects or characterise drug targets solely by studying the genome. Furthermore, proteins, not genes, are responsible for the phenotypes of cells. Determination of relative protein abundance levels allows for the identification of quantitative variations of individual proteins to be linked to physiological activity or other measurable phenotypic states of the cell. The main types of proteomics and their applications in biology are presented in Figure 6.1.



Mass spectrometry (MS) is a powerful proteomic technique that allows for quantification of compounds, including proteins (top-down proteomics) and peptides (bottom-up proteomics), within a sample and elucidation of their structure and chemical properties (Finehout and Lee, 2004; Angel *et al.*, 2012). There are many different types of MS, but all consist of three main parts: 1) an ion source, for the conversion of the samples under investigation into gaseous ions, 2) an analyser, for separating the ions based on their mass

to charge ratio (m/z), and 3) a detector, for detection of the ions and recording of their relative abundance. Moreover, a sample introduction system is needed for the introduction of the samples to the ion source. Notably, the instrument is controlled through a computer, which allows for the data to be acquired, manipulated, and then compared to reference libraries (Figure 6.2) (Graves and Haystead, 2002; de Hoffmann and Stroobant, 2013).

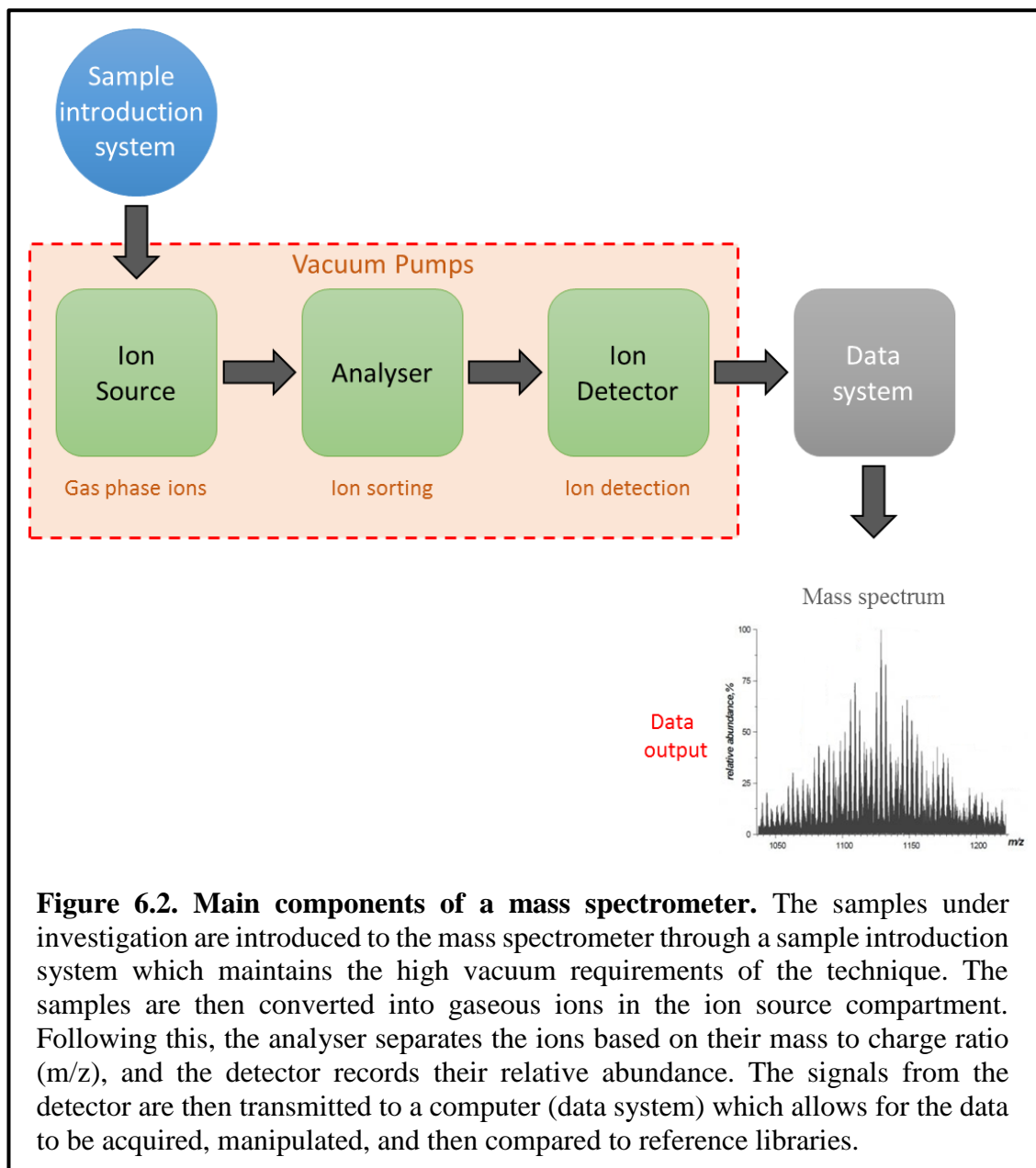
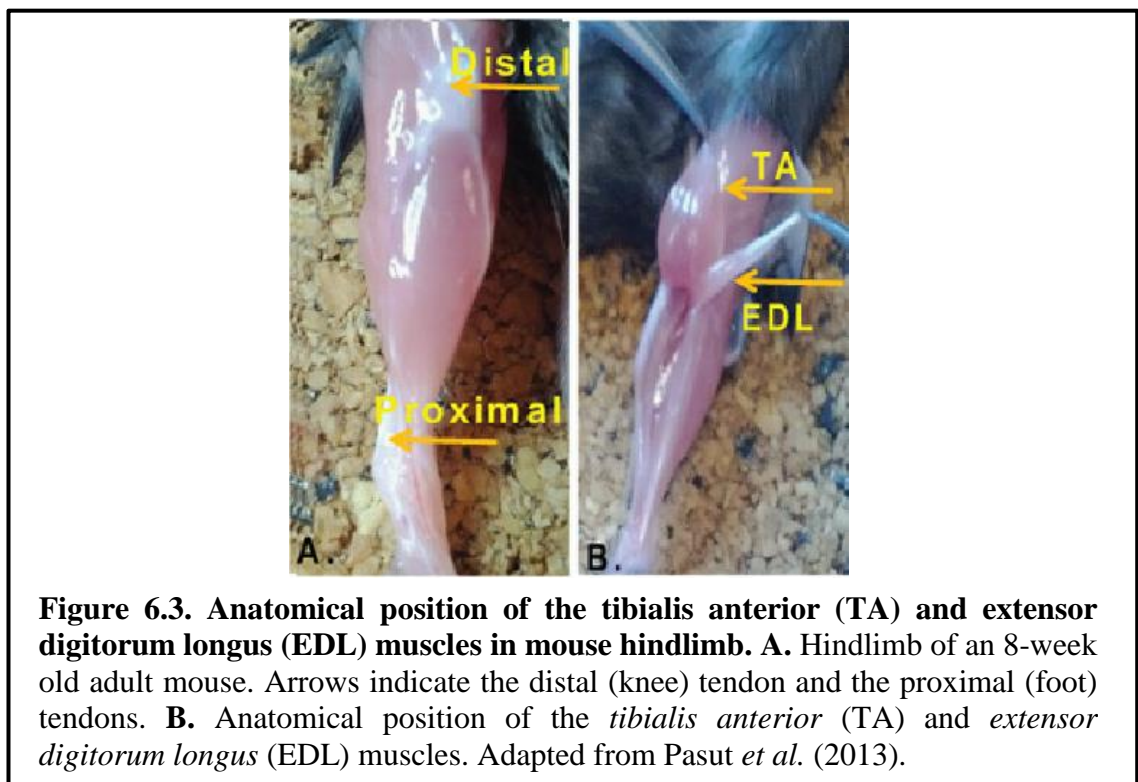


Figure 6.2. Main components of a mass spectrometer. The samples under investigation are introduced to the mass spectrometer through a sample introduction system which maintains the high vacuum requirements of the technique. The samples are then converted into gaseous ions in the ion source compartment. Following this, the analyser separates the ions based on their mass to charge ratio (m/z), and the detector records their relative abundance. The signals from the detector are then transmitted to a computer (data system) which allows for the data to be acquired, manipulated, and then compared to reference libraries.

Tandem mass spectrometry, also referred to as MS/MS, offers additional information about specific ions and allows for protein sequencing, the determination of the amino acid sequence of all or part of a protein or peptide. Therefore, it serves to identify the protein and its post-translational modifications. MS/MS involves at least two stages of mass analysis and incorporates fragmentation in-between stages. During the first stage of

MS/MS (MS^1), ions are formed in the ion source and separated by mass-to-charge ratio. Ions of a particular mass-to-charge ratio (precursor ions) are then selected and fragmented by ion-molecule reaction, collision-induced dissociation, photodissociation, or other process. Subsequently, the resulting ions are separated and detected in a second stage of mass spectrometry (MS^2). It is possible to increase the number of steps to yield MS^n experiments, where n refers to the number of generations of ions being analysed (Prasain, 2012; de Hoffmann and Stroobant, 2013).

The mass resolving and mass determining capabilities of MS can be enhanced by coupling it to chromatographic techniques (e.g. gas chromatography (GC) and liquid chromatography (LC)), which separate compounds chromatographically before they are introduced to the ion source and mass spectrometer. HPLC is the chromatographic method most commonly used to study biological samples by MS or MS/MS (LC-MS or LC-MS/MS, respectively), because the majority of biological samples are liquid and non-volatile (Tuli and Resson, 2009; Cutillas and Timms, 2011).



During this project, LC-MS/MS was employed for the proteome analysis of tibialis anterior (TA) muscles collected from two groups of mice: 1) *mdx* mice chronically treated with the NHE1 inhibitor KR-33028 for 28 weeks, and 2) vehicle-treated *mdx* mice, and aimed to investigate the effects of KR-33028 treatment on the proteome of dystrophic skeletal muscle. TA is a long, narrow muscle located in the anterior compartment of the

lower leg (Figure 6.3). It was chosen for the purposes of this study as it is a frequently used model system in pre-clinical DMD research that exhibits several signs of DMD pathology (Sacco *et al.*, 1992; Dellorusso *et al.*, 2001; van Putten *et al.*, 2012; Duddy *et al.*, 2015). Moreover, it has been previously used for profiling the proteome of dystrophic skeletal muscle (Ge *et al.*, 2004; Carberry *et al.*, 2012; Gamberi *et al.*, 2018).

Aims of proteomic analysis described in this chapter:

- To compare the proteomic signature of TA muscle samples collected from KR-33028- and vehicle-treated *mdx* mice.
- To carry out a gene ontology analysis of proteins found to be significantly altered in abundance in TA samples treated with KR-33028 when compared to vehicle-treated samples.

6.2 Proteome profiling of TA muscles collected from KR-33028-treated and vehicle-treated *mdx* mice

In an effort to define the effects of long-term treatment with the NHE1 inhibitor KR-33028 on the protein levels in dystrophic mouse muscle tissue, TA muscles collected from KR-33028-treated (n=3) and vehicle-treated (n=3) *mdx* mice were sent to the Leibniz-Institute for Analytical Science (ISAS), Germany, for proteomic analysis.

The use of LC-MS/MS allowed for the identification of a total of 801 proteins. For each protein, the average of the normalized abundances (obtained from Progenesis Qi) from the replicate analyses was calculated to determine the ratios between the KR-33028- and vehicle-treated mice. Out of the 801 proteins that were identified, the levels of 29 proteins were found to be significantly different between the drug- and vehicle-treated samples (ANOVA p-value ≤ 0.05) (Table 6.1).

Proteins with an average log₂ ratio that was either higher than the up-regulated cut-off or lower than the down-regulated cut-off was considered as regulated. The cut-off values were determined based on the 2x standard deviation and the normal distribution of the log₂ ratios from all identified proteins. Therefore, an average log₂ ratio of a protein below -0.79 or above 0.62 (corresponding to ~1.5-fold regulation; log₂ ratios of 0.96) were considered as regulated. The proteins: titin (TTN), 40S ribosomal protein S5 (RPS5), adenosylhomocysteinase (SAHH), vigilin (high density lipoprotein (HDL) binding protein; HDLBP), 40S ribosomal protein S15 (RPS15) and neurofilament heavy polypeptide (NEFH), when compared to the ones from vehicle-treated *mdx* mice, were found to be upregulated in TA samples collected from KR-33028-treated *mdx* mice. Conversely, the proteins: histone H1.0 (H1f0), phosphomannomutase 2 (PMM2), cytochrome b (mt-CYTB), and calcium binding protein 39 (CAB39), were found to be downregulated in TA samples collected from KR-33028-treated *mdx* mice.

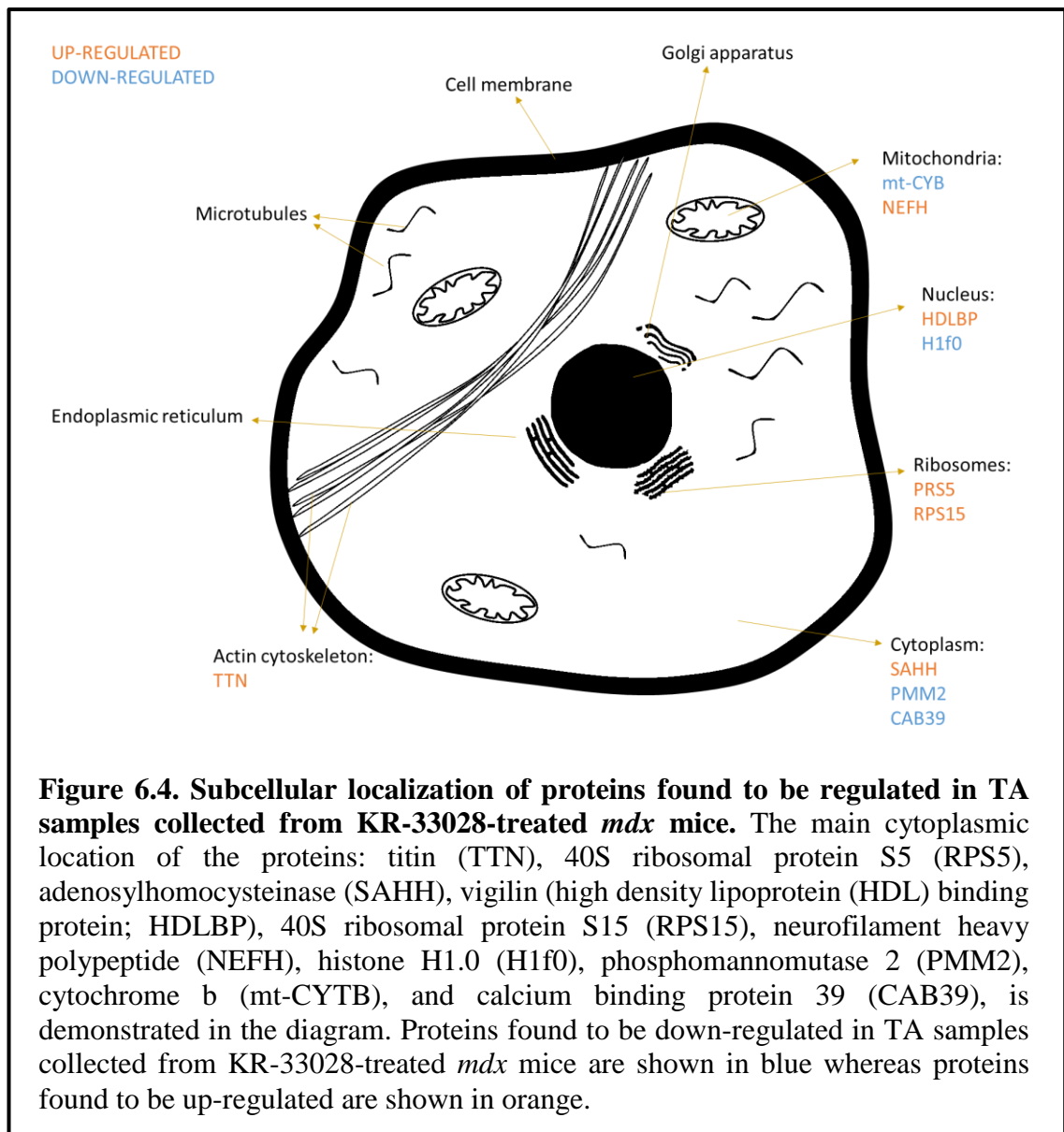
Accession	Protein	Unique peptides	ANOVA (p value)	Up/Down in KR-33028-treated <i>mdx</i> mice
A2ASS6	Titin (TTN)	855	0.00	UP (x2.79)
P97461	40S ribosomal protein S5 (RPS5)	3	0.00	UP (x1.85)
P50247	Adenosylhomocysteinase (SAHH)	2	0.00	UP (x1.77)
Q9R1P0	Proteasome subunit alpha type-4 (PSAM4)	2	0.02	UP (x1.32)
O08709	Peroxiredoxin-6 (PRDX6)	5	0.01	DOWN (1.32)
Q9CQ60	6-phosphogluconolactonase (6PGLS)	2	0.04	DOWN (x1.18)
P23506	Protein-L-isoaspartate(D-aspartate) O-methyltransferase (PCMT1)	5	0.02	DOWN (x1.23)
Q61171	Peroxiredoxin-2 (PRDX2)	4	0.02	DOWN (x1.26)
Q924M7	Mannose-6-phosphate isomerase (MPI)	4	0.05	DOWN (x0.79)
P10639	Thioredoxin (TXN1)	2	0.04	DOWN (x1.27)
Q99LY9	NADH dehydrogenase [ubiquinone] iron-sulphur protein 5 (NDUFS5)	2	0.03	DOWN (x1.38)
P62962	Profilin-1 (PFN1)	4	0.03	DOWN (x1.51)
Q8BIJ6	Isoleucine-tRNA ligase, mitochondrial (IARS2)	3	0.02	DOWN (x1.69)
P10922	Histone H1.0 (H1f0)	3	0.01	DOWN (x1.70)
Q8VDJ3	Vigilin (High density lipoprotein (HDL) binding protein; HDLBP)	1	0.03	UP (x1.85)
P62843	40S ribosomal protein S15 (RPS15)	1	0.01	UP (x1.72)
P19246	Neurofilament heavy polypeptide (NEFH)	1	0.02	UP (x1.65)
P48453	Serine/threonine-protein phosphatase 3 catalytic subunit beta isoform (PPP3CB)	1	0.01	UP (x1.32)
P62889	60S ribosomal protein L30 (RPL30)	1	0.00	UP (x1.32)
Q5DTJ9	Myopalladin (MYPN)	1	0.04	UP (x1.25)
Q9R0Q7	Prostaglandin E synthase 3 (PTGES3)	1	0.04	UP (x1.18)
Q61239	Protein farnesyltransferase/geranylgeranyltransferase type-1 subunit alpha (FNTA)	1	0.01	DOWN (x1.19)
Q8C0M9	Isoaspartyl peptidase/L-asparaginase (ASRGL1)	1	0.04	DOWN (x1.19)
P37804	Transgelin (TAGLN)	2	0.05	DOWN (x1.53)

P97315	Cysteine and glycine-rich protein 1 (CSRP1)	1	0.00	DOWN (x1.71)
Q9Z2M7	Phosphomannomutase 2 (PMM2)	1	0.04	DOWN (x1.87)
P00158	Cytochrome b (mt-CYTB)	1	0.03	DOWN (x5.00)
P63328	Serine/threonine-protein phosphatase 3 catalytic subunit alpha isoform (PPP3CA)	2	0.05	DOWN (x1.31)
Q06138	Calcium-binding protein 39 (CAB39)	1	0.05	DOWN (x1.89)

Table 6.1. Proteins found to be significantly different between the KR-33028- and vehicle-treated samples. Tibialis anterior (TA) muscles collected from KR-33028-treated *mdx* mice (n=3) and vehicle-treated *mdx* mice (n=3) were used for comparative proteome profile analysis. For each protein, the average of the normalized abundances (obtained from Progenesis Qi) from the replicate analyses was calculated to determine the ratios between the KR-33028- and vehicle-treated mice. Proteins which were a) commonly quantified in all the replicates, with b) unique peptides, c) an ANOVA p-value \leq 0.05 (Progenesis Qi) and d) an average log₂ ratio of which protein that was either higher than the up-regulated cut-off or lower than the down-regulated cut-off, was considered as regulated. The cut-off values were determined based on the 2x standard deviation and the normal distribution of the log₂ ratios from all identified proteins (found to be symmetric around the mean and had bell-shaped density curves). Therefore, an average log₂ ratio of a protein below -0.79 or above 0.62 (corresponding to approximately 1.5-fold regulation; log₂ ratios of 0.96), were considered as regulated. Down-regulated proteins are highlighted in blue and up-regulated proteins in orange.

6.3 Pathway and protein-protein interaction (PPI) analysis of proteins down- and up-regulated in KR-33028-treated TA samples

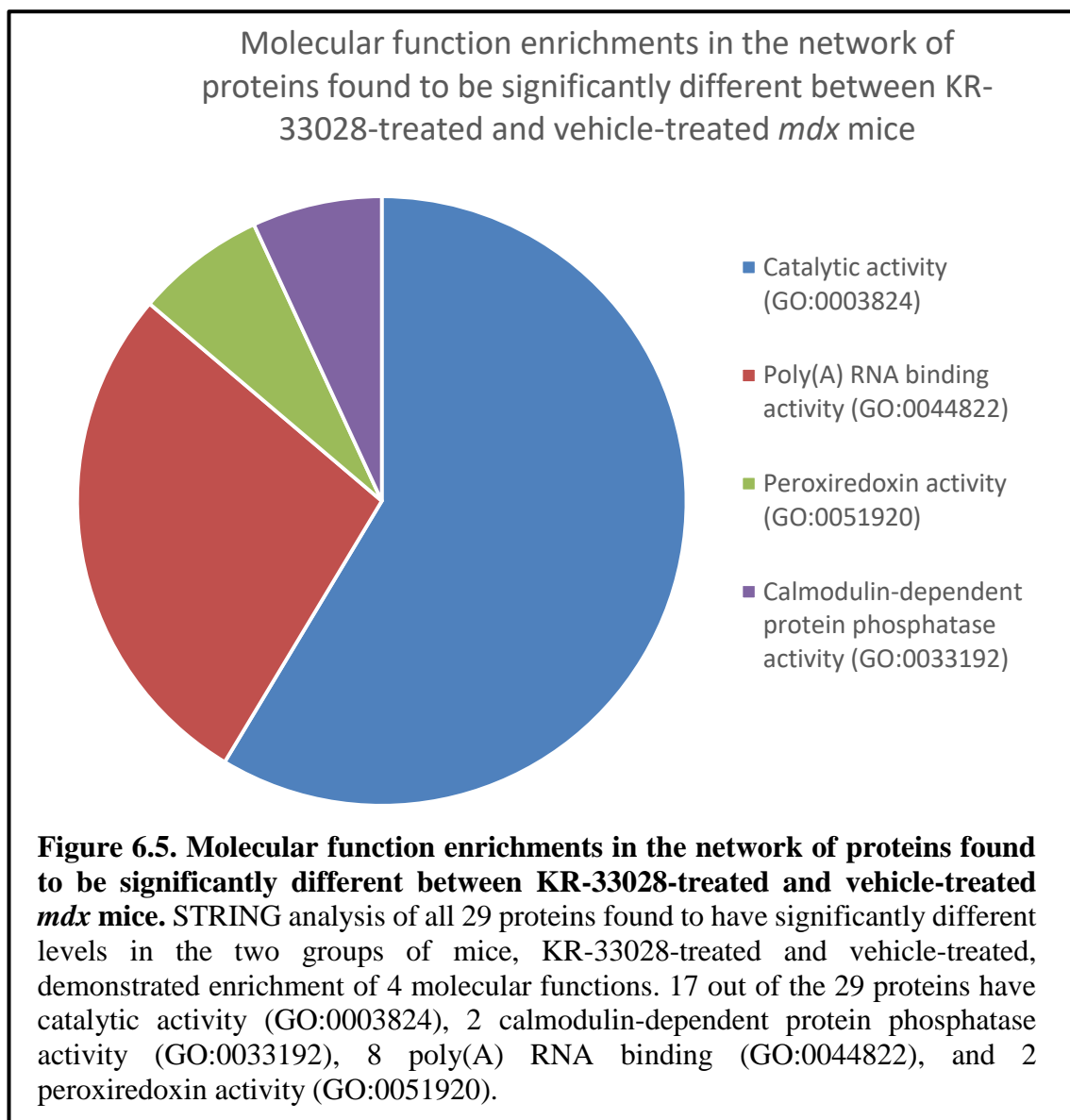
Proteins identified to be significantly different in abundance between KR-33028-treated and vehicle-treated *mdx* mice were further analysed for their enrichment in molecular function pathways and cytoplasmic locations. The primary cytoplasmic location of the proteins found to be up- or down-regulated in TA samples collected from KR-33028-treated *mdx* mice is demonstrated in Figure 6.4.



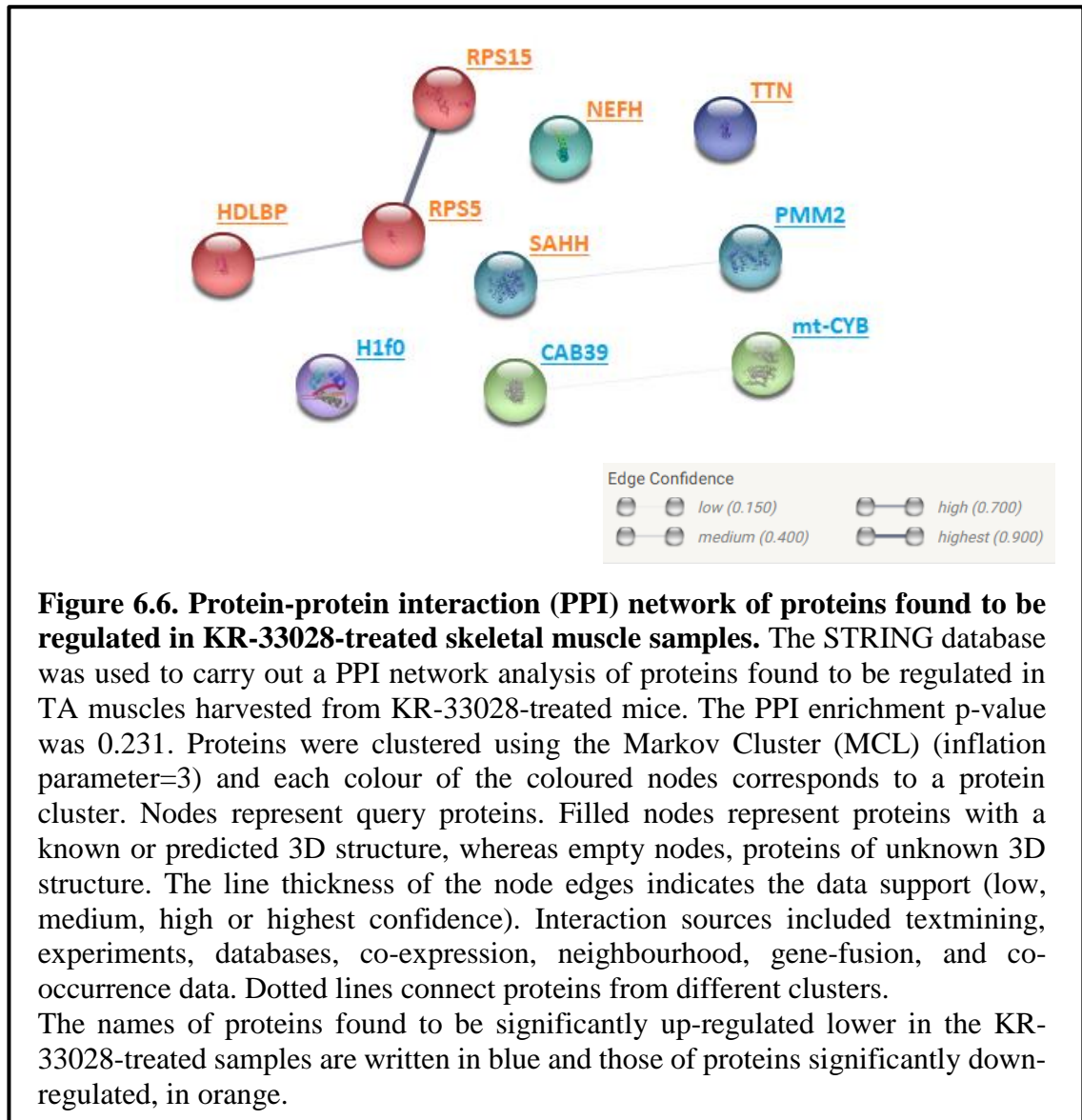
Analysis of the regulated proteins using the STRING database (<http://string-db.org>) showed no significant functional enrichments in the network. However, STRING analysis of all 29 proteins found to have significantly different levels in the two groups of mice,

KR-33028-treated and vehicle-treated, demonstrated significant enrichment of 4 molecular functions (Figure 6.5):

- 1) 17 out of the 29 proteins have catalytic activity – catalysis of biochemical reactions – (GO:0003824),
- 2) 2 proteins have calmodulin-dependent protein phosphatase activity – removal of phosphate group from protein serine/threonine phosphate, dependent on the presence of calcium-bound calmodulin – (GO:0033192),
- 3) 8 proteins have poly(A) RNA binding activity – selective and non-covalent interaction with an RNA molecule – (GO:0044822), and
- 4) 2 proteins have peroxiredoxin activity – catalysis of an oxidation-reduction (redox) reaction ($2 R'-SH = R'-S-S-R'$, where R' refers to peroxiredoxin itself) – (GO:0051920).



Additionally, the functional partnerships and interactions between these proteins were investigated and a protein-protein interaction (PPI) network was constructed using the STRING database. As demonstrated in Figure 6.6, PPI enrichments in the network of regulated proteins were not significant. However, PPI enrichments in the network of all proteins the abundance of which had significantly changed as a result of the KR-33028-treatment, were significant (p-value=1.12e-08, Figure 6.7).



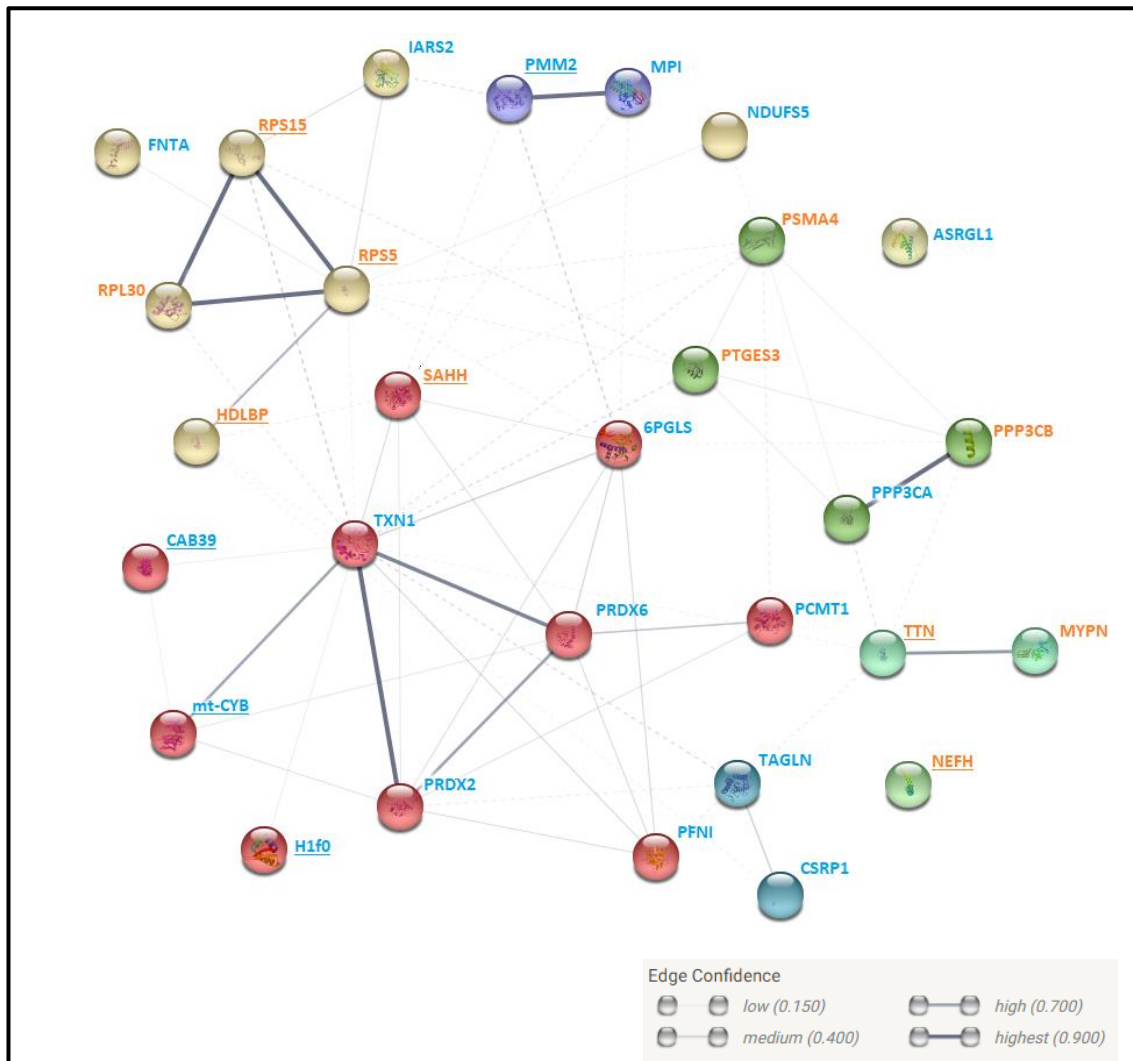


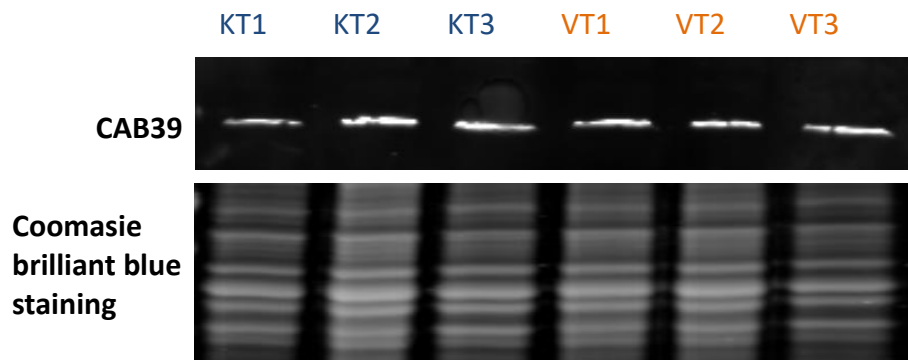
Figure 6.7. Protein-protein interaction (PPI) network of proteins found to be significantly altered in abundance in TA samples harvested from KR-33028-treated *mdx* mice. The STRING database was used to carry out a PPI network analysis of proteins the levels of which were found to be significantly different between drug- and vehicle-treated *mdx* mice. The PPI enrichment p-value was 1.12e-08. Proteins were clustered using the Markov Cluster (MCL) (inflation parameter=3) and each colour of the coloured nodes corresponds to a protein cluster. Nodes represent query proteins. Filled nodes represent proteins with a known or predicted 3D structure, whereas empty nodes proteins of unknown 3D structure. The line thickness of the node edges indicates the data support (low, medium, high or highest confidence). Interaction sources included textmining, experiments, databases, co-expression, neighborhood, gene-fusion, and co-occurrence data. Dotted lines connect proteins from different clusters. The names of proteins found to be significantly lower in abundance in the KR-33028-treated samples, when compared to the vehicle-treated ones, are written in blue and those of proteins significantly higher in orange. Regulated proteins are underlined.

6.4 Verification of proteomics data

Although quantitative proteomics strategies can generate great amounts of information, they are predicated on several assumptions and inherent to a number of limitations, including undersampling of complex proteomic samples, and limited capacity to detect low-abundance peptides (Kinoshita *et al.*, 2006; Chandramouli and Qian, 2009; Duncan *et al.*, 2010). It is therefore essential that LC-MS/MS findings are independently verified using more robust analytical techniques widely used for the quantitative detection of proteins such as western blot and immunohistochemistry.

As explained above, LC-MS/MS carried out as part of our project, demonstrated that the levels of a total of 10 proteins were significantly different between skeletal muscles harvested from KR-33028-treated *mdx* mice and the ones from vehicle-treated *mdx* mice. Due to limited resources and time constraints, it was not possible to verify the findings for all 10 proteins. A protein relevant to the initial hypothesis of our project – that treatment of dystrophic mice with KR-33028 would reduce the intracellular Ca^{2+} levels – was chosen for western blotting, i.e. CAB39, a Ca^{2+} -binding protein. Western blot analysis was carried out using protein extracted from TA muscles collected from treated and untreated *mdx* mice. It was demonstrated that levels of CAB39 are significantly lower ($p < 0.05$, Student's T-test) in the KR-33028-treated samples, when compared to the ones of vehicle-treated samples (Figure 6.8) further validating the findings of LC-MS/MS. The presence of CAB39 in the pool of proteins regulated in the treated muscle samples suggests that long-term treatment with KR-33028 can impact on the Ca^{2+} dynamics of dystrophin-deficient skeletal muscle.

In addition to CAB39, of great interest to our project was titin, a key cardiac and skeletal muscle protein (further explored in section 6.5), which was shown to be upregulated in KR-33028-treated muscles. However, due to its large size (3–3.7 MDa) (Opitz *et al.*, 2003) it was not possible to verify its levels in the KR-33028-treated vs vehicle-treated samples via western blot.



CAB39 levels in KR-33028- and vehicle-treated *mdx* mice determined through western blotting

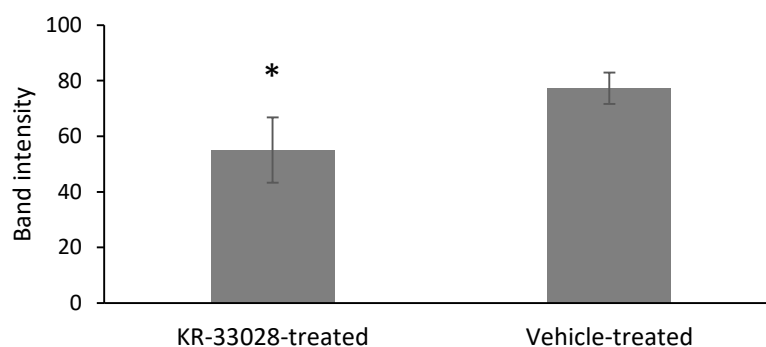


Figure 6.8. Western blot (WB) investigation of CAB39 levels in KR-33028- and vehicle-treated TA samples. Protein was extracted from TA muscles collected from three KR-33028-treated and three vehicle-treated *mdx* mice and was then quantified using the BCA assay. Equal quantities of protein extracts (25 µg) were then loaded on a 12% SDS polyacrylamide gel. Subsequently, proteins were transferred on a PVDF membrane which was then incubated with the CAB39 antibody. The protein bands were visualised using the Odyssey® CLx Imaging System (LI-COR Biosciences). The band intensity was determined using ImageJ software and was corrected against expression coefficient values determined by Coomassie brilliant blue staining.

KT: KR-33028-treated, and VT: vehicle-treated

6.5 Discussion and conclusions

This chapter aimed to investigate how long-term treatment with KR-33028 may impact on the proteomic signature of dystrophic muscle. TA muscles collected from *mdx* mice chronically treated (~28 weeks of treatment) with KR-33028 and vehicle-treated *mdx* mice were subjected to LC-MS/MS analysis. A total of 29 proteins were found to have significantly changed in abundance after the 28-week treatment with KR-33028, out of which 10 proteins were considered regulated based on a cut-off value.

Amongst the proteins that were found to be upregulated in the treated samples is a key cardiac and skeletal muscle protein, titin. Titin, formerly known as connectin, connects the Z to the M line of the sarcomere. It is the third most abundant protein in muscle (after myosin and actin) and is essential for the sarcomere assembly, and muscle elasticity and contraction (Trinick *et al.*, 1984; Labeit *et al.*, 1997; Trinick and Tskhovrebova, 1999; Sela, 2002; Tskhovrebova and Trinick, 2010). A series of studies have indicated that titin undergoes dynamic isoform and, possibly, phosphorylation changes in disease (LeWinter *et al.*, 2007; Linke, 2008; Kruger and Linke, 2011). Reports suggest that titin is degraded in muscles of DMD and other muscular dystrophy patients (Matsumura *et al.*, 1989; Rouillon *et al.*, 2014; Awano *et al.*, 2018). Moreover, mutations within the *TTN* gene are associated with a large number of genetic muscle diseases (Hackman *et al.*, 2002) but also the development of DCM (Itoh-Satoh *et al.*, 2002; Beqqali *et al.*, 2016; Perez-Serra *et al.*, 2016; Zhang *et al.*, 2017). In TA muscles collected from mice treated with KR-33028, titin was found to be upregulated, when compared to the titin levels in vehicle-treated mice. Activation of titin expression may represent the initiation of myofibre repair as a result of the long-term treatment with KR-33028.

Adenosylhomocysteinase (SAHH) is a metabolic enzyme that catalyses the reversible hydrolysis of S-adenosyl-L-homocysteine (AdoHcy) to adenosine (Ado) and L-homocysteine (Hcy) (De La Haba and Cantoni, 1959; Palmer and Abeles, 1979). Deficiency of SAHH has been shown to result in elevated serum CK concentrations, and hypermethioninaemia, an excess of methionine in the blood (Buist *et al.*, 2006). Since 2004, a series of cases of SAHH deficiency have been clinically described. They are characterized by white matter atrophy, retarded psychomotor development, delayed myelination, progressive myopathy, and mildly active chronic hepatitis (Barić *et al.*, 2004; Barić *et al.*, 2005; Buist *et al.*, 2006; Grubbs *et al.*, 2010; Honzík *et al.*, 2012; Stender *et al.*, 2015). Additionally, deficiency of SAHH may lead to cardiovascular diseases (Zaina

et al., 2005) and tumorigenesis (Leal *et al.*, 2008; Li *et al.*, 2014). The current study demonstrated an upregulation of SAHH in dystrophic skeletal muscles treated with KR-33028, when compared to untreated dystrophic samples. One might speculate that increased levels of SAHH in treated muscle also acts towards an antagonisation of dystrophin-deficient pathophysiology by reducing methionine levels and improving muscle function.

Proteins involved in the protein synthesis, i.e. the ribosomal proteins RPS5 and RPS15, and vigilin, have also been found to be upregulated in the KR-33028-treated samples. Vigilin, also known as HDLBP (high density lipoprotein binding protein), is associated with 80S ribosomes, interacts with several ribosomal proteins, and is involved in nuclear export of tRNA, cytoplasmic transport of RNA, and metabolism of specific mRNAs (Kruse *et al.*, 1998; Kruse *et al.*, 2003; Vollbrandt *et al.*, 2004). Furthermore, it plays an important role in the cellular sterol metabolism in human atherogenesis (Chiu *et al.*, 1997). Additionally, histone H1.0 (H1f0), a chromatin-associated DNA-binding protein, was found to be downregulated in KR-33028-treated samples. As a histone linker, H1f0 is involved in the regulation of chromatin architecture via protein-DNA interactions. Moreover, it interacts with a series of proteins essential for RNA metabolism in the nucleolus (Kalashnikova *et al.*, 2013; Kowalski, 2016). Conclusively, our findings suggest that protein synthesis increased as a result of the treatment with KR-33028, which might reflect an attempt of the skeletal muscle cells to restore the levels of proteins that are otherwise absent/downregulated in dystrophic muscle cells.

Additionally, NEFH, the heavy neurofilament protein, was found to be upregulated in treated TA muscles. NEFH has been linked to the development of amyotrophic lateral sclerosis (ALS) (Figlewicz *et al.*, 1994), a motor neuron disease, and axonal Charcot-Marie-Tooth disease 2CC (CMT2CC), an autosomal dominant peripheral neuropathy (Jacquier *et al.*, 2017; Khadilkar *et al.*, 2017). NEFH is located within the mitochondria and its loss of function has previously been associated with enhanced aerobic glycolysis and mitochondrial dysfunction (Kim *et al.*, 2010). Its upregulation in the treated samples might potentially signify an improved mitochondrial function and energy provision to the cells. Contradictory to these findings, the mitochondrial protein mt-CYB was amongst the pool of proteins found to be downregulated in the skeletal muscle of treated animals. Mt-CYB is a component of the mitochondrial complex III (CoQH2-cytochrome C reductase), a multiprotein enzyme complex essential for the biochemical generation of ATP via the oxidative phosphorylation (OXPHOS) system. Mutations within the *MT-*

CYB, the gene that encodes mt-*CYB*, usually manifest as exercise intolerance and fatigability (Andreu *et al.*, 1999; Gil Borlado *et al.*, 2010). They are the major cause of complex III deficiency, a clinically heterogeneous group of mitochondrial respiratory chain disorders (Benit *et al.*, 2009), and underlie a wide range of musculoskeletal and nervous system pathologies, including Leber's hereditary optic neuropathy (LHON) (Brown *et al.*, 1992), mitochondrial encephalomyopathy (Keightley *et al.*, 2000), hypertrophic or histiocytoid cardiomyopathy (Valnot *et al.*, 1999; Andreu *et al.*, 2000; Hagen *et al.*, 2013), sporadic mitochondrial myopathy (Andreu *et al.*, 1999) and fibromyalgia (Cordero *et al.*, 2016), and multisystem disorders (Wibrand *et al.*, 2001; Carossa *et al.*, 2014). Our findings suggest an alteration of the mitochondrial function as a result of the long-term treatment with KR-33028. However, and since our study is limited to the LC-MS/MS analysis, it was not possible to determine the exact mitochondrial functions affected by the treatment with KR-33028, and the extent of these effects. The levels of NEFH and mt-*CYB* in KR-33028- and vehicle-treated samples need to be verified via western blotting or immunohistochemistry. Additionally, further studies are needed to investigate the impact of KR-33028 treatment on mitochondrial function of skeletal and cardiac muscles.

The abundance of PMM2, an enzyme essential for the N-linked glycosylation of proteins (Sharma and Freeze, 2014), was significantly reduced in samples collected from KR-33028-treated mice. PMM2 deficiency causes congenital disorder of glycosylation type Ia (CDG Ia), a multisystem disorder caused by defective of serum glycoproteins and characterised by developmental and neurological abnormalities (Jaeken *et al.*, 1980; Matthijs *et al.*, 1999; Grünewald, 2009; Perez-Cerda *et al.*, 2017).

During this study, it was hypothesized that long-term treatment of dystrophic mice with the NHE1 inhibitor KR-33028 would reduce the elevated intracellular Ca^{2+} levels observed in dystrophic muscle. Proteomic analysis demonstrated that CAB39, a Ca^{2+} -binding protein also known as MO25 (Zeqiraj *et al.*, 2009; Filippi *et al.*, 2011), is downregulated in the KR-33028-treated TA muscle samples, suggesting that the treatment had an effect on the skeletal muscle Ca^{2+} machinery. CAB39 is involved in the activation of the sodium-potassium-chloride co-transporters (NKCCs) and inhibition of the potassium-chloride ion co-transporters (KCCs) (de Los Heros *et al.*, 2014). Moreover, the proteins PPP3CA and PPP3CB, found to have significantly changed in abundance in the treated samples, are Ca^{2+} -dependent and calmodulin-stimulated. Calmodulin (Ca^{2+} -modulated protein) is a multifunctional intermediate Ca^{2+} -binding messenger protein

(Chang *et al.*, 2016; Jingting *et al.*, 2017; Myers *et al.*, 2017). Titin also presents Ca²⁺- and calmodulin-binding activities (Labeit *et al.*, 2003; DuVall *et al.*, 2017). The change in abundance of proteins with Ca²⁺- and calmodulin-binding activities acts to further strengthen our hypothesis that long-term treatment of dystrophin-deficient skeletal muscle may act to reduce intracellular Ca²⁺ levels and subsequently improve DMD pathology.

Gene ontology analysis of the network of proteins identified to be regulated in the KR-33028-treated mice demonstrated the absence of any significant functional and PPI enrichments. However, analysis of all 29 proteins that were significantly different between the two groups of mice demonstrated functional enrichment of 4 molecular functions, catalytic activity (59%), calmodulin-dependent protein phosphatase activity (7%), poly(A) RNA binding activity (28%) and peroxiredoxin activity (7%). Furthermore, a PPI network analysis of proteins found to be significantly different in abundance between KR-33028-treated and vehicle-treated *mdx* mice (p-value=1.12e-08) demonstrated how the proteins are interconnected with each other.

In conclusion, proteomic analysis demonstrated that chronic treatment of dystrophic mice with KR-33028 resulted in a significant change of abundance of key skeletal muscle proteins and impacted on the Ca²⁺ machinery. The exact mechanisms by which the compound exerted its effects are not well established or understood, and further studies are required to investigate the networks of proteins that were affected by the treatment. Moreover, a critical investigation of how the proteome of the treated *mdx* mice compares to that of C57BL/10 control mice is warranted.

Chapter 7. General discussion and future directions

Development and approval of genetic treatment approaches to treat DMD will take time and even when approved they may only be suitable for a select patient population and/or able to alleviate pathology but not relieve them completely. Consequently, therapies that, either independently or in combination with other treatment strategies, improve disease pathology are needed (Hollinger and Selsby, 2013). In the present study, we focused our attention on the hypothesis that dysregulation of Ca^{2+} homeostasis contributes to DMD pathology (Vandebrouck *et al.*, 2002; van Deutekom *et al.*, 2007; Millay *et al.*, 2009).

The disruption of Ca^{2+} homeostasis observed in DMD muscle (Oberc and Engel, 1977; Duncan, 1978) contributes to increased activation of the Ca^{2+} -activated proteases, such as calpains, and the ubiquitin proteasome pathway, and thus may accelerate proteolysis in response to contractile activity, increase oxidative stress and inflammation, and, ultimately, lead to fibre death by necrosis (Hollinger and Selsby, 2013). Consequently, targeting the elevated intracellular Ca^{2+} levels has been proposed as a way of improving DMD pathology.

The elevation of intracellular Ca^{2+} levels has been attributed to the mechanical damage of the sarcolemma but also deficiencies in several Ca^{2+} -regulatory proteins (Vallejo-Illarramendi *et al.*, 2014; Burr and Molkenin, 2015). Recent evidence suggests that increased activity of the NHE1 exchanger also contributes to the dysregulation of Ca^{2+} homeostasis (Deval *et al.*, 2002; Iwata *et al.*, 2007; Burr *et al.*, 2014; Bkaily *et al.*, 2015). It is speculated that NHE1 over-activity leads to an increased influx of Na^+ , which in turn switches the NCX exchanger into reverse mode, resulting in an increased Ca^{2+} influx. The current study sought to investigate how inhibition of NHE1 may impact on the pathophysiology of DMD using the *mdx* mouse model of this disease. More specifically, the efficacy of the KR-33028 compound, a very specific and potent NHE1 inhibitor with a good safety and potency profile (Kim *et al.*, 2005; Jung *et al.*, 2006; Kim *et al.*, 2006; Kim *et al.*, 2007a; Kim *et al.*, 2007b; Kim *et al.*, 2007c; Oh *et al.*, 2007; Lee *et al.*, 2009), was investigated. It was hypothesised that long-term treatment of *mdx* mice with the KR-33028 NHE1 inhibitor would lead to a decrease of the intracellular Na^+ levels, reversal of the NCX back to normal and subsequent decrease of the Ca^{2+} influx within the skeletal and cardiac muscle cells.

7.1 Investigating the effects of KR-33028 *in vivo*

The *mdx* mouse model is genetically and biochemically homologous to human DMD, and although it presents a comparable mild phenotype (Anderson *et al.*, 1988; Lefaucheur *et al.*, 1995), it is the most commonly used DMD animal model for pre-clinical studies. For the purposes of this study, eleven *mdx* mice were treated with the KR-33028 compound for the period of ~6 months, which may be the most relevant time point to compare with human disease (Jørgensen *et al.*, 2011).

Ideally, the compound would have been administered through an IV injection which offers a more direct route of dosing by avoiding GI absorption and metabolism leading to greater drug exposure (Rang *et al.*, 2015). However, due to the workload involved in handling all the mice, administration through an IV injection was not feasible so the drug was formulated in standard mouse chow. The drug-formulated chow was formulated using 750 mg of KR-33028 per kg of chow. This dose was chosen based on the availability of the compound (~10 g), the number of mice that were treated (11), the length of treatment period (~6 months), and previous reports of efficacy and toxicity of the compound (Jung *et al.*, 2006; Kim *et al.*, 2007a; Kim *et al.*, 2007c; Oh *et al.*, 2007; Lee *et al.*, 2009). However, as demonstrated by HPLC analysis, formulation of the compound in chow was not 100% efficient. The chow contained ~590 mg of KR-33028 per kg, instead of 750 mg, which suggested that ~21% of the compound was lost during the formulation processes. Consequently, the mice were treated with a lower dose of compound (~94.4 mg/kg) than the one that was initially estimated (~120 mg/kg); the dose of compound was estimated based on the daily eating rate of the mice (~4 g of chow per day) and average mouse body weight (25 g).

Stability testing confirmed that storage of KR-33028-formulated chow at ambient temperature over the period of 6 months had minimal effects on the degradation of the compound in the chow, suggesting that the concentration of the compound remained stable over the 6-month treatment of the *mdx* mice.

In addition to stability testing, PK studies are an essential component of every drug-development study. We investigated the drug concentration in the plasma of *mdx* mice after administration via IV injection, oral gavage or drug-formulated chow. Notably, drug-formulated chow presented 19.30% bioavailability, which is comparable to the one of oral gavage, 18.07%. Moreover, the C_{\max} of the drug in plasma collected from mice fed with drug-formulated chow was 103.65 ng/mL and the plasma concentration did not

go below 30 ng/mL at any time during the treatment. Based on previous reports, it was postulated that the detected plasma concentrations were well above the minimum effective concentration of KR-33028 and within the therapeutic window (Kim *et al.*, 2007a). This suggests that the dose of KR-33028 given to the mice, although lower than the one that we initially intended to use, was high enough to reach appropriate plasma levels to achieve the desired therapeutic effects.

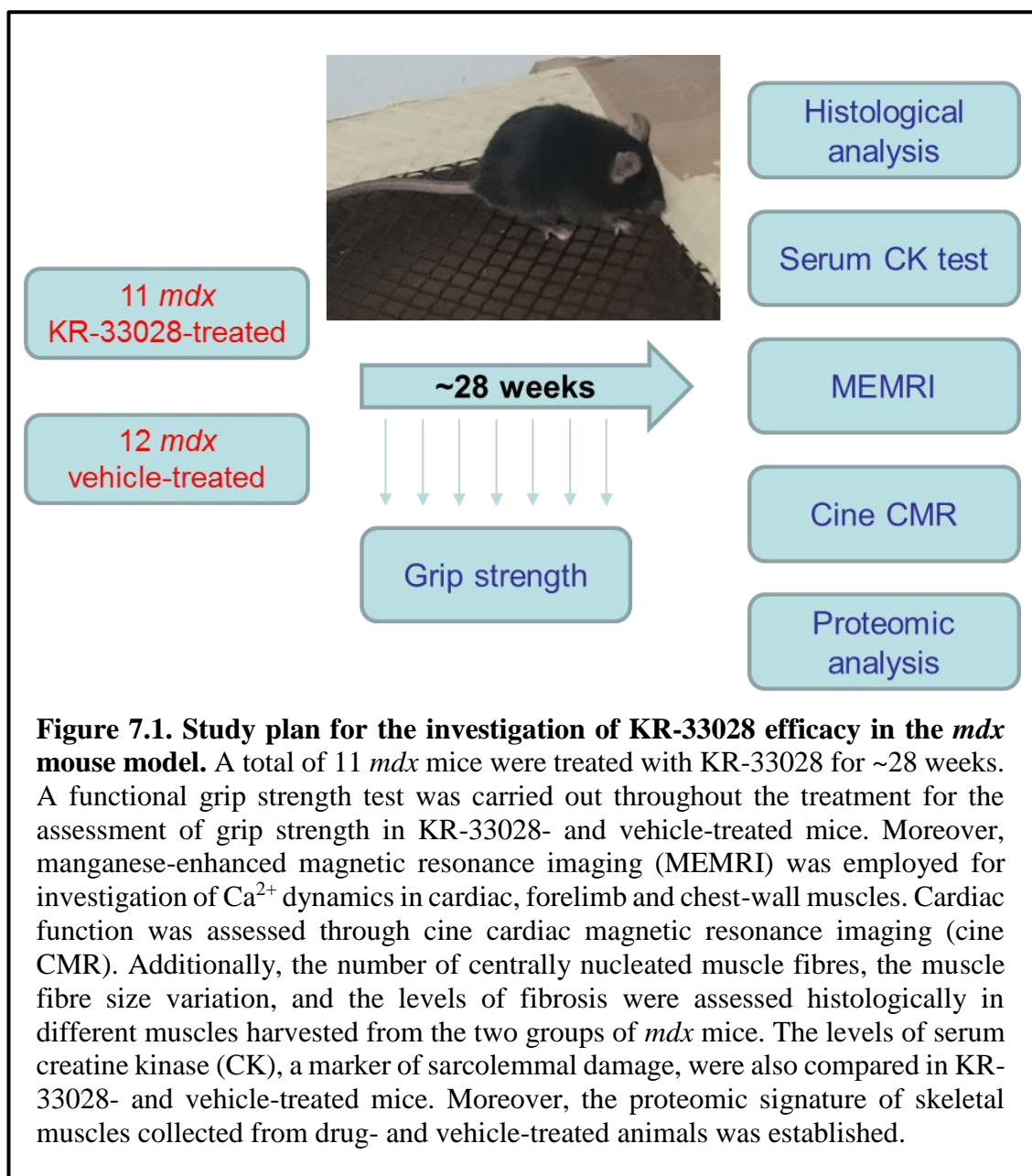


Figure 7.1. Study plan for the investigation of KR-33028 efficacy in the *mdx* mouse model. A total of 11 *mdx* mice were treated with KR-33028 for ~28 weeks. A functional grip strength test was carried out throughout the treatment for the assessment of grip strength in KR-33028- and vehicle-treated mice. Moreover, manganese-enhanced magnetic resonance imaging (MEMRI) was employed for investigation of Ca^{2+} dynamics in cardiac, forelimb and chest-wall muscles. Cardiac function was assessed through cine cardiac magnetic resonance imaging (cine CMR). Additionally, the number of centrally nucleated muscle fibres, the muscle fibre size variation, and the levels of fibrosis were assessed histologically in different muscles harvested from the two groups of *mdx* mice. The levels of serum creatine kinase (CK), a marker of sarcolemmal damage, were also compared in KR-33028- and vehicle-treated mice. Moreover, the proteomic signature of skeletal muscles collected from drug- and vehicle-treated animals was established.

The efficacy of KR-33028 was investigated by measuring the impact of 28 weeks of treatment on a series of functional, biochemical, imaging and histological parameters in the *mdx* mouse (Figure 7.1). More specifically, a functional hanging wire test was carried out throughout the treatment for the assessment of grip strength in KR-33028- and vehicle-treated mice. Moreover, MEMRI was employed for the investigation of Ca^{2+}

dynamics in cardiac, forelimb and chest-wall muscles. Cardiac function was assessed through cine CMR imaging. Additionally, the number of centrally nucleated muscle fibres, the muscle fibre size variation, and the levels of fibrosis were assessed histologically in different muscles harvested from the two groups of *mdx* mice. The levels of serum CK, a marker of sarcolemmal damage, were also compared in KR-33028- and vehicle-treated mice, as was the proteomic signature of TA muscles collected from drug- and vehicle-treated animals.

7.1.1 Efficacy of KR-33028 in improving DMD pathology of *mdx* skeletal muscles

The findings of the current study suggest that long-term treatment with KR-33028 improved DMD pathology of *mdx* skeletal muscles. The most encouraging finding was that functional grip strength of *mdx* mice treated with KR-33028 had significantly improved with progression of treatment. The maximum holding impulse that the group of drug-treated mice had achieved during the 28-week treatment was 74.86 N sec, in comparison to 43.61 N sec that the vehicle-treated mice achieved, and 91.30 N sec that control (C57BL/10) mice can achieve (unpublished data collected during the pilot study conducted prior the initiation of this project). This equates to a 65% improvement of functional grip strength as a result of the KR-33028 treatment. Additionally, long-term treatment with KR-33028 reduced fibrosis in the diaphragm. Although fibrosis in the femoral quadriceps muscles was not significantly impacted by the treatment, it has been proposed that this could be due to the variable disease severity in different muscle types of the *mdx* mouse (Moens *et al.*, 1993; Muller *et al.*, 2001; Ljubicic *et al.*, 2011). Notably, muscle fibre size variation, and the number of centrally nucleated fibres, markers of ongoing muscle fibre regeneration, in the diaphragm did not improve after the chronic treatment. As noted by Jørgensen *et al.* (2011), the presence of centrally located myonuclei does not depict the amount of times each individual muscle fibre has undergone a round of degeneration-regeneration. It can, therefore, be speculated that if the muscles have undergone fewer degeneration-regeneration cycles the satellite cell pool will not be exhausted enabling muscle fibre repair. This could potentially result in the pattern of regeneration (indicated by high muscle fibre size variation and number of centrally nucleated muscle fibres) accompanied by reduced fibrosis observed in diaphragm muscles of KR-33028-treated *mdx* mice.

Despite the histological and functional assessments demonstrating a positive effect of KR-33028 on the *mdx* muscle damage, the serum CK levels of the drug-treated mice were

not significantly different from the ones in vehicle-treated animals. It is, however, important to note that reducing the intracellular Ca^{2+} levels via inhibition of NHE1 might delay onset and/or improve disease pathology, but it will not correct the membrane fragility defect and microtears. As a result, soluble proteins such as CK might continue to leak out of the cell, which might explain why the serum CK levels were not impacted by the long-term treatment with KR-33028.

The above functional, biochemical and histological tests are standard tools employed for pre-clinical drug testing (Spurney *et al.*, 2009). In addition to these tests, we employed MEMRI in order to assess the Ca^{2+} dynamics of chest-wall and forelimb muscles of drug- and vehicle-treated animals. Previous MEMRI experiments have demonstrated that *mdx* mice, when compared to age-matched control (C57BL/10) mice, present elevated Ca^{2+} uptake in their myocardium, forelimb and chest-wall muscles (Greally *et al.*, 2012; Greally *et al.*, 2014). The pilot study conducted prior the initiation of this project demonstrated that treatment of *mdx* mice for 6 weeks (dosing via oral gavage, 20 mg/kg) significantly reduced Ca^{2+} uptake in both forelimb and chest-wall muscles (Burki *et al.*, 2014). However, the current study failed to detect any significant differences between the Ca^{2+} uptake in chest-wall and forelimb muscles of drug-treated mice and that of vehicle-treated animals. It is important to note that the MEMRI experiments carried out during our study assumed that Mn^{2+} can access any route that is available to Ca^{2+} . Nevertheless, although evidence exists to suggest that Mn^{2+} can enter the cardiac and skeletal muscle cells through different Ca^{2+} transporters, including L-type Ca^{2+} channels (Blain *et al.*, 2013; Greally *et al.*, 2013), no solid evidence exists, to our knowledge, to suggest that Mn^{2+} can also enter through the NCX exchanger. Moreover, it is possible that small transient changes were not detected by MEMRI due to the sensitivity of the technique. Therefore, the suitability of MEMRI for the assessment of the effect of KR-33028 on Ca^{2+} dynamics could not be proven during our study. Alternative techniques that could be used to investigate intracellular Ca^{2+} levels and dynamics in dystrophin-deficient muscle are further explored in section 7.2.

Of particular interest was the finding that 6-months treatment of dystrophic mice with KR-33028 resulted in a significant change of abundance of key skeletal muscle proteins, including titin, a key cardiac and skeletal muscle protein, which was found to be upregulated in TA muscles of treated mice. Activation of titin expression in the KR-33028-treated skeletal muscles may represent the initiation of myofibre repair as a result of the long-term treatment with KR-33028. Moreover, amongst the proteins that were

found to be regulated in the treated samples were the CAB39, PPP3CA and PPP3CB proteins, which present a Ca^{2+} - and calmodulin-binding activities. The change in abundance of these proteins acts to further strengthen our hypothesis that long-term treatment of dystrophin-deficient skeletal muscle may act to reduce intracellular Ca^{2+} levels and subsequently improve DMD pathology. Additionally, upregulation of NEFH and downregulation of mt-CYB, two mitochondrial proteins, in the KR-33028 samples suggest that some mitochondrial functions were affected by the treatment with KR-33028. However, and since our study was limited to LC-MS/MS, it was not possible to determine the extent of these effects. The levels of NEFH and mt-CYB in KR-33028- and vehicle-treated samples need to be verified via western blotting or immunohistochemistry. Additionally, further studies are needed to investigate the impact of KR-33028 treatment on mitochondrial function of skeletal and cardiac muscles. Our findings also suggest that protein synthesis had increased as a result of the treatment with KR-33028, which might reflect an attempt of the skeletal muscle cells to restore the levels of proteins that are otherwise absent/downregulated in dystrophic muscle cells. Furthermore, the levels of PMM2, a protein responsible for N-glycosylation of proteins, were found to be significantly reduced in KR-33028-treated TA samples. Notably, since data from control (C57BL/10) mice are not available, and due to the limitations that proteomics techniques present (Kinoshita *et al.*, 2006; Chandramouli and Qian, 2009; Duncan *et al.*, 2010), the proteomics results need to be treated with caution.

7.1.2 Efficacy of KR-33028 in improving DMD pathology of mdx cardiac muscles

DMD patients develop cardiomyopathy that leads to early death due to heart failure (Oldfors *et al.*, 1994; Toyo-oka *et al.*, 2002). Early assessment and treatment of heart failure in DMD is therefore essential (Romfh and McNally, 2010). A plethora of experimental studies have demonstrated that NHE1 inhibitors exert marked cardioprotective effects (Morris, 2002; Chahine *et al.*, 2005; Karmazyn, 2013; Bkaily *et al.*, 2015; Bkaily and Jacques, 2017). A number of NHE1 inhibitors have been shown to protect the myocardium against ischaemic and reperfusion injury, myocardial remodelling, and heart failure in different animal models, including the UM-X7.1 hereditary cardiomyopathic hamster (HCMH) (Bkaily *et al.*, 2015; Bkaily and Jacques, 2017), BIO14.6 hamsters (Iwata *et al.*, 2007) and *mdx* mice (Porte Thomé *et al.*, 2016; Gidaro *et al.*, 2017). KR-33028 has also been shown to have cardioprotective effects and

to reduce myocardial infarction due to ischaemia-reperfusion injury in rats and dogs (Kim *et al.*, 2006; Oh *et al.*, 2007).

Cine cardiac MRI was employed to assess the effects of KR-33028 treatment on the development and progression of cardiomyopathy in *mdx* mice during the current study. It was demonstrated that the left and right ventricular functions, including the LVMI, ESVI, SVI, CI, RVEDVI, RVSVI and RVEF, were significantly decreased in both groups of mice (vehicle- and KR-33028-treated) at the end of treatment, suggesting that the function of the hearts of the drug-treated mice was not significantly impacted by the treatment with KR-33028. The levels of fibrosis in hearts harvested from KR-33028-treated *mdx* mice were not impacted by the treatment either. On the other hand, MEMRI demonstrated that the long-term treatment with KR-33028 reversed the aged-related reduction in Ca^{2+} uptake in the myocardium of treated mice. These data suggest that long-term treatment with KR-33028 improved the Ca^{2+} levels in the hearts of dystrophin-deficient animals but not the heart function. However, due to the lack of wild type mice (C57BL/10) in our study design these data need to be further explored and validated.

The observed improvement of the skeletal and respiratory muscle phenotype is in discordance with the worsening of the cardiac muscle phenotype. Although worsening of skeletal muscle pathology has previously been suggested to worsen cardiac muscle pathology in *mdx* mice (Megney *et al.*, 1999), it is not clear why correction of skeletal muscle would worsen heart disease. Townsend *et al.* (2008), Townsend *et al.* (2009) and Jørgensen *et al.* (2011) argue that repaired skeletal muscle might enable increased exercise capacity, which would in turn place an additional load on the dystrophic heart and trigger heart remodelling. This is also supported by the studies of Kamogawa *et al.* (2001), Yasuda *et al.* (2005), and Townsend *et al.* (2007), which have indicated that dystrophin-deficient hearts are susceptible to increases in work load. This might also explain why the improvement of Ca^{2+} levels in hearts of treated animals (reversal of age-related effects) demonstrated by MEMRI was not accompanied by improvement of cardiac functions. No obvious behavioural changes were observed in the group of KR-33028-treated mice, and the animals appeared to be well-groomed and active. However, the possibility that the physical activity level is heightened as a result of the treatment should be tested using specific behaviour studies and exercise regimens.

7.2 Future directions

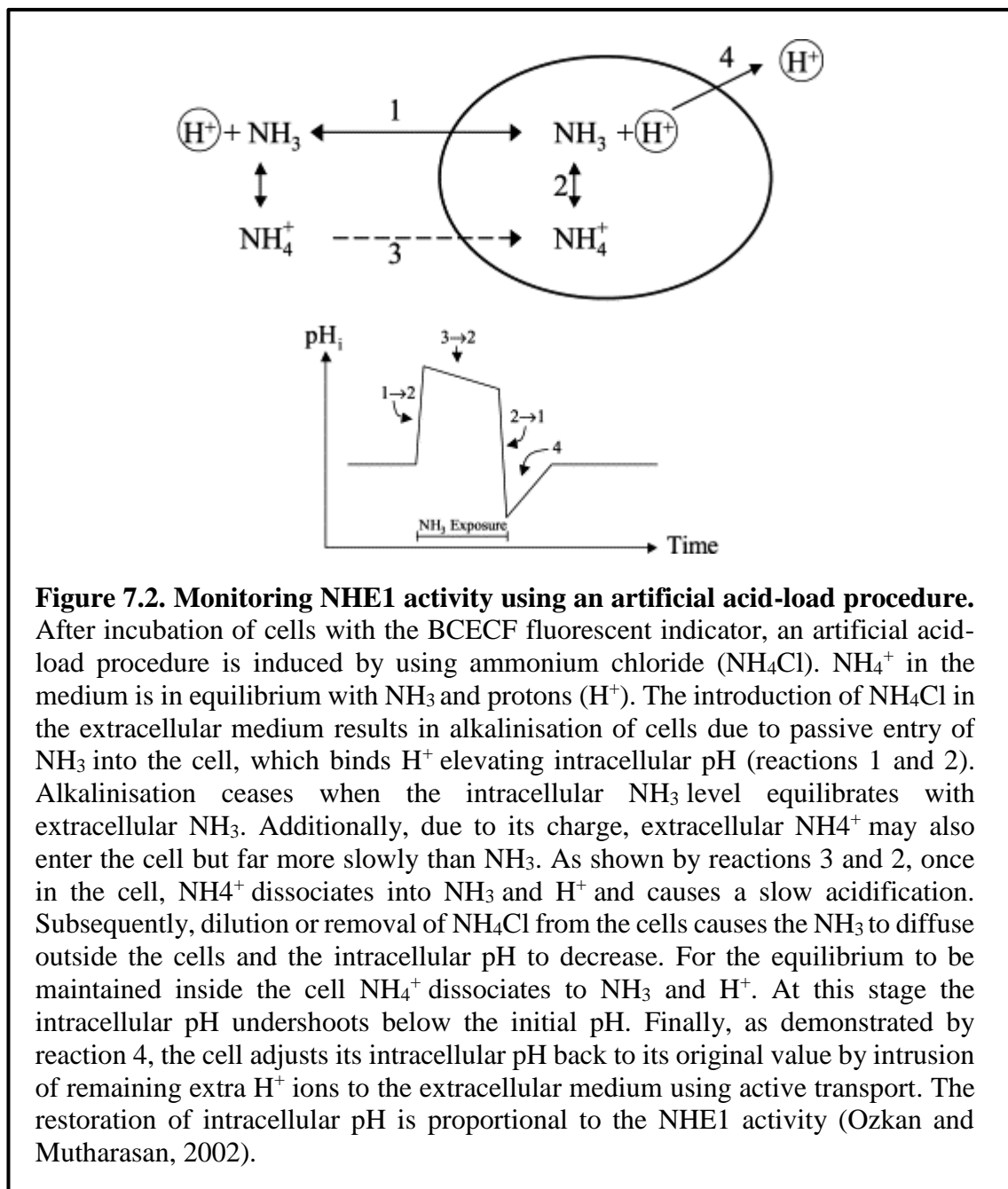
Our study is based on the hypothesis that NHE1 is overactive in DMD. It has been postulated that NHE1 inhibition will result in a decrease of intracellular Na^+ levels, reversal of NCX back to normal, and subsequent decrease of intracellular Ca^{2+} levels. In support of this hypothesis are the studies of a number of different groups (Deval *et al.*, 2002; Iwata *et al.*, 2007; Bkaily *et al.*, 2015; Porte Thomé *et al.*, 2016; Bkaily and Jacques, 2017; Gidaro *et al.*, 2017), which provide supportive evidence that NHE1 inhibition can ameliorate DMD pathology of both cardiac and skeletal muscles in dystrophic animals. The current study has demonstrated a positive effect of chronic treatment with KR-33028 on the DMD pathology of *mdx* skeletal muscles. Additionally, MEMRI and proteomic analysis that were carried out during this project suggest that chronic treatment with KR-33028 impacted on the Ca^{2+} machinery of cardiac and skeletal muscles further solidifying our theory. Nevertheless, further studies are needed to confirm the NHE1 over-activity and its downstream effects in DMD, and to demonstrate how KR-33028 engages its target, also known as ‘target engagement’ studies. Target engagement is a critical step for drug development because it allows for assessment of compound efficacy and confirmation of mode of action (Simon *et al.*, 2013; Schürmann *et al.*, 2016). Considerations for future preclinical investigations, as well as possible future studies for experimental testing of model claims, are suggested below:

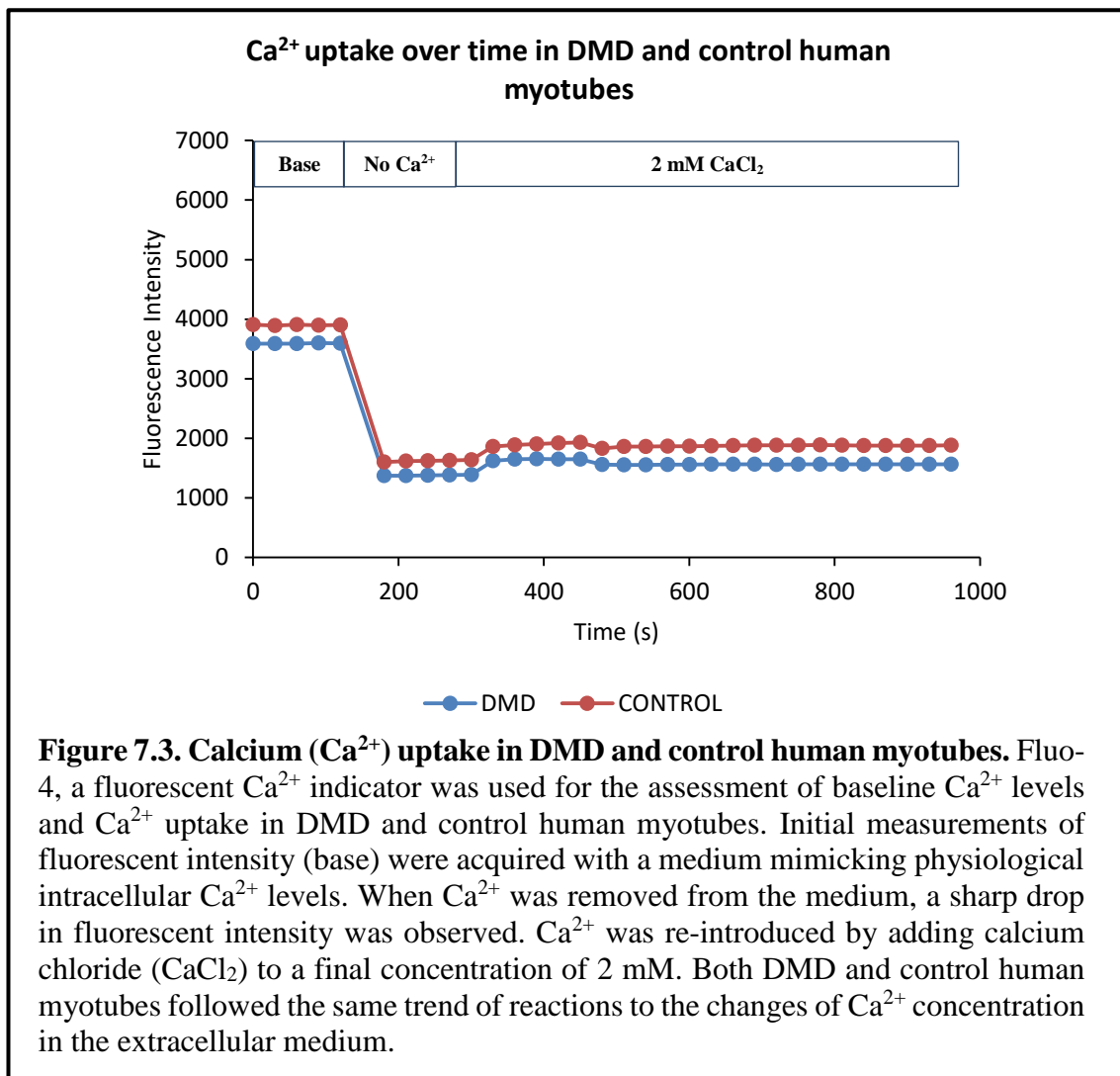
- **Verification of NHE1 over-activity and its impact on intracellular Ca^{2+} and Na^+ levels in DMD.**

In vitro fluorescent assays designed to assess intracellular pH, Na^+ and Ca^{2+} levels could be used to assess NHE1 activity and its impact on intracellular Ca^{2+} and Na^+ levels in DMD.

BCECF, a pH fluorescent indicator, has successfully been employed for the *in vitro* characterisation of NHE1 activity by a series of studies (Ozkan and Mutharasan, 2002; Touret *et al.*, 2003; Kim *et al.*, 2007a; Feger and Starnes, 2013). The proposed assay monitors NHE1 by measuring changes in intracellular pH following an artificial acid-load procedure induced by using ammonium chloride (NH_4Cl). The cells under investigation are incubated with the fluorescent dye, BCECF, and then NH_4Cl . The presence of NH_4Cl leads to the formation of ammonia (NH_3) in the cytoplasm, and subsequent alkalisation (demonstrated by increase of fluorescent signal, Figure 7.2). Following this step, NH_4Cl is diluted or removed from the cells, which causes NH_3 to

move outside the cell, and leaves a high concentration of protons (H^+) inside the cytoplasm (low pH, demonstrated by decrease of fluorescence signal, Figure 7.2). NHE1 is now responsible for the removal of the excess protons from the cytoplasm. This is seen as a slow increase of fluorescent signal, proportional to the NHE1 activity (reaction 4 Figure 7.2). Using this assay, the inhibitory effect of NHE1 inhibitors can also be investigated. Preliminary studies have already been conducted in our lab, optimising the use of BCECF-AM fluorescent indicator for the investigation of the NHE1 activity in DMD versus control myotubes, but also the inhibitory effect of KR-33028 on NHE1 (Appendix A).





During the course of our study we also attempted to test the impact of KR-33028 on intracellular Ca²⁺ levels by employing *in vitro* fluorescent Ca²⁺ assays. The levels of intracellular Ca²⁺ in DMD myotubes were not found to be significantly different from that of control myotubes (Figure 7.3) rendering this model unsuitable for the purpose of these assays. Consequently, we questioned the usability of other models, including single muscle fibres isolated from *mdx* FDB (flexor digitorum brevis; located medially at the sole of the foot) and EDL (extensor digitorum longus; located at the anterior lateral part of the leg) muscles. Although single muscle fibres were successfully isolated from these muscles, loading of the fibres with fluorescent Ca²⁺ dye was uneven, which suggests the presence of tears on the muscle membrane, a sign of DMD pathology and/or damage that occurred during the isolation of fibres. This shows that single muscle fibres might not be a suitable model for these assays either. In support of our findings are a series of studies that have shown no significant differences between the intracellular Ca²⁺ levels in skeletal muscle cells isolated from DMD patients or *mdx* mice and that of control muscle cells (Gailly *et al.*, 1993; Head, 1993; Pressmar *et al.*, 1994; Yeung *et al.*, 2005). Conversely,

a series of studies suggest that intracellular Ca^{2+} levels in dystrophic skeletal muscle cells and fibres are elevated (Turner *et al.*, 1988; Fong *et al.*, 1990; Imbert *et al.*, 2001). The controversy could be attributed to experimental variations between the different laboratories. Therefore, prospective studies need to take these variations into consideration.

In addition to the fluorescent assays, electrophysiological studies using patch-clamping techniques might be a great tool for assessing resting intracellular Ca^{2+} levels and rates of Ca^{2+} release and reuptake in DMD muscle cells, and the impact of NHE1 inhibition on them (Hamill *et al.*, 1981; Imbert *et al.*, 2001). Furthermore, recent studies have proposed the use of Ca^{2+} - and Na^{+} -sensitive microelectrodes for *in vivo* assessment of Ca^{2+} dynamics in dystrophic animals (Altamirano *et al.*, 2012; Altamirano *et al.*, 2013; Burr *et al.*, 2014).

- **Extend the findings of proteomic analysis with protein-protein interaction assays.**

Proteomic analysis of TA muscles isolated from drug- and vehicle-treated mice yielded interesting results. It was demonstrated that treatment with KR-33028 had an effect on the abundance of key skeletal muscle proteins and the Ca^{2+} machinery. However, the exact mechanisms by which the compound exerted its effects are not well established or understood. Additionally, proteomics present a number of limitations, including, undersampling of complex proteomic samples, and limited capacity to detect low-abundance peptides (Kinoshita *et al.*, 2006; Chandramouli and Qian, 2009; Duncan *et al.*, 2010). It is necessary that future studies verify the levels of proteins found to be regulated in the KR-33028-treated muscles and compare them to the ones of muscle samples harvested from control (C57BL/10) mice using techniques such as western blotting and immunohistochemistry. Additionally, the specific interactions between the proteins identified to be up- or down-regulated in treated animals need to be explored by, for example, employing pull-down assays, and immunofluorescence techniques. Notably, these experiments will also contribute to our understanding of the events occurring downstream of NHE1 inhibition.

- **Evaluation of the time-point of treatment initiation and the administered drug dose.**

Evidently, dystrophic pathological characteristics, including Ca^{2+} dysregulation and ultrastructural disturbances, appear at an early embryonic stage (Turkel *et al.*, 1981; Bertorini *et al.*, 1984). Similarly, the dystrophic process in the *mdx* mouse model begins

early in embryonic development and includes stem cell loss, structural muscle changes, and Ca^{2+} dysregulation (Merrick *et al.*, 2009; Jørgensen *et al.*, 2011). Consequently, correcting the intracellular Ca^{2+} levels through blockade of NHE1 from embryonic development may prevent initiation of DMD pathology or alleviate the pathology to a greater extent than postnatal treatment, a possibility that could be investigated by future studies.

In addition to the time-point of treatment initiation, the administered drug dose might also impact the effect of the treatment. The optimal dosage of a drug can be deduced from dose-response studies characterising drug tolerance, safety, and efficacy (Emilien *et al.*, 2000). Due to limited availability of the compound, the design of our study was limited to a single dose, which was estimated based on the number of mice that were treated, the length of the treatment, and previous drug efficacy and toxicity studies (Jung *et al.*, 2006; Kim *et al.*, 2007a; Kim *et al.*, 2007c; Oh *et al.*, 2007; Lee *et al.*, 2009). It is crucial that prospective studies obtain dose-response data for KR-33028. This will help to determine the optimal drug dose in the *mdx* mouse model, thus making the extrapolation of dose between species more accurate and the transition from pre-clinical to clinical investigations smoother.

- **Monitoring physical activity levels of animals during the course of treatment.**

Our study demonstrated that treatment of *mdx* mice with KR-33028 resulted in an improvement of skeletal and respiratory muscle pathology that was not accompanied by amelioration of cardiac muscle pathology. A series of studies have proposed that correction of skeletal muscle could result in increased physical activity which in turn could place an additional load on the dystrophic heart and worsen heart function (Townsend *et al.*, 2008; Townsend *et al.*, 2009; Jørgensen *et al.*, 2011). It is therefore essential that future studies monitor physical activity levels of treated animals using specific behaviour studies and exercise regimens during the course of treatment.

- **Extend the pharmacological study in other animal DMD models.**

The *mdx* mouse is the most commonly used and best understood animal model of DMD. It is a genetic homologue of the human disease and has therefore, been a great tool for elucidation of the molecular processes and underlying causes of the disease and developing novel therapeutic strategies (Willmann *et al.*, 2009; Manning and O'Malley, 2015). Although they present hallmark symptoms of the disease, *mdx* mice, compared to DMD patients, present a very mild clinical phenotype, which makes their clinical

relevance questionable. To resolve this, several groups have introduced forced exercise regimes that worsen the muscle pathology of the *mdx* mouse and which allow a better evaluation of the efficacy of experimental therapies (Vilquin *et al.*, 1998; Granchelli *et al.*, 2000; Hodgetts *et al.*, 2006). Consequently, exercised *mdx* mice might be a more compelling model for assessing the effects of NHE1 inhibition on DMD pathology.

Although less widely adopted, the GRMD canine DMD model, is more severely affected than the *mdx* mouse and phenotypically resembles human DMD (Sharp *et al.*, 1992; Howell *et al.*, 1997). Consequently, GRMD might present a more suitable model for evaluation of KR-33028 efficacy.

- **Correction of Ca²⁺ homeostasis in combination with other therapeutic interventions.**

The findings of the current study propose a positive impact of NHE1 inhibition by KR-33028 on the DMD skeletal muscle pathology. It is, however, important to note that although reducing the intracellular Ca²⁺ levels might delay onset and/or improve disease pathology, without concomitant correction of the membrane fragility defect, microtears, and non-specific Ca²⁺ uptake; eventually, muscle fibre degeneration, and necrosis will occur (Jørgensen *et al.*, 2011). It can therefore be speculated that combination of NHE1 inhibition with a gene replacement therapy may have more beneficial effects in improving DMD pathology (Spinazzola and Kunkel, 2016).

Furthermore, as highlighted before (section 7.1.2), correcting the Ca²⁺ homeostasis may benefit skeletal and respiratory muscles but not the heart. This is due to fundamental differences between the structure and function of the different types of muscles, but also the heightened physical activity levels observed in treated samples (Townsend *et al.*, 2009). Therefore, it might be beneficial to combine these treatments with cardioprotective agents.

7.3 Conclusion

Pre-clinical testing of drug efficacy in mouse models is a critical step in the process of moving promising therapies from the bench to the patient bedside. The current thesis presented promising results (i.e. functional grip strength, histology, MRI and proteomics data) on employing KR-33028 for the amelioration of DMD pathology and provided evidence for justification of further studies into these potential therapeutic compounds. It has also highlighted a series of limitations of pre-clinical investigations of drug efficacy, and the need for careful planning of such studies. Our study presented a series of limitations that came with collaborating with a commercial pharmaceutical company, including drug manufacturing restrictions (i.e. limited drug availability), time restraints, limited funds and regulatory aspects (e.g. I.P. and patents for drugs). Additionally, although the pharmacokinetic and pharmacodynamic data that we collected during this study are a valuable addition to the existing data, our efforts did not result in a standardised assay to demonstrate target engagement. Along with demonstration of target engagement, future studies will need to provide dose response and toxicology data, which are prerequisites for the drug progressing into clinical studies.

Appendix A.

In vitro fluorescent pH assay protocol to date

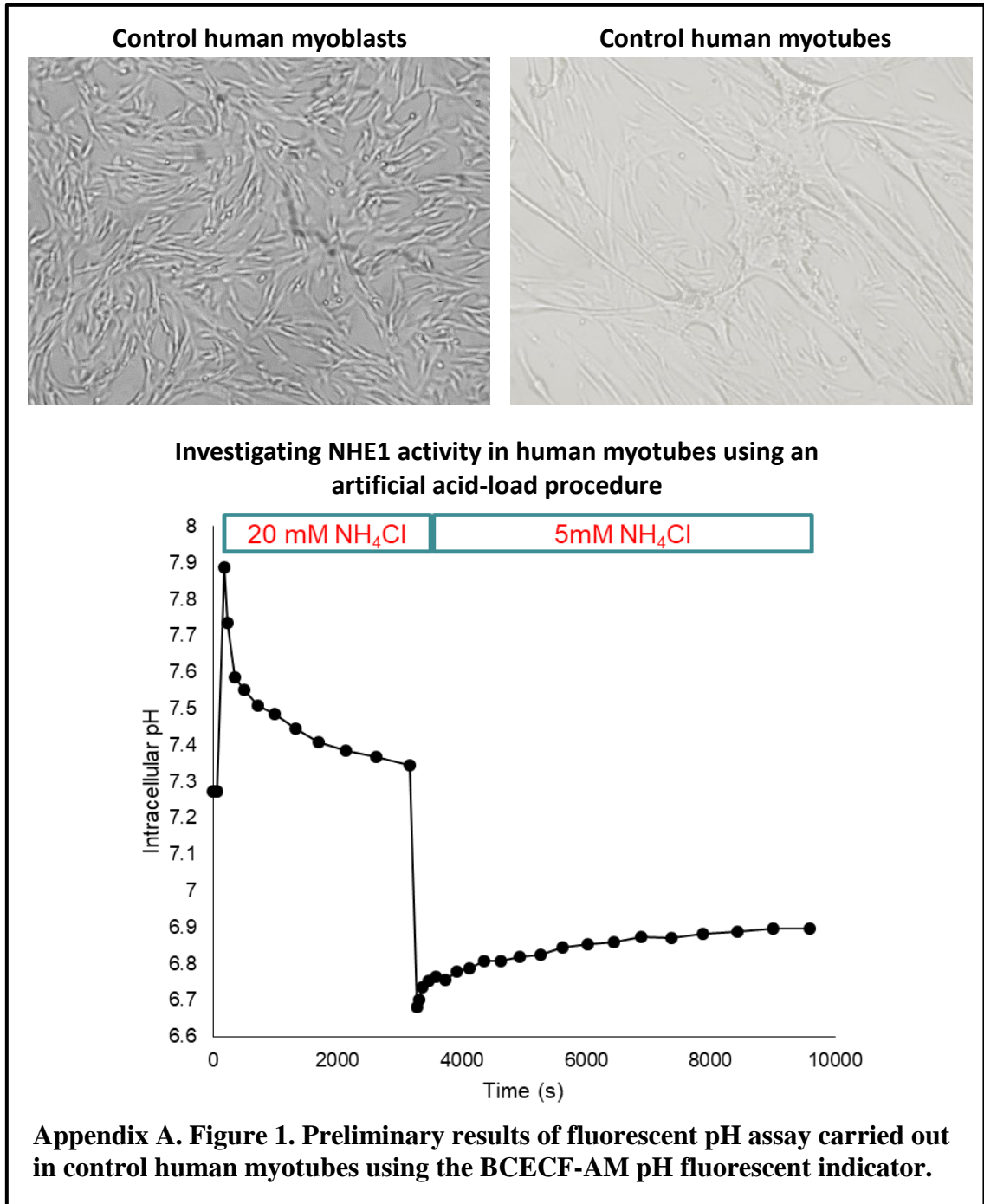
Solution	Composition
BCECF loading solution	10 μ M BCECF-AM, HBSS 1x, 20 mM HEPES, 2.5 mM probenecid
Acid load solution	200 mM NH_4Cl
Wash buffer	200 mM NH_4Cl , HBSS 1x, 20 mM HEPES, 2.5 mM probenecid
Compound diluent	HBSS 1x, 1 M HEPES, 250 mM probenecid
Calibration solution	135 mM KCl, 2 mM K_2HPO_2 , 20 mM HEPES, 1.2 mM CaCl_2 , 0.8 mM MgSO_4

Appendix A. Table 1. List of solutions used for fluorescent pH assay.

The composition of the solutions used for the pH fluorescent assay is shown in Appendix A. Table 1. The assay was carried out using control human myoblasts differentiated to myotubes, which were cultured in a black 96-well plate with clear bottom (Sigma Aldrich). The cells were loaded with BCECF-AM pH fluorescent indicator (Thermo Scientific) for 45 min at 37°C. Baseline fluorescence measurements were then obtained using the Thermo Scientific Varioskan LUX Multimode microplate reader (excitation: 440/490nm, emission: 535nm). To prepare for the acid load, ammonium chloride (NH_4Cl) was added to the cells to a final concentration of 20 mM and incubated for 15 min. Subsequently, the extracellular dye was washed out with wash buffer containing 20 mM NH_4Cl (3x washes) and fluorescence measurements were taken every 60 s for a total of 10 min. After the final wash, a small volume of medium was left covering the cells. This volume needed to be as small as possible to allow a large volume of fluid to be added in the wells to dilute out NH_4Cl . To initiate the acid load procedure, NH_4Cl was diluted 1 in 4 by adding the ‘compound diluent’, and fluorescence measurements were taken every 30 s for 10 min. Intracellular pH measurements with BCECF were made by determining the ratio of emission intensity at 535 nm when the dye was excited at 490 nm (pH-dependent) versus the emission intensity when the dye was excited at 440 nm (non pH-dependent).

BCECF fluorescence was calibrated *in situ* in the presence of 10 μ M nigericin (Sigma Aldrich) and a high potassium (K^+) solution (150 mM) at various external pH values

ranging from 5.5 to 8.5. Nigericin is a K^+/H^+ -exchanging ionophore that can equilibrate intracellular and extracellular pH when the extracellular concentration of potassium is in equilibrium with the intracellular concentration of potassium ($[K^+]_e = [K^+]_i$) (Ozkan and Mutharasan, 2002).



References

- Aartsma-Rus, A. and van Putten, M. (2014) 'Assessing Functional Performance in the *Mdx* Mouse Model', *Journal of Visualized Experiments : JoVE*, (85), p. 51303.
- Alderton, J.M. and Steinhardt, R.A. (2000) 'Calcium influx through calcium leak channels is responsible for the elevated levels of calcium-dependent proteolysis in dystrophic myotubes', *J Biol Chem*, 275(13), pp. 9452-60.
- Allen, D.G., Lamb, G.D. and Westerblad, H. (2008) 'Impaired calcium release during fatigue', *J Appl Physiol* (1985), 104(1), pp. 296-305.
- Allen, D.G. and Whitehead, N.P. (2011) 'Duchenne muscular dystrophy--what causes the increased membrane permeability in skeletal muscle?', *Int J Biochem Cell Biol*, 43(3), pp. 290-4.
- Altamirano, F., Lopez, J.R., Henriquez, C., Molinski, T., Allen, P.D. and Jaimovich, E. (2012) 'Increased resting intracellular calcium modulates NF-kappaB-dependent inducible nitric-oxide synthase gene expression in dystrophic *mdx* skeletal myotubes', *J Biol Chem*, 287(25), pp. 20876-87.
- Altamirano, F., Valladares, D., Henriquez-Olguin, C., Casas, M., Lopez, J.R., Allen, P.D. and Jaimovich, E. (2013) 'Nifedipine treatment reduces resting calcium concentration, oxidative and apoptotic gene expression, and improves muscle function in dystrophic *mdx* mice', *PLoS One*, 8(12), p. e81222.
- Amenta, A.R., Yilmaz, A., Bogdanovich, S., McKechnie, B.A., Abedi, M., Khurana, T.S. and Fallon, J.R. (2011) 'Biglycan recruits utrophin to the sarcolemma and counters dystrophic pathology in *mdx* mice', *Proc Natl Acad Sci U S A*, 108(2), pp. 762-7.
- Amith, S.R., Wilkinson, J.M. and Fliegel, L. (2016) 'KR-33028, a potent inhibitor of the Na⁺/H⁺ exchanger NHE1, suppresses metastatic potential of triple-negative breast cancer cells', *Biochem Pharmacol*, 118, pp. 31-39.
- Anaya-Segura, M.A., Garcia-Martinez, F.A., Montes-Almanza, L.A., Diaz, B.G., Avila-Ramirez, G., Alvarez-Maya, I., Coral-Vazquez, R.M., Mondragon-Teran, P., Escobar-Cedillo, R.E., Garcia-Calderon, N., Vazquez-Cardenas, N.A., Garcia, S. and Lopez-Hernandez, L.B. (2015) 'Non-Invasive Biomarkers for Duchenne Muscular Dystrophy and Carrier Detection', *Molecules*, 20(6), pp. 11154-72.
- Anderson, J.E., Bressler, B.H. and Ovalle, W.K. (1988) 'Functional regeneration in the hindlimb skeletal muscle of the *mdx* mouse', *J Muscle Res Cell Motil*, 9.
- Anderson, J.E., McIntosh, L.M. and Poettcker, R. (1996) 'Deflazacort but not prednisone improves both muscle repair and fiber growth in diaphragm and limb muscle in vivo in the *mdx* dystrophic mouse', *Muscle Nerve*, 19(12), pp. 1576-85.
- Andersson, D.C., Betzenhauser, M.J., Reiken, S., Meli, A.C., Umanskaya, A., Xie, W., Shiomi, T., Zalk, R., Lacampagne, A. and Marks, A.R. (2011) 'Ryanodine receptor oxidation causes intracellular calcium leak and muscle weakness in aging', *Cell Metab*, 14(2), pp. 196-207.

Andreu, A.L., Checcarelli, N., Iwata, S., Shanske, S. and DiMauro, S. (2000) 'A missense mutation in the mitochondrial cytochrome b gene in a revisited case with histiocytoid cardiomyopathy', *Pediatr Res*, 48(3), pp. 311-4.

Andreu, A.L., Hanna, M.G., Reichmann, H., Bruno, C., Penn, A.S., Tanji, K., Pallotti, F., Iwata, S., Bonilla, E., Lach, B., Morgan-Hughes, J. and DiMauro, S. (1999) 'Exercise intolerance due to mutations in the cytochrome b gene of mitochondrial DNA', *N Engl J Med*, 341(14), pp. 1037-44.

Andrews, M., Giger, M.L. and Roman, B.B. (2015) 'Manganese-enhanced MRI detection of impaired calcium regulation in a mouse model of cardiac hypertrophy', *NMR Biomed*, 28(2), pp. 255-63.

Angel, T.E., Aryal, U.K., Hengel, S.M., Baker, E.S., Kelly, R.T., Robinson, E.W. and Smith, R.D. (2012) 'Mass spectrometry-based proteomics: existing capabilities and future directions', *Chemical Society Reviews*, 41(10), pp. 3912-3928.

Awano, H., Matsumoto, M., Nagai, M., Shirakawa, T., Maruyama, N., Iijima, K., Nabeshima, Y.-i. and Matsuo, M. (2018) 'Diagnostic and clinical significance of the titin fragment in urine of Duchenne muscular dystrophy patients', *Clinica Chimica Acta*, 476(Supplement C), pp. 111-116.

Awano, H., Takeshima, Y., Okizuka, Y., Saiki, K., Yagi, M. and Matsuo, M. (2008) 'Wide ranges of serum myostatin concentrations in Duchenne muscular dystrophy patients', *Clin Chim Acta*, 391(1-2), pp. 115-7.

Baartscheer, A., Schumacher, C.A., van Borren, M.M., Belterman, C.N., Coronel, R., Opthof, T. and Fiolet, J.W. (2005) 'Chronic inhibition of Na⁺/H⁺-exchanger attenuates cardiac hypertrophy and prevents cellular remodeling in heart failure', *Cardiovasc Res*, 65(1), pp. 83-92.

Banihani, R., Smile, S., Yoon, G., Dupuis, A., Mosleh, M., Snider, A. and McAdam, L. (2015) 'Cognitive and Neurobehavioral Profile in Boys With Duchenne Muscular Dystrophy', *J Child Neurol*.

Barić, I., Čuk, M., Fumić, K., Vugrek, O., Allen, R.H., Glenn, B., Maradin, M., Pažanin, L., Pogribny, I., Radoš, M., Sarnavka, V., Schulze, A., Stabler, S., Wagner, C., Zeisel, S.H. and Mudd, S.H. (2005) 'S-Adenosylhomocysteine hydrolase deficiency: A second patient, the younger brother of the index patient, and outcomes during therapy', *Journal of Inherited Metabolic Disease*, 28(6), pp. 885-902.

Barić, I., Fumić, K., Glenn, B., Čuk, M., Schulze, A., Finkelstein, J.D., James, S.J., Mejaški-Bošnjak, V., Pažanin, L., Pogribny, I.P., Radoš, M., Sarnavka, V., Šćukanec-Špoljar, M., Allen, R.H., Stabler, S., Uzelac, L., Vugrek, O., Wagner, C., Zeisel, S. and Mudd, S.H. (2004) 'S-adenosylhomocysteine hydrolase deficiency in a human: A genetic disorder of methionine metabolism', *Proc Natl Acad Sci U S A*, 101(12), pp. 4234-4239.

Becker, P.E. (1957) '[New results of genetics of muscular dystrophy]', *Acta Genet Stat Med*, 7(2), pp. 303-10.

Becker, P.E. and Kiener, F. (1955) '[A new x-chromosomal muscular dystrophy]', *Arch Psychiatr Nervenkr Z Gesamte Neurol Psychiatr*, 193(4), pp. 427-48.

Bellinger, A.M., Reiken, S., Carlson, C., Mongillo, M., Liu, X., Rothman, L., Matecki, S., Lacampagne, A. and Marks, A.R. (2009) 'Hypernitrosylated ryanodine receptor calcium release channels are leaky in dystrophic muscle', *Nat Med*, 15(3), pp. 325-30.

Benedetti, M.S., Whomsley, R., Poggesi, I., Cawello, W., Mathy, F.X., Delporte, M.L., Papeleu, P. and Watelet, J.B. (2009) 'Drug metabolism and pharmacokinetics', *Drug Metab Rev*, 41(3), pp. 344-90.

Benit, P., Lebon, S. and Rustin, P. (2009) 'Respiratory-chain diseases related to complex III deficiency', *Biochim Biophys Acta*, 1, pp. 181-5.

Beqqali, A., Bollen, I.A., Rasmussen, T.B., van den Hoogenhof, M.M., van Deutekom, H.W., Schafer, S., Haas, J., Meder, B., Sorensen, K.E., van Oort, R.J., Mogensen, J., Hubner, N., Creemers, E.E., van der Velden, J. and Pinto, Y.M. (2016) 'A mutation in the glutamate-rich region of RNA-binding motif protein 20 causes dilated cardiomyopathy through missplicing of titin and impaired Frank-Starling mechanism', *Cardiovasc Res*, 112(1), pp. 452-63.

Berchtold, M.W., Brinkmeier, H. and Muntener, M. (2000) 'Calcium ion in skeletal muscle: its crucial role for muscle function, plasticity, and disease', *Physiol Rev*, 80(3), pp. 1215-65.

Berger, J., Berger, S., Hall, T.E., Lieschke, G.J. and Currie, P.D. (2010) 'Dystrophin-deficient zebrafish feature aspects of the Duchenne muscular dystrophy pathology', *Neuromuscul Disord*, 20(12), pp. 826-32.

Berridge, M.J., Bootman, M.D. and Roderick, H.L. (2003) 'Calcium signalling: dynamics, homeostasis and remodelling', *Nat Rev Mol Cell Biol*, 4(7), pp. 517-29.

Bertorini, T.E., Cornelio, F., Bhattacharya, S.K., Palmieri, G.M., Dones, I., Dworzak, F. and Brambati, B. (1984) 'Calcium and magnesium content in fetuses at risk and pre-necrotic Duchenne muscular dystrophy', *Neurology*, 34(11), pp. 1436-40.

Betteridge, D.J. (2000) 'What is oxidative stress?', *Metabolism*, 49(2 Suppl 1), pp. 3-8.

Bharath, S. (2013) *Pharmaceutical Technology: Concepts and applications*. Pearson Education India.

Bies, R.D., Friedman, D., Roberts, R., Perryman, M.B. and Caskey, C.T. (1992a) 'Expression and localization of dystrophin in human cardiac Purkinje fibers', *Circulation*, 86(1), pp. 147-53.

Bies, R.D., Phelps, S.F., Cortez, M.D., Roberts, R., Caskey, C.T. and Chamberlain, J.S. (1992b) 'Human and murine dystrophin mRNA transcripts are differentially expressed during skeletal muscle, heart, and brain development', *Nucleic Acids Res*, 20(7), pp. 1725-31.

Birnkrant, D.J., Bushby, K., Bann, C.M., Alman, B.A., Apkon, S.D., Blackwell, A., Case, L.E., Cripe, L., Hadjiyannakis, S., Olson, A.K., Sheehan, D.W., Bolen, J., Weber, D.R. and Ward, L.M. (2018a) 'Diagnosis and management of Duchenne muscular dystrophy, part 2: respiratory, cardiac, bone health, and orthopaedic management', *The Lancet Neurology*, 17(4), pp. 347-361.

Birnkrant, D.J., Bushby, K., Bann, C.M., Apkon, S.D., Blackwell, A., Brumbaugh, D., Case, L.E., Clemens, P.R., Hadjiyannakis, S., Pandya, S., Street, N., Tomezsko, J., Wagner, K.R., Ward, L.M. and Weber, D.R. (2018b) 'Diagnosis and management of Duchenne muscular dystrophy, part 1: diagnosis, and neuromuscular, rehabilitation, endocrine, and gastrointestinal and nutritional management', *The Lancet Neurology*, 17(3), pp. 251-267.

Birnkrant, D.J., Bushby, K., Bann, C.M., Apkon, S.D., Blackwell, A., Colvin, M.K., Cripe, L., Herron, A.R., Kennedy, A., Kinnett, K., Naprawa, J., Noritz, G., Poysky, J., Street, N., Trout, C.J., Weber, D.R. and Ward, L.M. (2018c) 'Diagnosis and management of Duchenne muscular dystrophy, part 3: primary care, emergency management, psychosocial care, and transitions of care across the lifespan', *The Lancet Neurology*, 17(5), pp. 445-455.

Bkaily, G., Chahine, M., Al-Khoury, J., Avedanian, L., Beier, N., Scholz, W. and Jacques, D. (2015) 'Na(+)-H(+) exchanger inhibitor prevents early death in hereditary cardiomyopathy', *Can J Physiol Pharmacol*, 93(11), pp. 923-34.

Bkaily, G. and Jacques, D. (2017) 'Na⁺-H⁺ exchanger and proton channel in heart failure associated with Becker and Duchenne muscular dystrophies', *Can J Physiol Pharmacol*, 95(10), pp. 1213-1223.

Bladen, C.L., Salgado, D., Monges, S., Foncuberta, M.E., Kekou, K., Kosma, K., Dawkins, H., Lamont, L., Roy, A.J., Chamova, T., Guerguelcheva, V., Chan, S., Korngut, L., Campbell, C., Dai, Y., Wang, J., Barisic, N., Brabec, P., Lahdetie, J., Walter, M.C., Schreiber-Katz, O., Karcagi, V., Garami, M., Viswanathan, V., Bayat, F., Buccella, F., Kimura, E., Koeks, Z., van den Bergen, J.C., Rodrigues, M., Roxburgh, R., Lusakowska, A., Kostera-Pruszczyk, A., Zimowski, J., Santos, R., Neagu, E., Artemieva, S., Rasic, V.M., Vojinovic, D., Posada, M., Bloetzer, C., Jeannet, P.Y., Joncourt, F., Diaz-Manera, J., Gallardo, E., Karaduman, A.A., Topaloglu, H., El Sherif, R., Stringer, A., Shatillo, A.V., Martin, A.S., Peay, H.L., Bellgard, M.I., Kirschner, J., Flanigan, K.M., Straub, V., Bushby, K., Verschuuren, J., Aartsma-Rus, A., Beroud, C. and Lochmuller, H. (2015) 'The TREAT-NMD DMD Global Database: analysis of more than 7,000 Duchenne muscular dystrophy mutations', *Hum Mutat*, 36(4), pp. 395-402.

Blain, A., Grealley, E., Laval, S., Blamire, A., Straub, V. and MacGowan, G.A. (2013) 'Beta-blockers, left and right ventricular function, and in-vivo calcium influx in muscular dystrophy cardiomyopathy', *PLoS One*, 8(2), p. e57260.

Blain, A., Grealley, E., Laval, S.H., Blamire, A.M., MacGowan, G.A. and Straub, V.W. (2015) 'Absence of Cardiac Benefit with Early Combination ACE Inhibitor and Beta Blocker Treatment in *mdx* Mice', *J Cardiovasc Transl Res*, 8(3), pp. 198-207.

Blake, D.J. and Kroger, S. (2000) 'The neurobiology of duchenne muscular dystrophy: learning lessons from muscle?', *Trends Neurosci*, 23(3), pp. 92-9.

Blake, D.J., Weir, A., Newey, S.E. and Davies, K.E. (2002) 'Function and genetics of dystrophin and dystrophin-related proteins in muscle', *Physiol Rev*, 82(2), pp. 291-329.

Bogdanovich, S., Krag, T.O., Barton, E.R., Morris, L.D., Whittemore, L.A., Ahima, R.S. and Khurana, T.S. (2002) 'Functional improvement of dystrophic muscle by myostatin blockade', *Nature*, 420(6914), pp. 418-21.

- Border, W.A. and Noble, N.A. (1994) 'Transforming growth factor beta in tissue fibrosis', *N Engl J Med*, 331(19), pp. 1286-92.
- Bostick, B., Yue, Y., Long, C., Marschalk, N., Fine, D.M., Chen, J. and Duan, D. (2009) 'Cardiac expression of a mini-dystrophin that normalizes skeletal muscle force only partially restores heart function in aged *Mdx* mice', *Mol Ther*, 17(2), pp. 253-61.
- Briguet, A., Courdier-Fruh, I., Foster, M., Meier, T. and Magyar, J.P. (2004) 'Histological parameters for the quantitative assessment of muscular dystrophy in the *mdx*-mouse', *Neuromuscul Disord*, 14(10), pp. 675-82.
- Brinkmeyer-Langford, C. and Kornegay, J.N. (2013) 'Comparative Genomics of X-linked Muscular Dystrophies: The Golden Retriever Model', *Curr Genomics*, 14(5), pp. 330-42.
- Brown, M.D., Voljavec, A.S., Lott, M.T., Torroni, A., Yang, C.C. and Wallace, D.C. (1992) 'Mitochondrial DNA complex I and III mutations associated with Leber's hereditary optic neuropathy', *Genetics*, 130(1), pp. 163-73.
- Buist, N.R.M., Glenn, B., Vugrek, O., Wagner, C., Stabler, S., Allen, R.H., Pogribny, I., Schulze, A., Zeisel, S.H., Barić, I. and Mudd, S.H. (2006) 'S-Adenosylhomocysteine hydrolase deficiency in a 26-year-old man', *Journal of inherited metabolic disease*, 29(4), pp. 538-545.
- Bulfield, G., Siller, W.G., Wight, P.A. and Moore, K.J. (1984) 'X chromosome-linked muscular dystrophy (*mdx*) in the mouse', *Proc Natl Acad Sci U S A*, 81(4), pp. 1189-92.
- Burch, P.M., Pogoryelova, O., Palandra, J., Goldstein, R., Bennett, D., Fitz, L., Guglieri, M., Bettolo, C.M., Straub, V., Evangelista, T., Neubert, H., Lochmuller, H. and Morris, C. (2017) 'Reduced serum myostatin concentrations associated with genetic muscle disease progression', *J Neurol*, 264(3), pp. 541-553.
- Burki, U., Grealley, E., Laval, S., Schäfer, S. and Straub, V. (2014) 'G.P.120: The Sodium/Hydrogen Exchanger (NHE-1): A promising novel target for DMD', *Neuromuscular Disorders*, 24(9), p. 836.
- Burr, A.R., Millay, D.P., Goonasekera, S.A., Park, K.H., Sargent, M.A., Collins, J., Altamirano, F., Philipson, K.D., Allen, P.D., Ma, J., Lopez, J.R. and Molkentin, J.D. (2014) 'Na⁺ dysregulation coupled with Ca²⁺ entry through NCX1 promotes muscular dystrophy in mice', *Mol Cell Biol*, 34(11), pp. 1991-2002.
- Burr, A.R. and Molkentin, J.D. (2015) 'Genetic evidence in the mouse solidifies the calcium hypothesis of myofiber death in muscular dystrophy', *Cell Death Differ*, 22(9), pp. 1402-12.
- Bushby, K., Finkel, R., Birnkrant, D.J., Case, L.E., Clemens, P.R., Cripe, L., Kaul, A., Kinnett, K., McDonald, C., Pandya, S., Poysky, J., Shapiro, F., Tomezsko, J. and Constantin, C. (2010) 'Diagnosis and management of Duchenne muscular dystrophy, part 1: diagnosis, and pharmacological and psychosocial management', *Lancet Neurol*, 9(1), pp. 77-93.
- Bushby, K., Finkel, R., Wong, B., Barohn, R., Campbell, C., Comi, G.P., Connolly, A.M., Day, J.W., Flanigan, K.M., Goemans, N., Jones, K.J., Mercuri, E., Quinlivan, R., Renfroe, J.B., Russman, B., Ryan, M.M., Tulinius, M., Voit, T., Moore, S.A., Lee Sweeney, H., Abresch, R.T., Coleman, K.L., Eagle, M., Florence, J., Gappmaier, E., Glanzman, A.M.,

- Henricson, E., Barth, J., Elfring, G.L., Reha, A., Spiegel, R.J., O'Donnell M, W., Peltz, S.W. and McDonald, C.M. (2014) 'Ataluren treatment of patients with nonsense mutation dystrophinopathy', *Muscle Nerve*, 50(4), pp. 477-87.
- Cacace, A.T., Brozoski, T., Berkowitz, B., Bauer, C., Odintsov, B., Bergkvist, M., Castracane, J., Zhang, J. and Holt, A.G. (2014) 'Manganese enhanced magnetic resonance imaging (MEMRI): a powerful new imaging method to study tinnitus', *Hear Res*, 311, pp. 49-62.
- Capogrosso, R.F., Cozzoli, A., Giustino, A., Mantuano, P., Massari, A.M., Conte, E., Cannone, M., Bellis, M.D., Liantonio, A., Camerino, G.M. and De Luca, A. (2014) 'G.P.90: Effects of S48168/Arm210, a new rycal® compound, on pathology related signs of exercised dystrophic *mdx* mouse', *Neuromuscular Disorders*, 24(9), pp. 821-822.
- Carberry, S., Zwyer, M., Swandulla, D. and Ohlendieck, K. (2012) 'Profiling of Age-Related Changes in the Tibialis Anterior Muscle Proteome of the *mdx* Mouse Model of Dystrophinopathy', *Journal of Biomedicine and Biotechnology*, 2012, p. 11.
- Carnwath, J.W. and Shotton, D.M. (1987) 'Muscular dystrophy in the *mdx* mouse: histopathology of the soleus and extensor digitorum longus muscles', *J Neurol Sci*, 80.
- Carossa, V., Ghelli, A., Tropeano, C.V., Valentino, M.L., Iommarini, L., Maresca, A., Caporali, L., La Morgia, C., Liguori, R., Barboni, P., Carbonelli, M., Rizzo, G., Tonon, C., Lodi, R., Martinuzzi, A., De Nardo, V., Rugolo, M., Ferretti, L., Gandini, F., Pala, M., Achilli, A., Olivieri, A., Torroni, A. and Carelli, V. (2014) 'A novel in-frame 18-bp microdeletion in MT-CYB causes a multisystem disorder with prominent exercise intolerance', *Hum Mutat*, 35(8), pp. 954-8.
- Carter, B.J. (2004) 'Adeno-associated virus and the development of adeno-associated virus vectors: a historical perspective', *Mol Ther*, 10(6), pp. 981-9.
- Cawello, W. and Antonucci, T. (1997) 'The correlation between pharmacodynamics and pharmacokinetics: basics of pharmacokinetics--pharmacodynamics modeling', *J Clin Pharmacol*, 37(1 Suppl), pp. 65s-69s.
- Cha, M., Lee, K., Lee, C., Cho, J.H., Cheong, C., Sohn, J.H. and Lee, B.H. (2016) 'Manganese-enhanced MR imaging of brain activation evoked by noxious peripheral electrical stimulation', *Neurosci Lett*, 613, pp. 13-8.
- Chahine, M., Bkaily, G., Nader, M., Al-Khoury, J., Jacques, D., Beier, N. and Scholz, W. (2005) 'NHE-1-dependent intracellular sodium overload in hypertrophic hereditary cardiomyopathy: prevention by NHE-1 inhibitor', *J Mol Cell Cardiol*, 38(4), pp. 571-82.
- Chakkalakal, J.V., Miura, P., Belanger, G., Michel, R.N. and Jasmin, B.J. (2008) 'Modulation of utrophin A mRNA stability in fast versus slow muscles via an AU-rich element and calcineurin signaling', *Nucleic Acids Res*, 36(3), pp. 826-38.
- Chamberlain, J.S. and Benian, G.M. (2000) 'Muscular dystrophy: the worm turns to genetic disease', *Curr Biol*, 10(21), pp. R795-7.
- Chamberlain, J.S., Metzger, J., Reyes, M., Townsend, D. and Faulkner, J.A. (2007) 'Dystrophin-deficient *mdx* mice display a reduced life span and are susceptible to spontaneous rhabdomyosarcoma', *Faseb j*, 21(9), pp. 2195-204.

Chandramouli, K. and Qian, P.-Y. (2009) 'Proteomics: Challenges, Techniques and Possibilities to Overcome Biological Sample Complexity', *Human Genomics and Proteomics : HGP*, 2009, p. 239204.

Chandrasekharan, K., Yoon, J.H., Xu, Y., deVries, S., Camboni, M., Janssen, P.M., Varki, A. and Martin, P.T. (2010) 'A human-specific deletion in mouse Cmah increases disease severity in the *mdx* model of Duchenne muscular dystrophy', *Sci Transl Med*, 2(42), p. 42ra54.

Chang, T.-H., Chen, M.-C., Chang, J.-P., Huang, H.-D., Ho, W.-C., Lin, Y.-S., Pan, K.-L., Huang, Y.-K., Liu, W.-H. and Wu, C.-C. (2016) 'Exploring Regulatory Mechanisms of Atrial Myocyte Hypertrophy of Mitral Regurgitation through Gene Expression Profiling Analysis: Role of NFAT in Cardiac Hypertrophy', *PLoS ONE*, 11(12), p. e0166791.

Chen, M.Y., Zhou, Z.G., Zeng, K., Sun, L.D. and Ding, L.F. (2005) '[Analysis of 34 cases of systemic lupus erythematosus with decreased platelet count]', *Di Yi Jun Yi Da Xue Xue Bao*, 25(10), pp. 1280-2.

Chen, X. and Li, Y. (2009) 'Role of matrix metalloproteinases in skeletal muscle: migration, differentiation, regeneration and fibrosis', *Cell Adh Migr*, 3(4), pp. 337-41.

Chiappalupi, S., Salvadori, L., Luca, G., Riuzzi, F., Calafiore, R., Donato, R. and Sorci, G. (2017) 'Employment of Microencapsulated Sertoli Cells as a New Tool to Treat Duchenne Muscular Dystrophy', *Journal of Functional Morphology and Kinesiology*, 2(4), p. 47.

Chiu, D.S., Oram, J.F., LeBoeuf, R.C., Alpers, C.E. and O'Brien, K.D. (1997) 'High-density lipoprotein-binding protein (HBP)/vigilin is expressed in human atherosclerotic lesions and colocalizes with apolipoprotein E', *Arterioscler Thromb Vasc Biol*, 17(11), pp. 2350-8.

Cirak, S., Arechavala-Gomez, V., Guglieri, M., Feng, L., Torelli, S., Anthony, K., Abbs, S., Garralda, M.E., Bourke, J., Wells, D.J., Dickson, G., Wood, M.J., Wilton, S.D., Straub, V., Kole, R., Shrewsbury, S.B., Sewry, C., Morgan, J.E., Bushby, K. and Muntoni, F. (2011) 'Exon skipping and dystrophin restoration in patients with Duchenne muscular dystrophy after systemic phosphorodiamidate morpholino oligomer treatment: an open-label, phase 2, dose-escalation study', *Lancet*, 378(9791), pp. 595-605.

Coleman, O., Henry, M., Clynes, M. and Meleady, P. (2017) 'Filter-Aided Sample Preparation (FASP) for Improved Proteome Analysis of Recombinant Chinese Hamster Ovary Cells', *Methods Mol Biol*, 1603, pp. 187-194.

Coley, W.D., Bogdanik, L., Vila, M.C., Yu, Q., Van Der Meulen, J.H., Rayavarapu, S., Novak, J.S., Nearing, M., Quinn, J.L., Saunders, A., Dolan, C., Andrews, W., Lammert, C., Austin, A., Partridge, T.A., Cox, G.A., Lutz, C. and Nagaraju, K. (2016) 'Effect of genetic background on the dystrophic phenotype in *mdx* mice', *Human Molecular Genetics*, 25(1), pp. 130-145.

Collins, C.A. and Morgan, J.E. (2003) 'Duchenne's muscular dystrophy: animal models used to investigate pathogenesis and develop therapeutic strategies', *Int J Exp Pathol*, 84(4), pp. 165-72.

Cooper, B.J., Winand, N.J., Stedman, H., Valentine, B.A., Hoffman, E.P., Kunkel, L.M., Scott, M.O., Fischbeck, K.H., Kornegay, J.N., Avery, R.J. and et al. (1988) 'The homologue of the Duchenne locus is defective in X-linked muscular dystrophy of dogs', *Nature*, 334(6178), pp. 154-6.

Cordero, M.D., Alcocer-Gomez, E., Marin-Aguilar, F., Rybkina, T., Cotan, D., Perez-Pulido, A., Alvarez-Suarez, J.M., Battino, M., Sanchez-Alcazar, J.A., Carrion, A.M., Culic, O., Navarro-Pando, J.M. and Bullon, P. (2016) 'Mutation in cytochrome b gene of mitochondrial DNA in a family with fibromyalgia is associated with NLRP3-inflammasome activation', *J Med Genet*, 53(2), pp. 113-22.

Cossu, G., Previtali, S.C., Napolitano, S., Cicalese, M.P., Tedesco, F.S., Nicastro, F., Noviello, M., Roostalu, U., Natali Sora, M.G., Scarlato, M., De Pellegrin, M., Godi, C., Giuliani, S., Ciotti, F., Tonlorenzi, R., Lorenzetti, I., Rivellini, C., Benedetti, S., Gatti, R., Markt, S., Mazzi, B., Tettamanti, A., Ragazzi, M., Imro, M.A., Marano, G., Ambrosi, A., Fiori, R., Sormani, M.P., Bonini, C., Venturini, M., Politi, L.S., Torrente, Y. and Ciceri, F. (2015) 'Intra - arterial transplantation of HLA - matched donor mesoangioblasts in Duchenne muscular dystrophy', *EMBO Molecular Medicine*, 7(12), pp. 1513-1528.

Cossu, G. and Sampaolesi, M. (2007) 'New therapies for Duchenne muscular dystrophy: challenges, prospects and clinical trials', *Trends Mol Med*, 13(12), pp. 520-6.

Coulton, G.R., Morgan, J.E., Partridge, T.A. and Sloper, J.C. (1988a) 'The *mdx* mouse skeletal muscle myopathy: I. A histological, morphometric and biochemical investigation', *Neuropathol Appl Neurobiol*, 14(1), pp. 53-70.

Coulton, G.R., Morgan, J.E., Partridge, T.A. and Sloper, J.C. (1988b) 'The *mdx* mouse skeletal muscle myopathy: I. A histological, morphometric and biochemical investigation', *Neuropathol Appl Neurobiol*, 14.

Crawford, G.E., Faulkner, J.A., Crosbie, R.H., Campbell, K.P., Froehner, S.C. and Chamberlain, J.S. (2000) 'Assembly of the dystrophin-associated protein complex does not require the dystrophin COOH-terminal domain', *J Cell Biol*, 150(6), pp. 1399-410.

Cutillas, P.R. and Timms, J.F. (2011) *LC-MS/MS in Proteomics: Methods and Applications*. Humana Press.

Dalkilic, I. and Kunkel, L.M. (2003) 'Muscular dystrophies: Genes to pathogenesis', *Current Opinion in Genetics and Development*, 13(3), pp. 231-238.

Dangain, J. and Vrbova, G. (1984) 'Muscle development in *mdx* mutant mice', *Muscle Nerve*, 7.

de Hoffmann, E. and Stroobant, V. (2013) *Mass Spectrometry: Principles and Applications*. Wiley.

De La Haba, G. and Cantoni, G.L. (1959) 'The enzymatic synthesis of S-adenosyl-L-homocysteine from adenosine and homocysteine', *J Biol Chem*, 234(3), pp. 603-8.

de Los Heros, P., Alessi, D.R., Gourlay, R., Campbell, D.G., Deak, M., Macartney, T.J., Kahle, K.T. and Zhang, J. (2014) 'The WNK-regulated SPAK/OSR1 kinases directly phosphorylate and inhibit the K⁺-Cl⁻ co-transporters', *Biochem J*, 458(3), pp. 559-73.

- Decary, S., Hamida, C.B., Mouly, V., Barbet, J.P., Hentati, F. and Butler-Browne, G.S. (2000) 'Shorter telomeres in dystrophic muscle consistent with extensive regeneration in young children', *Neuromuscul Disord*, 10.
- Deconinck, A.E., Rafael, J.A., Skinner, J.A., Brown, S.C., Potter, A.C., Metzinger, L., Watt, D.J., Dickson, J.G., Tinsley, J.M. and Davies, K.E. (1997) 'Utrophin-dystrophin-deficient mice as a model for Duchenne muscular dystrophy', *Cell*, 90(4), pp. 717-27.
- Deconinck, N. and Dan, B. (2007) 'Pathophysiology of duchenne muscular dystrophy: current hypotheses', *Pediatr Neurol*, 36(1), pp. 1-7.
- Dellorusso, C., Crawford, R.W., Chamberlain, J.S. and Brooks, S.V. (2001) 'Tibialis anterior muscles in *mdx* mice are highly susceptible to contraction-induced injury', *J Muscle Res Cell Motil*, 22(5), pp. 467-75.
- Deval, E., Levitsky, D.O., Marchand, E., Cantereau, A., Raymond, G. and Cognard, C. (2002) 'Na(+)/Ca(2+) exchange in human myotubes: intracellular calcium rises in response to external sodium depletion are enhanced in DMD', *Neuromuscul Disord*, 12(7-8), pp. 665-73.
- Doorenweerd, N., Mahfouz, A., van Putten, M., Kaliyaperumal, R., t' Hoen, P.A.C., Hendriksen, J.G.M., Aartsma-Rus, A.M., Verschuuren, J.J.G.M., Niks, E.H., Reinders, M.J.T., Kan, H.E. and Lelieveldt, B.P.F. (2017) 'Timing and localization of human dystrophin isoform expression provide insights into the cognitive phenotype of Duchenne muscular dystrophy', *Scientific Reports*, 7, p. 12575.
- Drousiotou, A., Ioannou, P., Georgiou, T., Mavrikiou, E., Christopoulos, G., Kyriakides, T., Voyasianos, M., Argyriou, A. and Middleton, L. (1998) *Neonatal Screening for Duchenne Muscular Dystrophy: A Novel Semiquantitative Application of the Bioluminescence Test for Creatine Kinase in a Pilot National Program in Cyprus*.
- Duchenne, G.B. (1868) *De la paralysie musculaire pseudo-hypertrophique ou paralysie myo-sclérosique*. P. Asselin.
- Duchenne, G.B.A. (1861) *De l'électrisation localisée et de son application à la pathologie et à la thérapeutique*.
- Duddy, W., Duguez, S., Johnston, H., Cohen, T.V., Phadke, A., Gordish-Dressman, H., Nagaraju, K., Gnocchi, V., Low, S. and Partridge, T. (2015) 'Muscular dystrophy in the *mdx* mouse is a severe myopathy compounded by hypotrophy, hypertrophy and hyperplasia', *Skeletal Muscle*, 5(1), p. 16.
- Dudley, R.W.R., Danialou, G., Govindaraju, K., Lands, L., Eidelman, D.H. and Petrof, B.J. (2006) 'Sarcolemmal Damage in Dystrophin Deficiency Is Modulated by Synergistic Interactions between Mechanical and Oxidative/Nitrosative Stresses', *The American Journal of Pathology*, 168(4), pp. 1276-1287.
- Duncan, C.J. (1978) 'Role of intracellular calcium in promoting muscle damage: a strategy for controlling the dystrophic condition', *Experientia*, 34(12), pp. 1531-5.
- Duncan, M.W., Aebersold, R. and Caprioli, R.M. (2010) 'The pros and cons of peptide-centric proteomics', *Nature Biotechnology*, 28, p. 659.

- DuVall, M.M., Jinha, A., Schappacher-Tilp, G., Leonard, T.R. and Herzog, W. (2017) 'Differences in titin segmental elongation between passive and active stretch in skeletal muscle', *J Exp Biol*, 220(Pt 23), pp. 4418-4425.
- Egar, J., Ali, A., Howlett, S.E., Friesen, C.H. and O'Blenes, S. (2014) 'The Na⁺/Ca²⁺ exchange inhibitor SEA0400 limits intracellular Ca²⁺ accumulation and improves recovery of ventricular function when added to cardioplegia', *J Cardiothorac Surg*, 9(11), pp. 1749-8090.
- Elkina, Y., von Haehling, S., Anker, S.D. and Springer, J. (2011) 'The role of myostatin in muscle wasting: an overview', *J Cachexia Sarcopenia Muscle*, 2(3), pp. 143-151.
- Ellis, J.A., Vroom, E. and Muntoni, F. (2013) '195th ENMC International Workshop: Newborn screening for Duchenne muscular dystrophy 14-16th December, 2012, Naarden, The Netherlands', *Neuromuscul Disord*, 23(8), pp. 682-9.
- Emery, A.E. (1993) 'Duchenne muscular dystrophy -Meryon's disease', *Neuromuscul Disord*, 3(4), pp. 263-6.
- Emery, A.E.H. (1991) 'Population frequencies of inherited neuromuscular diseases—A world survey', *Neuromuscular Disorders*, 1(1), pp. 19-29.
- Emery, A.E.H. (2002) 'The muscular dystrophies', *The Lancet*, 359(9307), pp. 687-695.
- Emilien, G., van Meurs, W. and Maloteaux, J.-M. (2000) 'The dose-response relationship in Phase I clinical trials and beyond: use, meaning, and assessment', *Pharmacology & Therapeutics*, 88(1), pp. 33-58.
- Erb, W.H. (1884) 'Über die "juvenile Form" der progressiven Muskelatrophie und ihre Beziehungen zur sogenannten Pseudohypertrophie der Muskeln', *Dtsch Arch Klin Med* 34, pp. 467-519.
- Ervasti, J.M. (2007) 'Dystrophin, its interactions with other proteins, and implications for muscular dystrophy', *Biochim Biophys Acta*, 1772(2), pp. 108-17.
- Ervasti, J.M. and Campbell, K.P. (1991) 'Membrane organization of the dystrophin-glycoprotein complex', *Cell*, 66(6), pp. 1121-31.
- Ervasti, J.M., Ohlendieck, K., Kahl, S.D., Gaver, M.G. and Campbell, K.P. (1990) 'Deficiency of a glycoprotein component of the dystrophin complex in dystrophic muscle', *Nature*, 345(6273), pp. 315-9.
- Fairclough, R.J., Wood, M.J. and Davies, K.E. (2013) 'Therapy for Duchenne muscular dystrophy: renewed optimism from genetic approaches', *Nat Rev Genet*, 14(6), pp. 373-8.
- Feger, B.J. and Starnes, J.W. (2013) 'Exercise alters the regulation of myocardial Na⁺/H⁺ exchanger-1 activity', *American Journal of Physiology-Regulatory, Integrative and Comparative Physiology*, 305(10), pp. R1182-R1189.
- Figlewicz, D.A., Krizus, A., Martinoli, M.G., Meininger, V., Dib, M., Rouleau, G.A. and Julien, J.P. (1994) 'Variants of the heavy neurofilament subunit are associated with the development of amyotrophic lateral sclerosis', *Hum Mol Genet*, 3(10), pp. 1757-61.

Filippi, B.M., de los Heros, P., Mehellou, Y., Navratilova, I., Gourlay, R., Deak, M., Plater, L., Toth, R., Zeqiraj, E. and Alessi, D.R. (2011) 'MO25 is a master regulator of SPAK/OSR1 and MST3/MST4/YSK1 protein kinases', *Embo j*, 30(9), pp. 1730-41.

Finehout, E.J. and Lee, K.H. (2004) 'An introduction to mass spectrometry applications in biological research', *Biochemistry and Molecular Biology Education*, 32(2), pp. 93-100.

Finkel, R.S., Flanigan, K.M., Wong, B., Bonnemann, C., Sampson, J., Sweeney, H.L., Reha, A., Northcutt, V.J., Elfring, G., Barth, J. and Peltz, S.W. (2013) 'Phase 2a study of ataluren-mediated dystrophin production in patients with nonsense mutation Duchenne muscular dystrophy', *PLoS One*, 8(12), p. e81302.

Finley, J.W. (1998) 'Manganese uptake and release by cultured human hepato-carcinoma (Hep-G2) cells', *Biol Trace Elem Res*, 64(1-3), pp. 101-18.

Flanigan, K.M., Dunn, D.M., von Niederhausern, A., Soltanzadeh, P., Gappmaier, E., Howard, M.T., Sampson, J.B., Mendell, J.R., Wall, C., King, W.M., Pestronk, A., Florence, J.M., Connolly, A.M., Mathews, K.D., Stephan, C.M., Laubenthal, K.S., Wong, B.L., Morehart, P.J., Meyer, A., Finkel, R.S., Bonnemann, C.G., Medne, L., Day, J.W., Dalton, J.C., Margolis, M.K., Hinton, V.J. and Weiss, R.B. (2009) 'Mutational spectrum of DMD mutations in dystrophinopathy patients: application of modern diagnostic techniques to a large cohort', *Hum Mutat*, 30(12), pp. 1657-66.

Fong, P.Y., Turner, P.R., Denetclaw, W.F. and Steinhardt, R.A. (1990) 'Increased activity of calcium leak channels in myotubes of Duchenne human and *mdx* mouse origin', *Science*, 250(4981), pp. 673-6.

Frohlich, T., Kemter, E., Flenkenthaler, F., Klymiuk, N., Otte, K.A., Blutke, A., Krause, S., Walter, M.C., Wanke, R., Wolf, E. and Arnold, G.J. (2016) 'Progressive muscle proteome changes in a clinically relevant pig model of Duchenne muscular dystrophy', *Sci Rep*, 6, p. 33362.

Fuster, D.G. and Alexander, R.T. (2014) 'Traditional and emerging roles for the SLC9 Na⁺/H⁺ exchangers', *Pflugers Arch*, 466(1), pp. 61-76.

Gailly, P. (2002) 'New aspects of calcium signaling in skeletal muscle cells: implications in Duchenne muscular dystrophy', *Biochim Biophys Acta*, 1600(1-2), pp. 38-44.

Gailly, P., Boland, B., Himpens, B., Casteels, R. and Gillis, J.M. (1993) 'Critical evaluation of cytosolic calcium determination in resting muscle fibres from normal and dystrophic (*mdx*) mice', *Cell Calcium*, 14(6), pp. 473-83.

Gallagher, S. and Chakavarti, D. (2008) 'Staining proteins in gels', *J Vis Exp*, (17).

Gamberi, T., Fiaschi, T., Valocchia, E., Modesti, A., Mantuano, P., Rolland, J.-F., Sanarica, F., De Luca, A. and Magherini, F. (2018) 'Proteome analysis in dystrophic *mdx* mouse muscle reveals a drastic alteration of key metabolic and contractile proteins after chronic exercise and the potential modulation by anti-oxidant compounds', *Journal of Proteomics*, 170(Supplement C), pp. 43-58.

Gauthier-Rouviere, C. and Bonet-Kerrache, A. (2009) 'RhoA leads to up-regulation and relocalization of utrophin in muscle fibers', *Biochem Biophys Res Commun*, 384(3), pp. 322-8.

- Ge, Y., Molloy, M.P., Chamberlain, J.S. and Andrews, P.C. (2004) 'Differential expression of the skeletal muscle proteome in *mdx* mice at different ages', *Electrophoresis*, 25(15), pp. 2576-85.
- Gibbs, E.M., Horstick, E.J. and Dowling, J.J. (2013) 'Swimming into prominence: the zebrafish as a valuable tool for studying human myopathies and muscular dystrophies', *FEBS J*, 280(17), pp. 4187-97.
- Gidaro, T., Servais, L., Previtali, S., Zambon, A., Pitchforth, J., Maresh, K., Diaz, J., Laveille, C., Gray, J., Porte-Thomé, F., Gheit, H., Annoussamy, M., Che, V., Duchene, D., Sora, M., Gerevini, S., Vidal, N., Groves, K., Brimble, J. and Muntoni, F. (2017) 'Rimeporide: safety, tolerability and pharmacokinetic results from a phase Ib study in DMD boys as well as exploratory biomarkers', *Neuromuscular Disorders*, 27, pp. S215-S216.
- Gieseler, K., Grisoni, K. and Segalat, L. (2000) 'Genetic suppression of phenotypes arising from mutations in dystrophin-related genes in *Caenorhabditis elegans*', *Curr Biol*, 10(18), pp. 1092-7.
- Gil Borlado, M.C., Moreno Lastres, D., Gonzalez Hoyuela, M., Moran, M., Blazquez, A., Pello, R., Marin Buera, L., Gabaldon, T., Garcia Peñas, J.J., Martín, M.A., Arenas, J. and Ugalde, C. (2010) 'Impact of the Mitochondrial Genetic Background in Complex III Deficiency', *PLoS One*, 5(9), p. e12801.
- Giliberto, F., Radic, C.P., Luce, L., Ferreiro, V., de Brasi, C. and Szijan, I. (2014) 'Symptomatic female carriers of Duchenne muscular dystrophy (DMD): genetic and clinical characterization', *J Neurol Sci*, 336(1-2), pp. 36-41.
- Gilson, W.D. and Kraitchman, D.L. (2007) 'Cardiac Magnetic Resonance Imaging in Small Rodents using Clinical 1.5T and 3.0T Scanners', *Methods (San Diego, Calif.)*, 43(1), pp. 35-45.
- Goemans, N. and Buyse, G. (2014) 'Current treatment and management of dystrophinopathies', *Curr Treat Options Neurol*, 16(5), p. 287.
- Goonasekera, S.A., Lam, C.K., Millay, D.P., Sargent, M.A., Hajjar, R.J., Kranias, E.G. and Molkentin, J.D. (2011) 'Mitigation of muscular dystrophy in mice by SERCA overexpression in skeletal muscle', *J Clin Invest*, 121(3), pp. 1044-52.
- Gorospe, J.R., Tharp, M.D., Hinckley, J., Kornegay, J.N. and Hoffman, E.P. (1994) 'A role for mast cells in the progression of Duchenne muscular dystrophy? Correlations in dystrophin-deficient humans, dogs, and mice', *J Neurol Sci*, 122(1), pp. 44-56.
- Goyenvalle, A., Seto, J.T., Davies, K.E. and Chamberlain, J. (2011) 'Therapeutic approaches to muscular dystrophy', *Hum Mol Genet*, 20(R1), pp. R69-78.
- Grady, R.M., Teng, H., Nichol, M.C., Cunningham, J.C., Wilkinson, R.S. and Sanes, J.R. (1997) 'Skeletal and cardiac myopathies in mice lacking utrophin and dystrophin: a model for Duchenne muscular dystrophy', *Cell*, 90(4), pp. 729-38.
- Gramolini, A.O. and Jasmin, B.J. (1997) 'Duchenne muscular dystrophy and the neuromuscular junction: the utrophin link', *Bioessays*, 19(9), pp. 747-50.

- Granchelli, J.A., Pollina, C. and Hudecki, M.S. (2000) 'Pre-clinical screening of drugs using the *mdx* mouse', *Neuromuscul Disord*, 10(4-5), pp. 235-9.
- Graves, P.R. and Haystead, T.A.J. (2002) 'Molecular Biologist's Guide to Proteomics', *Microbiology and Molecular Biology Reviews*, 66(1), pp. 39-63.
- Greally, E., Blain, A., Blamire, A.M., MacGowan, G., Laval, S.H. and Straub, V. (2012) 'D.P.18 Manganese enhanced MRI as an outcome measure in assessing skeletal muscle calcium uptake in muscular dystrophy mouse models', *Neuromuscular Disorders*, 22(9), p. 823.
- Greally, E., Blain, A.M., Ahmed, S.T., Laval, S.H., Blamire, A.M. and Straub, V. (2014) 'G.P.125', *Neuromuscular Disorders*, 24(9), p. 838.
- Greally, E., Davison, B.J., Blain, A., Laval, S., Blamire, A., Straub, V. and MacGowan, G.A. (2013) 'Heterogeneous abnormalities of in-vivo left ventricular calcium influx and function in mouse models of muscular dystrophy cardiomyopathy', *J Cardiovasc Magn Reson*, 15, p. 4.
- Greenberg, B. (2015) 'Gene therapy for heart failure', *Journal of Cardiology*, 66(3), pp. 195-200.
- Gregorevic, P., Allen, J.M., Minami, E., Blankinship, M.J., Haraguchi, M., Meuse, L., Finn, E., Adams, M.E., Froehner, S.C., Murry, C.E. and Chamberlain, J.S. (2006) 'rAAV6-microdystrophin preserves muscle function and extends lifespan in severely dystrophic mice', *Nat Med*, 12(7), pp. 787-9.
- Grubbs, R., Vugrek, O., Deisch, J., Wagner, C., Stabler, S., Allen, R., Barić, I., Rados, M. and Mudd, S.H. (2010) 'S-adenosylhomocysteine hydrolase deficiency: two siblings with fetal hydrops and fatal outcomes', *Journal of Inherited Metabolic Disease*, 33(6), pp. 705-713.
- Grünewald, S. (2009) 'The clinical spectrum of phosphomannomutase 2 deficiency (CDG-1a)', *Biochimica et Biophysica Acta (BBA) - Molecular Basis of Disease*, 1792(9), pp. 827-834.
- Guglieri, M. and Bushby, K. (2010) 'Molecular treatments in Duchenne muscular dystrophy', *Curr Opin Pharmacol*, 10(3), pp. 331-7.
- Guiraud, S. and Davies, K.E. (2017) 'Pharmacological advances for treatment in Duchenne muscular dystrophy', *Current Opinion in Pharmacology*, 34, pp. 36-48.
- Guiraud, S., Squire, S.E., Edwards, B., Chen, H., Burns, D.T., Shah, N., Babbs, A., Davies, S.G., Wynne, G.M., Russell, A.J., Elsey, D., Wilson, F.X., Tinsley, J.M. and Davies, K.E. (2015) 'Second-generation compound for the modulation of utrophin in the therapy of DMD', *Hum Mol Genet*.
- Hackman, P., Vihola, A., Haravuori, H., Marchand, S., Sarparanta, J., de Seze, J., Labeit, S., Witt, C., Peltonen, L., Richard, I. and Udd, B. (2002) 'Tibial Muscular Dystrophy Is a Titinopathy Caused by Mutations in TTN, the Gene Encoding the Giant Skeletal-Muscle Protein Titin', *American Journal of Human Genetics*, 71(3), pp. 492-500.
- Hagen, C.M., Aidt, F.H., Havndrup, O., Hedley, P.L., Jespersgaard, C., Jensen, M., Kanters, J.K., Moolman-Smook, J.C., Moller, D.V., Bundgaard, H. and Christiansen, M.

- (2013) 'MT-CYB mutations in hypertrophic cardiomyopathy', *Mol Genet Genomic Med*, 1(1), pp. 54-65.
- Hakim, C.H., Wasala, N.B., Pan, X., Kodippili, K., Yue, Y., Zhang, K., Yao, G., Haffner, B., Duan, S.X., Ramos, J., Schneider, J.S., Yang, N.N., Chamberlain, J.S. and Duan, D. (2017) 'A Five-Repeat Micro-Dystrophin Gene Ameliorated Dystrophic Phenotype in the Severe DBA/2J-*mdx* Model of Duchenne Muscular Dystrophy', *Molecular Therapy - Methods & Clinical Development*, 6, pp. 216-230.
- Hamill, O.P., Marty, A., Neher, E., Sakmann, B. and Sigworth, F.J. (1981) 'Improved patch-clamp techniques for high-resolution current recording from cells and cell-free membrane patches', *Pflugers Arch*, 391(2), pp. 85-100.
- Harper, S.Q., Hauser, M.A., DelloRusso, C., Duan, D., Crawford, R.W., Phelps, S.F., Harper, H.A., Robinson, A.S., Engelhardt, J.F., Brooks, S.V. and Chamberlain, J.S. (2002) 'Modular flexibility of dystrophin: implications for gene therapy of Duchenne muscular dystrophy', *Nat Med*, 8(3), pp. 253-61.
- Hauser, E., Hoger, H., Bittner, R., Widhalm, K., Herkner, K. and Lubec, G. (1995) 'Oxyradical damage and mitochondrial enzyme activities in the *mdx* mouse', *Neuropediatrics*, 26(5), pp. 260-2.
- Haycock, J.W., MacNeil, S., Jones, P., Harris, J.B. and Mantle, D. (1996) 'Oxidative damage to muscle protein in Duchenne muscular dystrophy', *Neuroreport*, 8(1), pp. 357-61.
- Head, S.I. (1993) 'Membrane potential, resting calcium and calcium transients in isolated muscle fibres from normal and dystrophic mice', *J Physiol*, 469, pp. 11-9.
- Hess, J.W., Macdonald, R.P., Frederick, R.J., Jones, R.N., Neely, J. and Gross, D. (1964) 'Serum Creatine Phosphokinase (Cpk) Activity in Disorders of Heart and Skeletal Muscle', *Ann Intern Med*, 61, pp. 1015-28.
- Heydemann, A., Huber, J.M., Demonbreun, A., Hadhazy, M. and McNally, E.M. (2005) 'Genetic background influences muscular dystrophy', *Neuromuscul Disord*, 15(9-10), pp. 601-9.
- Hilal-Dandan, R., Knollman, B. and Brunton, L. (2017) *Goodman and Gilman's The Pharmacological Basis of Therapeutics, 13th Edition*. McGraw-Hill Education.
- Hodgetts, S., Radley, H., Davies, M. and Grounds, M.D. (2006) 'Reduced necrosis of dystrophic muscle by depletion of host neutrophils, or blocking TNF α function with Etanercept in *mdx* mice', *Neuromuscular Disorders*, 16(9), pp. 591-602.
- Hogrel, J.Y., Zagnoli, F., Canal, A., Fraysse, B., Bouchard, J.P., Skuk, D., Fardeau, M. and Tremblay, J.P. (2013) 'Assessment of a symptomatic Duchenne muscular dystrophy carrier 20 years after myoblast transplantation from her asymptomatic identical twin sister', *Neuromuscul Disord*, 23(7), pp. 575-9.
- Hollinger, K. and Selsby, J.T. (2013) 'The physiological response of protease inhibition in dystrophic muscle', *Acta Physiol (Oxf)*, 208(3), pp. 234-44.
- Honzík, T., Magner, M., Krijt, J., Sokolová, J., Vugrek, O., Belužić, R., Barić, I., Hansíková, H., Elleder, M., Veselá, K., Bauerová, L., Ondrušková, N., Ješina, P., Zeman,

J. and Kožich, V. (2012) 'Clinical picture of S-adenosylhomocysteine hydrolase deficiency resembles phosphomannomutase 2 deficiency', *Molecular Genetics and Metabolism*, 107(3), pp. 611-613.

Howell, J.M., Fletcher, S., Kakulas, B.A., O'Hara, M., Lochmuller, H. and Karpati, G. (1997) 'Use of the dog model for Duchenne muscular dystrophy in gene therapy trials', *Neuromuscul Disord*, 7(5), pp. 325-8.

Hu, T.C., Pautler, R.G., MacGowan, G.A. and Koretsky, A.P. (2001) 'Manganese-enhanced MRI of mouse heart during changes in inotropy', *Magn Reson Med*, 46(5), pp. 884-90.

Ignotz, R.A. and Massague, J. (1986) 'Transforming growth factor-beta stimulates the expression of fibronectin and collagen and their incorporation into the extracellular matrix', *J Biol Chem*, 261(9), pp. 4337-45.

Ileana, T., Anna, M., Pamela, S., Fernanda, V., Stefano, B. and Livio, L. (2016) 'Ranolazine promotes muscle differentiation and reduces oxidative stress in C2C12 skeletal muscle cells', *Endocrine*, 8(10), pp. 016-1181.

Imbert, N., Vandebrouck, C., Duport, G., Raymond, G., Hassoni, A.A., Constantin, B., Cullen, M.J. and Cognard, C. (2001) 'Calcium currents and transients in co-cultured contracting normal and Duchenne muscular dystrophy human myotubes', *The Journal of Physiology*, 534(Pt 2), pp. 343-355.

Inoue, T., Majid, T. and Pautler, R.G. (2011) 'Manganese enhanced MRI (MEMRI): neurophysiological applications', *Rev Neurosci*, 22(6), pp. 675-94.

Itoh-Satoh, M., Hayashi, T., Nishi, H., Koga, Y., Arimura, T., Koyanagi, T., Takahashi, M., Hohda, S., Ueda, K., Nouchi, T., Hiroe, M., Marumo, F., Imaizumi, T., Yasunami, M. and Kimura, A. (2002) 'Titin mutations as the molecular basis for dilated cardiomyopathy', *Biochem Biophys Res Commun*, 291(2), pp. 385-93.

Iwata, Y., Katanosaka, Y., Arai, Y., Shigekawa, M. and Wakabayashi, S. (2009) 'Dominant-negative inhibition of Ca²⁺ influx via TRPV2 ameliorates muscular dystrophy in animal models', *Hum Mol Genet*, 18(5), pp. 824-34.

Iwata, Y., Katanosaka, Y., Hisamitsu, T. and Wakabayashi, S. (2007) 'Enhanced Na⁺/H⁺ exchange activity contributes to the pathogenesis of muscular dystrophy via involvement of P2 receptors', *Am J Pathol*, 171(5), pp. 1576-87.

Jacquier, A., Delorme, C., Belotti, E., Juntas-Morales, R., Sole, G., Dubourg, O., Giroux, M., Maurage, C.A., Castellani, V., Rebelo, A., Abrams, A., Zuchner, S., Stojkovic, T., Schaeffer, L. and Latour, P. (2017) 'Cryptic amyloidogenic elements in mutant NEFH causing Charcot-Marie-Tooth 2 trigger aggresome formation and neuronal death', *Acta Neuropathol Commun*, 5(1), pp. 017-0457.

Jaeken, J., Vanderschueren-Lodeweyckx, M., Casaer, P., L. Snoeck, L., Corbeel, L., Eggermont, E. and Eeckels, R. (1980) *Familial psychomotor retardation with markedly fluctuating serum prolactin, FSH and GH levels, partial TBG-deficiency, increased serum arylsulphatase A and increased CSF protein: A new syndrome?*

Jambhekar, S. and Breen, P.J. (2009) *Basic Pharmacokinetics*. Pharmaceutical Press.

- Jaski, B.E., Jessup, M.L., Mancini, D.M., Cappola, T.P., Pauly, D.F., Greenberg, B., Borow, K., Dittrich, H., Zsebo, K.M. and Hajjar, R.J. (2009) 'Calcium upregulation by percutaneous administration of gene therapy in cardiac disease (CUPID Trial), a first-in-human phase 1/2 clinical trial', *J Card Fail*, 15(3), pp. 171-81.
- Jin, L., Jiang, X.-M., Du, P., Xu, J., Gong, G.-q., Wang, Q.-j. and Xu, Y.-g. (2011) 'Synthesis and Na⁺/H⁺ exchanger inhibitory activity of benzoylguanidine derivatives', *European Journal of Medicinal Chemistry*, 46(9), pp. 4107-4116.
- Jingting, S., Qin, X., Yanju, S., Ming, Z., Yunjie, T., Gaige, J., Zhongwei, S. and Jianmin, Z. (2017) 'Oxidative and glycolytic skeletal muscles show marked differences in gene expression profile in Chinese Qingyuan partridge chickens', *PLoS One*, 12(8), p. e0183118.
- Johnstone, V.P.A., Viola, H.M. and Hool, L.C. (2017) 'Dystrophic Cardiomyopathy—Potential Role of Calcium in Pathogenesis, Treatment and Novel Therapies', *Genes*, 8(4), p. 108.
- Jørgensen, L.H., Blain, A., Grealley, E., Laval, S.H., Blamire, A.M., Davison, B.J., Brinkmeier, H., MacGowan, G.A., Schrøder, H.D., Bushby, K., Straub, V. and Lochmüller, H. (2011) 'Long-Term Blocking of Calcium Channels in *mdx* Mice Results in Differential Effects on Heart and Skeletal Muscle', *The American Journal of Pathology*, 178(1), pp. 273-283.
- Judge, D.P., Kass, D.A., Thompson, W.R. and Wagner, K.R. (2011) 'Pathophysiology and therapy of cardiac dysfunction in Duchenne muscular dystrophy', *Am J Cardiovasc Drugs*, 11(5), pp. 287-94.
- Jung, Y.S., Kim, M.Y., Kim, M.J., Oh, K.S., Yi, K.Y., Lee, S., Yoo, S.E. and Lee, B.H. (2006) 'Pharmacological profile of KR-33028, a highly selective inhibitor of Na⁺/H⁺ exchanger', *Eur J Pharmacol*, 535(1-3), pp. 220-7.
- Kalashnikova, A.A., Winkler, D.D., McBryant, S.J., Henderson, R.K., Herman, J.A., DeLuca, J.G., Luger, K., Prenni, J.E. and Hansen, J.C. (2013) 'Linker histone H1.0 interacts with an extensive network of proteins found in the nucleolus', *Nucleic Acids Research*, 41(7), pp. 4026-4035.
- Kamogawa, Y., Biro, S., Maeda, M., Setoguchi, M., Hirakawa, T., Yoshida, H. and Tei, C. (2001) 'Dystrophin-deficient myocardium is vulnerable to pressure overload in vivo', *Cardiovascular Research*, 50(3), pp. 509-515.
- Kar, N.C. and Pearson, C.M. (1979) 'Catalase, superoxide dismutase, glutathione reductase and thiobarbituric acid-reactive products in normal and dystrophic human muscle', *Clin Chim Acta*, 94(3), pp. 277-80.
- Karmazyn, M. (2013) 'NHE-1: still a viable therapeutic target', *J Mol Cell Cardiol*, 61, pp. 77-82.
- Karpati, G. and Carpenter, S. (1986) 'Small-caliber skeletal muscle fibers do not suffer deleterious consequences of dystrophic gene expression', *Am J Med Genet*, 25(4), pp. 653-8.
- Karpati, G., Carpenter, S. and Prescott, S. (1988) 'Small-caliber skeletal muscle fibers do not suffer necrosis in *mdx* mouse dystrophy', *Muscle Nerve*, 11(8), pp. 795-803.

- Katsetos, C.D., Koutzaki, S. and Melvin, J.J. (2013) 'Mitochondrial dysfunction in neuromuscular disorders', *Semin Pediatr Neurol*, 20(3), pp. 202-15.
- Keightley, J.A., Anitori, R., Burton, M.D., Quan, F., Buist, N.R. and Kennaway, N.G. (2000) 'Mitochondrial encephalomyopathy and complex III deficiency associated with a stop-codon mutation in the cytochrome b gene', *Am J Hum Genet*, 67(6), pp. 1400-10.
- Kendall, G.C., Mokhonova, E.I., Moran, M., Sejbuk, N.E., Wang, D.W., Silva, O., Wang, R.T., Martinez, L., Lu, Q.L., Damoiseaux, R., Spencer, M.J., Nelson, S.F. and Miceli, M.C. (2012) 'Dantrolene enhances antisense-mediated exon skipping in human and mouse models of Duchenne muscular dystrophy', *Sci Transl Med*, 4(164), p. 164ra160.
- Kerper, L.E. and Hinkle, P.M. (1997) 'Cellular uptake of lead is activated by depletion of intracellular calcium stores', *J Biol Chem*, 272(13), pp. 8346-52.
- Khadilkar, S.V., Patil, N.D., Kadam, N.D., Mansukhani, K.A. and Patel, B.A. (2017) 'Clinico-Electrophysiological and Genetic Overlaps and Magnetic Resonance Imaging Findings in Charcot-Marie-Tooth Disease: A Pilot Study from Western India', *Ann Indian Acad Neurol*, 20(4), pp. 425-429.
- Kharraz, Y., Guerra, J., Pessina, P., Serrano, A.L. and Munoz-Canoves, P. (2014) 'Understanding the process of fibrosis in Duchenne muscular dystrophy', *Biomed Res Int*, 2014, p. 965631.
- Khouzami, L., Bourin, M.-C., Christov, C., Damy, T., Escoubet, B., Caramelle, P., Perier, M., Wahbi, K., Meune, C., Pavoine, C. and Pecker, F. (2010) 'Delayed Cardiomyopathy in Dystrophin Deficient *mdx* Mice Relies on Intrinsic Glutathione Resource', *The American Journal of Pathology*, 177(3), pp. 1356-1364.
- Khurana, T.S., Prendergast, R.A., Alameddine, H.S., Tome, F.M., Fardeau, M., Arahata, K., Sugita, H. and Kunkel, L.M. (1995) 'Absence of extraocular muscle pathology in Duchenne's muscular dystrophy: role for calcium homeostasis in extraocular muscle sparing', *J Exp Med*, 182(2), pp. 467-75.
- Kikuchi, K. and Poss, K.D. (2012) 'Cardiac Regenerative Capacity and Mechanisms', *Annual review of cell and developmental biology*, 28, pp. 719-741.
- Kim, H., Yoon, Y.J., Kim, H., Cha, E.Y., Lee, H.S., Kim, J.H., Yi, K.Y., Lee, S., Cheon, H.G., Yoo, S.E., Lee, S.S., Shin, J.G. and Liu, K.H. (2005) 'In vitro metabolism of a new cardioprotective agent, KR-33028 in the human liver microsomes and cryopreserved human hepatocytes', *Arch Pharm Res*, 28(11), pp. 1287-92.
- Kim, H., Yoon, Y.J., Kim, H., Kang, S., Cheon, H.G., Yoo, S.E., Shin, J.G. and Liu, K.H. (2006) 'Characterization of the cytochrome P450 enzymes involved in the metabolism of a new cardioprotective agent KR-33028', *Toxicol Lett*, 166(2), pp. 105-14.
- Kim, J., Jung, Y.S., Han, W., Kim, M.Y., Namkung, W., Lee, B.H., Yi, K.Y., Yoo, S.E., Lee, M.G. and Kim, K.H. (2007a) 'Pharmacodynamic characteristics and cardioprotective effects of new NHE1 inhibitors', *Eur J Pharmacol*, 567(1-2), pp. 131-8.
- Kim, M.S., Chang, X., LeBron, C., Nagpal, J.K., Lee, J., Huang, Y., Yamashita, K., Trink, B., Ratovitski, E.A. and Sidransky, D. (2010) 'Neurofilament Heavy Polypeptide Regulates the Akt- β -Catenin Pathway in Human Esophageal Squamous Cell Carcinoma', *PLoS ONE*, 5(2), p. e9003.

Kim, Y.H., Ji, H.Y., Lee, S., Yi, K.Y., Kim, Y.S., Lee, K.H. and Lee, H.S. (2007b) 'Determination of a selective Na⁺/H⁺ exchanger inhibitor, 4-cyano(benzo[b]thiophene-2-carbonyl)guanidine (KR-33028) in rat plasma by liquid chromatography-tandem mass spectrometry', *Biomed Chromatogr*, 21(8), pp. 810-5.

Kim, Y.H., Yoo, S.D., Kim, Y.S., Lee, K.H. and Lee, H.S. (2007c) 'Dose-dependent pharmacokinetics of a new Na⁺/H⁺ exchanger inhibitor KR-33028 in rats', *Biopharm Drug Dispos*, 28(8), pp. 423-9.

Kinali, M., Arechavala-Gomez, V., Feng, L., Cirak, S., Hunt, D., Adkin, C., Guglieri, M., Ashton, E., Abbs, S., Nihoyannopoulos, P., Garralda, M.E., Rutherford, M., McCulley, C., Popplewell, L., Graham, I.R., Dickson, G., Wood, M.J., Wells, D.J., Wilton, S.D., Kole, R., Straub, V., Bushby, K., Sewry, C., Morgan, J.E. and Muntoni, F. (2009) 'Local restoration of dystrophin expression with the morpholino oligomer AVI-4658 in Duchenne muscular dystrophy: a single-blind, placebo-controlled, dose-escalation, proof-of-concept study', *Lancet Neurol*, 8(10), pp. 918-28.

Kinoshita, Y., Uo, T., Jayadev, S., Garden, G.A., Conrads, T.P., Veenstra, T.D. and Morrison, R.S. (2006) 'Potential applications and limitations of proteomics in the study of neurological disease', *Arch Neurol*, 63(12), pp. 1692-6.

Klingler, W., Jurkat-Rott, K., Lehmann-Horn, F. and Schleip, R. (2012) 'The role of fibrosis in Duchenne muscular dystrophy', *Acta Myol*, 31(3), pp. 184-95.

Klymiuk, N., Blutke, A., Graf, A., Krause, S., Burkhardt, K., Wuensch, A., Krebs, S., Kessler, B., Zakhartchenko, V., Kurome, M., Kemter, E., Nagashima, H., Schoser, B., Herbach, N., Blum, H., Wanke, R., Aartsma-Rus, A., Thirion, C., Lochmuller, H., Walter, M.C. and Wolf, E. (2013) 'Dystrophin-deficient pigs provide new insights into the hierarchy of physiological derangements of dystrophic muscle', *Hum Mol Genet*, 22(21), pp. 4368-82.

Koenig, M., Hoffman, E.P., Bertelson, C.J., Monaco, A.P., Feener, C. and Kunkel, L.M. (1987) 'Complete cloning of the Duchenne muscular dystrophy (DMD) cDNA and preliminary genomic organization of the DMD gene in normal and affected individuals', *Cell*, 50(3), pp. 509-17.

Koliakos, G., Paletas, K. and Kaloyianni, M. (2008) 'NHE-1: a molecular target for signalling and cell matrix interactions', *Connect Tissue Res*, 49(3), pp. 157-61.

Kolthammer, J. and Korjonen-Close, H. (2007) *Pharmacokinetics, a Beginner's Guide*. Institute of Clinical Research Publishing.

Kornegay, J.N. (2017) 'The golden retriever model of Duchenne muscular dystrophy', *Skelet Muscle*, 7(1), p. 9.

Kornegay, J.N., Bogan, J.R., Bogan, D.J., Childers, M.K., Li, J., Nghiem, P., Detwiler, D.A., Larsen, C.A., Grange, R.W., Bhavaraju-Sanka, R.K., Tou, S., Keene, B.P., Howard, J.F., Jr., Wang, J., Fan, Z., Schatzberg, S.J., Styner, M.A., Flanigan, K.M., Xiao, X. and Hoffman, E.P. (2012) 'Canine models of Duchenne muscular dystrophy and their use in therapeutic strategies', *Mamm Genome*, 23(1-2), pp. 85-108.

Kornegay, J.N., Tuler, S.M., Miller, D.M. and Levesque, D.C. (1988) 'Muscular dystrophy in a litter of golden retriever dogs', *Muscle Nerve*, 11(10), pp. 1056-64.

- Kowalski, A. (2016) 'Nuclear and nucleolar activity of linker histone variant H1.0', *Cell Mol Biol Lett*, 21(15), pp. 016-0014.
- Krag, T.O.B., Bogdanovich, S., Jensen, C.J., Fischer, M.D., Hansen-Schwartz, J., Javazon, E.H., Flake, A.W., Edvinsson, L. and Khurana, T.S. (2004) 'Heregulin ameliorates the dystrophic phenotype in *mdx* mice', *Proceedings of the National Academy of Sciences of the United States of America*, 101(38), pp. 13856-13860.
- Kruger, M. and Linke, W.A. (2011) 'The giant protein titin: a regulatory node that integrates myocyte signaling pathways', *J Biol Chem*, 286(12), pp. 9905-12.
- Kruse, C., Grunweller, A., Willkomm, D.K., Pfeiffer, T., Hartmann, R.K. and Muller, P.K. (1998) 'tRNA is entrapped in similar, but distinct, nuclear and cytoplasmic ribonucleoprotein complexes, both of which contain vigilin and elongation factor 1 alpha', *Biochem J*, 329(Pt 3), pp. 615-21.
- Kruse, C., Willkomm, D., Gebken, J., Schuh, A., Stossberg, H., Vollbrandt, T. and Muller, P.K. (2003) 'The multi-KH protein vigilin associates with free and membrane-bound ribosomes', *Cell Mol Life Sci*, 60(10), pp. 2219-27.
- Kunkel, L.M., Beggs, A.H. and Hoffman, E.P. (1989) 'Molecular genetics of Duchenne and Becker muscular dystrophy: emphasis on improved diagnosis', *Clin Chem*, 35(7 Suppl), pp. B21-4.
- Labeit, D., Watanabe, K., Witt, C., Fujita, H., Wu, Y., Lahmers, S., Funck, T., Labeit, S. and Granzier, H. (2003) 'Calcium-dependent molecular spring elements in the giant protein titin', *Proceedings of the National Academy of Sciences*, 100(23), pp. 13716-13721.
- Labeit, S., Kolmerer, B. and Linke, W.A. (1997) 'The giant protein titin. Emerging roles in physiology and pathophysiology', *Circ Res*, 80(2), pp. 290-4.
- Laing, N.G., Davis, M.R., Bayley, K., Fletcher, S. and Wilton, S.D. (2011) 'Molecular diagnosis of duchenne muscular dystrophy: past, present and future in relation to implementing therapies', *Clin Biochem Rev*, 32(3), pp. 129-34.
- Larcher, T., Lafoux, A., Tesson, L., Remy, S., Thepenier, V., François, V., Le Guiner, C., Goubin, H., Dutilleul, M., Guigand, L., Toumaniantz, G., De Cian, A., Boix, C., Renaud, J.-B., Chereil, Y., Giovannangeli, C., Concordet, J.-P., Anegon, I. and Huchet, C. (2014) 'Characterization of Dystrophin Deficient Rats: A New Model for Duchenne Muscular Dystrophy', *PLoS ONE*, 9(10), p. e110371.
- Le Guiner, C., Servais, L., Montus, M., Larcher, T., Fraysse, B., Moullec, S., Allais, M., Francois, V., Dutilleul, M., Malerba, A., Koo, T., Thibaut, J.L., Matot, B., Devaux, M., Le Duff, J., Deschamps, J.Y., Barthelemy, I., Blot, S., Testault, I., Wahbi, K., Ederhy, S., Martin, S., Veron, P., Georger, C., Athanasopoulos, T., Masurier, C., Mingozi, F., Carlier, P., Gjata, B., Hogrel, J.Y., Adjali, O., Mavilio, F., Voit, T., Moullier, P. and Dickson, G. (2017) 'Long-term microdystrophin gene therapy is effective in a canine model of Duchenne muscular dystrophy', *Nat Commun*, 8, p. 16105.
- Leal, J.F., Ferrer, I., Blanco-Aparicio, C., Hernandez-Losa, J., Ramon, Y.C.S., Carnero, A. and Leonart, M.E. (2008) 'S-adenosylhomocysteine hydrolase downregulation contributes to tumorigenesis', *Carcinogenesis*, 29(11), pp. 2089-95.

- Lee, B.K., Lee, D.H., Park, S., Park, S.L., Yoon, J.S., Lee, M.G., Lee, S., Yi, K.Y., Yoo, S.E., Lee, K.H., Kim, Y.S., Lee, S.H., Baik, E.J., Moon, C.H. and Jung, Y.S. (2009) 'Effects of KR-33028, a novel Na⁺/H⁺ exchanger-1 inhibitor, on glutamate-induced neuronal cell death and ischemia-induced cerebral infarct', *Brain Res*, 1248, pp. 22-30.
- Lefaucheur, J.P., Pastoret, C. and Sebillé, A. (1995) 'Phenotype of dystrophinopathy in old *mdx* mice', *Anat Rec*, 242(1), pp. 70-6.
- Leung, D.G. and Wagner, K.R. (2013) 'Therapeutic advances in muscular dystrophy', *Ann Neurol*, 74(3), pp. 404-11.
- LeWinter, M.M., Wu, Y., Labeit, S. and Granzier, H. (2007) 'Cardiac titin: structure, functions and role in disease', *Clin Chim Acta*, 375(1-2), pp. 1-9.
- Li, Q., Mao, L., Wang, R., Zhu, L. and Xue, L. (2014) 'Overexpression of S-adenosylhomocysteine hydrolase (SAHH) in esophageal squamous cell carcinoma (ESCC) cell lines: effects on apoptosis, migration and adhesion of cells', *Molecular Biology Reports*, 41(4), pp. 2409-2417.
- Li, Z.B., Kollias, H.D. and Wagner, K.R. (2008) 'Myostatin directly regulates skeletal muscle fibrosis', *J Biol Chem*, 283(28), pp. 19371-8.
- Linke, W.A. (2008) 'Sense and stretchability: The role of titin and titin-associated proteins in myocardial stress-sensing and mechanical dysfunction†', *Cardiovascular Research*, 77(4), pp. 637-648.
- Liu, M., Yue, Y., Harper, S.Q., Grange, R.W., Chamberlain, J.S. and Duan, D. (2005) 'Adeno-associated virus-mediated microdystrophin expression protects young *mdx* muscle from contraction-induced injury', *Mol Ther*, 11(2), pp. 245-56.
- Ljubicic, V., Miura, P., Burt, M., Boudreault, L., Khogali, S., Lunde, J.A., Renaud, J.M. and Jasmin, B.J. (2011) 'Chronic AMPK activation evokes the slow, oxidative myogenic program and triggers beneficial adaptations in *mdx* mouse skeletal muscle', *Hum Mol Genet*, 20(17), pp. 3478-93.
- Loehr, J.A., Stinnett, G.R., Hernandez-Rivera, M., Roten, W.T., Wilson, L.J., Pautler, R.G. and Rodney, G.G. (2016) 'Eliminating Nox2 reactive oxygen species production protects dystrophic skeletal muscle from pathological calcium influx assessed in vivo by manganese-enhanced magnetic resonance imaging', *J Physiol*, 594(21), pp. 6395-6405.
- Loftsson, T. (2015) *Essential Pharmacokinetics: A Primer for Pharmaceutical Scientists*. Elsevier Science.
- London, R.E., Toney, G., Gabel, S.A. and Funk, A. (1989) 'Magnetic resonance imaging studies of the brains of anesthetized rats treated with manganese chloride', *Brain Res Bull*, 23(3), pp. 229-35.
- Lynch, G.S., Hinkle, R.T., Chamberlain, J.S., Brooks, S.V. and Faulkner, J.A. (2001) 'Force and power output of fast and slow skeletal muscles from *mdx* mice 6-28 months old', *J Physiol*, 535(Pt 2), pp. 591-600.
- Mackrill, J.J. (2010) 'Ryanodine receptor calcium channels and their partners as drug targets', *Biochem Pharmacol*, 79(11), pp. 1535-43.

- Mah, J.K., Selby, K., Campbell, C., Nadeau, A., Tarnopolsky, M., McCormick, A., Dooley, J.M., Kolski, H., Skalsky, A.J., Smith, R.G., Buckley, D., Ray, P.N. and Yoon, G. (2011) 'A population-based study of dystrophin mutations in Canada', *Can J Neurol Sci*, 38(3), pp. 465-74.
- Majid, T., Ali, Y.O., Venkitaramani, D.V., Jang, M.K., Lu, H.C. and Pautler, R.G. (2014) 'In vivo axonal transport deficits in a mouse model of fronto-temporal dementia', *Neuroimage Clin*, 4, pp. 711-7.
- Malerba, A., Kang, J.K., McClorey, G., Saleh, A.F., Popplewell, L., Gait, M.J., Wood, M.J.A. and Dickson, G. (2012) 'Dual Myostatin and Dystrophin Exon Skipping by Morpholino Nucleic Acid Oligomers Conjugated to a Cell-penetrating Peptide Is a Promising Therapeutic Strategy for the Treatment of Duchenne Muscular Dystrophy', *Molecular Therapy. Nucleic Acids*, 1(12), p. e62.
- Malheiros, J.M., Paiva, F.F., Longo, B.M., Hamani, C. and Covolan, L. (2015) 'Manganese-Enhanced MRI: Biological Applications in Neuroscience', *Frontiers in Neurology*, 6, p. 161.
- Mallick, P. and Kuster, B. (2010) 'Proteomics: a pragmatic perspective', *Nat Biotechnol*, 28(7), pp. 695-709.
- Malo, M.E. and Fliegel, L. (2006) 'Physiological role and regulation of the Na⁺/H⁺ exchanger', *Can J Physiol Pharmacol*, 84(11), pp. 1081-95.
- Mandel, J.L. (1989) 'Dystrophin. The gene and its product', *Nature*, 339(6226), pp. 584-6.
- Mann, C.J., Perdiguero, E., Kharraz, Y., Aguilar, S., Pessina, P., Serrano, A.L. and Munoz-Canoves, P. (2011) 'Aberrant repair and fibrosis development in skeletal muscle', *Skelet Muscle*, 1(1), p. 21.
- Manning, J. and O'Malley, D. (2015) 'What has the *mdx* mouse model of duchenne muscular dystrophy contributed to our understanding of this disease?', *Journal of Muscle Research and Cell Motility*, 36(2), pp. 155-167.
- Manole, E. (1995) 'The dystrophin gene and its product--a view', *Rom J Neurol Psychiatry*, 33(2), pp. 109-19.
- Mao, D., Xu, Y., Hu, X., Zhang, G., Dong, J. and Gong, G. (2009) 'Synthesis and Na⁽⁺⁾/H⁽⁺⁾ exchanger-1 inhibitory activity of substituted (quinolinecarbonyl)guanidine derivatives', *Chem Biodivers*, 6(10), pp. 1727-36.
- Masereel, B. (2003) 'An overview of inhibitors of Na⁺/H⁺ exchanger', *European Journal of Medicinal Chemistry*, 38(6), pp. 547-554.
- Mason, M.J., Mayer, B. and Hymel, L.J. (1993) 'Inhibition of Ca²⁺ transport pathways in thymic lymphocytes by econazole, miconazole, and SKF 96365', *Am J Physiol*, 264(3 Pt 1), pp. C654-62.
- Massaad, C.A. and Pautler, R.G. (2011) 'Manganese-enhanced magnetic resonance imaging (MEMRI)', *Methods Mol Biol*, 711, pp. 145-74.

- Matsuda, T., Arakawa, N., Takuma, K., Kishida, Y., Kawasaki, Y., Sakaue, M., Takahashi, K., Takahashi, T., Suzuki, T., Ota, T., Hamano-Takahashi, A., Onishi, M., Tanaka, Y., Kameo, K. and Baba, A. (2001) 'SEA0400, a novel and selective inhibitor of the Na⁺-Ca²⁺ exchanger, attenuates reperfusion injury in the in vitro and in vivo cerebral ischemic models', *J Pharmacol Exp Ther*, 298(1), pp. 249-56.
- Matsumura, C.Y., Pertille, A., Albuquerque, T.C., Santo Neto, H. and Marques, M.J. (2009) 'Diltiazem and verapamil protect dystrophin-deficient muscle fibers of MDX mice from degeneration: a potential role in calcium buffering and sarcolemmal stability', *Muscle Nerve*, 39(2), pp. 167-76.
- Matsumura, K., Shimizu, T., Nonaka, I. and Mannen, T. (1989) 'Immunochemical study of connectin (titin) in neuromuscular diseases using a monoclonal antibody: connectin is degraded extensively in Duchenne muscular dystrophy', *Journal of the Neurological Sciences*, 93(2), pp. 147-156.
- Matthijs, G., Schollen, E., Heykants, L. and Grünewald, S. (1999) 'Phosphomannomutase Deficiency: The Molecular Basis of the Classical Jaeken Syndrome (CDGS Type Ia)', *Molecular Genetics and Metabolism*, 68(2), pp. 220-226.
- McGreevy, J.W., Hakim, C.H., McIntosh, M.A. and Duan, D. (2015) 'Animal models of Duchenne muscular dystrophy: from basic mechanisms to gene therapy', *Disease Models & Mechanisms*, 8(3), pp. 195-213.
- McManus, L.M. and Mitchell, R.N. (2014) *Pathobiology of Human Disease: A Dynamic Encyclopedia of Disease Mechanisms*. Elsevier Science.
- Megeney, L.A., Kablar, B., Perry, R.L.S., Ying, C., May, L. and Rudnicki, M.A. (1999) 'Severe cardiomyopathy in mice lacking dystrophin and MyoD', *Proceedings of the National Academy of Sciences of the United States of America*, 96(1), pp. 220-225.
- Mei, Y., Xu, L., Kramer, H.F., Tomberlin, G.H., Townsend, C. and Meissner, G. (2013) 'Stabilization of the skeletal muscle ryanodine receptor ion channel-FKBP12 complex by the 1,4-benzothiazepine derivative S107', *PLoS One*, 8(1), p. e54208.
- Mendell, J.R., Goemans, N., Lowes, L.P., Alfano, L.N., Berry, K., Shao, J., Kaye, E.M. and Mercuri, E. (2016) 'Longitudinal effect of eteplirsen versus historical control on ambulation in Duchenne muscular dystrophy', *Ann Neurol*, 79(2), pp. 257-71.
- Mendell, J.R., Rodino-Klapac, L.R., Sahenk, Z., Roush, K., Bird, L., Lowes, L.P., Alfano, L., Gomez, A.M., Lewis, S., Kota, J., Malik, V., Shontz, K., Walker, C.M., Flanigan, K.M., Corridore, M., Kean, J.R., Allen, H.D., Shilling, C., Melia, K.R., Sazani, P., Saoud, J.B. and Kaye, E.M. (2013) 'Eteplirsen for the treatment of Duchenne muscular dystrophy', *Ann Neurol*, 74(5), pp. 637-47.
- Merrick, D., Stadler, L.K., Larner, D. and Smith, J. (2009) 'Muscular dystrophy begins early in embryonic development deriving from stem cell loss and disrupted skeletal muscle formation', *Dis Model Mech*, 2.
- Meryon, E. (1852) 'On Granular and Fatty Degeneration of the Voluntary Muscles', *Med Chir Trans*, 35, pp. 73-84 1.

- Mihaila, R.G. (2015) 'A minireview on NHE1 inhibitors. A rediscovered hope in oncohematology', *Biomed Pap Med Fac Univ Palacky Olomouc Czech Repub*, 159(4), pp. 519-26.
- Millay, D.P., Goonasekera, S.A., Sargent, M.A., Maillet, M., Aronow, B.J. and Molkentin, J.D. (2009) 'Calcium influx is sufficient to induce muscular dystrophy through a TRPC-dependent mechanism', *Proc Natl Acad Sci U S A*, 106(45), pp. 19023-8.
- Millay, D.P., Sargent, M.A., Osinska, H., Baines, C.P., Barton, E.R., Vuagniaux, G., Sweeney, H.L., Robbins, J. and Molkentin, J.D. (2008) 'Genetic and pharmacologic inhibition of mitochondrial-dependent necrosis attenuates muscular dystrophy', *Nature medicine*, 14(4), pp. 442-447.
- Missiaen, L., Robberecht, W., van den Bosch, L., Callewaert, G., Parys, J.B., Wuytack, F., Raeymaekers, L., Nilius, B., Eggermont, J. and De Smedt, H. (2000) 'Abnormal intracellular Ca^{2+} homeostasis and disease', *Cell Calcium*, 28(1), pp. 1-21.
- Miura, P., Chakkalakal, J.V., Boudreault, L., Belanger, G., Hebert, R.L., Renaud, J.M. and Jasmin, B.J. (2009) 'Pharmacological activation of PPAR β /delta stimulates utrophin A expression in skeletal muscle fibers and restores sarcolemmal integrity in mature *mdx* mice', *Hum Mol Genet*, 18(23), pp. 4640-9.
- Moens, P., Baatsen, P.H. and Marechal, G. (1993) 'Increased susceptibility of EDL muscles from *mdx* mice to damage induced by contractions with stretch', *J Muscle Res Cell Motil*, 14(4), pp. 446-51.
- Moorwood, C., Lozynska, O., Suri, N., Napper, A.D., Diamond, S.L. and Khurana, T.S. (2011) 'Drug Discovery for Duchenne Muscular Dystrophy via Utrophin Promoter Activation Screening', *PLoS ONE*, 6(10), p. e26169.
- Moorwood, C., Soni, N., Patel, G., Wilton, S.D. and Khurana, T.S. (2013) 'A cell-based high-throughput screening assay for posttranscriptional utrophin upregulation', *J Biomol Screen*, 18(4), pp. 400-6.
- Morgan, J.E., Fletcher, R.M. and Partridge, T.A. (1996) 'Yields of muscle from myogenic cells implanted into young and old *mdx* hosts', *Muscle Nerve*, 19(2), pp. 132-9.
- Morgan, J.E., Hoffman, E.P. and Partridge, T.A. (1990) 'Normal myogenic cells from newborn mice restore normal histology to degenerating muscles of the *mdx* mouse', *J Cell Biol*, 111(6 Pt 1), pp. 2437-49.
- Morine, K.J., Sleeper, M.M., Barton, E.R. and Sweeney, H.L. (2010) 'Overexpression of SERCA1a in the *mdx* diaphragm reduces susceptibility to contraction-induced damage', *Hum Gene Ther*, 21(12), pp. 1735-9.
- Morris, K. (2002) 'Targeting the myocardial sodium-hydrogen exchange for treatment of heart failure', *Expert Opin Ther Targets*, 6(3), pp. 291-8.
- Mosqueira, M., Willmann, G., Ruohola-Baker, H. and Khurana, T.S. (2010) 'Chronic Hypoxia Impairs Muscle Function in the Drosophila Model of Duchenne's Muscular Dystrophy (DMD)', *PLoS ONE*, 5(10), p. e13450.

Mosqueira, M., Zeiger, U., Forderer, M., Brinkmeier, H. and Fink, R.H. (2013) 'Cardiac and respiratory dysfunction in Duchenne muscular dystrophy and the role of second messengers', *Med Res Rev*, 33(5), pp. 1174-213.

Mouly, V., Aamiri, A., Perie, S., Mamchaoui, K., Barani, A., Bigot, A., Bouazza, B., Francois, V., Furling, D., Jacquemin, V., Negroni, E., Riederer, I., Vignaud, A., St Guily, J.L. and Butler-Browne, G.S. (2005) 'Myoblast transfer therapy: is there any light at the end of the tunnel?', *Acta Myol*, 24(2), pp. 128-33.

Muir, L.A. and Chamberlain, J.S. (2009) 'Emerging strategies for cell and gene therapy of the muscular dystrophies', *Expert Rev Mol Med*, 11, p. e18.

Muller, J., Vayssiere, N., Royuela, M., Leger, M.E., Muller, A., Bacou, F., Pons, F., Hugon, G. and Mornet, D. (2001) 'Comparative evolution of muscular dystrophy in diaphragm, gastrocnemius and masseter muscles from old male *mdx* mice', *J Muscle Res Cell Motil*, 22(2), pp. 133-9.

Muntoni, F., Torelli, S. and Ferlini, A. (2003) 'Dystrophin and mutations: one gene, several proteins, multiple phenotypes', *Lancet Neurol*, 2(12), pp. 731-40.

Murphy, V.A., Smith, Q.R. and Rapoport, S.I. (1991) 'Saturable transport of Ca into CSF in chronic hypo- and hypercalcemia', *J Neurosci Res*, 30(2), pp. 421-6.

Myers, C.T., Stong, N., Mountier, E.I., Helbig, K.L., Freytag, S., Sullivan, J.E., Ben Zeev, B., Nissenkorn, A., Tzadok, M., Heimer, G., Shinde, D.N., Rezazadeh, A., Regan, B.M., Oliver, K.L., Ernst, M.E., Lippa, N.C., Mulhern, M.S., Ren, Z., Poduri, A., Andrade, D.M., Bird, L.M., Bahlo, M., Berkovic, S.F., Lowenstein, D.H., Scheffer, I.E., Sadleir, L.G., Goldstein, D.B., Mefford, H.C. and Heinzen, E.L. (2017) 'De Novo Mutations in PPP3CA Cause Severe Neurodevelopmental Disease with Seizures', *Am J Hum Genet*, 101(4), pp. 516-524.

Nagamine, Y., Medcalf, R.L. and Munoz-Canoves, P. (2005) 'Transcriptional and posttranscriptional regulation of the plasminogen activator system', *Thromb Haemost*, 93(4), pp. 661-75.

Nakamura, A. and Takeda, S.i. (2011) 'Mammalian Models of Duchenne Muscular Dystrophy: Pathological Characteristics and Therapeutic Applications', *Journal of Biomedicine and Biotechnology*, 2011, p. 8.

Nakamura, K., Fujii, W., Tsuboi, M., Tanihata, J., Teramoto, N., Takeuchi, S., Naito, K., Yamanouchi, K. and Nishihara, M. (2014) 'Generation of muscular dystrophy model rats with a CRISPR/Cas system', *Scientific Reports*, 4, p. 5635.

Nigro, G., Comi, L.I., Politano, L. and Bain, R.J.I. (1990) 'The incidence and evolution of cardiomyopathy in Duchenne muscular dystrophy', *International Journal of Cardiology*, 26(3), pp. 271-277.

Nigro, V. and Piluso, G. (2015) 'Spectrum of muscular dystrophies associated with sarcolemmal-protein genetic defects', *Biochim Biophys Acta*, 1852(4), pp. 585-93.

Nudel, U., Zuk, D., Einat, P., Zeelon, E., Levy, Z., Neuman, S. and Yaffe, D. (1989) 'Duchenne muscular dystrophy gene product is not identical in muscle and brain', *Nature*, 337(6202), pp. 76-8.

- Oberc, M.A. and Engel, W.K. (1977) 'Ultrastructural localization of calcium in normal and abnormal skeletal muscle', *Lab Invest*, 36(6), pp. 566-77.
- Oh, K.S., Seo, H.W., Yi, K.Y., Lee, S., Yoo, S.E. and Lee, B.H. (2007) 'Effects of KR-33028, a novel Na⁺/H⁺ exchanger-1 inhibitor, on ischemia and reperfusion-induced myocardial infarction in rats and dogs', *Fundam Clin Pharmacol*, 21(3), pp. 255-63.
- Ohlendieck, K., Ervasti, J.M., Matsumura, K., Kahl, S.D., Leveille, C.J. and Campbell, K.P. (1991) 'Dystrophin-related protein is localized to neuromuscular junctions of adult skeletal muscle', *Neuron*, 7(3), pp. 499-508.
- Oldfors, A., Eriksson, B.O., Kyllerman, M., Martinsson, T. and Wahlstrom, J. (1994) 'Dilated cardiomyopathy and the dystrophin gene: an illustrated review', *Br Heart J*, 72(4), pp. 344-8.
- Opitz, C.A., Kulke, M., Leake, M.C., Neagoe, C., Hinssen, H., Hajjar, R.J. and Linke, W.A. (2003) 'Damped elastic recoil of the titin spring in myofibrils of human myocardium', *Proceedings of the National Academy of Sciences of the United States of America*, 100(22), pp. 12688-12693.
- Ozkan, P. and Mutharasan, R. (2002) 'A rapid method for measuring intracellular pH using BCECF-AM', *Biochim Biophys Acta*, 1572(1), pp. 143-8.
- Palmer, J.L. and Abeles, R.H. (1979) 'The mechanism of action of S-adenosylhomocysteinase', *J Biol Chem*, 254(4), pp. 1217-26.
- Pantoja, M. and Ruohola-Baker, H. (2013) 'Drosophila as a starting point for developing therapeutics for the rare disease Duchenne Muscular Dystrophy', *Rare Diseases*, 1, p. e24995.
- Park, K.S., Poburko, D., Wollheim, C.B. and Demarex, N. (2009) 'Amiloride derivatives induce apoptosis by depleting ER Ca(2⁺) stores in vascular endothelial cells', *British Journal of Pharmacology*, 156(8), pp. 1296-1304.
- Parsons, E.P., Bradley, D.M. and Clarke, A.J. (2003) 'Newborn screening for Duchenne muscular dystrophy', *Archives of Disease in Childhood*, 88(1), p. 91.
- Partridge, T.A., Morgan, J.E., Coulton, G.R., Hoffman, E.P. and Kunkel, L.M. (1989) 'Conversion of *mdx* myofibres from dystrophin-negative to -positive by injection of normal myoblasts', *Nature*, 337(6203), pp. 176-9.
- Pastoret, C. and Seville, A. (1995) '*mdx* mice show progressive weakness and muscle deterioration with age', *J Neurol Sci*, 129(2), pp. 97-105.
- Pasut, A., Jones, A.E. and Rudnicki, M.A. (2013) 'Isolation and culture of individual myofibers and their satellite cells from adult skeletal muscle', *J Vis Exp*, (73), p. e50074.
- Pearce, J.M. (2005) 'Early observations on duchenne-meryon muscular dystrophy', *Eur Neurol*, 54(1), pp. 46-8.
- Perez-Cerda, C., Giros, M.L., Serrano, M., Ecay, M.J., Gort, L., Perez Duenas, B., Medrano, C., Garcia-Alix, A., Artuch, R., Briones, P. and Perez, B. (2017) 'A Population-Based Study on Congenital Disorders of Protein N- and Combined with O-Glycosylation Experience in Clinical and Genetic Diagnosis', *J Pediatr*, 183, pp. 170-177.e1.

- Perez-Serra, A., Toro, R., Sarquella-Brugada, G., de Gonzalo-Calvo, D., Cesar, S., Carro, E., Llorente-Cortes, V., Iglesias, A., Brugada, J., Brugada, R. and Campuzano, O. (2016) 'Genetic basis of dilated cardiomyopathy', *Int J Cardiol*, 224, pp. 461-472.
- Perie, S., Trollet, C., Mouly, V., Vanneaux, V., Mamchaoui, K., Bouazza, B., Marolleau, J.P., Laforet, P., Chapon, F., Eymard, B., Butler-Browne, G., Larghero, J. and St Guily, J.L. (2014) 'Autologous myoblast transplantation for oculopharyngeal muscular dystrophy: a phase I/IIa clinical study', *Mol Ther*, 22(1), pp. 219-25.
- Perrin, C., Unterborn, J.N., Ambrosio, C.D. and Hill, N.S. (2004) 'Pulmonary complications of chronic neuromuscular diseases and their management', *Muscle Nerve*, 29(1), pp. 5-27.
- Petrof, B.J., Shrager, J.B., Stedman, H.H., Kelly, A.M. and Sweeney, H.L. (1993) 'Dystrophin protects the sarcolemma from stresses developed during muscle contraction', *Proceedings of the National Academy of Sciences of the United States of America*, 90(8), pp. 3710-3714.
- Philip, B., Lu, Z. and Gao, Y. (2005) 'Regulation of GDF-8 signaling by the p38 MAPK', *Cell Signal*, 17(3), pp. 365-75.
- Phillips, M.F. and Quinlivan, R. (2008) 'Calcium antagonists for Duchenne muscular dystrophy', *Cochrane Database Syst Rev*, (4), p. Cd004571.
- Plantie, E., Migocka-Patrzalek, M., Daczewska, M. and Jagla, K. (2015) 'Model organisms in the fight against muscular dystrophy: lessons from drosophila and Zebrafish', *Molecules*, 20(4), pp. 6237-53.
- Porte Thomé, F., Su, J., Barthelemy, I., Blanchard-Gutton, N., Bkaily, G., Yu, Q., Nagaraju, K., Galeh, B. and Blot, S. (2016) 'Translational development of rimeporide, a sodium-hydrogen exchanger (NHE-1) inhibitor, for patients with Duchenne muscular dystrophy', *Neuromuscular Disorders*, 26, p. S155.
- Pouyssegur, J., Chambard, J.C., Franchi, A., Paris, S. and Van Obberghen-Schilling, E. (1982) 'Growth factor activation of an amiloride-sensitive Na⁺/H⁺ exchange system in quiescent fibroblasts: coupling to ribosomal protein S6 phosphorylation', *Proc Natl Acad Sci U S A*, 79(13), pp. 3935-9.
- Prasain, J.K. (2012) *Tandem Mass Spectrometry - Applications and Principles*. InTech.
- Pressmar, J., Brinkmeier, H., Seewald, M.J., Naumann, T. and Rüdell, R. (1994) 'Intracellular Ca²⁺ concentrations are not elevated in resting cultured muscle from Duchenne (DMD) patients and in MDX mouse muscle fibres', *Pflügers Archiv*, 426(6), pp. 499-505.
- Price, A.N., Cheung, K.K., Cleary, J.O., Campbell, A.E., Riegler, J. and Lythgoe, M.F. (2010) 'Cardiovascular Magnetic Resonance Imaging in Experimental Models', *The Open Cardiovascular Medicine Journal*, 4, pp. 278-292.
- Putney, L.K., Denker, S.P. and Barber, D.L. (2002) 'The changing face of the Na⁺/H⁺ exchanger, NHE1: structure, regulation, and cellular actions', *Annu Rev Pharmacol Toxicol*, 42, pp. 527-52.

- Quinlan, J.G., Hahn, H.S., Wong, B.L., Lorenz, J.N., Wenisch, A.S. and Levin, L.S. (2004) 'Evolution of the *mdx* mouse cardiomyopathy: physiological and morphological findings', *Neuromuscul Disord*, 14(8-9), pp. 491-6.
- Rafael-Fortney, J.A., Chimanji, N.S., Schill, K.E., Martin, C.D., Murray, J.D., Ganguly, R., Stangland, J.E., Tran, T., Xu, Y., Canan, B.D., Mays, T.A., Delfin, D.A., Janssen, P.M. and Raman, S.V. (2011) 'Early treatment with lisinopril and spironolactone preserves cardiac and skeletal muscle in Duchenne muscular dystrophy mice', *Circulation*, 124(5), pp. 582-8.
- Ragusa, R.J., Chow, C.K., St Clair, D.K. and Porter, J.D. (1996) 'Extraocular, limb and diaphragm muscle group-specific antioxidant enzyme activity patterns in control and *mdx* mice', *J Neurol Sci*, 139(2), pp. 180-6.
- Rang, H.P., Ritter, J.M., Flower, R.J. and Henderson, G. (2015) *Rang and Dale's Pharmacology*. Elsevier Health Sciences.
- Reid, W.D. and MacGowan, N.A. (1998) 'Respiratory muscle injury in animal models and humans', *Mol Cell Biochem*, 179(1-2), pp. 63-80.
- Reinig, A.M., Mirzaei, S. and Berlau, D.J. (2017) 'Advances in the Treatment of Duchenne Muscular Dystrophy: New and Emerging Pharmacotherapies', *Pharmacotherapy*, 37(4), pp. 492-499.
- Richardson, G.D., Laval, S. and Owens, W.A. (2015) 'Cardiomyocyte Regeneration in the *mdx* Mouse Model of Nonischemic Cardiomyopathy', *Stem Cells and Development*, 24(14), pp. 1672-1679.
- Ricotti, V., Spinty, S., Roper, H., Hughes, I., Tejura, B., Robinson, N., Layton, G., Davies, K., Muntoni, F. and Tinsley, J. (2016) 'Safety, Tolerability, and Pharmacokinetics of SMT C1100, a 2-Arylbenzoxazole Utrophin Modulator, following Single- and Multiple-Dose Administration to Pediatric Patients with Duchenne Muscular Dystrophy', *PLoS ONE*, 11(4), p. e0152840.
- Rodino-Klapac, L.R., Chicoine, L.G., Kaspar, B.K. and Mendell, J.R. (2007) 'Gene therapy for duchenne muscular dystrophy: expectations and challenges', *Arch Neurol*, 64(9), pp. 1236-41.
- Rodrigues, M., Echigoya, Y., Fukada, S.I. and Yokota, T. (2016) 'Current Translational Research and Murine Models For Duchenne Muscular Dystrophy', *J Neuromuscul Dis*, 3(1), pp. 29-48.
- Rodriguez, O., Schaefer, M.L., Wester, B., Lee, Y.C., Boggs, N., Conner, H.A., Merkle, A.C., Fricke, S.T., Albanese, C. and Koliatsos, V.E. (2016) 'Manganese-Enhanced Magnetic Resonance Imaging as a Diagnostic and Dispositional Tool after Mild-Moderate Blast Traumatic Brain Injury', *J Neurotrauma*, 33(7), pp. 662-71.
- Roig, M., Roma, J., Fargas, A. and Munell, F. (2004) 'Longitudinal pathologic study of the gastrocnemius muscle group in *mdx* mice', *Acta Neuropathol*, 107(1), pp. 27-34.
- Rombouts, I., Lagrain, B., Brunnbauer, M., Delcour, J.A. and Koehler, P. (2013) 'Improved identification of wheat gluten proteins through alkylation of cysteine residues and peptide-based mass spectrometry', *Scientific Reports*, 3, p. 2279.

- Romfh, A. and McNally, E.M. (2010) 'Cardiac assessment in duchenne and becker muscular dystrophies', *Curr Heart Fail Rep*, 7(4), pp. 212-8.
- Roos, A., Thompson, R., Horvath, R., Lochmuller, H. and Sickmann, A. (2017) *Intersection of Proteomics and Genomics to "Solve the Unsolved" in Rare Disorders such as Neurodegenerative and Neuromuscular Diseases*.
- Rosenbaum, S.E. (2011) *Basic Pharmacokinetics and Pharmacodynamics: An Integrated Textbook and Computer Simulations*. Wiley.
- Rouillon, J., Zocevic, A., Leger, T., Garcia, C., Camadro, J.M., Udd, B., Wong, B., Servais, L., Voit, T. and Svinartchouk, F. (2014) 'Proteomics profiling of urine reveals specific titin fragments as biomarkers of Duchenne muscular dystrophy', *Neuromuscul Disord*, 24(7), pp. 563-73.
- Ryan, N.J. (2014) 'Ataluren: first global approval', *Drugs*, 74(14), pp. 1709-14.
- Sacco, A., Mourkioti, F., Tran, R., Choi, J., Llewellyn, M., Kraft, P., Shkreli, M., Delp, S., Pomerantz, J.H., Artandi, S.E. and Blau, H.M. (2010) 'Short telomeres and stem cell exhaustion model Duchenne muscular dystrophy in *mdx/mTR* mice', *Cell*, 143(7), pp. 1059-71.
- Sacco, P., Jones, D.A., Dick, J.R. and Vrbova, G. (1992) 'Contractile properties and susceptibility to exercise-induced damage of normal and *mdx* mouse tibialis anterior muscle', *Clin Sci (Lond)*, 82(2), pp. 227-36.
- Sardet, C., Franchi, A. and Pouyssegur, J. (1989) 'Molecular cloning, primary structure, and expression of the human growth factor-activatable Na⁺/H⁺ antiporter', *Cell*, 56(2), pp. 271-80.
- Schatzberg, S.J., Olby, N.J., Breen, M., Anderson, L.V., Langford, C.F., Dickens, H.F., Wilton, S.D., Zeiss, C.J., Binns, M.M., Kornegay, J.N., Morris, G.E. and Sharp, N.J. (1999) 'Molecular analysis of a spontaneous dystrophin 'knockout' dog', *Neuromuscul Disord*, 9(5), pp. 289-95.
- Schmidt, W.M., Uddin, M.H., Dysek, S., Moser-Thier, K., Pirker, C., Hoger, H., Ambros, I.M., Ambros, P.F., Berger, W. and Bittner, R.E. (2011) 'DNA damage, somatic aneuploidy, and malignant sarcoma susceptibility in muscular dystrophies', *PLoS Genet*, 7(4), p. e1002042.
- Schroeder, M.P., Weiss, C., Procissi, D., Wang, L. and Disterhoft, J.F. (2016) 'Activity-induced manganese-dependent MRI (AIM-MRI) and functional MRI in awake rabbits during somatosensory stimulation', *Neuroimage*, 126, pp. 72-80.
- Schultz, E. and Lipton, B.H. (1982) 'Skeletal muscle satellite cells: changes in proliferation potential as a function of age', *Mech Ageing Dev*, 20(4), pp. 377-83.
- Schürmann, M., Janning, P., Ziegler, S. and Waldmann, H. (2016) 'Small-Molecule Target Engagement in Cells', *Cell Chemical Biology*, 23(4), pp. 435-441.
- Sela, B.A. (2002) '[Titin: some aspects of the largest protein in the body]', *Harefuah*, 141(7), pp. 631-5, 665.

- Selsby, J.T., Morine, K.J., Pendrak, K., Barton, E.R. and Sweeney, H.L. (2012) 'Rescue of dystrophic skeletal muscle by PGC-1 α involves a fast to slow fiber type shift in the *mdx* mouse', *PLoS One*, 7(1), p. e30063.
- Selsby, J.T., Ross, J.W., Nonneman, D. and Hollinger, K. (2015) 'Porcine Models of Muscular Dystrophy()', *ILAR Journal*, 56(1), pp. 116-126.
- Shareef, M.A., Anwer, L.A. and Poizat, C. (2014) 'Cardiac SERCA2A/B: therapeutic targets for heart failure', *Eur J Pharmacol*, 724, pp. 1-8.
- Sharma, A., Sane, H., Badhe, P., Gokulchandran, N., Kulkarni, P., Lohiya, M., Biju, H. and Jacob, V.C. (2013) 'A clinical study shows safety and efficacy of autologous bone marrow mononuclear cell therapy to improve quality of life in muscular dystrophy patients', *Cell Transplant*, 22 Suppl 1, pp. S127-38.
- Sharma, A., Sane, H., Paranjape, A., Bhagawanani, K., Gokulchandran, N. and Badhe, P. (2014) 'Autologous bone marrow mononuclear cell transplantation in Duchenne muscular dystrophy – a case report', *The American Journal of Case Reports*, 15, pp. 128-134.
- Sharma, V. and Freeze, H. (2014) 'Phosphomannomutase 1,2 (PMM1,2)', in Taniguchi, N., Honke, K., Fukuda, M., Narimatsu, H., Yamaguchi, Y. and Angata, T. (eds.) *Handbook of Glycosyltransferases and Related Genes*. Tokyo: Springer Japan, pp. 1591-1598.
- Sharp, N.J., Kornegay, J.N., Van Camp, S.D., Herbstreith, M.H., Secore, S.L., Kettle, S., Hung, W.Y., Constantinou, C.D., Dykstra, M.J., Roses, A.D. and et al. (1992) 'An error in dystrophin mRNA processing in golden retriever muscular dystrophy, an animal homologue of Duchenne muscular dystrophy', *Genomics*, 13(1), pp. 115-21.
- Sheehan, D.C. and Hrapchak, B.B. (1980) *Theory and practice of histotechnology*. Mosby, Incorporated.
- Shen, W., Li, Y., Zhu, J., Schwendener, R. and Huard, J. (2008) 'Interaction between macrophages, TGF- β 1, and the COX-2 pathway during the inflammatory phase of skeletal muscle healing after injury', *J Cell Physiol*, 214(2), pp. 405-12.
- Shin, J., Tajrishii, M.M., Ogura, Y. and Kumar, A. (2013) 'Wasting mechanisms in muscular dystrophy', *Int J Biochem Cell Biol*, 45(10), pp. 2266-79.
- Sicinski, P., Geng, Y., Ryder-Cook, A.S., Barnard, E.A., Darlison, M.G. and Barnard, P.J. (1989) 'The molecular basis of muscular dystrophy in the *mdx* mouse: a point mutation', *Science*, 244(4912), pp. 1578-80.
- Sienkiewicz, D., Kulak, W., Okurowska-Zawada, B., Paszko-Patej, G. and Kawnik, K. (2015) 'Duchenne muscular dystrophy: current cell therapies', *Therapeutic Advances in Neurological Disorders*, 8(4), pp. 166-177.
- Silva, A.C. and Bock, N.A. (2008) 'Manganese-enhanced MRI: an exceptional tool in translational neuroimaging', *Schizophr Bull*, 34(4), pp. 595-604.
- Simon, G.M., Niphakis, M.J. and Cravatt, B.F. (2013) 'Determining target engagement in living systems', *Nature chemical biology*, 9(4), pp. 200-205.

Skuk, D., Goulet, M., Roy, B., Piette, V., Cote, C.H., Chapdelaine, P., Hogrel, J.Y., Paradis, M., Bouchard, J.P., Sylvain, M., Lachance, J.G. and Tremblay, J.P. (2007) 'First test of a "high-density injection" protocol for myogenic cell transplantation throughout large volumes of muscles in a Duchenne muscular dystrophy patient: eighteen months follow-up', *Neuromuscul Disord*, 17(1), pp. 38-46.

Slepkov, E.R., Rainey, J.K., Sykes, B.D. and Fliegel, L. (2007) 'Structural and functional analysis of the Na⁺/H⁺ exchanger', *Biochem J*, 401(3), pp. 623-33.

Smith, J.P., Hicks, P.S., Ortiz, L.R., Martinez, M.J. and Mandler, R.N. (1995) 'Quantitative measurement of muscle strength in the mouse', *Journal of Neuroscience Methods*, 62(1), pp. 15-19.

Soltanzadeh, P., Friez, M.J., Dunn, D., von Niederhausern, A., Gurvich, O.L., Swoboda, K.J., Sampson, J.B., Pestronk, A., Connolly, A.M., Florence, J.M., Finkel, R.S., Bönnemann, C.G., Medne, L., Mendell, J.R., Mathews, K.D., Wong, B.L., Sussman, M.D., Zonana, J., Kovak, K., Gospe Jr, S.M., Gappmaier, E., Taylor, L.E., Howard, M.T., Weiss, R.B. and Flanigan, K.M. (2010) 'Clinical and genetic characterization of manifesting carriers of DMD mutations', *Neuromuscular Disorders*, 20(8), pp. 499-504.

Sonnemann, K.J., Heun-Johnson, H., Turner, A.J., Baltgalvis, K.A., Lowe, D.A. and Ervasti, J.M. (2009) 'Functional substitution by TAT-utrophin in dystrophin-deficient mice', *PLoS Med*, 6(5), p. e1000083.

Spinazzola, J.M. and Kunkel, L.M. (2016) 'Pharmacological therapeutics targeting the secondary defects and downstream pathology of Duchenne muscular dystrophy', *Expert opinion on orphan drugs*, 4(11), pp. 1179-1194.

Spurney, C.F., Gordish-Dressman, H., Guerron, A.D., Sali, A., Pandey, G.S., Rawat, R., Van Der Meulen, J.H., Cha, H.-J., Pistilli, E.E., Partridge, T.A., Hoffman, E.P. and Nagaraju, K. (2009) 'Preclinical drug trials in the *mdx* mouse: assessment of reliable and sensitive outcome measures', *Muscle & nerve*, 39(5), pp. 591-602.

St Andre, M., Johnson, M., Bansal, P.N., Wellen, J., Robertson, A., Opsahl, A., Burch, P.M., Bialek, P., Morris, C. and Owens, J. (2017) 'A mouse anti-myostatin antibody increases muscle mass and improves muscle strength and contractility in the *mdx* mouse model of Duchenne muscular dystrophy and its humanized equivalent, domagrozumab (PF-06252616), increases muscle volume in cynomolgus monkeys', *Skelet Muscle*, 7(1), p. 25.

Stedman, H.H., Sweeney, H.L., Shrager, J.B., Maguire, H.C., Panettieri, R.A., Petrof, B., Narusawa, M., Lefterovich, J.M., Sladky, J.T. and Kelly, A.M. (1991) 'The *mdx* mouse diaphragm reproduces the degenerative changes of Duchenne muscular dystrophy', *Nature*, 352(6335), pp. 536-9.

Stender, S., Chakrabarti, R.S., Xing, C., Gotway, G., Cohen, J.C. and Hobbs, H.H. (2015) 'Adult-onset liver disease and hepatocellular carcinoma in S-adenosylhomocysteine hydrolase deficiency', *Mol Genet Metab*, 116(4), pp. 269-74.

Straub, V. and Campbell, K.P. (1997) 'Muscular dystrophies and the dystrophin-glycoprotein complex', *Curr Opin Neurol*, 10(2), pp. 168-75.

Stuckey, D.J., Carr, C.A., Camelliti, P., Tyler, D.J., Davies, K.E. and Clarke, K. (2012) 'In vivo MRI characterization of progressive cardiac dysfunction in the *mdx* mouse model of muscular dystrophy', *PLoS One*, 7(1), p. e28569.

Szklarczyk, D., Franceschini, A., Wyder, S., Forslund, K., Heller, D., Huerta-Cepas, J., Simonovic, M., Roth, A., Santos, A., Tsafou, K.P., Kuhn, M., Bork, P., Jensen, L.J. and von Mering, C. (2015) 'STRING v10: protein-protein interaction networks, integrated over the tree of life', *Nucleic Acids Res*, 43(Database issue), pp. D447-52.

Takeda, A. (2003) 'Manganese action in brain function', *Brain Research Reviews*, 41(1), pp. 79-87.

Takehima, Y., Yagi, M., Okizuka, Y., Awano, H., Zhang, Z., Yamauchi, Y., Nishio, H. and Matsuo, M. (2010) 'Mutation spectrum of the dystrophin gene in 442 Duchenne/Becker muscular dystrophy cases from one Japanese referral center', *J Hum Genet*, 55(6), pp. 379-88.

Takehita, H., Yamamoto, K., Nozato, S., Inagaki, T., Tsuchimochi, H., Shirai, M., Yamamoto, R., Imaizumi, Y., Hongyo, K., Yokoyama, S., Takeda, M., Oguro, R., Takami, Y., Itoh, N., Takeya, Y., Sugimoto, K., Fukada, S.-i. and Rakugi, H. (2017) 'Modified forelimb grip strength test detects aging-associated physiological decline in skeletal muscle function in male mice', *Scientific Reports*, 7, p. 42323.

Tanabe, Y., Esaki, K. and Nomura, T. (1986) 'Skeletal muscle pathology in X chromosome-linked muscular dystrophy (*mdx*) mouse', *Acta Neuropathol*, 69.

Terrill, J.R., Radley-Crabb, H.G., Iwasaki, T., Lemckert, F.A., Arthur, P.G. and Grounds, M.D. (2013) 'Oxidative stress and pathology in muscular dystrophies: focus on protein thiol oxidation and dysferlinopathies', *Febs j*, 280(17), pp. 4149-64.

Tinsley, J.M., Fairclough, R.J., Storer, R., Wilkes, F.J., Potter, A.C., Squire, S.E., Powell, D.S., Cozzoli, A., Capogrosso, R.F., Lambert, A., Wilson, F.X., Wren, S.P., De Luca, A. and Davies, K.E. (2011) 'Daily treatment with SMTC1100, a novel small molecule utrophin upregulator, dramatically reduces the dystrophic symptoms in the *mdx* mouse', *PLoS One*, 6(5), p. e19189.

Torelli, S., Ferlini, A., Obici, L., Sewry, C. and Muntoni, F. (1999) 'Expression, regulation and localisation of dystrophin isoforms in human foetal skeletal and cardiac muscle', *Neuromuscul Disord*, 9(8), pp. 541-51.

Touret, N., Tanneur, V., Godart, H., Seidler, R., Taki, N., Bürger, E., Dämmgen, J. and Counillon, L. (2003) 'Characterization of sabiporide, a new specific NHE-1 inhibitor exhibiting slow dissociation kinetics and cardioprotective effects', *European Journal of Pharmacology*, 459(2), pp. 151-158.

Townsend, D., Blankinship, M.J., Allen, J.M., Gregorevic, P., Chamberlain, J.S. and Metzger, J.M. (2007) 'Systemic administration of micro-dystrophin restores cardiac geometry and prevents dobutamine-induced cardiac pump failure', *Mol Ther*, 15(6), pp. 1086-92.

Townsend, D., Yasuda, S., Chamberlain, J. and Metzger, J.M. (2009) 'Cardiac consequences to skeletal muscle-centric therapeutics for Duchenne muscular dystrophy', *Trends Cardiovasc Med*, 19(2), pp. 50-55.

- Townsend, D., Yasuda, S., Li, S., Chamberlain, J.S. and Metzger, J.M. (2008) 'Emergent dilated cardiomyopathy caused by targeted repair of dystrophic skeletal muscle', *Mol Ther*, 16(5), pp. 832-5.
- Toyo-oka, T., Kawada, T., Xi, H., Nakazawa, M., Masui, F., Hemmi, C., Nakata, J., Tezuka, A., Iwasawa, K., Urabe, M., Monahan, J. and Ozawa, K. (2002) 'Gene therapy prevents disruption of dystrophin-related proteins in a model of hereditary dilated cardiomyopathy in hamsters', *Heart Lung Circ*, 11(3), pp. 174-81.
- Trinick, J., Knight, P. and Whiting, A. (1984) 'Purification and properties of native titin', *Journal of Molecular Biology*, 180(2), pp. 331-356.
- Trinick, J. and Tskhovrebova, L. (1999) 'Titin: a molecular control freak', *Trends Cell Biol*, 9(10), pp. 377-80.
- Tskhovrebova, L. and Trinick, J. (2010) 'Roles of titin in the structure and elasticity of the sarcomere', *J Biomed Biotechnol*, 2010, p. 612482.
- Tuffery-Giraud, S., Beroud, C., Leturcq, F., Yaou, R.B., Hamroun, D., Michel-Calemard, L., Moizard, M.P., Bernard, R., Cossee, M., Boisseau, P., Blayau, M., Creveaux, I., Guiochon-Mantel, A., de Martinville, B., Philippe, C., Monnier, N., Bieth, E., Khau Van Kien, P., Desmet, F.O., Humbertclaude, V., Kaplan, J.C., Chelly, J. and Claustres, M. (2009) 'Genotype-phenotype analysis in 2,405 patients with a dystrophinopathy using the UMD-DMD database: a model of nationwide knowledgebase', *Hum Mutat*, 30(6), pp. 934-45.
- Tuli, L. and Ransom, H.W. (2009) 'LC-MS Based Detection of Differential Protein Expression', *J Proteomics Bioinform*, 2, pp. 416-438.
- Turkel, S.B., Howell, R., Iseri, A.L. and Chui, L. (1981) 'Ultrastructure of muscle in fetal Duchenne's dystrophy', *Arch Pathol Lab Med*, 105(8), pp. 414-8.
- Turner, P.R., Westwood, T., Regen, C.M. and Steinhardt, R.A. (1988) 'Increased protein degradation results from elevated free calcium levels found in muscle from *mdx* mice', *Nature*, 335(6192), pp. 735-8.
- Tyler, K.L. (2003) 'Origins and early descriptions of "Duchenne muscular dystrophy"', *Muscle and Nerve*, 28(4), pp. 402-422.
- Uygur, A. and Lee, R.T. (2016) 'Mechanisms of Cardiac Regeneration', *Dev Cell*, 36(4), pp. 362-74.
- Valentine, B.A., Cooper, B.J., de Lahunta, A., O'Quinn, R. and Blue, J.T. (1988) 'Canine X-linked muscular dystrophy. An animal model of Duchenne muscular dystrophy: clinical studies', *J Neurol Sci*, 88(1-3), pp. 69-81.
- Valentine, B.A., Winand, N.J., Pradhan, D., Moise, N.S., de Lahunta, A., Kornegay, J.N. and Cooper, B.J. (1992) 'Canine X-linked muscular dystrophy as an animal model of Duchenne muscular dystrophy: a review', *Am J Med Genet*, 42(3), pp. 352-6.
- Vallejo-Illarramendi, A., Toral-Ojeda, I., Aldanondo, G. and Lopez de Munain, A. (2014) 'Dysregulation of calcium homeostasis in muscular dystrophies', *Expert Rev Mol Med*, 16, p. e16.

- Valnot, I., Kassis, J., Chretien, D., de Lonlay, P., Parfait, B., Munnich, A., Kachaner, J., Rustin, P. and Rotig, A. (1999) 'A mitochondrial cytochrome b mutation but no mutations of nuclearly encoded subunits in ubiquinol cytochrome c reductase (complex III) deficiency', *Hum Genet*, 104(6), pp. 460-6.
- van Deutekom, J.C., Janson, A.A., Ginjaar, I.B., Frankhuizen, W.S., Aartsma-Rus, A., Bremmer-Bout, M., den Dunnen, J.T., Koop, K., van der Kooi, A.J., Goemans, N.M., de Kimpe, S.J., Ekhart, P.F., Venneker, E.H., Platenburg, G.J., Verschuuren, J.J. and van Ommen, G.J. (2007) 'Local dystrophin restoration with antisense oligonucleotide PRO051', *N Engl J Med*, 357(26), pp. 2677-86.
- van Putten, M., Kumar, D., Hulsker, M., Hoogaars, W.M., Plomp, J.J., van Opstal, A., van Iterson, M., Admiraal, P., van Ommen, G.J., t Hoen, P.A. and Aartsma-Rus, A. (2012) 'Comparison of skeletal muscle pathology and motor function of dystrophin and utrophin deficient mouse strains', *Neuromuscul Disord*, 22(5), pp. 406-17.
- Van Ruiten, H.J., Marini Bettolo, C., Cheetham, T., Eagle, M., Lochmuller, H., Straub, V., Bushby, K. and Guglieri, M. (2016) 'Why are some patients with Duchenne muscular dystrophy dying young: An analysis of causes of death in North East England', *Eur J Paediatr Neurol*, 20(6), pp. 904-909.
- Vandebrouck, C., Martin, D., Colson-Van Schoor, M., Debaix, H. and Gailly, P. (2002) 'Involvement of TRPC in the abnormal calcium influx observed in dystrophic (*mdx*) mouse skeletal muscle fibers', *J Cell Biol*, 158(6), pp. 1089-96.
- Vidal, B., Serrano, A.L., Tjwa, M., Suelves, M., Ardite, E., De Mori, R., Baeza-Raja, B., Martinez de Lagran, M., Lafuste, P., Ruiz-Bonilla, V., Jardi, M., Gherardi, R., Christov, C., Dierssen, M., Carmeliet, P., Degen, J.L., Dewerchin, M. and Munoz-Canoves, P. (2008) 'Fibrinogen drives dystrophic muscle fibrosis via a TGFbeta/alternative macrophage activation pathway', *Genes Dev*, 22(13), pp. 1747-52.
- Vilquin, J.T., Brussee, V., Asselin, I., Kinoshita, I., Gingras, M. and Tremblay, J.P. (1998) 'Evidence of *mdx* mouse skeletal muscle fragility in vivo by eccentric running exercise', *Muscle Nerve*, 21(5), pp. 567-76.
- Voisin, V. and de la Porte, S. (2005) '[Pharmacological treatments for Duchenne and Becker dystrophies]', *J Soc Biol*, 199(1), pp. 17-28.
- Vollbrandt, T., Willkomm, D., Stossberg, H. and Kruse, C. (2004) 'Vigilin is co-localized with 80S ribosomes and binds to the ribosomal complex through its C-terminal domain', *Int J Biochem Cell Biol*, 36(7), pp. 1306-18.
- von Mering, C., Jensen, L.J., Snel, B., Hooper, S.D., Krupp, M., Foglierini, M., Jouffre, N., Huynen, M.A. and Bork, P. (2005) 'STRING: known and predicted protein-protein associations, integrated and transferred across organisms', *Nucleic Acids Research*, 33(Database Issue), pp. D433-D437.
- Waghorn, B., Yang, Y., Baba, A., Matsuda, T., Schumacher, A., Yanasak, N. and Hu, T.C. (2009) 'Assessing manganese efflux using SEA0400 and cardiac T1-mapping manganese-enhanced MRI in a murine model', *NMR Biomed*, 22(8), pp. 874-81.
- Wakabayashi, S., Hisamitsu, T. and Nakamura, T.Y. (2013) 'Regulation of the cardiac Na(+)/H(+) exchanger in health and disease', *J Mol Cell Cardiol*, 61, pp. 68-76.

- Walker, J.M. (1994) 'The bicinchoninic acid (BCA) assay for protein quantitation', *Methods Mol Biol*, 32, pp. 5-8.
- Wallimann, T., Tokarska-Schlattner, M. and Schlattner, U. (2011) 'The creatine kinase system and pleiotropic effects of creatine', *Amino Acids*, 40(5), pp. 1271-96.
- Wang, B., Li, J., Fu, F.H. and Xiao, X. (2009a) 'Systemic human minidystrophin gene transfer improves functions and life span of dystrophin and dystrophin/utrophin-deficient mice', *J Orthop Res*, 27(4), pp. 421-6.
- Wang, B., Li, J. and Xiao, X. (2000) 'Adeno-associated virus vector carrying human minidystrophin genes effectively ameliorates muscular dystrophy in *mdx* mouse model', *Proc Natl Acad Sci U S A*, 97(25), pp. 13714-9.
- Wang, Y., Marino-Enriquez, A., Bennett, R.R., Zhu, M., Shen, Y., Eilers, G., Lee, J.C., Henze, J., Fletcher, B.S., Gu, Z., Fox, E.A., Antonescu, C.R., Fletcher, C.D., Guo, X., Raut, C.P., Demetri, G.D., van de Rijn, M., Ordog, T., Kunkel, L.M. and Fletcher, J.A. (2014) 'Dystrophin is a tumor suppressor in human cancers with myogenic programs', *Nat Genet*, 46(6), pp. 601-6.
- Wang, Z., Chamberlain, J.S., Tapscott, S.J. and Storb, R. (2009b) 'Gene therapy in large animal models of muscular dystrophy', *ILAR J*, 50(2), pp. 187-98.
- Watkins, S.C. and Cullen, M.J. (1982) 'Muscle fibre size and shape in Duchenne muscular dystrophy', *Neuropathol Appl Neurobiol*, 8(1), pp. 11-7.
- Webster, C., Silberstein, L., Hays, A.P. and Blau, H.M. (1988) 'Fast muscle fibers are preferentially affected in Duchenne muscular dystrophy', *Cell*, 52(4), pp. 503-13.
- Whitehead, N.P., Yeung, E.W. and Allen, D.G. (2006) 'Muscle damage in *mdx* (dystrophic) mice: role of calcium and reactive oxygen species', *Clin Exp Pharmacol Physiol*, 33(7), pp. 657-62.
- Whittemore, L.A., Song, K., Li, X., Aghajanian, J., Davies, M., Girgenrath, S., Hill, J.J., Jalenak, M., Kelley, P., Knight, A., Maylor, R., O'Hara, D., Pearson, A., Quazi, A., Ryerson, S., Tan, X.Y., Tomkinson, K.N., Veldman, G.M., Widom, A., Wright, J.F., Wudyka, S., Zhao, L. and Wolfman, N.M. (2003) 'Inhibition of myostatin in adult mice increases skeletal muscle mass and strength', *Biochem Biophys Res Commun*, 300(4), pp. 965-71.
- Wibrand, F., Ravn, K., Schwartz, M., Rosenberg, T., Horn, N. and Vissing, J. (2001) 'Multisystem disorder associated with a missense mutation in the mitochondrial cytochrome b gene', *Ann Neurol*, 50(4), pp. 540-3.
- Wicklund, M.P. (2013) 'The muscular dystrophies', *Continuum (Minneap Minn)*, 19(6 Muscle Disease), pp. 1535-70.
- Wilkins, M.R., Appel, R.D., Williams, K.L. and Hochstrasser, D.F. (2008) *Proteome Research: Concepts, Technology and Application*. Springer Berlin Heidelberg.
- Willmann, R., De Luca, A., Benatar, M., Grounds, M., Dubach, J., Raymackers, J.M. and Nagaraju, K. (2012) 'Enhancing translation: guidelines for standard pre-clinical experiments in *mdx* mice', *Neuromuscul Disord*, 22(1), pp. 43-9.

- Willmann, R., Possekkel, S., Dubach-Powell, J., Meier, T. and Ruegg, M.A. (2009) 'Mammalian animal models for Duchenne muscular dystrophy', *Neuromuscul Disord*, 19(4), pp. 241-9.
- Xu, W.T., Jin, N., Xu, J., Xu, Y.G., Wang, Q.J. and You, Q.D. (2009) 'Design, synthesis and biological evaluation of novel substituted benzoylguanidine derivatives as potent Na⁺/H⁺ exchanger inhibitors', *Bioorg Med Chem Lett*, 19(12), pp. 3283-7.
- Yang, J., Li, Q., Wang, M., Cao, X., Ding, Y., Wang, G. and Liao, C. (2016) 'Semiquantitative assessment of optic nerve injury using manganese-enhanced MRI', *Jpn J Radiol*, 34(5), pp. 356-65.
- Yasuda, S., Townsend, D., Michele, D.E., Favre, E.G., Day, S.M. and Metzger, J.M. (2005) 'Dystrophic heart failure blocked by membrane sealant poloxamer', *Nature*, 436(7053), pp. 1025-9.
- Yeung, E.W., Whitehead, N.P., Suchyna, T.M., Gottlieb, P.A., Sachs, F. and Allen, D.G. (2005) 'Effects of stretch-activated channel blockers on [Ca²⁺]_i and muscle damage in the *mdx* mouse', *The Journal of Physiology*, 562(Pt 2), pp. 367-380.
- Yiu, E.M. and Kornberg, A.J. (2015) 'Duchenne muscular dystrophy', *Journal of Paediatrics and Child Health*.
- Yu, H.-H., Zhao, H., Qing, Y.-B., Pan, W.-R., Jia, B.-Y., Zhao, H.-Y., Huang, X.-X. and Wei, H.-J. (2016) 'Porcine Zygote Injection with Cas9/sgRNA Results in DMD-Modified Pig with Muscle Dystrophy', *International Journal of Molecular Sciences*, 17(10), p. 1668.
- Yu, X., Bao, B., Echigoya, Y. and Yokota, T. (2015) 'Dystrophin-deficient large animal models: translational research and exon skipping', *Am J Transl Res*, 7(8), pp. 1314-31.
- Zacharias, J.M. and Anderson, J.E. (1991) 'Muscle regeneration after imposed injury is better in younger than older *mdx* dystrophic mice', *J Neurol Sci*, 104(2), pp. 190-6.
- Zaina, S., Lindholm, M.W. and Lund, G. (2005) 'Nutrition and aberrant DNA methylation patterns in atherosclerosis: more than just hyperhomocysteinemia?', *J Nutr*, 135(1), pp. 5-8.
- Zeqiraj, E., Filippi, B.M., Deak, M., Alessi, D.R. and van Aalten, D.M. (2009) 'Structure of the LKB1-STRAD-MO25 complex reveals an allosteric mechanism of kinase activation', *Science*, 326(5960), pp. 1707-11.
- Zhang, C., Zhang, H., Wu, G., Luo, X., Zhang, C., Zou, Y., Wang, H., Hui, R., Wang, J. and Song, L. (2017) 'Titin-Truncating Variants Increase the Risk of Cardiovascular Death in Patients With Hypertrophic Cardiomyopathy', *Can J Cardiol*, 33(10), pp. 1292-1297.
- Zhao, D.W., Zhang, L.T., Cheng, H.Y., Zhang, Y.L., Min, J.Y., Xiao, H.L. and Wang, Y. (2015) 'Monitoring dynamic alterations in calcium homeostasis by T1-mapping manganese-enhanced MRI (MEMRI) in the early stage of small intestinal ischemia-reperfusion injury', *NMR Biomed*, 28(8), pp. 958-66.
- Zhou, L., Rafael-Fortney, J.A., Huang, P., Zhao, X.S., Cheng, G., Zhou, X., Kaminski, H.J., Liu, L. and Ransohoff, R.M. (2008) 'Haploinsufficiency of utrophin gene worsens

skeletal muscle inflammation and fibrosis in *mdx* mice', *J Neurol Sci*, 264(1-2), pp. 106-11.

Zhu, J., Li, Y., Shen, W., Qiao, C., Ambrosio, F., Lavasani, M., Nozaki, M., Branca, M.F. and Huard, J. (2007) 'Relationships between transforming growth factor-beta1, myostatin, and decorin: implications for skeletal muscle fibrosis', *J Biol Chem*, 282(35), pp. 25852-63.